Response functions of semiconductors and insulators : from the Bethe-Salpeter equation to time-dependent density functional theory

Francesco Sottile

Thèse présentée pour obtenir le grade de

DOCTEUR DE L'ÉCOLE POLYTECHNIQUE

par

FRANCESCO SOTTILE

Response functions of semiconductors and insulators: from the Bethe-Salpeter equation to time-dependent density functional theory

Soutenue le 29 Septembre 2003 devant le jury composé de :

M. Friedhelm	BECHSTEDT	Rapporteur
M. George	BERTSCH	
M. Xavier	BLASE	Rapporteur
M. Fabio	FINOCCHI	
M.me Lucia	REINING	Directeur
M. Jean-Claude	TOLEDANO	Directeur

Laboratoire des Solides Irradiés UMR 7642
CNRS-CEA/DSM, École POLYTECHNIQUE, F-91128 Palaiseau, France

Francesco Sottile `francesco.sottile@polytechnique.fr`

Response functions of semiconductors and insulators: from the Bethe-Salpeter equation to time-dependent density functional theory

Pdf file available at the page
`http://theory.polytechnique.fr/people/sottile/Tesi_dot.pdf`

2003

This manuscript has been conceived only using free software: LaTeX, Ghostscript, Kile.
Figures and graphs were created with Xfig, The Gimp, Grace, PStoEdit and GNUPlot.

Acknowledgments

Le Laboratoire des Solides Irradiés de l'École Polytechnique, dirigé par Guillaume Petite, m'a accueilli avec la plus grande sympathie et je tiens à leur exprimer à tous ma reconnaissance.

I would like to express my profound gratitude to my supervisor, Lucia Reining, for supporting, guiding, and working very closely with me for the last three years. In particular, I will never forget our discussions at 7.30 in the morning. This thesis owes its existence to Lucia.

I am very grateful to Prof. Toledano who agreed to be my supervisor. He left me free to work as I preferred, and was always available to help me.

I would like to thank all those who I have collaborated with: first of all, Valerio Olevano, for providing the computational codes I worked on, and for the endless discussions on kernels, fortran, latex and home-cinema; Angel Rubio, who worked with me at the very beginning of the thesis, on finite systems; Giovanni Onida, Andrea Marini and Rodolfo Del Sole, for useful discussions about kernels; Ferdi Aryasetiawan and Krister Karlsson, for a fruitful work on model kernels we have been carrying out together.

I acknowledge my gratitude also to the NANOPHASE Network, to which I have had the privilege to belong. My scientific background also originated from the several meetings we have had in these years. Let me take this opportunity to thank the European Community, but also the three organisms which the laboratory depends on (CNRS, CEA, Polytechnique), for covering living and travel expenses in many occasions, and also Marie Madeleine Lemartinel and Catherine Julien for helping me to get along with all these administrative things.

Je tiens à remercier chaleureusement toute l'équipe théorique du laboratoire, pour toutes nos discussions et pour le temps passé ensemble : Silvana Botti, Apostolos Marinopoulos, Nathalie Vast, Fabien Bruneval, Andrea Cucca, Louise Dash and Virginie Quequet ; Marc Hayoun et Olivier Hardouin Duparc pour avoir écouté mes exposés et m'avoir également aidé avec le français ; en particulier Olivier, avec qui j'ai partagé le bureau dans une très bonne ambiance.

I'm deeply indebted to my university supervisor, Prof. Pietro Ballone, who taught me a lot, and introduced me into the Palaiseau group.

My gratitude goes to the Rapporteurs, Friedhelm Bechstedt and Xavier Blase, who accepted the work of examining and reporting; I'm also grateful to the Examinateurs, George Bertsch for chairing the jury and Fabio Finocchi, who also gave me the possibility to teach in a DEA for the first time.

Un grazie sincero a tutti gli amici "parigini", per aver trascorso bei momenti di svago insieme, molti dei quali a tavola.

Ai miei genitori, Nuccia e Gianni, devo tutta la mia gratitudine, per tutto l'aiuto e l'incoraggiamento avuto da parte loro, non importa quanto lontano stiano.

Finally my deepest gratitude to my girlfriend, Daniella, for her understanding and love. Her support and encouragement has made this work possible.

Francesco

Contents

List of abbreviations, acronyms and symbols

Eq.(s)	equation(s)
Tab.	table
Fig.	figure
Ref.(s)	reference(s)
Par.	paragraph
exp.	experiment

BZ	Brillouin zone
(TD)DFT	(time dependent) density functional theory
BSE	Bethe-Salpeter equation
MBPT	many-body perturbation theory
SCF	self-consistent field
RPA	random phase approximation
(A)LDA	(adiabatic) local density approximation
HK	Hohenberg-Kohn
HF	Hartree-Fock
KS	Kohn-Sham
GWA	GW approximation for the self-energy
GW-RPA	RPA polarizability with (GW) corrected eigenvalues

$x-c$	exchange-correlation
$e-h$	electron-hole
ϵ_i	one-particle eigenvalues
E_i	quasi-particle eigenvalues
ϕ	one-particle wavefunctions
Ψ	quasi-particle wavefunctions
φ	many-body wave function

Jungle of Polarizabilities

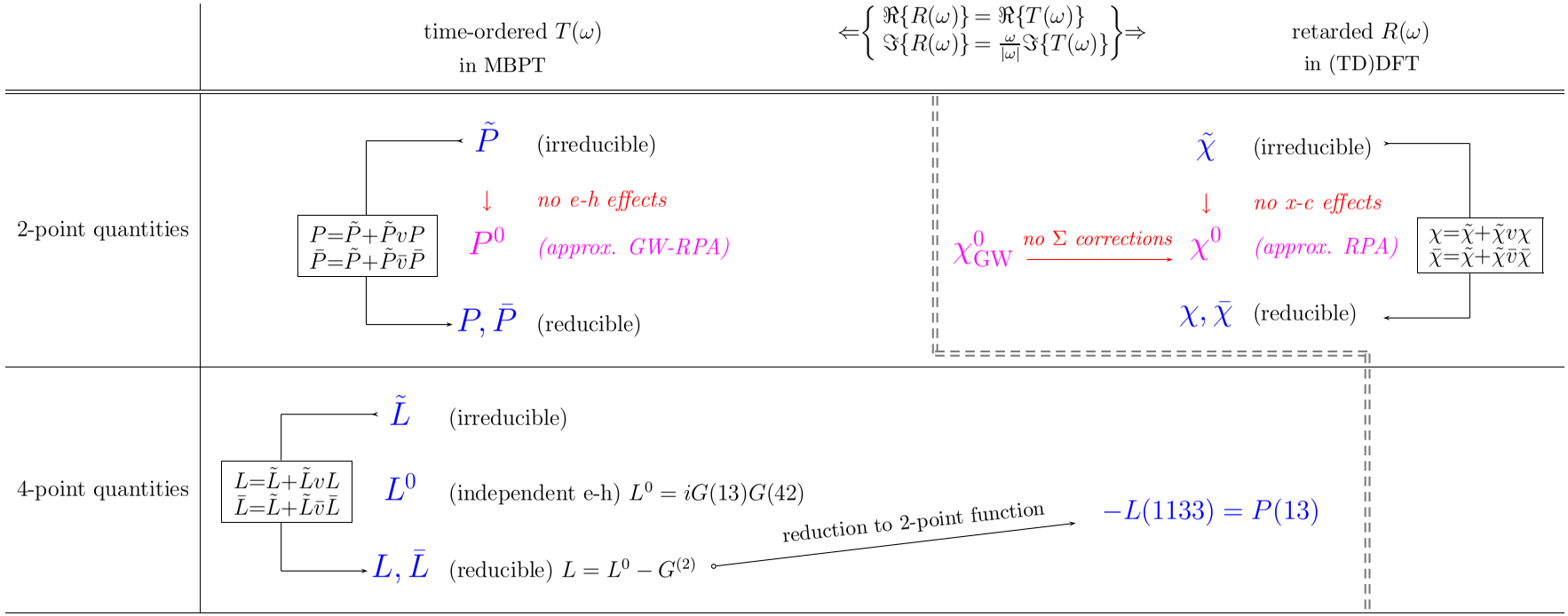

in the dielectric function ε

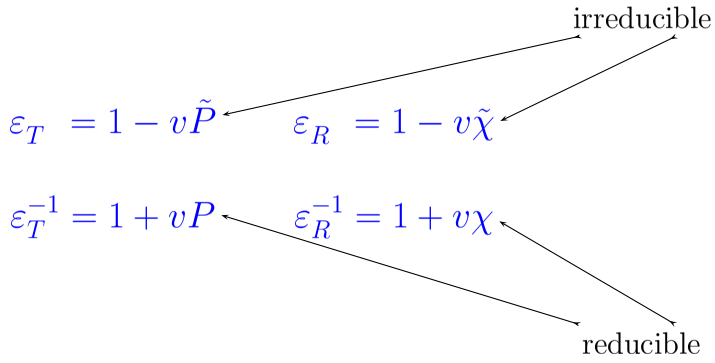

Introduction

pedo mellon a minno

from West Gate of Moria Inscription

Electronic excitations, caused for example by irradiation with electrons, light or modern photon sources (synchrotron, ultra-fast lasers), are key quantities for the study of materials, ranging from solids to atoms, from surface to nanoscale systems. An accurate understanding and prediction of the interaction of radiation and matter can even favor remarkable technological breakthroughs, like new functionalities for bulk systems (e.g. in optoelectronics) or, in the long term, in biological applications ("bottom-up" assembling or molecular machines[1]).

Experimental techniques measuring electronic excitations have seen rapid progress (high spatial resolution, short measurement time, low temperature), which continuously requires and stimulates a more precise theoretical description. The joint use of theory and computer simulation has in fact, over the last decades, permitted to achieve big improvements in the description of optical properties of both finite and infinite systems.

The problem of calculating electronic excitations is strongly related to the challenging problem of electron correlation. The energy gap of a bulk material, for example, crucially depends on electron correlation. Correlation prevents the ground and excited states many-body wave function φ of a system to be simply a symmetrized product of independent single-particle orbitals ϕ_i. Methods that aim at calculating the many-electron wave function (and hence at calculating, from first principles, the electron correlation) are the Configuration Interaction method [6–8], the Coupled Electron Pair Approximation [9–11] and Coupled Cluster method [9, 10, 12, 13], and, more recently, the Quantum Monte Carlo [14–19]. These methods can yield results of very high accuracy. However, unless seriously approximated, they are restricted to systems of a few electrons, due to an unfavorable scaling with system size, or due to size-consistency problems [20, 21]. In this thesis, instead, we will exclusively follow methods which do not require the knowledge of the many-body wave function of the system, being density-based (Time-independent and

[1] "Scientists have discovered how to use a single plastic molecule to drive a tiny machine. One frequency of light causes the molecule to contract and another causes it to expand, making it move a board down and up repeatedly" [1]. For details on molecular machines set in action by light, see Ref.s [2–5].

Dependent Density Functional Theory (TD)DFT, chapters 2 and 4) or Green function-based (many body perturbation theory MBPT, chapter 3). The approximations involved in these theories (regarding the exchange-correlation potential or the self-energy) are essentially an "ansatz" for the electron correlation.

The theoretical description of electronic excitations in the framework of many-body perturbation theory (chapter 3) has undergone a rapid development since new approaches and the increase of computer power have made numerical calculations feasible for real systems. Within many-body perturbation theory one can calculate with a good precision charged excitations (i.e. electron addition and removal energies), using e.g. Hedin's GW approximation [22] for the electron self-energy. In the same framework, neutral excitations (e.g. optical and energy-loss spectra) are also well described today through the solution of the Bethe-Salpeter equation (BSE). An optical absorption experiment creates an *interacting* electron-hole pair, the *exciton*. Good agreement between theory and experiment can only be achieved taking into account the electron-hole interaction, especially if the system is a semiconductor or an insulator (small-gap semiconductors and metals, instead, screen this electron-hole interaction, and the resulting contribution can therefore be negligible). The Bethe-Salpeter couples indeed the electron and the hole, and it has been very successful for the calculation of absorption spectra of a large variety of systems: insulators, semiconductors, atoms, clusters, surfaces or polymers. However, the intrinsic two-particle nature of the Bethe-Salpeter equation makes the calculations very cumbersome, since a four-point equation (due to the propagation of two particles) has to be solved. Therefore, in spite of the excellent results obtained with the BSE for moderately simple systems, the efficient description of electron-hole excited states in realistic materials is still considered to be an unsolved problem in condensed matter theory.

A quite different approach, the time-dependent density-functional theory (TDDFT, chapter 4) might be an advantageous alternative to the BSE formalism because, as in the case of the very successful static density-functional theory (DFT), this theory relies on the (now time-dependent) electron density $n(\mathbf{r}, t)$ instead of the one-particle Green function, the propagator $G(\mathbf{r}, t, \mathbf{r}', t')$. Two-point response functions are involved in the formalism instead of the four-point ones required in the BSE approach. However, the time-dependent exchange-correlation (xc) potential $v_{xc}[n](\mathbf{r}, t)$ is unknown, as well as its density variations. In the framework of linear response, the quantity to be described is the xc kernel $f_{xc}[n](\mathbf{r}, t, \mathbf{r}', t') = \delta v_{xc}[n](\mathbf{r}, t)/\delta n(\mathbf{r}', t')$. A widely used approximation is the adiabatic local-density approximation (ALDA) which defines a short-ranged xc-kernel as the functional derivative with respect to the density of the xc-potential in the static local-density approximation. Unfortunately, this approximation turned out not to be a systematically good approximation, and in general yields a rather bad description of optical properties of infinite systems.

Up to three years ago, at the beginning of this thesis work, the application of TDDFT, to the description of absorption spectra of solids (in practice done almost exclusively

within the adiabatic local density approximation), was therefore considered to be a failure.

In this thesis, instead, we show that the time dependent density functional theory could become *the method* to calculate the absorption spectrum of solids, including the excitonic effects, and obtaining results of the same precision as the Bethe-Salpeter method.

A general theoretical background is provided in Part I, in which we link the macroscopic measured quantities to the microscopic response of the system to an external perturbation. We also remind that the response function equations in time dependent density functional theory and in the Bethe-Salpeter framework have the same structure and can be described by the same type of equation

$$S = S^0 + S^0 K S.$$

The kernel K of this Dyson-like screening equation, that links the response function S^0, of a system of independent (Kohn-Sham or quasi-) particles, to the full response S, is composed of two terms: 1) a bare Coulomb interaction, which is the same in both approaches. Its role will be investigated in chapter 6; 2) the exchange-correlation (in TDDFT) or electron-hole (in BSE) contribution, which is, instead, different in time dependent density functional theory and Bethe-Salpeter. The importance of this contribution will be analyzed in chapter 7, showing, in particular, that very simple approximations can lead to satisfying spectra for both semiconductors and insulators. In chapter 8 we combine the knowledge gained from BSE, with the advantages of TDDFT, in order to obtain exchange-correlation kernels, to be used in time dependent density functional theory. They are fully *ab initio*, and parameter-free, and they *are* able to describe the optical spectra of solids. The results are in fact extremely promising. We show the optical absorption of bulk semiconductors (chapter 9) and insulators (chapter 10) in good agreement with the experiments, almost indistinguishable from those of the BSE approach. This is, to our opinion, an important step towards the solution of the long-standing problem of how to calculate *ab initio* realistic absorption spectra of materials, without solving the BSE.

The conclusions, with a brief summary of the main topics addressed in this work, end the thesis.

Part I

Background

Chapter 1

Dielectric and optical properties in solids

> I never satisfy myself until I can make a mechanical model of a thing. If I can make a mechanical model I can understand it. As long as I cannot make a mechanical model all the way through I cannot understand; and that is why I cannot get the electromagnetic theory.
>
> Sir William Thomson, Lord Kelvin

The aim of this chapter is to establish a relation between the microscopic and macroscopic description of the interaction between a material and the electro-magnetic field [23]. In microscopic terms, we use concepts like the excitation of an electron as a consequence of the absorption of a photon, or like the creation of an electron-hole pair, etc. From a macroscopic point of view we talk in terms of Maxwell's equations to define macroscopic quantities like absorption, light scattering, reflectivity, that are measurable by spectroscopy experiments. The importance of this relation is therefore clear: on one hand, the knowledge of the band structure of a solid, and more in particular of electronic excited states, is crucial to describe and predict results of experiments; on the other hand, optical properties of solids provide a very efficient tool for studying band structure, excitons, but also for detecting defects and impurities, or lattice vibrations. The central quantity that makes the link is the frequency-dependent dielectric function $\varepsilon(\omega)$ (and conductivity σ).

1.1 Complex dielectric function and complex conductivity

In the presence of matter, Maxwell's equations are [24–26]

$$\begin{aligned} \nabla \times \mathsf{H} &= \frac{1}{c}\frac{\partial \mathsf{D}}{\partial t} + \frac{4\pi}{c}\mathbf{j}_{ext} \\ \nabla \times \mathsf{E} &= -\frac{1}{c}\frac{\partial \mathsf{B}}{\partial t} \\ \nabla \cdot \mathsf{D} &= 4\pi\rho_{ext} \\ \nabla \cdot \mathsf{B} &= 0 \end{aligned} \tag{1.1}$$

where E and H are the electric and magnetic fields, D is the electric displacement, B is the magnetic induction, ρ_{ext} is the external charge (or free charge) density and $\mathbf{j}_{ext}$ the external current density. By combining the first and the third of the Eq. (1.1) we have the continuity equation

$$\frac{\partial \rho_{ext}}{\partial t} + \nabla \cdot \mathbf{j}_{ext} = 0$$

which takes into account the conservation of the charge. The complex dielectric function and complex conductivity are introduced once the constitutive equations

$$\begin{aligned} \mathsf{D} &= \mathsf{D}\left[\mathsf{E}, \mathsf{H}\right] \\ \mathsf{B} &= \mathsf{B}\left[\mathsf{E}, \mathsf{H}\right] \\ \mathbf{j} &= \mathbf{j}\left[\mathsf{E}, \mathsf{H}\right] \end{aligned}$$

are specified. When non-linear effects are neglected we can write *linear* relations for the constitutive equations. So let's define the complex tensors ε,μ, σ through

$$\begin{aligned} \mathsf{D}(\mathbf{r},t) &= \int d\mathbf{r}' \int dt' \varepsilon(\mathbf{r},\mathbf{r}',t-t')\mathsf{E}(\mathbf{r}',t') \\ \mathsf{B}(\mathbf{r},t) &= \int d\mathbf{r}' \int dt' \mu(\mathbf{r},\mathbf{r}',t-t')\mathsf{H}(\mathbf{r}',t') \\ \mathbf{j}(\mathbf{r},t) &= \int d\mathbf{r}' \int dt' \sigma(\mathbf{r},\mathbf{r}',t-t')\mathsf{E}(\mathbf{r}',t'). \end{aligned} \tag{1.2}$$

These equations define the complex quantities ε,μ,σ. The latter are in general tensors, but from now on, this fact will be ignored.[1] In frequency domain the equations read:

$$\begin{aligned} \mathsf{D}(\omega) &= \varepsilon(\omega)\mathsf{E}(\omega) \\ \mathsf{B}(\omega) &= \mu(\omega)\mathsf{H}(\omega) \\ \mathbf{j}(\omega) &= \sigma(\omega)\mathsf{E}(\omega) \end{aligned} \tag{1.3}$$

[1] This is however correct for an isotropic medium or a crystal having cubic symmetry.

where ε, μ and σ are the dielectric tensor, the permeability tensor and the conductivity of the medium, respectively. Since all the vectors $\mathsf{D}(\mathbf{r},t)$, $\mathsf{B}(\mathbf{r},t)$, $\mathsf{H}(\mathbf{r},t)$ $\mathsf{E}(\mathbf{r},t)$, $\mathbf{j}(\mathbf{r},t)$ are real, we also have the important relations:

$$\begin{aligned}\varepsilon(-\omega) &= \varepsilon^*(\omega)\\ \mu(-\omega) &= \mu^*(\omega)\\ \sigma(-\omega) &= \sigma^*(\omega).\end{aligned}$$

We can also relate the electric and magnetic fields E and B with their derived fields D and H, by the *polarisation* $\mathcal{P}$ and the *magnetisation* $\mathcal{M}$, via

$$\begin{aligned}\mathsf{D} &= \mathsf{E} + 4\pi\mathcal{P}\\ \mathsf{H} &= \mathsf{B} - 4\pi\mathcal{M}.\end{aligned} \tag{1.4}$$

The quantities $\mathcal{P}$ and $\mathcal{M}$ can be (linearly) related to the macroscopic fields via the

$$\begin{aligned}\mathcal{P} &= \chi_e\mathsf{E}\\ \mathcal{M} &= \chi_m\mathsf{H}\end{aligned} \tag{1.5}$$

where χ_e and χ_m are the (electric) susceptibility and (magnetic) permeability of the medium, respectively. From Eq.s (1.3), (1.4) and (1.5) we have

$$\begin{aligned}\varepsilon &= 1 + 4\pi\chi_e\\ \mu &= 1 + 4\pi\chi_m.\end{aligned} \tag{1.6}$$

For non magnetic media one can set $\mu = 1$, $\chi_m = 0$.

When the external sources are zero, the Maxwell's equations in frequency domain read

$$\begin{aligned}\nabla\times\mathsf{H}(\omega) &= -\frac{i\omega}{c}\mathsf{D}(\omega)\\ \nabla\times\mathsf{E}(\omega) &= \frac{i\omega}{c}\mathsf{B}(\omega)\\ \nabla\cdot\mathsf{D}(\omega) &= 0\\ \nabla\cdot\mathsf{B}(\omega) &= 0.\end{aligned} \tag{1.7}$$

Now from the first of Eq. (1.7) and the first of Eq. (1.3) we have

$$\nabla\times\mathsf{H}(\omega) = -\frac{i\omega\varepsilon(\omega)}{c}\mathsf{E}(\omega) \tag{1.8}$$

which is also equal to (using Eq.s (1.5) and (1.6))

$$\nabla\times\mathsf{H}(\omega) = -\frac{i\omega}{c}\mathsf{E}(\omega) - \frac{i\omega 4\pi}{c}\mathcal{P}(\omega)$$

or

$$\nabla \times \mathsf{H}(\omega) = -\frac{i\omega}{c}\mathsf{E}(\omega) + \frac{4\pi}{c}\mathbf{j}_{ind}(\omega)$$

where the induced current density has been introduced. From the Ohm's law (Eq. (1.3))

$$\varepsilon = 1 + \frac{4\pi i\sigma}{\omega} \tag{1.9}$$

which shows the link between the dielectric function ε and the conductivity σ of a material.

1.2 Complex refraction index and absorption coefficient

Without external sources, Maxwell's equations yield

$$\nabla \times \nabla \times \mathsf{E} = -\frac{1}{c}\frac{\partial}{\partial t}(\nabla \times \mathsf{B})$$

$$\nabla(\nabla \cdot \mathsf{E}) - \nabla^2\mathsf{E} = -\frac{1}{c}\frac{\partial}{\partial t}\left(\frac{\mu}{c}\frac{\partial \mathsf{D}}{\partial t}\right)$$

$$\nabla^2\mathsf{E} = \frac{\mu\varepsilon}{c^2}\frac{\partial^2\mathsf{E}}{\partial t^2}. \tag{1.10}$$

The general solution of Eq. (1.10) is

$$\mathsf{E} = \mathsf{E}_0 e^{i(\mathbf{K}\cdot\mathbf{r}-\omega t)}$$

with

$$|\mathbf{K}|^2 = \frac{\omega^2}{c^2}\mu\varepsilon.$$

If we suppose that the propagation vector is in $\hat{\mathbf{x}}$ direction,

$$\mathbf{K} = \frac{\omega}{c}\sqrt{\mu\varepsilon}\hat{\mathbf{x}}$$

and

$$\mathsf{E}(x,t) = \mathsf{E}_0 e^{i\frac{\omega}{c}x\sqrt{\mu\varepsilon}} e^{-i\omega t}.$$

For the wave propagation in vacuum ($\sigma = 0, \mu = \varepsilon = 1$)

$$\mathsf{E}(x,t) = \mathsf{E}_0 e^{i\omega\left(\frac{x}{c}-t\right)}$$

which represents the plane wave solution.
The solution of (1.10) inside a medium of finite conductivity is the damped wave[2]

$$\mathsf{E}(x,t) = \mathsf{E}_0 e^{\frac{i\omega}{c}x\mathcal{N}} e^{-i\omega t} \tag{1.11}$$

where the *complex refractive index*

$$\mathcal{N} = \sqrt{\varepsilon} = \nu + i\kappa \tag{1.12}$$

has been introduced. The real and the imaginary part of $\mathcal{N}$ are the *refraction index* and the *extinction coefficient*, respectively, and they are related to the real ε_1 and the imaginary part ε_2 of ε, as

$$\begin{aligned} \varepsilon_1 &= \nu^2 - \kappa^2 \\ \varepsilon_2 &= 2\nu\kappa \end{aligned}$$

ν and κ being not independent, since ε_1 and ε_2 are related by the Kramers Kronig relations (see Appendix A). Eq. (1.11) becomes

$$\mathsf{E}(x,t) = \mathsf{E}_0 e^{i\frac{\omega}{c}\nu x} e^{-\frac{\omega}{c}\kappa x} e^{-i\omega t}$$

so we can define the *optical skin depth* δ as the distance where the amplitude of the field is reduced by $1/e$, and the *absorption coefficient* α as the inverse distance where the intensity[3] of the field is reduced by $1/e$:

$$\delta = \frac{c}{\omega\kappa} \tag{1.13}$$

$$\alpha = \frac{2\omega\kappa}{c} = \frac{\omega\varepsilon_2}{\nu c} \tag{1.14}$$

the latter giving a linear relation between the absorption coefficient and the imaginary part of the dielectric function. All these quantities are, in the most general case, frequency dependent.

In experiments concerning optical properties of solids often the *normal incidence reflectivity* is involved. Following Fig. 1.I, one can see an incident beam which impinges normally at the surface of a solid, with an amplitude given by E_i, and a reflected beam, with the same frequency but an amplitude $E_r < E_i$. So in the vacuum the wave is:

$$E_z = E_i e^{i\left(\frac{\omega x}{c} - \omega t\right)} + E_r e^{-i\left(\frac{\omega x}{c} + \omega t\right)} \qquad x < 0,$$

where we imagine the beam polarised along z; inside the solid, one can see the transmitted wave

$$E_z = E_t e^{i(kx - \omega t)} \qquad x > 0.$$

[2]I.e. the amplitude of the wave exponentially decays over a characteristic distance δ (see text above).
[3]The intensity of an electromagnetic field is proportional to $|\mathsf{E}(x)|^2$, i.e. $I(x) = I_0 e^{-2\frac{\omega}{c}\kappa x}$.

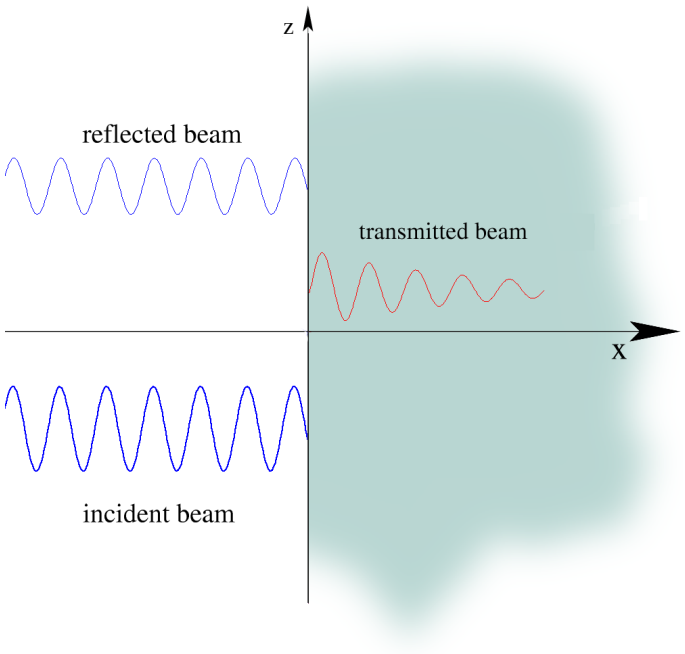

Figure 1.I: Schematic diagram of incident, reflected and transmitted electromagnetic wave at the surface.

Imposing the boundary condition to the tangential component of the electric field[4]

$$E_z(x \to 0^+) = E_z(x \to 0^-)$$

we have

$$E_i + E_r = E_t.$$

The second boundary condition has to be applied to the tangential component of the magnetic field H_y:

$$-\partial_x E_z = \frac{i\omega\mu}{c} H_y$$

$$\frac{\omega}{c}(E_i - E_r) = kE_t = \frac{\omega}{c}\mathcal{N}E_t \Rightarrow E_i - E_r = \mathcal{N}E_t.$$

We define the *normal incidence reflectivity* $\mathcal{R}$ as

$$\mathcal{R} = \left|\frac{E_r}{E_i}\right|^2 < 1$$

[4]Let $\hat{\mathbf{n}}$ be a normal (unit) vector to the surface separating the two materials. We have, for the normal components, the two relations: $(\mathsf{D}_2 - \mathsf{D}_1)\cdot\hat{\mathbf{n}} = 4\pi\rho_s$ and $(\mathsf{B}_2 - \mathsf{B}_1)\cdot\hat{\mathbf{n}} = 0$; while for the tangential components: $\hat{\mathbf{n}}\times(\mathsf{E}_2 - \mathsf{E}_1) = 0$ and $\hat{\mathbf{n}}\times(\mathsf{H}_2 - \mathsf{H}_1) = \frac{4\pi}{c}\mathbf{j}_s$, with ρ_s and $\mathbf{j}_s$ the surface density and surface current respectively [26].

which becomes

$$\mathcal{R} = \left| \frac{(1-\nu)^2 + \kappa^2}{(1+\nu)^2 + \kappa^2} \right| < 1.$$

The knowledge of the optical constants implies hence the knowledge of the reflectivity, which can be compared, e.g., with the experiment. But the opposite procedure is more interesting, because we can measure the reflectivity, and then deduce the optical constants. Since there are two optical constants involved (ν and κ), we need two reflectivity experiments or just one experiment, but in a very large frequency range, in order to exploit the Kramers-Kronig relation between ν and κ.

Another measurable quantity, useful in the description of a surface, is the *surface impedance* $\mathcal{Z}$ defined as

$$\mathcal{Z} = \frac{4\pi}{c} \frac{\mathsf{E}(0)}{\mathsf{B}(0)}$$

which can also be related to the optical refractive index $\mathcal{N}$ by $\mathcal{Z} = \frac{4\pi}{c\mathcal{N}}$.

Today, one frequently applied technique to probe the optical properties of a sample is the optical *ellipsometry*. Ellipsometry deals with measurements of polarised light undergoing oblique reflection (or transmission) from a sample surface. The quantities measured are the ellipsometric angles φ and δ related to the complex ratio of Fresnel reflection (or refraction) coefficient R_p and R_n for light polarised parallel (p-component) and normal (n-component) to the plane of incidence

$$\zeta = \frac{R_p}{R_n} = \mathrm{tg}\varphi \, e^{i\delta}$$

characterizing the different changes in amplitude and phase. Ellipsometry experiments [27–29] can be carried out at multiple frequency (spectroscopic ellipsometry) and also at different angles of incidence (variable angle spectroscopic ellipsometry, V.A.S.E). In Fig. 1.II a schematic example of reflection ellipsometry is reported. Knowing the ratio ζ and the incidence angle θ the complex dielectric function is

$$\varepsilon = \sin^2\theta + \sin^2\theta \tan^2\theta \left(\frac{1-\zeta}{1+\zeta} \right)^2 . \tag{1.15}$$

1.3 Electron Energy Loss

1.3.1 Fundamental relations

Given an external charge density $\rho_{ext}(\mathbf{r}, t)$, that we can write in Fourier space as $\rho_{ext}(\mathbf{k}, \omega)$, one can obtain the external potential $V_{ext}(\mathbf{k}, \omega)$ via the Poisson equation, where only the

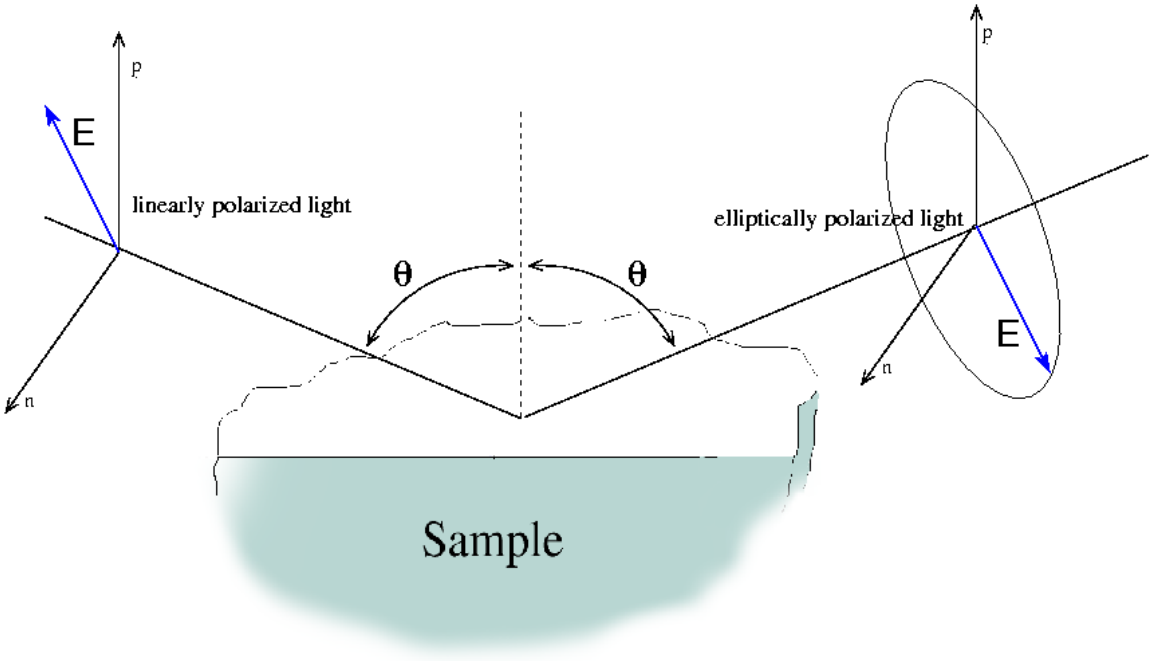

Figure 1.II: Schematic representation of a reflection ellipsometry experiment.

electrostatic nature of the charge is taken into account:

$$k^2 V_{ext}(\mathbf{k},\omega) = 4\pi\rho_{ext}(\mathbf{k},\omega). \tag{1.16}$$

There can also be an induced density $\rho_{ind}(\mathbf{k},\omega)$ as the response of the system to an external perturbation $V_{ext}(\mathbf{k},\omega)$. $\rho_{ind}(\mathbf{k},\omega)$ is linked to the external potential by the response function χ.[5] In the linear response formalism (see Appendix A),

$$\rho_{ind}(\mathbf{k},\omega) = \chi(\mathbf{k},\omega)V_{ext}(\mathbf{k},\omega). \tag{1.17}$$

The induced potential $V_{ind}(\mathbf{k},\omega)$ is then

$$k^2 V_{ind}(\mathbf{k},\omega) = 4\pi\rho_{ind}(\mathbf{k},\omega) \tag{1.18}$$

. The sum of the induced potential and the external potential constitutes the total or "effective potential" acting on the system.

$$k^2 V_{tot}(\mathbf{k},\omega) = 4\pi\left[\rho_{ind}(\mathbf{k},\omega) + \rho_{ext}(\mathbf{k},\omega)\right]. \tag{1.19}$$

[5]Eq. (1.17) is not rigorously general. If the system were not homogeneous, in fact, one should have $\rho_{ind}(\mathbf{k},\omega) = \int d\mathbf{k}'\chi(\mathbf{k},\mathbf{k}',\omega)V_{ext}(\mathbf{k}',\omega)$.

From (1.16) and (1.17), the latter is

$$k^2 V_{tot}(\mathbf{k},\omega) = 4\pi \left[\frac{k^2}{4\pi} V_{ext}(\mathbf{k},\omega) + \chi(\mathbf{k},\omega) V_{ext}(\mathbf{k},\omega) \right]$$

and

$$V_{tot}(\mathbf{k},\omega) = \left[1 + \frac{4\pi}{k^2}\chi(\mathbf{k},\omega) \right] V_{ext}(\mathbf{k},\omega) = \varepsilon^{-1}(\mathbf{k},\omega) V_{ext}(\mathbf{k},\omega)$$

where we have defined

$$V_{tot}(\mathbf{k},\omega) = \varepsilon^{-1}(\mathbf{k},\omega) V_{ext}(\mathbf{k},\omega). \tag{1.20}$$

The quantity χ is called polarizability of the system and ε is the dielectric function of the system. The relation between the external charge and the total potential acting on the system is given by

$$V_{tot}(\mathbf{k},\omega) = \frac{4\pi}{k^2}\varepsilon^{-1}(\mathbf{k},\omega)\rho_{ext}(\mathbf{k},\omega). \tag{1.21}$$

1.3.2 Energy loss by a fast charged particle

Let's specify the external perturbation ρ_{ext}. The charge density of a particle (e^-) moving with velocity $\mathbf{v}$ is

$$\rho_{ext}(\mathbf{r},t) = e\delta(\mathbf{r} - \mathbf{v}t).$$

In Fourier space it becomes

$$\begin{aligned} \rho_{ext}(\mathbf{k},\omega) &= \frac{e}{(2\pi)^4} \int d\mathbf{r} \int dt\; e^{-i\mathbf{k}\cdot\mathbf{r}}\; e^{i\omega t} \delta(\mathbf{r} - \mathbf{v}t) \\ &= \frac{e}{(2\pi)^4} \int dt\; e^{i\omega t}\; e^{-i\mathbf{k}\cdot\mathbf{v}t} = \frac{e}{(2\pi)^3}\delta(\omega - \mathbf{k}\cdot\mathbf{v}) \end{aligned} \tag{1.22}$$

where we have used the convention

$$f(\mathbf{r}) = \int d\mathbf{k}\; e^{i\mathbf{k}\cdot\mathbf{r}} \tilde{f}(\mathbf{k}) \qquad \tilde{f}(\mathbf{k}) = \frac{1}{(2\pi)^3} \int d\mathbf{r}\; e^{-i\mathbf{k}\cdot\mathbf{r}} f(\mathbf{r})$$

$$f(t) = \int d\omega\; e^{-i\omega t} \tilde{f}(\omega) \qquad \tilde{f}(\omega) = \frac{1}{2\pi} \int dt\; e^{i\omega t} f(t)$$

and the relations

$$\int d\mathbf{r} f(\mathbf{r})\delta(\mathbf{r} - \mathbf{a}) = f(\mathbf{a}) \quad ; \quad \frac{1}{2\pi}\int dt\; e^{i\omega t} = \delta(\omega).$$

From Eq.s (1.21) and (1.22) we have

$$\begin{aligned} V_{tot}(\mathbf{k},\omega) &= \frac{4\pi}{k^2}\varepsilon^{-1}(\mathbf{k},\omega)\rho_{ext}(\mathbf{k},\omega) \\ &= \frac{e}{2\pi^2 k^2}\varepsilon^{-1}(\mathbf{k},\omega)\delta(\omega - \mathbf{k}\cdot\mathbf{v}). \end{aligned} \tag{1.23}$$

Now we make the important assumption that the probe, the fast electron, could be treated classically, in order, on one hand, to justify the previous classical derivation for the induced potential (by the Poisson equation), and, then, to simply derive the total electric field E_{tot} as

$$\begin{aligned} \mathsf{E}_{tot}(\mathbf{r},t) &= -\nabla_{\mathbf{r}} V_{tot}(\mathbf{r},t) \\ \mathsf{E}_{tot}(\mathbf{k},\omega) &= -i\mathbf{k} V_{tot}(\mathbf{k},\omega) \end{aligned}$$

$$\mathsf{E}_{tot}(\mathbf{k},\omega) = -\frac{ie}{2\pi^2 k^2}\varepsilon^{-1}(\mathbf{k},\omega)\delta(\omega-\mathbf{k}\cdot\mathbf{v})\mathbf{k}. \tag{1.24}$$

The energy lost by the electron in unit time is

$$\frac{dW}{dt} = \int d\mathbf{r}\ \mathbf{j}\cdot\mathsf{E}_{tot} \tag{1.25}$$

where the current density is $\mathbf{j} = -e\mathbf{v}\delta(\mathbf{r}-\mathbf{v}t)$. In order to use Eq. (1.25), we also need Eq. (1.24) in real space

$$\mathsf{E}_{tot}(\mathbf{r},t) = \int d\mathbf{k}\int d\omega\ e^{i(\mathbf{k}\cdot\mathbf{r}-\omega t)}\mathsf{E}_{tot}(\mathbf{k},\omega)$$

so

$$\begin{aligned} \frac{dW}{dt} &= \int d\mathbf{r}\ e\mathbf{v}\delta(\mathbf{r}-\mathbf{v}t)\int d\mathbf{k}\int d\omega\ e^{i(\mathbf{k}\cdot\mathbf{r}-\omega t)}\frac{ie}{2\pi\mathbf{k}^2}\,\mathbf{k}\,\varepsilon^{-1}(\mathbf{k},\omega)\delta(\omega-\mathbf{k}\cdot\mathbf{v}) \\ &= \frac{ie^2}{2\pi}\int d\mathbf{k}\int d\omega\ \mathbf{v}\cdot\mathbf{k}\,\frac{1}{k^2}\,e^{i(\mathbf{v}\cdot\mathbf{k}-\omega)t}\varepsilon^{-1}(\mathbf{k},\omega)\delta(\omega-\mathbf{k}\cdot\mathbf{v}) \end{aligned} \tag{1.26}$$

and

$$\frac{dW}{dt} = -\frac{e^2}{\pi^2}\int\frac{d\mathbf{k}}{k^2}\,\Im\left\{\frac{\omega}{\varepsilon(\mathbf{k},\omega)}\right\} \tag{1.27}$$

which is the *electron energy loss rate per unit time*, with $\omega = \mathbf{v}\cdot\mathbf{k}$. The function $-\Im\{\varepsilon^{-1}\}$ is therefore called the loss function. In order to derive Eq. (1.27) from Eq. (1.26):

$$\begin{aligned} \int_{-\infty}^{\infty}\omega\varepsilon^{-1}(\omega)d\omega &= \int_{-\infty}^{0}\omega\varepsilon^{-1}(\omega)d\omega + \int_{0}^{\infty}\omega\varepsilon^{-1}(\omega)d\omega \\ &= -\int_{0}^{\infty}\omega\varepsilon^{-1}(-\omega)d\omega + \int_{0}^{\infty}\omega\varepsilon^{-1}(\omega)d\omega \\ &= -\int_{0}^{\infty}\omega\left[\varepsilon^{-1}(\omega)-\left(\varepsilon^{-1}\right)^{*}(\omega)\right]d\omega = \int_{0}^{\infty}\omega\,\Im\left\{\varepsilon^{-1}(\omega)\right\}\frac{1}{2i} \end{aligned}$$

where we have used $\varepsilon^{-1}(-\omega) = \left(\varepsilon^{-1}\right)^{*}(\omega)$.

1.4 Microscopic-Macroscopic connection

The Hamiltonian H_0 of a N-electrons system, when subject to an electro-magnetic perturbation, changes its kinetic term according to

$$\sum_j \frac{1}{2}\mathbf{p}_j^2 \quad \longrightarrow \quad \sum_j \frac{1}{2}\left(\mathbf{p}_j - \frac{\mathbf{A}(\mathbf{r}_j,t)}{c}\right)^2$$

where $\mathbf{p}_j - \mathbf{A}(\mathbf{r}_j,t)/c$ can be viewed as a generalized velocity $\mathbf{v}$ [30] and $\mathbf{A}$ is the vector potential of the electro-magnetic field in the Coulomb gauge ($\nabla \cdot \mathbf{A} = 0$ and scalar potential $\phi = 0$). Neglecting the non-linear effects in $\frac{1}{c}$, the perturbed Hamiltonian becomes $H = H_0 + H_1$, where the radiation perturbative field is

$$H_1 = -\frac{1}{c}\sum_j \mathbf{A}(\mathbf{r}_j,t)\cdot\mathbf{p}_j.$$

This term can be treated within the well known time-dependent perturbation theory, in order to find the transition probability (per unit time), which gives rise to the absorption of the incoming radiation:

$$P_{i\to f} = 2\pi\left|\langle f|\mathbf{A}(\mathbf{r}_j,t)\cdot\mathbf{p}_i|i\rangle\right|^2\delta(E_f - E_i - \omega)$$

where the initial and final states $|i>, |f>$ and $\{E_i\}$ are eigenfunctions and eigenvalues of the many-body Hamiltonian H_0, respectively. If now, one specifies the perturbation $\mathbf{A}$

$$\mathbf{A}(\mathbf{r},t) = A_0\hat{\mathbf{e}}e^{i(\mathbf{q}\cdot\mathbf{r}-\omega t)} + c.c.$$

with $\hat{\mathbf{e}}$ = polarisation vector and $\mathbf{q}$ = wave vector of the radiation, the transition probability becomes

$$P_{i\to f} = 2\pi\left(\frac{A_0}{c}\right)^2|\hat{\mathbf{e}}\cdot\mathbf{M}_{if}|^2\delta(E_f - E_i - \omega) \tag{1.28}$$

and $\mathbf{M}_{if} =< f|e^{i\mathbf{q}\cdot\mathbf{r}}\mathbf{p}|i >$.

The absorption coefficient is defined as the energy absorbed in the unit time in the unit volume divided by the flux of energy

$$\alpha(\omega) = \frac{\omega W(\omega)}{u(c/\nu)}$$

where c/ν is the speed of the light in the matter, the average energy density u is

$$u = \frac{\nu^2 A_0^2\omega^2}{2\pi c^2}$$

and the number of transition per unit time per unit volume $W(\omega)$ is given by the sum of (1.28) over all possible transitions. Hence $\alpha(\omega)$ becomes

$$\alpha = \frac{4\pi^2}{\nu\omega c}\sum_{i,f}|\hat{\mathbf{e}}\cdot\mathbf{M}_{if}|^2\delta(E_f - E_i - \omega).$$

In a single particle picture, and if the system is a solid, the many-body level i can be substituted by a double index $v, \mathbf{k}$, band and wave vector indices (the latter contained in the first Brillouin zone). Moreover, since the wavelength $\mathbf{q}$ of light is very small ($\sim 5\cdot 10^{-2} nm^{-1}$) the transmitted momentum can usually be neglected. Therefore we are going to consider only vertical transitions, i.e. from an occupied state $v, \mathbf{k}$ to an empty state $c, \mathbf{k}$, and, in order to better exploit the translational invariance of an infinite solid, we work in reciprocal space. We can therefore obtain the imaginary part of the complex dielectric function, ε_2, from (1.14)[6]

$$\varepsilon_2 = 2\frac{4\pi^2}{\Omega}\lim_{\mathbf{q}\to 0}\frac{1}{q^2}\sum_{v,c,\mathbf{k}}\left|\langle c\,\mathbf{k}+\mathbf{q}|e^{i\mathbf{q}\cdot\mathbf{r}}|v\,\mathbf{k}\rangle\right|^2\delta(\epsilon_{c\,\mathbf{k}+\mathbf{q}} - \epsilon_{v\,\mathbf{k}} - \omega). \tag{1.29}$$

The expression of the real part $\varepsilon_1(\omega)$ can be obtained via the Kramers-Kronig relations (see Appendix A).

The important Eq. (1.29) permits us to write a connection between the macroscopic optical constants (absorption index, refractivity, etc.) and the microscopic structure of the material, namely the band structure for a solid. More complicated relations are obtained when the single particle approximation is dropped.

1.5 Electronic Spectra

We have seen the importance of the dielectric function ε both for absorption coefficient (last paragraph) and for electron energy loss function (Par. 1.3). In particular we have seen the connection between the microscopic point of view (band structure, levels of energy, etc.) and the macroscopic one (relying on the Maxwell's equations). Eq. (1.29), for example, which is a macroscopic function, is an *average* (i.e. a spatial integral) carried on microscopic quantities like wave functions. The dielectric function is, in fact, in the most general case, a frequency (or time) dependent matrix $\varepsilon(\mathbf{r}, \mathbf{r}', \omega)$, as it stems out from (1.2), which is called *microscopic dielectric function*, and some macroscopic average has to be taken in order to obtain, e.g. an absorption spectrum. When the system to deal with is a solid, it is more convenient to write the microscopic dielectric function in Fourier space, as $\varepsilon_{\mathbf{G}\mathbf{G}'}(\mathbf{q}, \omega)$, with the wave vector $\mathbf{q}$ contained in the Brillouin zone and $\mathbf{G}$= reciprocal lattice vector. In order to make a comparison with an optical

[6]Here the relation $p_l = \lim_{q\to 0}[H, e^{iqr_l}]/q$ has been used, with $l = x, y, z$.

absorption measure, we need to define a *macroscopic dielectric function* ε_M. The connection between a microscopic and macroscopic dielectric function necessarily involves an average operation. In Eq. (1.29), this average had implicitly been taken into account as $\varepsilon'_M(\omega) \sim \lim_{\mathbf{q}\to 0} \int d\mathbf{r} d\mathbf{r}' e^{i\mathbf{q}\cdot(\mathbf{r}-\mathbf{r}')}\varepsilon(\mathbf{r},\mathbf{r}',\omega)$. However the "total" electric field E is related to the external "applied" field D, via $\mathsf{E} = \varepsilon^{-1}\mathsf{D}$, and the correct and physically meaningful average is therefore to be taken on ε^{-1}. Hence, following the works of Adler and Wiser [31, 32], the macroscopic dielectric function is given by

$$\varepsilon_M(\omega) \equiv \lim_{\mathbf{q}\to 0} \frac{1}{\left[\varepsilon^{-1}(\mathbf{q},\omega)\right]_{\mathbf{G}=\mathbf{G}'=0}}, \tag{1.30}$$

which is, in the most general case, a tensor of rank one.

The physical meanings of all these definitions will be clarified throughout the thesis; here we want only to introduce the formalism. Following Par.s (1.1) and (1.3), the imaginary part of ε_M or of $1/\varepsilon_M$ then, determine the measured absorption (Abs) and Electron Energy Loss Spectra (EELS) for vanishing momentum transfer,[7] through the quantities

$$\text{Abs} = \Im\left\{\varepsilon_M\right\} \qquad ; \qquad \text{EELS} = -\Im\left\{\frac{1}{\varepsilon_M}\right\}.$$

As pointed out above, the average implicitly used in (1.29) in order to obtain a macroscopic function is not the one defined in (1.30), but, in Fourier space,

$$\varepsilon'_M(\omega) = \lim_{\mathbf{q}\to 0} \varepsilon(\mathbf{q},\omega)_{\mathbf{G}=\mathbf{G}'=0}. \tag{1.31}$$

The important difference with (1.30) will be clarified in Chap. 6.

1.5.1 Alternative formulation for the spectra

It will be very useful in the following, to have a unified description of Absorption and EELS, at vanishing momentum transfer. To do so, first of all, we have to introduce the microscopic polarizability $\tilde{\chi}_{\mathbf{G},\mathbf{G}'}(\mathbf{q},\omega)$ which is related to the microscopic dielectric function, via (see also the first of Eq.s (1.6))

$$\varepsilon = 1 - v\tilde{\chi}. \tag{1.32}$$

In fact, when the system is not polarizable, $\tilde{\chi} = 0$ and the total field assumes the same value of the external applied field, $\mathsf{E} = \varepsilon^{-1}\mathsf{D} = \mathsf{D}$. A crucial point now is to make a more consistent comparison between the Absorption and EELS. To this purpose, we define two more microscopic functions, namely the function χ that yields $\varepsilon^{-1} = 1 + v\chi$, and the

[7] The vanishing momentum transfer is, for the electron energy loss spectroscopy, only one particular case in a wide range of possibilities. See Chap. 6 and Appendix D for further discussion.

function $\bar{\chi}$ for which $\varepsilon_M = 1 - v\bar{\chi}_{\mathbf{G}=\mathbf{G}'=0}(\mathbf{q},\omega)$. In this way both spectra can be described by a *generalized spectrum* $Z(\omega)$ where only the long range part ($\mathbf{G} = 0$) of the coulomb potential $v_0(\mathbf{q})$ appears

$$Z(\omega) \equiv -\Im\Big\{ \lim_{\mathbf{q}\to 0} v_0(\mathbf{q}) S_{\mathbf{G}=\mathbf{G}'=0}(\mathbf{q},\omega)\Big\}. \tag{1.33}$$

In this equation, the matrix S stands for the modified polarisation function $\bar{\chi}$ in the case of absorption and the microscopic response function χ for EELS. In order to find the link between $\bar{\chi}$ and $\tilde{\chi}$, we recall the analytical inversion of the microscopic dielectric function leading to ε_M (for details of the derivation, see Appendix B). χ, on the other hand, can be found by comparing its definition $\varepsilon^{-1} = 1 + v\chi$ with $\varepsilon^{-1} = (1 - v\tilde{\chi})^{-1} = 1 + v\tilde{\chi}(1 - v\tilde{\chi})^{-1}$.

One finds hence that $\bar{\chi}$ and χ are obtained by solving a Dyson-like screening equation in terms of the bare coulomb potential and the irreducible polarisation function $\tilde{\chi}$, defined in (1.32), as:

$$\begin{cases} \bar{\chi} = \tilde{\chi} + \tilde{\chi}\bar{v}\bar{\chi} \\ \chi = \tilde{\chi} + \tilde{\chi}v\chi. \end{cases} \tag{1.34}$$

Here $\bar{v}$ represents the Coulomb term without the long range component v_0

$$\bar{v} = \begin{cases} v_{\mathbf{G}} & \mathbf{G} \neq 0 \\ 0 & \mathbf{G} = 0 \end{cases} \tag{1.35}$$

and its role will be elucidated more in detail in Par. 6.1.

We have seen that if the system is not polarizable ($\tilde{\chi} = 0$), the total potential has the same value as the external potential. In case of independent particles, $\tilde{\chi}$ is approximated by a function called independent-particle polarizability χ^0. This is the Random Phase Approximation (RPA) for $\tilde{\chi}$ and it will be better defined and discussed in Chap. 3. The formula (1.29) instead describes an RPA spectrum where the macroscopic average is performed on $\varepsilon = 1 - v\chi^0$, i.e. the approximation (1.31), instead[8] of the correct average (1.30). The consequences of this will be clarified throughout the thesis.

However, in order to obtain qualitative and quantitative agreement with experiments, one often has to go beyond the independent-particle approximation for $\tilde{\chi}$, e.g. through the Bethe-Salpeter or the Time Dependent Density Functional Theory. This will be the main subject of the thesis, and will be discussed in Chap.s 3 and 4, respectively.

But first, the ground state configuration of the system has to be calculated. For crystals, a widely used method to obtain ground state properties and an approximated band structure is represented by the density functional theory, briefly described in the next chapter.

[8] This approximation is also called independent-particle Random Phase Approximation [33], for reasons we will soon discuss.

Chapter 2

Density Functional Theory

> I have yet to see any problem, however complicated, which, when you looked at it in the right way, did not become still more complicated.
>
> Poul Anderson

2.1 The many-body problem

The fundamental problem of condensed matter physics is the determination of the eigenstates of the Hamiltonian

$$H\Big(\{\mathbf{r},\mathbf{p}\};\{\mathbf{R},\mathbf{P}\}\Big) = \sum_{i=1}^{N}\frac{\mathbf{p}_i^2}{2m} + \sum_{I=1}^{M}\frac{\mathbf{P}_I^2}{2M_I} + \sum_{i<j}\frac{e^2}{|\mathbf{r}_i-\mathbf{r}_j|} - \\ - \sum_{i<j}\frac{Z_I e^2}{|\mathbf{r}_i-\mathbf{R}_I|} + \sum_{I<J}\frac{Z_I Z_J e^2}{|\mathbf{R}_I-\mathbf{R}_J|}$$

that governs the evolution of any system composed by electrons (represented by coordinates $\mathbf{r}_i$ and momenta $\mathbf{p}_i$, with mass m) and atomic nuclei (represented by coordinates $\mathbf{R}_I$ and momenta $\mathbf{P}_I$, with mass M_I and atomic number Z_I). For the huge number of interactions involved, this problem is enormously complex. It is possible, however, to introduce a hierarchy of approximations, due to the different scales of energy occurring. The first approximation allows us to separate the motion of the electrons from that of the nuclei, because electrons are so much faster than ions (three order of magnitude of difference), that they can be considered to be in their ground state for each ionic configuration. We can translate this sentence in the quantum mechanics language by the Born-Oppenheimer (also called *adiabatic*) approximation [34].

2.1.1 The Born-Oppenheimer approximation

The original eigenvalues equation

$$\left(T_e + T_I + V_{ee} + V_{Ie} + V_{II}\right) \tilde{\Psi}\left(\mathbf{r}, \mathbf{R}\right) = E_{tot} \tilde{\Psi}\left(\mathbf{r}, \mathbf{R}\right)$$

(where we have substituted all the sums in the Hamiltonian with the symbols T for kinetic energy and V for the potential energy) with $\mathbf{r} = \{\mathbf{r}_i\}$ electronic coordinates and $\mathbf{R} = \{\mathbf{R}_I\}$ ionic coordinates, can be separated in two coupled equations

$$\Big[T_e + V_{ee} + V_{Ie}\Big] \varphi_{\mathbf{R}}(\mathbf{r}) = E_{\mathbf{R}} \varphi_{\mathbf{R}}(\mathbf{r})$$

$$\Big[T_I + V_{II} + E_{\mathbf{R}}\Big] \Phi(\mathbf{R}) = E_{tot} \Phi(\mathbf{R})$$

for the two eigenfunctions $\varphi_{\mathbf{R}}(\mathbf{r})$ e $\Phi(\mathbf{R})$, for electrons and ions respectively; we observe that the ionic potential parametrically occurs in the equation for the electrons (ions considered *frozen*) and that the presence of electrons also occurs in the equation for ions via the *adiabatic* term E_R, which represents a sort of *electronic glue* for the lattice.
To obtain this separation we rewrite the Hamiltonian:

$$\begin{aligned} H = \left[-\sum_I \frac{\hbar^2}{2M_I} \cdot \frac{\partial^2}{\partial \mathbf{R}_I} + V_{II}\left(\{\mathbf{R}_I\}\right) \right] + \left[-\sum_i \frac{\hbar^2}{2m} \cdot \frac{\partial^2}{\partial \mathbf{r}_i} + \right. \\ \left. + \frac{1}{2} \sum_{i \neq j} \frac{e^2}{|\mathbf{r}_i - \mathbf{r}_j|} + V_{Ie}\left(\{\mathbf{r}_i, \mathbf{R}_I\}\right) \right] = \\ = H_I\left(\{\mathbf{R}_I\}\right) + H'\left(\{\mathbf{r}_i, \mathbf{R}_I\}\right). \end{aligned} \tag{2.1}$$

As a consequence of this partial separation of variables, we can factorize the full wave function corresponding to the equation for the Hamiltonian (2.1)

$$\tilde{\Psi}\left(\mathbf{r}, \mathbf{R}\right) \equiv \varphi\left(\mathbf{r}, \mathbf{R}\right) \Phi\left(\mathbf{R}\right) \tag{2.2}$$

with $\varphi\left(\mathbf{r}, \mathbf{R}\right)$ solution of

$$H'\left(\{\mathbf{r}_i, \mathbf{R}_I\}\right) \varphi\left(\mathbf{r}, \mathbf{R}\right) = E_{\mathbf{R}} \varphi\left(\mathbf{r}, \mathbf{R}\right) \tag{2.3}$$

i.e. the Schrödinger equation for a system of interacting electrons in the external field V_{Ie} generated by the ions frozen in the position $\{\mathbf{R}_I\}$.
If we now apply the operator (2.1) to (2.2), we obtain:

$$\begin{aligned} H\tilde{\Psi} = \varphi\left(\mathbf{r}, \mathbf{R}\right) H_I\left(\{\mathbf{R}_I\}\right) \Phi\left(\mathbf{R}\right) + \Phi\left(\mathbf{R}\right) H'\left(\{\mathbf{r}_i, \mathbf{R}_I\}\right) \varphi\left(\mathbf{r}, \mathbf{R}\right) + \\ + \sum_I \left[\frac{\partial \Phi\left(\mathbf{R}\right)}{\partial \mathbf{R}_I} \cdot \frac{\partial \varphi\left(\mathbf{r}, \mathbf{R}\right)}{\partial \mathbf{R}_I} - \frac{\hbar^2}{2M} \cdot \frac{\partial^2 \varphi\left(\mathbf{r}, \mathbf{R}\right)}{\partial \mathbf{R}_I^2} \Phi\left(\mathbf{R}\right) \right] = E_{tot} \tilde{\Psi}. \end{aligned} \tag{2.4}$$

The separation would be concluded if we could neglect the last line in Eq. (2.4). In fact, without the last line, Eq. (2.4) would lead to (2.3) for electrons and to

$$\Big[T_I + V_{II} + E_{\mathbf{R}}\Big]\Phi(\mathbf{R}) = E_{tot}\Phi(\mathbf{R}) \tag{2.5}$$

for the nuclei. Now we want to verify how (and when) we can neglect the last line of (2.4). The expectation value $\left\langle \tilde{\Psi}|H|\tilde{\Psi} \right\rangle$ using the first term of the last line of (2.4) leads to integrals such as:

$$\int d\mathbf{R}\Phi^*\left(\mathbf{R}\right)\frac{\partial\Phi\left(\mathbf{R}\right)}{\partial\mathbf{R}}\cdot\int d\mathbf{r}\varphi^*\left(\mathbf{r},\mathbf{R}\right)\frac{\partial\varphi\left(\mathbf{r},\mathbf{R}\right)}{\partial\mathbf{R}} + \text{c.c.}$$

that are proportional to

$$\int d\mathbf{r}\left(\varphi^*\left(\mathbf{r},\mathbf{R}\right)\frac{\partial\varphi\left(\mathbf{r},\mathbf{R}\right)}{\partial\mathbf{R}} + \varphi\left(\mathbf{r},\mathbf{R}\right)\frac{\partial\varphi^*\left(\mathbf{r},\mathbf{R}\right)}{\partial\mathbf{R}}\right) = \frac{\partial}{\partial\mathbf{R}}\int d\mathbf{r}\left|\varphi\right|^2 = \frac{\partial \mathrm{N}}{\partial\mathbf{R}};$$

this term is zero if the number of electrons does not change with respect to the variation of position of nuclei.[1] The conservation of N is not trivial. In metal → superconductor phase transition, for example, electrons couple themselves building Cooper couples, which are bosons; and this is exactly due to the interaction between electrons and lattice vibrations. For what concerns the second term of the last line of (2.4) we can imagine, as a first approximation, that the electrons belong to the atoms instead of being totally delocalized over the entire system. So

$$\varphi(\mathbf{r},\mathbf{R}) = \varphi(\mathbf{r}-\mathbf{R})$$

and then

$$\frac{\partial^2\varphi}{\partial\mathbf{R}^2} = \frac{\partial^2\varphi}{\partial\mathbf{r}^2}$$

In this case the expectation value is

$$\int d\mathbf{r}\varphi^*\left(\mathbf{r},\mathbf{R}\right)\left(-\frac{\hbar^2}{2M}\right)\frac{\partial^2\varphi\left(\mathbf{r},\mathbf{R}\right)}{\partial\mathbf{R}^2} =$$
$$\frac{m}{M}\int d\mathbf{r}\varphi^*\left(\mathbf{r},\mathbf{R}\right)\left(-\frac{\hbar^2}{2M}\right)\frac{\partial^2\varphi\left(\mathbf{r},\mathbf{R}\right)}{\partial\mathbf{r}^2}$$

i.e. m/M times the electronic kinetic energy, which is a negligible contribution to the total energy.

[1] If one wanted also to calculate the non-diagonal matrix elements of the many body Hamiltonian $\langle\Psi_1|H|\Psi_2\rangle$, between two different states Ψ_1, Ψ_2, another term would appear, proportional to $\varphi_1^*(\mathbf{r},\mathbf{R})\frac{\partial\varphi_2(\mathbf{r},\mathbf{R})}{\partial\mathbf{R}}$ which leads to electronic transitions induced by the ionic motion (electron-phonon interaction). However, the energy separation between two electronic states φ_1 and φ_2 is in general much larger than the energies involved in the ionic motion, so that these off-diagonal terms can be neglected [35].

A further approximation, frequently used in condensed matter theory, is to assume, not only the adiabatic separation between electrons and nuclei, but also that the motion of the ions could be treated classically, substituting Eq. (2.5) with

$$M\ddot{\mathbf{R}}_I = -\frac{\partial V_{II}}{\partial \mathbf{R}_I} - \frac{\partial E_{\mathbf{R}}}{\partial \mathbf{R}_I}.$$

This approximation is intuitively justified by the fact that the De Broglie wave length associated to nuclei is much smaller than the inter-atomic distances, but a more rigorous demonstration is given by the Hellmann-Feynman theorem [36–38].

2.1.2 The electronic problem

Even when one accepts the separation of electron and ionic degrees of freedom, one is still left with the solution of Eq. (2.3), which is still a formidable task, that requires in many cases serious approximations. An important class of approximations reduces the problem to the study of a Hamiltonian of *non interacting* particles like

$$H_0 = \sum_i H_i$$

so that the wave function of the system can be separated

$$\varphi\left(\mathbf{r}_1, \mathbf{r}_2, .., \mathbf{r}_N, t\right) = \phi_1\left(\mathbf{r}_1, t\right) \cdot \cdot \phi_N\left(\mathbf{r}_N, t\right)$$

and

$$i\hbar \frac{\partial \phi_i}{\partial t} = H_i \phi_i.$$

This reduction, of the original Hamiltonian to an independent-particle one, occurs as follows (from now on, since only the electrons will be considered explicitly, we substitute $\frac{\partial^2}{\partial \mathbf{r}_i^2} \rightarrow \nabla_i^2$). From the initial Hamiltonian

$$H = \sum_i -\frac{\hbar^2}{2m}\nabla_i^2 + V_{ext}(\mathbf{r}_i) + \frac{1}{2}\sum_{i \neq j} v_{ij}(|\mathbf{r}_i - \mathbf{r}_j|)$$

of interacting electrons subject to an external potential V_{ext}, one chooses an auxiliary one-body potential $\mathcal{V}_i$ so that

$$H = \left(\sum_i -\frac{\hbar^2}{2m}\nabla_i^2 + V_{ext}(\mathbf{r}_i) + \mathcal{V}_i\right) + \left(\frac{1}{2}\sum_{i \neq j} v_{ij}(|\mathbf{r}_i - \mathbf{r}_j|) - \mathcal{V}_i\right) = H_0 + H_{\text{res}}$$

For a convenient choice of $\mathcal{V}_i$, the term H_{res} is small and can be treated as a perturbation. It is easy to recognize in this procedure the well known mean-field approach.[2]

[2]This procedure is very important not only for electron structure problems, but for most of the many-body problems, both classical and quantistic.

In the case of electrons in their ground state, this mean-field method can be reformulated in a variational scheme: one searches for the minimum of a certain quantity (typically the total energy) expressed in terms of functions. In this category we have Hartree [39], Hartree-Fock [40] and Density Functional Theory (DFT) techniques. But while Hartree single particle solutions (later improved by Fock to take into account the correct symmetry of fermions) represent approximated solutions, the DFT [41, 42] allows us to reduce the initial problem to an *exact* non-interacting particles problem, with an evident conceptual advantage. Approximations occur later, in the determination of the exchange-correlation potential, as we will discuss later in the chapter.

2.2 The Hohenberg and Kohn theorem

Since an important part of the thesis is dedicated to the generalization of DFT to TDDFT, it is worthwhile to present the fundaments of DFT [41, 43–45] in detail, following the original formulation of Hohenberg and Kohn [41] and the more recent work of Dreizler and Gross [44].

From now on, and throughout the thesis, we will use the atomic units.[3] Thus the electron density n will coincide with the charge density ρ.

Let H be the Hamiltonian of a system of N interacting electrons:

$$H = T + W + V$$

$$T = \sum_i -\frac{1}{2}\nabla_i^2 \quad ; \quad W = \sum_i V_{ext}(\mathbf{r}_i) \quad ; \quad V = \frac{1}{2}\sum_{i\neq j} v_{ij}(|\mathbf{r}_i - \mathbf{r}_j|)$$

which represent the kinetic term, the interaction with an external field (usually represented by the nuclei potential) and electron-electron interaction respectively. The following theorem establishes exact results for the ground state of an interacting-electrons system.

Theorem of Hohenberg and Kohn

a) The ground state expectation value of any physical observable of a many-electrons system is a unique functional of the electron density $n(\mathbf{r})$

$$\langle\varphi^0|O|\varphi^0\rangle = O\big[n\big]$$

with $|\varphi^0\rangle$ many-body ground state wave function.
b) In particular the total energy defines a *universal functional* which has a minimum, the

[3] $\hbar = m = e^2 = 1 \quad ; \quad \varepsilon_0 = 1/4\pi$.

ground state energy E_0, corresponding to the ground state density n_0.

$$E_{V_{ext}}[n] = \langle\varphi|T+W+V|\varphi\rangle = \langle\varphi|T+V|\varphi\rangle + \int d\mathbf{r} V_{ext}(\mathbf{r}) n(\mathbf{r}) = \\ = F_{HK}[n] + \int d\mathbf{r} V_{ext}(\mathbf{r}) n(\mathbf{r})$$

with $F_{HK}[n] = \langle\varphi|T+V|\varphi\rangle$ universal functional[4] because it does not depend on the external potential, and

$$\min_{\varphi\in\Psi}\langle\varphi|T+W+V|\varphi\rangle = \langle\varphi^0|H|\varphi^0\rangle = \min_{n\in N} E_{V_{ext}}\big[n\big]$$

where Ψ represents the space of the ground state wave functions and N the ensemble of all electron densities.

Before giving a demonstration (close to the original) of the HK theorem, formulated for a system with a non-degenerate ground state, we want to observe that the derivation is restricted to all those densities that can be realized for some external potential; this class of densities is called v-*representable*[5] ensemble. A lot of extensions (degenerated ground state [55], N-representable functionals [44, 53], bosons [56], spin-polarised systems [57, 58], superconductors [59, 60], relativistic systems [61–63], etc.) of the theorem are available in literature.

Demonstration of the theorem

When the Schrödinger equation leads to a non-degenerated ground state for a N-electron system,

$$H|\varphi^0\rangle = E_0|\varphi^0\rangle$$

defines the relation $C : W \to \Psi$ between the ensemble W, constituted by all external potentials, and Ψ, constituted by all possible ground state wave functions. The relation C

[4]The universal functional F_{HK} can also be seen as a "free-energy HK functional" in the (functional) Legendre-transformation picture, common in thermodynamics [46]. This point of view, presented in Ref.s [47–49], is important not only for an intuitive introduction to the DFT, but also to derive some properties of F_{HK} as properties of the Legendre transformations, or to infer efficient numerical schemes for solving the DFT problem in practice [50]. Besides, this free-energy HK functional is also the classical analogue of the F_{HK} in the "classical" version [51] of the Hohenberg-Kohn-Mermin theorem [52] for finite temperature *gran-canonical ensembles*.

[5]Up to the seventies, it was known that given a density field, it is always possible to find, solving the inverse problem of the Schrödinger equation, the corresponding potential. Levy [53] showed in 1982 that there is a wider class of densities that do not correspond, in the ground state, to a *unique* external potential. This class is called *N-representable* ensemble, because it is a set of densities obtained from some antisymmetric N-particle wave function $\Psi(x_1, ..., x_N)$ (not necessarily the ground state of any Hamiltonian); this set of course contains the v-representable ensemble. For the N representability problem, see Ref. [54].

is surjective by construction.[6] At the same time we can build the ground state electronic densities by

$$n(\mathbf{r}) = \langle\varphi^0|\hat{n}(\mathbf{r})|\varphi^0\rangle$$

which defines a new relation, still surjective, $D : \Psi \to N$. If the two mappings C and D were also injective, they would be biunivocals too. This would permit us to define a full invertible relation between N and W:

$$(D \circ C) : W \to N \qquad ; \qquad (D \circ C)^{-1} : N \to W$$

and to associate to any charge density $n(\mathbf{r})$, one and only one external potential $V_{ext}(\mathbf{r})$. So, once T, V and $n(\mathbf{r})$ are known, we can determine the Hamiltonian and the expectation value of each observable in the ground state, i.e.

$$\langle\varphi^0|O|\varphi^0\rangle = O\big[n\big]$$

concluding the demonstration of the first part of the theorem.

Now we have got to show that both C and D are injective and we can do that by following a *reductio ad absurdum*. So let's assume that two different external potentials lead to the same ground state wave function:

$$\begin{aligned}(T + W_1 + V)\,|\varphi^0\rangle &= E_1^0|\varphi^0\rangle \\ (T + W_2 + V)\,|\varphi^0\rangle &= E_2^0|\varphi^0\rangle.\end{aligned}$$

Subtracting one equation from the other, we obtain $\Rightarrow \quad (W_1 - W_2)|\varphi^0\rangle = (E_1^0 - E_2^0)|\varphi^0\rangle$, which means that $W_1 = W_2 + \text{constant}$, which contradicts our initial hypothesis ($W_1 \neq W_2$). So C is injective, and also biunivocal. For what concerns D, we assume that two different ground state wave functions lead to the same ground state density. Since C is injective two different wave functions imply two different external potentials, i.e. two different Hamiltonians (T and V are given) H_1 and H_2 with:

$$H_1 = H_2 + W_1 - W_2$$

We can then write

$$\begin{aligned}\langle\varphi_1^0|H_1|\varphi_1^0\rangle &= \langle\varphi_1^0|H_2|\varphi_1^0\rangle + \langle\varphi_1^0|W_1 - W_2|\varphi_1^0\rangle \\ \langle\varphi_2^0|H_1|\varphi_2^0\rangle &= \langle\varphi_2^0|H_2|\varphi_2^0\rangle + \langle\varphi_2^0|W_1 - W_2|\varphi_2^0\rangle.\end{aligned} \tag{2.6}$$

Since $\langle\varphi_1^0|W_1 - W_2|\varphi_1^0\rangle = \int d\mathbf{r} n(\mathbf{r})(V_{ext,1} - V_{ext,2}) = \langle\varphi_2^0|W_1 - W_2|\varphi_2^0\rangle$, subtracting the first of (2.6) from the second, we have

$$\langle\varphi_1^0|H_1|\varphi_1^0\rangle - \langle\varphi_2^0|H_1|\varphi_2^0\rangle = \langle\varphi_1^0|H_2|\varphi_1^0\rangle - \langle\varphi_2^0|H_2|\varphi_2^0\rangle. \tag{2.7}$$

[6] In fact, given T and V, there is not any element of Ψ not corresponding to an element of W.

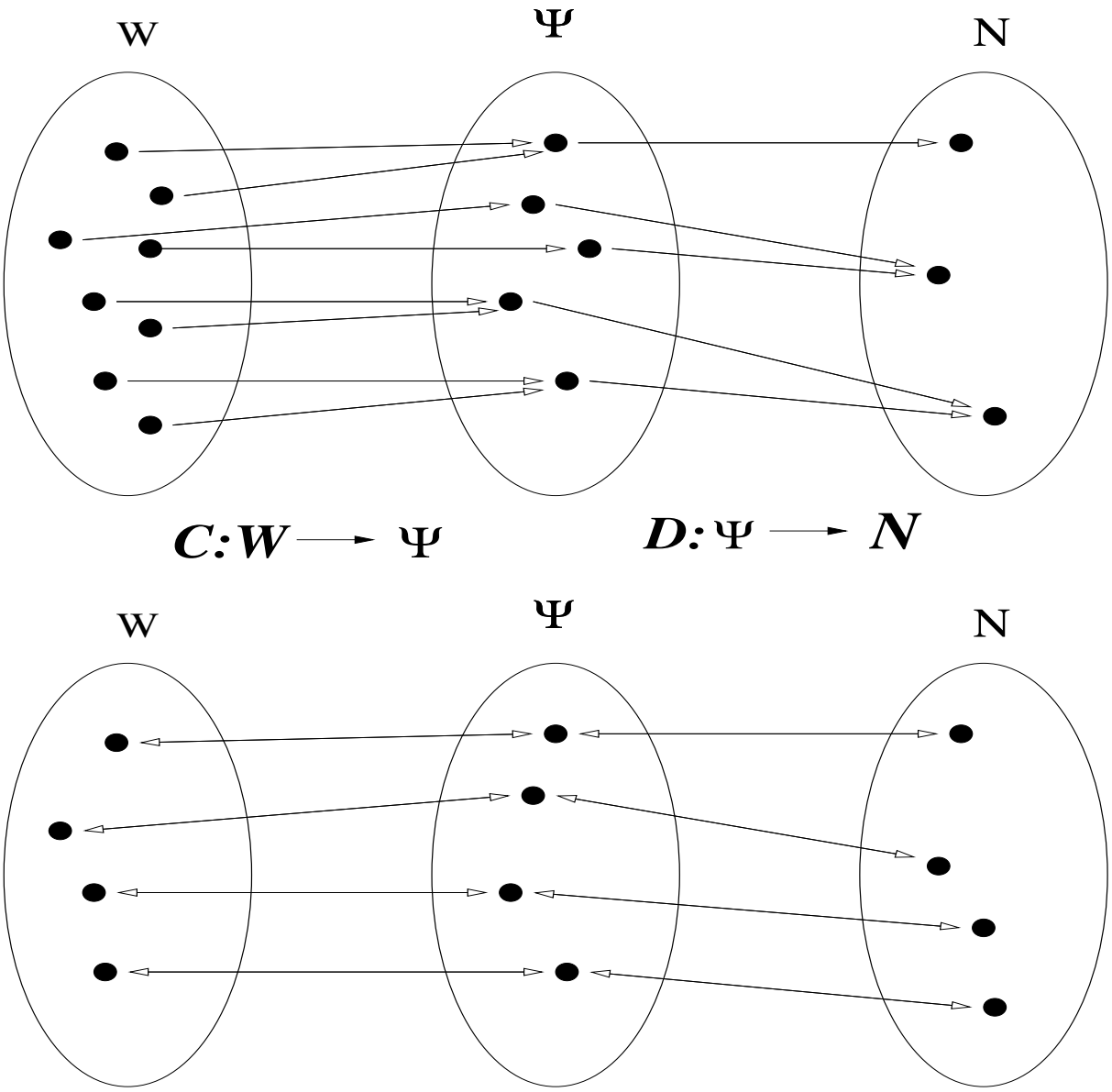

Figure 2.I: A graphical illustration of the HK theorem. One shows that the two relations are injective, so biunivocal, then fully invertible.

Now the Ritz variational principle says that

$$\begin{cases} \langle\varphi_1^0|H_1|\varphi_1^0\rangle - \langle\varphi_2^0|H_1|\varphi_2^0\rangle < 0 \\ \langle\varphi_1^0|H_2|\varphi_1^0\rangle - \langle\varphi_2^0|H_2|\varphi_2^0\rangle > 0 \end{cases} \tag{2.8}$$

because $|\varphi_1^0\rangle$ is the ground state of H_1 and $|\varphi_2^0\rangle$ is the ground state of H_2 by hypothesis. Clearly (2.7) and (2.8) are in contrast, so the function D is injective, too.

It is now easy to show the second part of the theorem. We take $O = H$ and build

$$E_{V_{ext}}[n] = \langle\varphi|H|\varphi\rangle = \langle\varphi|T + W + V|\varphi\rangle$$

which is unique. For the Ritz principle

$$\min_{\varphi\in\Psi}\langle\varphi|H|\varphi\rangle = \langle\varphi^0|H|\varphi^0\rangle = E_0$$

then

$$\min_{n\in N} E_{V_{ext}}[n] = E_0 = E_{V_{ext}}[n_0] \quad ; \quad n_0 = \langle\varphi^0|\hat{n}(\mathbf{r})|\varphi^0\rangle.$$

Observations:

- The HK theorem shows the existence of a universal functional without determining it. We should know, at least for one system, the *general solution*, i.e. for any density.
- The request of minimizing the functional of the density could be a convenient approach, from a computational point of view. However, since the functionals are not known, and in particular approximations for $T[n]$ lead to big errors, the theory has been reformulated in order to find an efficient scheme for applications, like a self-consistent scheme, similar to the Hartree or Hartree-Fock methods, which involve single particle orbitals.

In fact, the initial scepticism about the practical usefulness of DFT disappeared when Kohn and Sham introduced what would be later called the Kohn and Sham equations, and when it turned out that a very simple approximation they proposed, namely the local density approximation (see Par. 2.4), could already yield very good results.

2.3 The Kohn Sham method

Kohn and Sham [42] considered a system of non-interacting particles (without requiring any physical meaning) whose density would be the same as that of the associated interacting particle system. So, given a (real) system of N interacting electrons with Hamiltonian $H = T + W + V$, let's consider an auxiliary system of N *non-interacting* electrons with Hamiltonian $H' = T' + W'$ and the same density as the interacting system.[7,8] Here W', the KS potential, represents an effective or total (and local) potential for the single electrons and, we can anticipate, it is composed of three parts: the external potential, the

[7]We assume that the v-representable interacting density is also v-representable non-interacting.

[8]It is clear that if this system exists, it is also unique, because of the HK theorem.

Hartree potential and the so-called exchange-correlation potential. The latter is an unknown functional of the density, containing all the exchange (effects due to the fermion nature of the electrons) and correlation effects. We assume for the discussion that this auxiliary system exists (we will come back later on this point) and that the ground state is not degenerate. We have in this case the following scheme, called Kohn-Sham (KS) scheme, which permits one to accurately approximate the kinetic energy of the electrons, and to simplify the identification of simple and efficient shapes for the remaining density functional. Since

$$n(\mathbf{r}) = n'(\mathbf{r}) = \sum_{i}^{\text{occ.}} |\phi_i(\mathbf{r})|^2$$

where the ϕ_i are the single particle orbitals of the non-interacting system, we obtain the N *exact* single-particle equations (KS equations):

$$\left[-\frac{1}{2}\cdot\nabla_i^2 + V_{tot}(\mathbf{r})\right]\phi_i(\mathbf{r}) = \epsilon_i\phi_i(\mathbf{r}) \tag{2.9}$$

where

$$V_{tot}(\mathbf{r}) = V_{ext}(\mathbf{r}) + \int d\mathbf{r}' v(\mathbf{r},\mathbf{r}')n(\mathbf{r}') + V_{xc}\left([n],\mathbf{r}\right). \tag{2.10}$$

$V_{tot}(\mathbf{r})$ represents the effective single particle potential, which we mentioned above, containing all the many-body effects, and $V_H(\mathbf{r}) = \int d\mathbf{r}' v(\mathbf{r},\mathbf{r}')n(\mathbf{r}')$ is the Hartree potential. The KS scheme is obtained as follows.
The HK functional of the real system is

$$E[n] = F[n] + \int d\mathbf{r} V_{ext}(\mathbf{r})n(\mathbf{r}) \tag{2.11}$$

while that of the auxiliary system is

$$E'[n] = T'[n] + \int d\mathbf{r} V_{tot}(\mathbf{r})n(\mathbf{r}) \tag{2.12}$$

with

$$T'[n] = \sum_{i}^{\text{occ.}} \langle\phi_i| - \frac{1}{2}\nabla_i^2|\phi_i\rangle. \tag{2.13}$$

Adding and subtracting in (2.11) the quantity

$$T'[n] + \frac{1}{2}\int d\mathbf{r}\int d\mathbf{r}' v(\mathbf{r},\mathbf{r}')n(\mathbf{r})n(\mathbf{r}'),$$

the HK functional becomes

$$E[n] = T'[n] + \int d\mathbf{r} V_{ext}(\mathbf{r})n(\mathbf{r}) + \frac{1}{2}\int d\mathbf{r}\int d\mathbf{r}' v(\mathbf{r},\mathbf{r}')n(\mathbf{r})n(\mathbf{r}') + E_{xc}[n] \tag{2.14}$$

with

$$E_{xc}[n] = T[n] + V[n] - \frac{1}{2}\int d\mathbf{r}\int d\mathbf{r}' v(\mathbf{r},\mathbf{r}')n(\mathbf{r})n(\mathbf{r}') - T'[n] \tag{2.15}$$

which represents the *exchange-correlation energy*. If we impose the stationarity condition ($\delta E[n] = 0$):

$$\delta T'[n] + \int d\mathbf{r}\delta n(\mathbf{r})\left[V_{ext}(\mathbf{r}) + \int d\mathbf{r}' v(\mathbf{r},\mathbf{r}')n(\mathbf{r}') + \frac{\delta E_{xc}[n]}{\delta n(\mathbf{r})}\right] = 0,$$

and use, from (2.12)

$$\delta T'[n] = -\int d\mathbf{r} V_{tot}(\mathbf{r})\delta n(\mathbf{r}),$$

we find directly Eq. (2.10) where $\frac{\delta E_{xc}[n]}{\delta n(\mathbf{r})} = V_{xc}$ is the *exchange-correlation potential*. The central equation of the scheme is Eq. (2.14) where:

- The first term is the kinetic energy of the auxiliary system of non-interacting electrons.
- The second is the "exact" interaction energy with the external field.
- The third (with $v(\mathbf{r},\mathbf{r}') = 1/|\mathbf{r}-\mathbf{r}'|$) is the electrostatic classical energy associated to a charge distribution and it is usually called *Hartree energy*.
- The last term contains the exchange and correlation effects for the electrons. The accuracy of DFT calculations depends on the choice of the approximation for this unknown term (and hence for V_{xc}), which takes, by definition, into account all the effects beyond the Hartree theory.

Before talking about approximations for V_{xc}, let's have another look at the main point of the KS scheme: the problem of the existence of an auxiliary non-interacting-particle system associated to the interacting system. One can reformulate the request asking if it is possible to find, given a density field $n_0(\mathbf{r})$, a non-interacting representation of the system. We can observe that, if the functional derivative of $E'[n]$ is well defined in n_0, it is possible to find the minimum of the functional with the normalization condition for the number of particles (Lagrange multipliers method)

$$E'[n] - \mu\left(\int d\mathbf{r} n(\mathbf{r}) - N\right) = T'[n] + \int d\mathbf{r}\left(V_{tot}(\mathbf{r}) - \mu\right)n(\mathbf{r}) + \mu N.$$

The functional derivative at $n(\mathbf{r}) = n_0(\mathbf{r})$ leads to the Euler-Lagrange equation

$$\left.\frac{\delta T'[n]}{\delta n(\mathbf{r})}\right|_{n_0(\mathbf{r})} + V_{tot}(\mathbf{r}) - \mu = 0$$

which is satisfied by the total potential

$$V_{tot}(\mathbf{r}) = \left.\frac{\delta T'[n]}{\delta n(\mathbf{r})}\right|_{n_0(\mathbf{r})} + \mu. \tag{2.16}$$

We can conclude that a non-interacting representation of $n_0(\mathbf{r})$ exists *if* $\frac{\delta T'[n]}{\delta n(\mathbf{r})}$ is well defined in $n_0(\mathbf{r})$, and that it is given by the total potential (2.16). So the problem has moved to the study of the differentiability of $T'[n]$. It is possible to show [64, 65] that $T'[n]$ **has a well defined functional derivative for all v-representable densities**.[9] As a consequence, for these densities, the KS scheme is applicable.

2.4 Local Density Approximation (LDA)

The first and simplest approximation for the exchange-correlation energy is represented by the local density approximation (LDA) [42]. The LDA assumes that the functional dependence of E_{xc}, on the density, can be approximated by a local relation, i.e:

$$E_{xc}^{LDA}[n] \approxeq \int n(\mathbf{r})\varepsilon_{xc}^{\text{heg}}(n(\mathbf{r}))d\mathbf{r} \tag{2.17}$$

where $\varepsilon_{xc}^{\text{heg}}(n)$ is the exchange-correlation energy per electron in a homogeneous electron gas of density n. The $\varepsilon_{xc}(n)$ is known exactly in the high-density limit, and can be accurately computed at any density, using Quantum Monte Carlo simulations [66–68] (so, without free parameters). Eq. (2.17) is, by construction, exact for the homogeneous electron gas and we can expect it to work well for systems where the density has small spatial variations,[10] or where the electron-electron interaction is well-screened.
The domain of applicability of LDA has been unexpectedly found to go much beyond the nearly-free electron gas and accurate results can be obtained for inhomogeneous systems like atoms or molecules. The problem now is to understand why this simple approximation works. In order to answer this question, we can give a formally equivalent way to write the exchange-correlation energy :

$$E_{xc}[n] = \frac{1}{2}\int d\mathbf{r} n(\mathbf{r}) \int d\mathbf{r}' \frac{n_{xc}(\mathbf{r}, \mathbf{r}' - \mathbf{r})}{|\mathbf{r} - \mathbf{r}'|} \tag{2.18}$$

where $n_{xc}(\mathbf{r}, \mathbf{r}' - \mathbf{r})$ is the exchange-correlation hole that is defined in terms of the pair correlation function $g(\mathbf{r}, \mathbf{r}', \lambda)$ for a system of density $n(\mathbf{r})$ but with the reduced electron

[9] In reality the Englisch and Englisch [64, 65] demonstration regards a wider set of densities, the class of *ensemble* v-*representable*, the class of densities obtainable via a statistical treating of pure states in terms of density matrix.

[10] The adimensional quantity $\frac{\delta n}{|n|^{4/3}}$ can be taken as a measure of the *inhomogeneity* of the system.

interaction $\frac{\lambda}{|\mathbf{r}-\mathbf{r}'|}$:

$$n_{xc}(\mathbf{r}, \mathbf{r}' - \mathbf{r}) = n(\mathbf{r}') \int_0^1 [g(\mathbf{r}, \mathbf{r}', \lambda) - 1]\, d\lambda.$$

The exchange-correlation hole is normalized to -1:

$$\int n_{xc}(\mathbf{r}, \mathbf{r}' - \mathbf{r}) d\mathbf{r}' = -1, \tag{2.19}$$

i.e. the depletion in charge around the electron corresponds to exactly one unit of charge. Given the isotropic character of the Coulomb interaction, the exchange-correlation energy depends only on the spherical average of $n_{xc}(\mathbf{r}, \mathbf{r}'-\mathbf{r})$ for a given $\mathbf{r}$. In fact, if we represent the exchange-correlation hole as an expansion in spherical harmonics

$$n_{xc}(\mathbf{r}, \mathbf{r}' - \mathbf{r}) = \sum_{l=0}^{\infty} \sum_{m=-l}^{l} \rho_{lm}(\mathbf{r}, |\mathbf{r}' - \mathbf{r}|) \mathrm{Y}_l^m(\Omega)$$

we have

$$\begin{aligned} E_{xc} = & \tfrac{1}{2} \int d\mathbf{r} n(\mathbf{r}) \int_0^{\infty} dR \cdot R^2 \frac{1}{R} \cdot \sum_{l=0}^{\infty} \sum_{m=-l}^{l} \rho_{lm}(\mathbf{r}, R) \int d\Omega \cdot \mathrm{Y}_l^m(\Omega) \\ = & \tfrac{1}{2} \int d\mathbf{r} n(\mathbf{r}) \int_0^{\infty} dR \cdot R \cdot \rho_{00}(\mathbf{r}, R) \end{aligned}$$

where $|\mathbf{r} - \mathbf{r}'| = R$, and the property $\int d\Omega \cdot \mathrm{Y}_l^m(\Omega) = \delta_{l,0}\delta_{m,0}$ has been used.
It has been proved [69] that LDA satisfies the sum-rule (2.19) for the exchange-correlation hole and reproduces rather well the spherical average of the hole even if the exact hole is not so well reproduced. These results can explain why the LDA works so remarkably well.

2.5 Beyond LDA

One improvement with respect to LDA, which is very often implemented is the local spin density approximation (LSDA) [70], motivated in part by the fact that the exchange-correlation hole is very different for electrons with parallel and anti-parallel spins.

The next step is to allow ε_{xc} to depend not only on the local densities, but also on the variation of the densities, by adding gradient corrections. However, it was found that such corrections do not necessarily improve the LDA results. The reason was given to the missing fulfilling of sum rules for the exchange-correlation hole [69]. A more general

approach, the generalized gradient approximation (GGA), developed by Perdew and coworkers [71–73], was constructed to fulfill the sum rule for the exchange-correlation hole, with a consequent improvement in the results.

Recently, efforts have been done to go even beyond the GGA functionals. One possibility is to construct fully non-local density functional (examples and discussions can be found in Ref.s [74, 75] and references therein), but this goal seems quite ambitious, leading to functionals that are at present rather useless for practical purpose; a more practical way is to construct density functionals, casting additional semi-local informations (in some cases the self-interaction problem, i.e. the fact that an approximate exchange term does not correctly cancel the self-interaction of electrons in the Hartree term, can be eliminated; see Ref.s [76, 77]) like in meta-GGA [78–80] functionals. Another possibility is represented by hybrid Hartree-Fock/DFT models (based on a linear combination of HF exchange and DFT exchange-correlation contribution), the most popular implementation being represented by the so-called B3LYP [81].

2.6 Excited States in DFT

It is interesting to note that the first HK theorem implies that the ground state electronic density determines (within an additive constant) the external potential. This latter determines the Hamiltonian, so one can establish a connection between the ground state density and any excited state

$$|\phi_i\rangle = |\phi_i[n]\rangle.$$

Thus any expectation value with respect to an excited state, in particular an excited state energy, can be considered as a functional of the ground state density. So DFT can, in principle, be used to calculate excitation energies. The problem now is to find a *practical* scheme for determining the excited states.

The one-particle KS eigenvalues have been used as (quasi-)particle energies and their differences interpreted as photoemission gaps or optical excitations energies without any formal justification. In fact the KS eigenvalues enter in (2.9) as Lagrange multipliers (normalization condition) and their physical meaning is very ambiguous. The interpretation of KS eigenvalues appears to be much more complicated in DFT than that of eigenvalues in the traditional schemes of quantum chemistry. In Hartree-Fock theory, e.g., the Koopmans' theorem [82] gives a clear meaning to the eigenvalues of the HF single electron equations:

$$\epsilon_i^{HF} = E(f_1, .., f_i, .., f_n) - E(f_1, .., f_i - 1, .., f_n) \tag{2.20}$$

where ϵ_i^{HF} is a HF eigenvalue and $E(f_1, .., f_n)$ the total energy of a system of $N = f_1 + .. + f_n$ electrons.

I.e., neglecting relaxations effects[11] (conditio sine qua non), the energy required to remove an electron from the orbital i (ionization energy) is ϵ_i^{HF}, eigenvalue of the i$^{\text{th}}$ orbital of the HF solution. In DFT this correspondence between KS eigenvalues and excitation energies is not valid. However the eigenvalue of the highest occupied state, in an "exact" DFT scheme, gives the exact work function for a metal, or the ionization energy for a finite system [83, 84]. For all the other KS eigenvalues we can only write

$$\epsilon_i(f_1, .., f_n) = \frac{\partial E}{\partial f_i}$$

which means that

$$E(f_1, .., f_i, .., f_n) - E(f_1, .., f_i - 1, .., f_n) = \int_0^1 df \cdot \epsilon_i(f_1, .., f_i + f - 1, .., f_n)$$

rather different from Eq. (2.20). Although the previous observations are well known, the KS eigenvalues have been used to discuss the spectra of solids, molecules and atoms, giving rise to the well known band-gap problem. In LDA, e.g., the predicted band-gap is typically 30-50% (or even 100%) smaller than the band-gap observed in direct plus inverse photoemission experiments (Tab. 2.1).

	DFT	HF	Exp.
Ge	0.5[a]	4.3[b]	1.0[b]
C	5.6[c]	15.0[c]	7.3[c]
Si	2.6[c]	9.4[c]	3.4[c]
Ne	21.2[c]	25.1[c]	21.4[c]
Ar	8.3[c]	18.5[c]	14.3[c]
Kr	6.8[c]	16.4[c]	11.6[c]
LiF	10.0[d]	22.4[e]	14.9[d]
MgO	4.2[d]	18.0[f]	7.6[d]

Table 2.1: Comparison of calculated (DFT,HF) minimum direct band-gaps (expressed in eV) with experiment. References are the following: [a][85], [b][86], [c][87], [d][88], [e][89], [f][90].

On the contrary, the correlation (totally) missing in the Hartree-Fock theory is responsible for the large overestimation of the band-gap energy, as reported in Tab. 2.1.

2.6.1 ΔSCF

The simplest DFT scheme for the computation of electron removal energies has been the evaluation of the total energy difference between the final state (excited state) and initial state (ground state). This method is called Δ Self-Consistent-Field method (ΔSCF) . It is based on the idea that DFT should be valid for the lowest state of a given symmetry

[11] The removal of an electron from an orbital i does not imply the relaxation of the other orbitals to a new equilibrium configuration.

and a given number of electrons. So ΔSCF energies are calculated by simply performing two DFT calculations, one with the ground state and the other with an excited state configuration, taking, at the end, the energy difference. When applicable[12] this method has permitted a quite good estimation of excitation energies of atoms and molecules [91–93]. A crucial point for the success of the ΔSCF is represented by the fact that the electrons are localized, and consequently, by the Hartree relaxation effects (see Ref. [94] and discussions therein). In infinite systems, when one deals with Bloch states for the electrons, these effects are lost [95], and ΔSCF does not yield useful results.

2.7 Electronic Spectra in KS-DFT

In spite of these difficulties, a first investigation of electronic spectra, within the (static) DFT is useful, and the meaning and limits will be clarified throughout the thesis.

Once the DFT-KS band structure,[13] schematically represented in Fig. 2.II with one valence and one conduction band, has been found by solving (2.9), we can write down the KS independent-particle polarizability χ^0, (see also Appendix A) that we have firstly defined in Par. 1.5.1, as a sum over *independent transitions*

$$\chi^0 = 2\sum_{v,c} \frac{|<\phi_c|e^{i\mathbf{q}\cdot\mathbf{r}}|\phi_v>|^2}{\omega - (\epsilon_c - \epsilon_v) + i\eta} \tag{2.21}$$

with ϕ_i, ϵ_i KS eigenfunctions and eigenvalues, respectively.[14]

The connection with some measurable quantity is done via the dielectric function

$$\varepsilon = 1 - v\chi^0, \tag{2.22}$$

whose imaginary part (neglecting the subtleties of the correct macroscopic average, see previous chapter) permits one to describe the absorption spectrum

$$Abs = \Im\{\varepsilon\} = \Im\{1 - v\chi^0\} = -v\Im\{\chi^0\}, \tag{2.23}$$

and the imaginary part of the inverse ε^{-1} describes the electron energy loss spectrum (EELS)

$$EELS = -\Im\left\{\frac{1}{\varepsilon}\right\} = -v\Im\left\{\frac{\chi^0}{1 - v\chi^0}\right\}.$$

Eq. (2.23) corresponds to Eq. (1.29) (where the wavefunctions and eigenvalues have been specified as the KS ones), i.e. a Random Phase approximation of the irreducible polarizability $\tilde{\chi}$, but using the approximation (1.31) instead of (1.30) to get the macroscopic

[12] This approach is formally exact for the first ionization potential, or, more generally, for the lowest excited state of a given symmetry.

[13] Let's restrict the target of the paragraph to solids only.

[14] Any single-particle picture can be used here to find ϕ_i, ϵ_i, like, e.g., Hartree or Hartree-Fock theory.

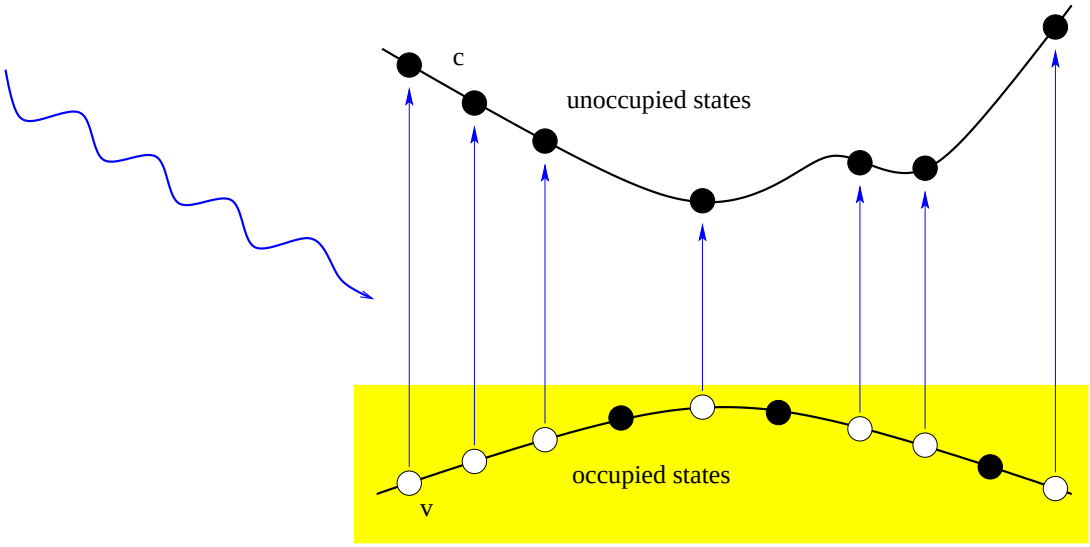

Figure 2.II: Independent transitions. The energy of the photon ω is given by the conservation of energy.

measurable quantity (optical absorption spectrum). For the absorption spectrum we have, more explicitly

$$Abs = \Im\{\varepsilon\} \propto \sum_{v,c} \left| < \phi_c | e^{i\mathbf{q}\cdot\mathbf{r}} | \phi_v > \right|^2 \delta\left(\omega - (\epsilon_c - \epsilon_v)\right) \tag{2.24}$$

which is nothing but the one-electron approximation of Fermi's golden rule (sum over all independent transitions times the delta function, representing the conservation of energy).

Despite its (low) level of sophistication, this approximation[15] can be used for a qualitative, and sometimes quantitative, description of electronic spectra. The description of EELS in graphite or silicon, are examples where this method can be in quite good agreement with the experimental results [96, 97].

However, with the exception of few cases, the one-electron KS level can not be satisfactory for the description of electronic spectra. In Fig. 2.III the absorption spectrum of bulk silicon is taken as example, showing that the application of (2.24) does not lead (continuous curve) to satisfactory results, if compared to the experiment [98] (dots). The fact to have used an average operation like (1.31) instead of the correct (1.30), to obtain the macroscopic function, is not, in this case, responsible for the missing agreement between the experimental and calculated spectra. In order to use the (1.30), we should

[15]It is also called independent-particle Random Phase Approximation [33], for reasons we will soon discuss.

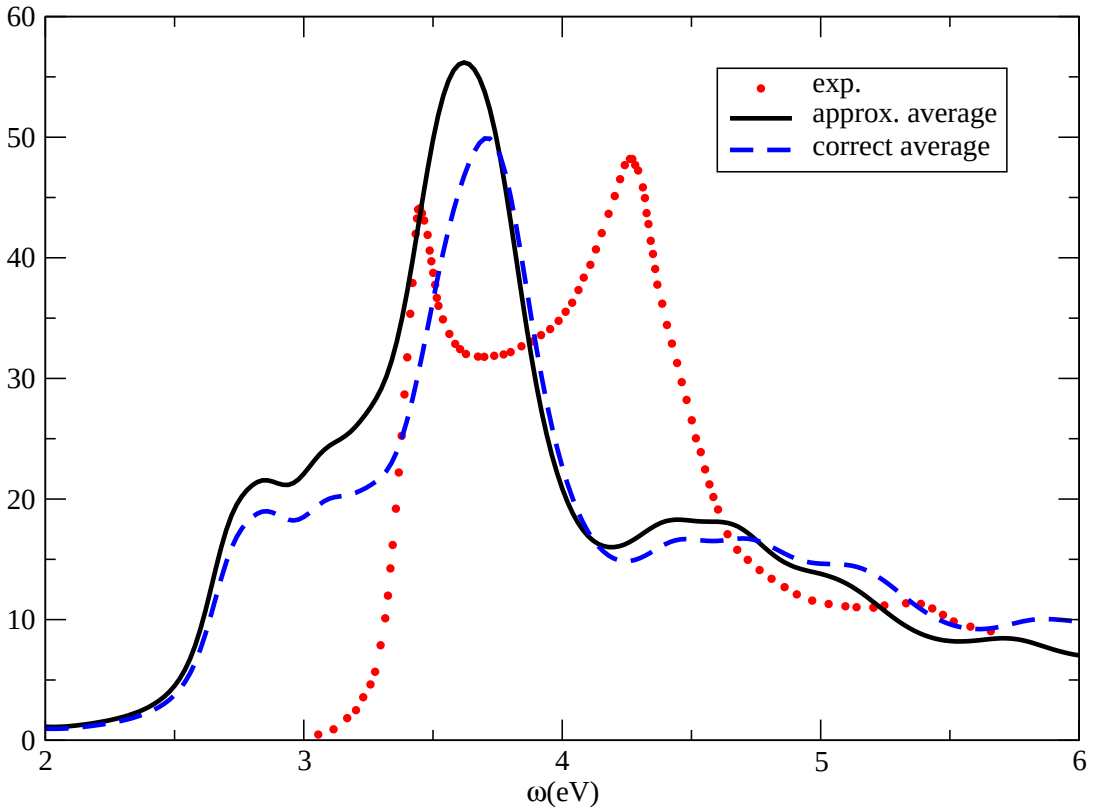

Figure 2.III: Absorption spectrum of solid silicon. Continuous line: Eq. (2.24) used. Dashed line: Eq.s (2.25) and (1.30) used.

define the KS independent-particle polarizability χ^0 as

$$\chi^0(\mathbf{G};\mathbf{G}',\omega) = 2\sum_{vc} \frac{\langle v|e^{-i\mathbf{G}\cdot\mathbf{r}}|c\rangle \langle c|e^{i\mathbf{G}'\cdot\mathbf{r}'}|v\rangle}{\omega - (\epsilon_c - \epsilon_v) + i\eta} \tag{2.25}$$

and, via $\varepsilon = 1 - v\chi^0$, have used (1.30). The difference with (2.23), however, is very small for solid silicon, as it is shown by the dashed curve in Fig. 2.III.

In order to have a more realistic description of the spectra, several aspects have to be considered and included in the theory: the aim of next chapters is to introduce more appropriate theories (Bethe-Salpeter equation and Time Dependent Density Functional Theory) for the description of electronic spectra, well beyond the Eq. (2.24), and leading to better results than that in Fig. 2.III.

2.8 DFT in solids

The crystal has become the main target system of this thesis. When dealing with solids some further details have to be specified, namely the use of periodic boundary conditions,[16] the use of a basis development for the wavefunctions, and the use of pseudo-potentials.

- A (ideal) solid is invariant under translations, so one can apply periodic boundary conditions to one unit cell and predict the properties of the whole crystal. Now the quantum numbers to deal with also include the wave vector $\mathbf{k}$, called crystal momentum.

- The one-particle wavefunctions ϕ_i have to be expanded in a basis. The simplest (and the most convenient for periodic systems) representation is given by plane waves

$$\phi_{n\mathbf{k}}(\mathbf{r}) = \frac{1}{\sqrt{\Omega_{cell}}} e^{i\mathbf{k}\cdot\mathbf{r}} \sum_{\mathbf{G}} c_{n\mathbf{k}}(\mathbf{G}) e^{i\mathbf{G}\cdot\mathbf{r}} = e^{i\mathbf{k}\cdot\mathbf{r}} u_{n\mathbf{k}}(\mathbf{r}) \tag{2.26}$$

  where $u_{n\mathbf{k}}(\mathbf{r})$ has the same periodicity as the crystal. The vector $\mathbf{k}$ lies in the first BZ, while $\mathbf{G}$ is a reciprocal lattice vector. In order for the calculation to be numerically feasible we need to truncate this expansion, one criterion being represented, for example, by the convergence of the total energy. This convergence can be achieved by gradually increasing the cutoff energy E_{cutoff}

$$\frac{1}{2}|\mathbf{k}+\mathbf{G}|^2 \leq E_{cutoff}$$

  to include more and more plane waves. The number of plane waves N_{pw} scales as $N_{pw} \propto \Omega_{cell}(E_{cutoff})^{3/2}$, with the volume of the cell Ω_{cell}, and the cutoff.

- Since the core electrons are very localized close to the nuclei, 1) they do not take part in chemical bonds; 2) the corresponding wave functions are very difficult to expand in plane waves. Thus it would be great to get rid of core electrons and represent their influence on valence electrons by an effective ("pseudo") potential, which reproduces the same valence eigenvalues and scattering properties of the atom. This is exactly the idea of the *pseudo-potential method*, largely used throughout this thesis, with the double advantage to decrease the cutoff energy (we need relatively few plane waves for valence electrons) and to deal with a reduced number of electrons (only the valence ones). Concerning the theory, we refer to the rich literature.[17]

[16] For an introductory course on solid state physics, see, e.g., Ref.s [23, 99–101].

[17] The original concepts are dated 1934 [102] and 1959 [103]. See also [104] (and references therein) for a review of the method.

2.9 Technical details of the ground state calculations in this thesis

All the ground state calculations have been performed using two plane-waves codes: the first, local code[18] (CP-LSI) has been used only for the ground state calculation of beryllium (Chap. 6), whereas the Abinit code [106] has been used for all other ground state calculations. We have used Troullier-Martins [107] pseudo-potentials[19] for silicon, carbon and argon, and Hamann pseudo-potential [109] for the beryllium. The ground state cutoffs are the following: 20 Hartrees for silicon, 30 Hartrees for silicon carbide, 30 Hartrees for argon and 25 Hartrees for beryllium. The Brillouin zone has been sampled using 256 Monkhorst-Pack [110] k-points (corresponding to 10 special k-points in the irreducible Brillouin zone) for all the systems, except the beryllium atom, for which only the Γ point (0,0,0) has been used.

[18] For details about the codes, see Ref. [105]
[19] Downloaded from [108].

Chapter 3

Green functions approach

Thinking in terms of one
Is easily done -
One room, one bed, one chair,
One person there,
Makes perfect sense; one set
Of wishes can be met,
One coffin filled.
But counting up to two
Is harder to do;
For one must be denied
Before it's tried.

Philip Larkin

The fact that an interacting system can be mapped onto a non-interacting one, easier to handle, has made the DFT approach very useful, and successfully applied to a wide range of materials, at least for what concerns ground-state properties.

However, in order to describe the electronic excited-state properties of materials, one has to go beyond the static DFT, as it is witnessed by Tab. 2.1 for the excitation energies or by Fig. 2.III for the absorption spectrum. This is the aim of the Green functions theory and of Time Dependent DFT (TDDFT). In this chapter we introduce the former, while the next chapter will be centered on TDDFT.

The Green function method has been successfully applied in the last three decades, to describe one-particle and two-particle excitations, and still represents a very powerful tool to deal with excitation energies (and today even ground-state total energy) like quasi-particle energies, absorption spectra, collective excitations.

3.1 Quasi-particle formulation

We have seen that, in the DFT-KS scheme, the response of a system of interacting electrons, of Hamiltonian

$$H = \sum_{i=1}^{N} \left[-\frac{1}{2}\nabla_i^2 + V_{ext}(\mathbf{r}_i) \right] + \sum_{i<j}^{N} \frac{1}{|\mathbf{r}_i - \mathbf{r}_j|} \tag{3.1}$$

to an external potential V_{ext} is that of independent particles responding to an "effective" potential.

A similar, though much older, idea is that the long-range, and relatively strong, Coulomb forces could screen the individual electrons, with a surrounding charge cloud of the other electrons. This leads us to the concept of *quasi-particle*,[1] i.e. an electron plus its screening cloud. Thus, the response of strongly interacting particles, can be described in terms of weakly interacting quasi-particles (Fig. 3.I). The latter interact via a screened

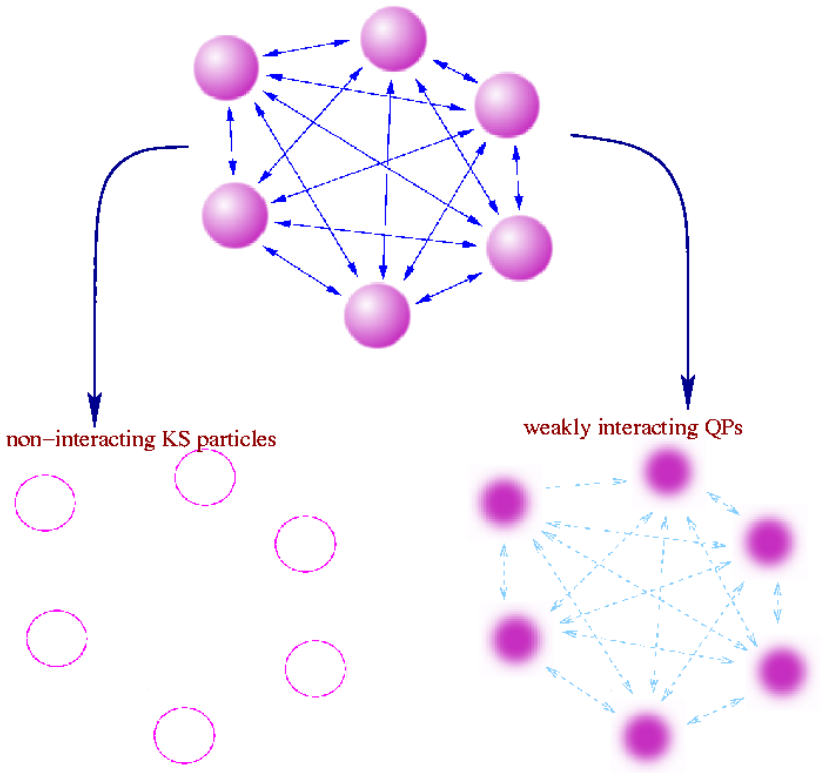

Figure 3.I: An interacting particles system can be mapped onto a non-interacting particles system (DFT-KS theory) or onto a weakly interacting particles (quasi-particles) system (Green functions).

[1] Primarily due to Landau [111–113]. See also [114, 115]

rather than the bare Coulomb potential. This scheme has also the two advantages of (1) to better represent the electrons in a many-body framework,[2] and (2) to permit one to use a perturbative expansion, with respect to the quasi-particle interaction, which has given to this approach the name "Many Body Perturbation Theory" (MBPT).[3]

Quasi-particles states are not eigenstates of the N-electrons Hamiltonian (3.1), therefore their lifetimes are not infinite. Moreover, the screening can lead to an "effective mass" different from that of the bare particle. All the differences between quasi-particles and bare particles[4] can be contained in a non-local, non-hermitian, energy-dependent operator Σ, the *self-energy*, which contains all the many-body exchange and correlation effects. In this MBPT theory, the quasi-particle energies and wavefunctions are determined by solving the Schrödinger-like equation

$$\left[-\frac{1}{2}\nabla^2 + V_{ext}(\mathbf{r}) + V_H(\mathbf{r})\right]\Psi_i(\mathbf{r},\omega) + \int d\mathbf{r}'\Sigma(\mathbf{r},\mathbf{r}',\omega)\Psi_i(\mathbf{r}',\omega) = E_i(\omega)\Psi_i(\mathbf{r},\omega) \quad (3.2)$$

for $\omega = E_i(\omega)$, called quasi-particle equation, where $V_H(\mathbf{r})$ is the Hartree potential and $V_{ext}(\mathbf{r})$ is the usual external potential (e.g. the ions potential). In a solid, the index i can represent the usual couple $\mathbf{k}, n$, wave vector and band index. One can recognize the similarity of the latter with Eq. (2.9) of the KS-DFT, to which it is led by the substitution[5]

$$\Sigma(\mathbf{r},\mathbf{r}',E_i) = V_{xc}[n](\mathbf{r})\delta(\mathbf{r}-\mathbf{r}'). \quad (3.3)$$

3.1.1 Green functions

The expectation value (on the ground state $|N\rangle$) of any single-particle operator is determined by the knowledge of the time ordered single-particle Green function [133]

$$\begin{aligned} G(1,2) &= -i\left\langle N|\mathcal{T}\left[\psi(1)\psi^\dagger(2)\right]|N\right\rangle \\ &= \begin{cases} -i\left\langle N|\psi(1)\psi^\dagger(2)|N\right\rangle & t_1 > t_2 \\ i\left\langle N|\psi^\dagger(2)\psi(1)|N\right\rangle & t_1 < t_2 \end{cases} \end{aligned} \quad (3.4)$$

[2]When the many-body interaction is switched on, talking about quasi-particles makes more sense than talking about bare particles.

[3]Technical details about MBPT can be found in [116–120], whereas interesting discussions on the breakdowns of the theory are in [121–123]. However the approach briefly mentioned in this chapter is more based on the Schwinger's functional approach [22, 118, 119, 124–132].

[4]The bare particles, as defined in the following, are however subject to the Hartree potential.

[5]Also the Hartree and Hartree-Fock equations resemble the quasi-particle equation. In particular Eq. (3.2) is seen as an extension of the Hartree-Fock, in which the self-energy Σ is the bare exchange term, whereas it is here an exchange *and correlation* term. However, while Hartree and Hartree-Fock obey Koopmans' theorem and can therefore be actually considered as approximations of Eq. (3.2), the eigenvalues of the DFT-KS are, of course, not meant to be measurable quasi-particle energies. DFT-KS (exact theory) should be therefore called a "starting point" rather than an "approximation" to (3.2).

with $\psi^\dagger$ and ψ representing the creation and annihilation field operators, and where the five coordinates $(\mathbf{r}_i, \sigma_i = \pm\frac{1}{2}, t_i)$ of the i-th electron are represented by the symbol (i). By inserting a complete set of (N-1) and (N+1) particles state in (3.4) and taking the Fourier transform in time, it can be seen that G has poles at the electron addition and removal energies. Among the observables described by single-particle operator, there are the density, the quasi-particle energies and lifetimes, or even the total energy of the system.[6] The Green function $G(1,2)$ is also called *propagator* since it describes the probability amplitude for the propagation of an electron from position $\mathbf{r}_2$ at time t_2 to the position $\mathbf{r}_1$ at time t_1. If $t_1 < t_2$, the same $G(1,2)$ describes the propagation of a hole.

The many-body Hamiltonian (3.1) becomes, in second quantization framework, $H = T + W + V$ where

$$\begin{aligned} T &= -\frac{1}{2}\int d\mathbf{r}\psi^\dagger(\mathbf{r})\nabla^2\psi(\mathbf{r}) \\ W &= \int d\mathbf{r}\psi^\dagger(\mathbf{r})V_{ext}(\mathbf{r})\psi(\mathbf{r}) \\ V &= \frac{1}{2}\int d\mathbf{r}d\mathbf{r}'\psi^\dagger(\mathbf{r})\psi^\dagger(\mathbf{r}')v(\mathbf{r}-\mathbf{r}')\psi(\mathbf{r}')\psi(\mathbf{r}). \end{aligned}$$

From the Heisenberg equation of motion for the field operator

$$i\frac{\partial\psi}{\partial t} = [\psi, H]$$

we can derive the equation of motion of the Green function

$$\left[i\frac{\partial}{\partial t_1} - H_0(1)\right]G(1,2) - \int d3\Sigma(1,3)G(3,2) = \delta(1,2) \tag{3.5}$$

with

$$H_0(1) = -\frac{1}{2}\nabla_1^2 + V_{ext}(1) + V_H(1)$$

and where the self-energy Σ has been implicitly introduced (it is related to the two-particle Green functions G_2).
It is also useful to introduce the "mass operator" M via

$$\left[i\frac{\partial}{\partial t_1} + \frac{1}{2}\nabla_1^2 - V_{ext}(1)\right]G(1,2) - \int d3M(1,3)G(3,2) = \delta(1,2), \tag{3.6}$$

which includes the whole many-body interaction (Hartree potential included).

[6] For the ground state energy, one needs to calculate the potential energy, which involves a two-particle operator. It could seem necessary to use the two-particle creation and annihilation field operators, i.e. a two-particle Green functions. However it is possible to demonstrate [133, 134] that even the potential energy (if it is restricted to two-body forces) can be written in terms of one-particle Green functions.

The condition $\Sigma = 0$ defines an equation similar to (3.5) for the non-interacting (it still contains the Hartree potential) Green function G^0

$$\left[i\frac{\partial}{\partial t_1} - H_0(1) \right] G^0(1,2) = \delta(1,2). \tag{3.7}$$

From Eq.s (3.5) and (3.7), we have

$$G(1,2) = G^0(1,2) + \int d(34) G^0(1,3)\Sigma(3,4)G(4,2) \tag{3.8}$$

which represents the Dyson [135, 136] equation for the Green function.

Spectral Function and connection with experiments

As we can see, comparing Eq.s (3.2) and (3.5), the Green function represents the formal solution (the "resolvent")[7] of Eq. (3.2). This directly leads to a spectral representation

$$G(\mathbf{r}, \mathbf{r}', \omega) = \sum_i \frac{\Psi_i(\mathbf{r}, \omega)\Psi_i^*(\mathbf{r}', \omega)}{\omega - E_i(\omega)}$$

for the Green function in the space and in frequency domain, where, of course, $\{\Psi_i, E_i\}$ are the solutions of Eq. (3.2).

The imaginary part of the Green function is called *spectral function*

$$A(\mathbf{r}, \mathbf{r}', \omega) = -\frac{1}{\pi}\Im\{G(\mathbf{r}, \mathbf{r}', \omega)\}$$

which is closely connected to direct and inverse photoemission spectra. In fact, if we look at the non-interacting Green function

$$G^0(\mathbf{r}, \mathbf{r}', \omega) = \sum_i \frac{\phi_i(\mathbf{r})\phi_i^*(\mathbf{r}')}{\omega - \epsilon_i},$$

i labelling the non-interacting states, its spectral function is a series of δ-functions at the eigenvalues of the Hamiltonian of non-interacting electrons (e.g. Hartree eigenvalues, if (3.7) is used), as schematically represented in Fig. 3.II. Now, from Dyson equation (3.8), we have for a diagonal element of the spectral function of the full Green function,

$$A(\omega) = \frac{1}{\pi}\sum_i \frac{\Im\{\Sigma(\omega)\}}{|\omega - \epsilon_i - \Re\{\Sigma(\omega)\}|^2 + |\Im\{\Sigma(\omega)\}|^2} \tag{3.9}$$

[7] Given $(z - \mathcal{L})|u >= |f >$, with $\mathcal{L}$ differential operator, the Green function is the inverse operator of the associated homogeneous equation, i.e. $G(z) = (z - \mathcal{L})^{-1}$. For the mathematical properties of the resolvent, see Ref.s [137–140].

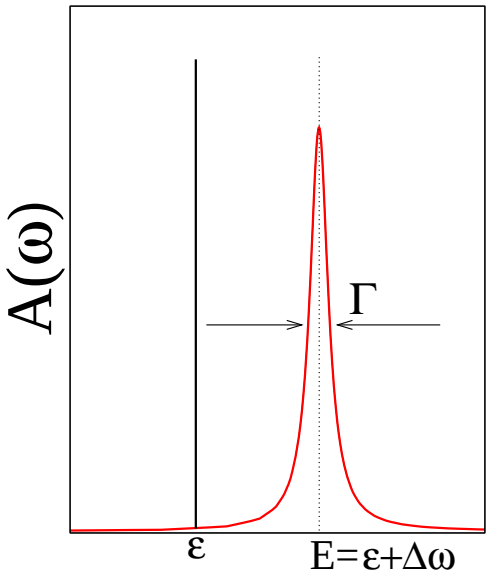

Figure 3.II: Schematic representation of the spectral function. The position of the quasi-particle peak represents the quasi-particle energy, while its width (at half maximum) is the inverse quasi-particle lifetime. On the left the independent-particle spectral function (a delta function) is shown.

using $E_i = \epsilon_i + \Re\{\Sigma\} + i\Im\{\Sigma\}$. The shape of the spectral function can be, within quasi-particle approximation,[8]

$$A(\omega) \approx \frac{\Gamma}{(\omega - \epsilon - \Delta\omega)^2 + \Gamma^2} = \frac{\Gamma}{(\omega - E)^2 + \Gamma^2}$$

as reported in Fig. 3.II. The quasi-particle position is at the excitation energy $\omega = E = \epsilon + \Delta\omega$, i.e. shifted with respect to the non-interacting eigenvalue, by a contribution $\Re\{\Sigma\}$. The width of the peak (it is no longer a delta function, as for the non-interacting case, but a Lorentzian) represents the inverse lifetime of the corresponding quasi-particle.

Experimentally, direct and inverse photoemission measurements offer a method for the approximate determination of the spectral function and hence, when the quasi-particle approximation holds, of the electronic energy levels, both occupied and empty [141]. Based on the photo-electric effect, the direct photoemission concerns a monochromatic radiation (a photon) of energy $h\nu$ that impinges on the sample. The system of electrons absorbs the energy and a photo-electron is emitted with energy E_K given by, following Fig. 3.III

$$E_K = h\nu + E_i$$

where E_i is the quasi-particle energy of the level i, calculated with respect to the vacuum level. In the inverse photoemission experiment, an electron impinging on the system can lose its energy and be captured by the system, via the emission of a photon of energy $h\nu$. The latter equation still holds. The energy levels of a molecule or the band structure

[8] If the spectral function is much different from a Lorentzian function, it is not possible to speak about quasi-particles anymore.

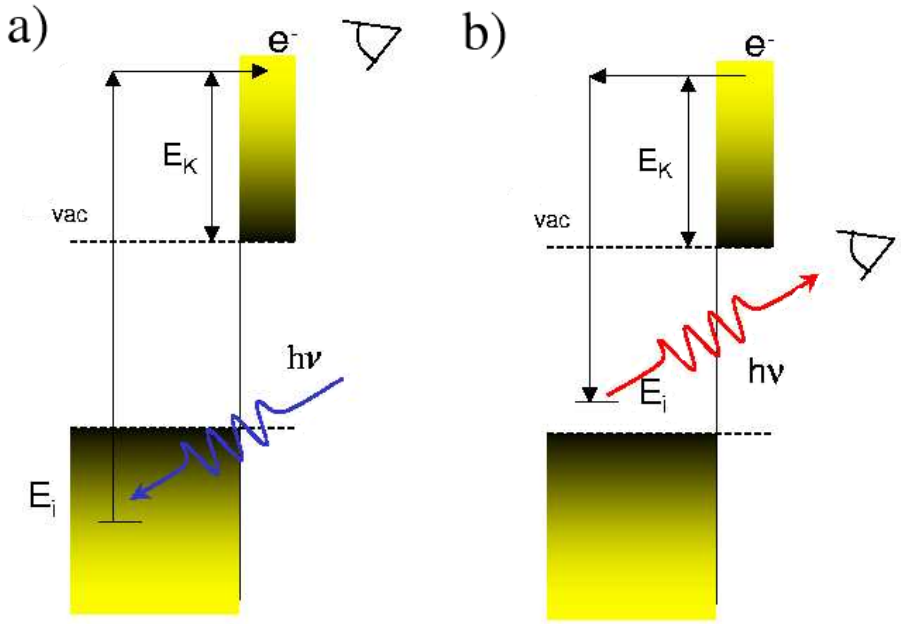

Figure 3.III: a) Direct photoemission experiment. Investigation of *occupied* quasi-particle states. b) Inverse photo-emission experiment. Investigation of *empty* quasi-particle states.

of a solid can hence be calculated by determining the eigenvalues of the quasi-particle Eq. (3.2), once an expression for the self-energy has been found.

3.1.2 Hedin's pentagon

A systematic way to approximate the self-energy Σ was proposed by Hedin in 1965 [142] and then detailed in 1969 [22]. This scheme consists of five (one is the Dyson equation (3.8) for the Green function) coupled integral equations

$$\Sigma(1,2) = i \int d(34) G(1,3) \Gamma(3,2,4) W(4,1^+) \tag{3.10}$$

$$G(1,2) = G^0(1,2) + \int d(34) G^0(1,3) \Sigma(3,4) G(4,2) \tag{3.11}$$

$$\Gamma(1,2,3) = \delta(1,2)\delta(1,3) + \int d(4567) \frac{\delta \Sigma(1,2)}{\delta G(4,5)} G(4,6) G(7,5) \Gamma(6,7,3) \tag{3.12}$$

$$W(1,2) = v(1,2) + \int d(34) v(1,3) \tilde{P}(3,4) W(4,2) \tag{3.13}$$

$$\tilde{P}(1,2) = -i \int d(34) G(1,3) G(4,1^+) \Gamma(3,4,2) \tag{3.14}$$

to be solved iteratively. Here $1^+ = (\mathbf{r}_1, \sigma_1, t_1 + \delta)$ where δ is a positive infinitesimal. The equations involve G, Σ, the *irreducible polarizability* $\tilde{P}$

$$\tilde{P}(1,2) = \frac{\delta n(1)}{\delta U(2)} = \frac{\delta n(1)}{\delta \left(V_{ext}(2) + V_H(2) \right)},$$

the screened Coulomb interaction W, the *vertex* function

$$\Gamma(1,2,3) = -\frac{\delta G^{-1}(1,2)}{\delta U(3)} = \delta(1,2)\delta(1,3) + \frac{\delta \Sigma(1,2)}{\delta U(3)},$$

and the independent-particle Green function G^0. Defined the time-ordered dielectric function as

$$\varepsilon(1,2) = \delta(1,2) - \int d3 v(1,3) \tilde{P}(3,2), \tag{3.15}$$

the screening equation (3.13) becomes $W = \varepsilon^{-1} v$, linking the screened to the bare Coulomb interaction.

In order to solve Eq.s (3.10-3.14), one possible strategy could be to start from the top of the pentagon, with $\Sigma = 0$, and obtain in the order: the Green function G (at this step the Hartree independent-particle G^0), the vertex function (only a delta function), the polarizability (at this step it is the independent-particle polarizability P^0 or Random Phase Approximation (RPA) polarizability[9]), the screening (which corresponds to the RPA screening $W^{\mathrm{RPA}} = W^0$), and the self-energy $\Sigma = iG^0W^0$ which now has been updated. In principle this process should continue until self-consistency is reached. But in practice, a full self-consistent resolution of the Hedin's equations has never been pursued.

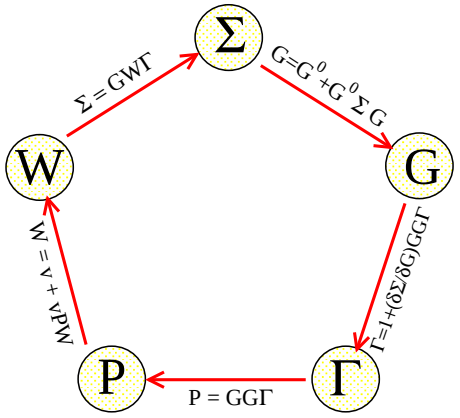

Instead, real calculations usually stop once obtained the $\Sigma = G^0W^0$ (i.e. after one round), or search for the self-consistency of a reduced set of equations, short-cutting the vertex function. These approximations are called non-self-consistent and self-consistent GW approximations (GWA), respectively.

[9] This is a definition of the Random Phase Approximation for the polarizability, i.e. the $P = -iG^0G^0$ shape. The connection with the original diagrammatic bubble expansion [114, 115], or even with linearized time dependent Hartree [143] is done via the formal use of a product of two one-particle Green functions. From now on, and throughout the thesis, the RPA polarizability will be considered of the form $P = -iG^0G^0$.

3.1.3 Real calculations and GWA

Standard GWA

The *GW* approximation (GWA) consists, hence, in short-cutting the Hedin's pentagon, avoiding the calculation of the vertex function Γ set to a delta function

$$\Gamma^{GWA}(1,2,3) = \delta(1,2)\delta(1,3).$$

In practical calculations, one needs a starting point for the independent-particle Green function G^0 that is more realistic than the Hartree one. A good choice can be represented by the solution of the KS equations.[10] Once G^0 has been obtained, the (independent-particle) polarizability P^0, the (RPA) screening W^0 and the self-energy Σ^{GW} become

$$\begin{aligned} P^0(1,2) &= -iG^0(1,2)G^0(2,1^+) \\ W^0(1,2) &= v(1,2) + \int d(34)v(1^+,3)P^0(3,4)W^0(4,2) \\ \Sigma(1,2) &= iG^0(1,2)W^0(1^+,2). \end{aligned} \tag{3.16}$$

This self-energy $\Sigma^{\mathrm{GW}} = G^0W^0$ can be used to calculate the quasi-particle energies, via the quasi-particle equation (3.2). The similarity of (2.9) and (3.2) suggests to treat the difference of the self-energy and the KS potential as a perturbation. In fact it has turned out that the quasi-particle wavefunctions and the KS-LDA ones are similar, at least for many simple bulk materials.[11] This leads, in first order, to the quasi-particle energies:

$$\underset{\Uparrow}{E_i} = \epsilon_i + \left\langle \phi_i^{\mathrm{LDA}} \right| \Sigma(\underset{\Uparrow}{E_i}) - V_{xc}^{\mathrm{LDA}} \left| \phi_i^{\mathrm{LDA}} \right\rangle$$

where the ϵ_i represent the KS eigenvalues. One can see that the quasi-particle energies appear also as argument of the self-energy. What is usually done, in this so called "*standard* GW approximation", is to expand (with Taylor) at the first order the $\Sigma(E_i)$, around ϵ_i

$$\langle \Sigma(E_i) \rangle = \langle \Sigma(\epsilon_i) \rangle + (E_i - \epsilon_i) \left\langle \left. \frac{\partial \Sigma(\omega)}{\partial \omega} \right|_{\omega=\epsilon_i} \right\rangle + O\left[(E_i - \epsilon_i)^2 \right]$$

in order to find the GW corrections (to first order) with respect to the KS energies

$$E_i - \epsilon_i = \frac{\langle \Sigma(\varepsilon_i) \rangle - \langle V_{xc} \rangle}{1 - \left\langle \left. \frac{\partial \Sigma(\omega)}{\partial \omega} \right|_{\omega=\epsilon_i} \right\rangle} = Z_i \left[\langle \Sigma(\varepsilon_i) \rangle - \langle V_{xc} \rangle \right] \tag{3.17}$$

[10] Caution: the DFT-LDA wavefunctions are eigenstates of a system of independent particles, but where exchange and correlation effects are partially (i.e. within the local density approximation) taken into account by the V_{xc}^{LDA}. While in the definition of G^0, by (3.7), all these effects ($\Sigma = 0$) are zero. So, if DFT-LDA wavefunctions are used to build the independent-particle Green function, for example the spectral function $A(\omega)$ has to be rewritten as $A(\omega) = \frac{1}{\pi} \sum_i \frac{\Im\{\Sigma(\omega)\}}{|\omega - \epsilon_i - \Re\{\Sigma(\omega) - V_i^{xc}\}|^2 + |\Im\{\Sigma(\omega)\}|^2}$, as a consequence of the fact that $G = G^0 + G^0(\Sigma - V_{xc}^{\mathrm{LDA}})G$ should replace Eq. (3.8).

[11] E.g. in silicon $\left\langle \phi^{\mathrm{LDA}} | \Psi^{\mathrm{QP}} \right\rangle > 0.999$. For details and discussions, see Ref.s [144, 145].

which also defines a renormalization factor Z_i.

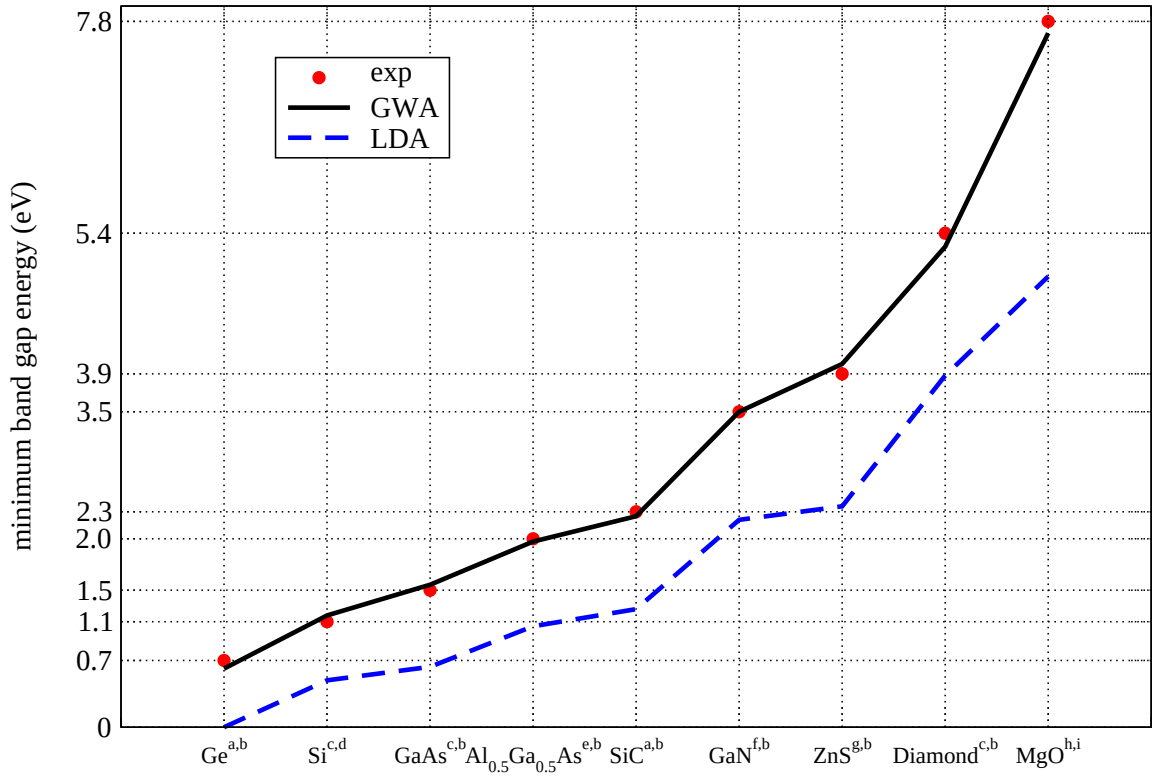

Figure 3.IV: Minimum band-gap energies for several solid materials. The references (as exponent, calculated first, experiment later) are the following: [a][146], [b][147], [c][148], [d][149], [e][150], [f][151], [g][152], [h][153], [i][154].

The standard GW approximation here described [155, 156], represents a valid tool to obtain accurate results for excitation energies [144, 145, 148, 157–159], quasi-particle band-gaps of solids, as one can see in Fig. 3.IV, and quasi-particle lifetimes [160–167]. It is therefore worthwhile to summarize the principal steps of the method:

1. DFT ground-state calculation (e.g. LDA) and construction of G^0.

2. Calculation of P^0, W^0 and Σ^{GW}, using Eq.s (3.16).

3. Calculation of the quasi-particle energies/correction using Eq. (3.17).[12]

The GW approximation in its practical implementations coincides, hence, with a first iteration of Hedin's pentagon, together with a number of choices and approximations.

[12] Or, less frequently, using [168] Eq. (3.2).

Plasmon-pole model

Another approximation that is often used concerns W. In the calculation of $W = \varepsilon^{-1}v$, the inverse dielectric function is a frequency dependent matrix. The so called *plasmon-pole model* [145, 169–171] consists in substituting the frequency dependence of the imaginary part of every element of the matrix with just a narrow Lorentzian peak, which is related to the plasmon excitations of the system, since $-\Im\{\varepsilon^{-1}\}$ is the loss function. Using the Kramers-Kronig relations, the resulting dielectric function is, then, in reciprocal space,

$$\varepsilon^{-1}_{\mathbf{G},\mathbf{G}'} = \delta_{\mathbf{G}\mathbf{G}'} + \frac{\Omega^2_{\mathbf{G}\mathbf{G}'}(\mathbf{q})}{\omega^2 - \bar{\omega}^2_{\mathbf{G}\mathbf{G}'}(\mathbf{q})}$$

where Ω and $\bar{\omega}$ are parameters giving the strength and the position of the poles, respectively. They can be obtained, for example, using the static screening and sum rules [144] or fitted to a full calculation along the imaginary energy axis (we use the latter option). The effects of this approximation have been discussed in Ref. [172]. For the results contained in this thesis, we always have made use of this approximation for all GW calculations.

Self-consistent GWA

In order to go beyond the first order expression (3.17), another possibility to calculate the quasi-particle energies but also the quasi-particle wavefunction is to perform a self-consistent resolution of the set of Eq.s (3.16) plus the Dyson equation for the Green function.

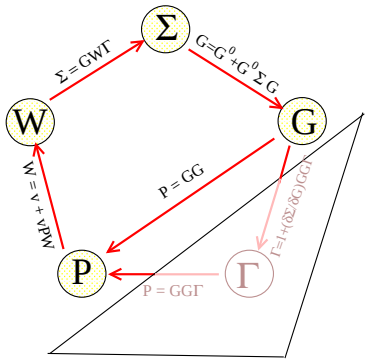

This coincides with a short-circuit of the Hedin's pentagon, as shown in the scheme, but it is of course, computationally much more cumbersome than the "standard" not self-consistent GWA.

Some examples of self-consistent GW calculations can be found in Ref.s [173, 174] for semi-conductors,[13] but, in these works, the results turned out to be worse than those of the non self-consistent calculations, at least concerning the quasi-particle energies (often the quasi-particle gap is overestimated) or the spectra. Improvements due to the self-consistency can be found, instead, for the description of total energies [178–180]. This is partially explained with the fulfilling of certain sum rules [129, 181–183] (conservation of number of particles, conservation of the total momentum) by the self-consistent GW scheme, which are instead not fulfilled by the non self-consistent GWA. Then, why does the latter work better than the self-consistent GWA

[13] Previous self-consistent GW calculations, on the homogeneous electron gas, have also been performed, see [175–177].

for the description of the quasi-particle gap? This has been attributed to the cancellation between the GW self-consistency and the vertex correction (that are both neglected in the standard GW) [173, 184, 185]. More recently, the band-gap problem in semiconductors has been revisited by Ku and Eguiluz [186], who show that an all-electron self consistent GW calculation can lead, contrary to the previous lore, to a good estimation of the quasi-particle gap and also infer about quasi-particle lifetime. However these results still have to be confirmed, especially because the inclusion of the core-electron worsens the convergence of the GW calculations [187]. Most people working in the field of GW still claim that a non-self-consistent GW calculation is a suitable approach for determining quasi-particle energies, at least in simple bulk systems. This is also the approach we have adopted in this thesis.

3.2 Response functions

In Par. (3.1.2) we have briefly introduced the polarizability $\tilde{P}$ and the dielectric function ε. In the spirit of linear response (see Appendix A) we can better clarify all these concepts.

The *reducible* response function P is defined [22] as

$$P(1,2) = \frac{\delta n(1)}{\delta V_{ext}(2)} = -i\frac{\delta G(1,1^+)}{\delta V_{ext}(2)} \tag{3.18}$$

and represents the variation of the induced density upon a variation of the external field V_{ext}. The *irreducible* polarizability $\tilde{P}$ is, instead, defined as

$$\tilde{P}(1,2) = \frac{\delta n(1)}{\delta U(2)} = -i\frac{\delta G(1,1^+)}{\delta \left[V_{ext}(2) + V_H(2)\right]} \tag{3.19}$$

i.e. the variation of the induced density with respect to a variation of a (classical) total potential, here given by the external plus the Hartree potential. The inverse dielectric function ε^{-1} is

$$\begin{aligned} \varepsilon^{-1}(1,2) = \frac{\delta U(1)}{\delta V_{ext}(2)} = \delta(1,2) + \int d3v(1,3)\frac{\delta n(3)}{\delta V_{ext}(2)} = \\ = \delta(1,2) + \int d3v(1,3)P(3,2) \end{aligned} \tag{3.20}$$

and it is also related to the polarizability $\tilde{P}$ via Eq. (3.15). Eq.s (3.20) and (3.15) are very important equations because of their role to connect the dielectric function (that is, in its retarded version, related to macroscopic measurable quantities, see Chap. 1) with the polarizability $\tilde{P}$, ingredient of Hedin's equations. The relation between P and $\tilde{P}$ is given by the retarded version of Eq.s (1.34). Putting, in fact, the second of (1.34) into

(3.20) we have

$$\begin{aligned}\varepsilon^{-1} &= 1 + v\left(1-\tilde{P}v\right)^{-1}\tilde{P} = 1 + \left(v^{-1}-\tilde{P}\right)^{-1}\tilde{P} = \\ &= 1 + \left(1-v\tilde{P}\right)^{-1}v\tilde{P} = \left(1-v\tilde{P}\right)^{-1}\left(1-v\tilde{P}\right) + \left(1-v\tilde{P}\right)^{-1}v\tilde{P} = \\ &= \left(1-v\tilde{P}\right)^{-1}\left(1-v\tilde{P}+v\tilde{P}+\right) = \left(1-v\tilde{P}\right)^{-1}\end{aligned}$$

and then (3.15).

As mentioned above, we should remember that all the quantities we have defined up to now are time ordered. To make a direct comparison with the retarded functions of the linear response theory we have the relations

$$\begin{aligned}\Re\left\{\chi_R(\omega)\right\} &= \Re\left\{P_T(\omega)\right\} \\ \Im\left\{\chi_R(\omega)\right\} &= \mathrm{sign}(\omega)\,\Im\left\{P_T(\omega)\right\}\end{aligned} \tag{3.21}$$

where the suffixes $\square_T$ and $\square_R$ stand for time-ordered and retarded, respectively. As one can see, if only the $\omega > 0$ part of the response function is considered, the retarded and time ordered response functions have the same value.

Spectra in GWA

We have seen in Fig. 3.IV that the standard GWA scheme led to important improvements concerning the band-gap energies of a large variety of semi-conductors and insulators. One could think to use the same level of approximation to infer even on neutral excitations spectra, like the absorption spectrum.
The substitution of DFT (e.g. LDA) eigenvalues with the quasi-particle energies E_i into (2.25) directly leads to the "GW-RPA polarizability"

$$\chi^0_{GW}(\mathbf{G};\mathbf{G}',\omega) = 2\sum_{i,j}\frac{\left\langle\phi_i|e^{-i\mathbf{G}\cdot\mathbf{r}}|\phi_j\right\rangle\left\langle\phi_j|e^{i\mathbf{G}'\cdot\mathbf{r}'}|\phi_i\right\rangle}{\omega-(E_j-E_i)+i\eta}. \tag{3.22}$$

In spite of the improvements achieved by the GWA, concerning the energy levels and photoemission spectra, the use of (3.22) for neutral excitations spectra often leads to poor results. In Ref.s [33, 188] some examples concerning semiconductors are reported. Generally the calculated spectrum shows a blue-shift with respect to the RPA one (also with respect to experiment), and the line-shape is not systematically improved. An example, the absorption spectrum of solid silicon, is shown in Fig. 3.V, where the GW-RPA curve has been added to the previous Fig. 2.III. This failure can be easily explained: in GWA, self-consistent or not, we describe excitations that change the number of particle of the system, adding or removing an electron (or a hole). This also explains the good results

for the description of energy levels, quasi-particle gaps, photoemission spectra. But absorption, reflectivity or fluorescence spectroscopies involve neutral excitations, with the number of electrons of the system which remains constant. An absorption experiment for example, removes an electron from an occupied level, leaving a hole, putting it in an empty level, of higher energy, thus describing a two-particle excitation. The GWA

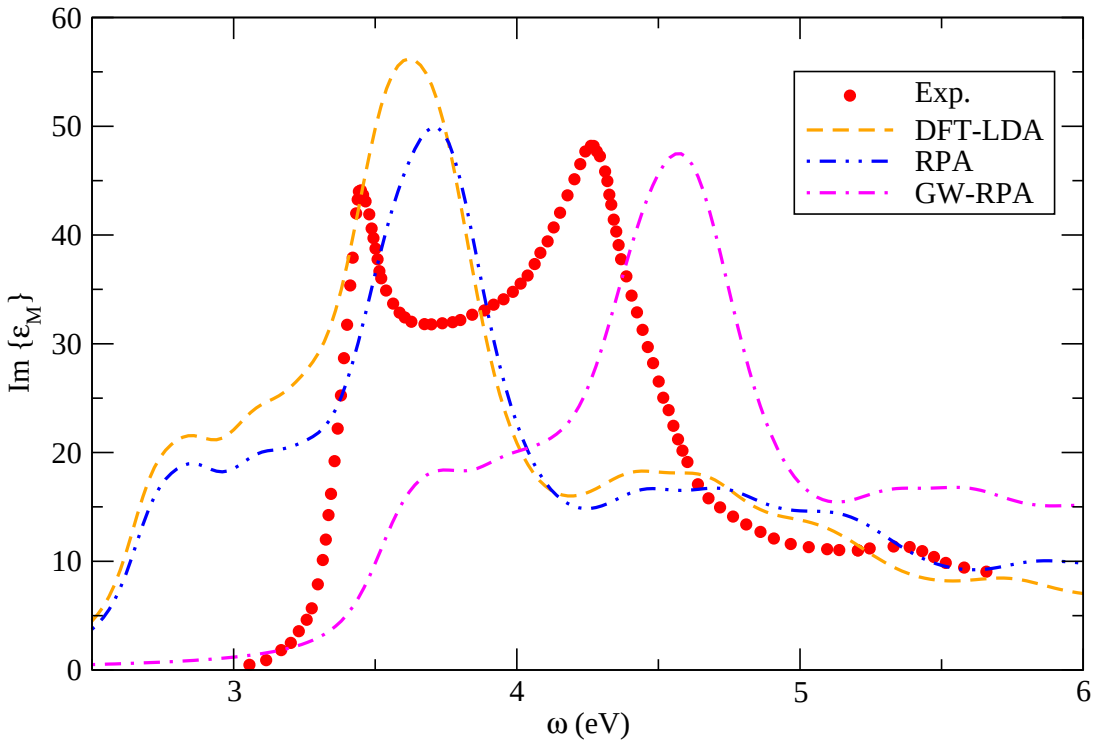

Figure 3.V: Absorption Spectrum of solid silicon. DFT-LDA, RPA and GW-RPA results compared to the experiment [189].

cannot properly describe this mechanism because of its definition of the polarizability (3.16), which excludes any possible interaction between the electron (whose propagation is described by $G(1,2)$) and the hole (described by $G(2,1^+)$). The inclusion of the vertex function $\Gamma(1,2,3)$ as follows from Hedin's equations (3.13), is then crucial for the description of two-particle excitations.

This is the aim (and the success) of the Bethe-Salpeter[14] equation (BSE).

[14]The original work can be found in Ref. [190].

3.3 Bethe-Salpeter Equation

Processes involving two-particle excitations are normally described (implicitly or explicitly) via a two-particle Green function

$$G(1,2,3,4) = (-i)^2 \left\langle N \left| T\left[\psi(1)\psi(3)\psi^\dagger(4)\psi^\dagger(2)\right] \right| N \right\rangle .$$

We can now introduce a 4-point (*reducible*) polarizability L

$$L(1,2,3,4) = L^0(1,2,3,4) - G(1,2,3,4)$$

where the independent-electron-hole polarizability

$$L^0(1,2,3,4) = iG(1,3)G(4,2)$$

describes the propagation of a hole and an electron separately.
The function L (and $\bar{L}$ defined in analogy to (1.34)) also satisfies a Dyson equation, known as *Bethe-Salpeter equation* (BSE)

$$\begin{aligned} L(1,2,3,4) &= L^0(1,2,3,4) + \int d(5678)\, L^0(1,2,5,6)K(5,6,7,8)L(7,8,3,4) \\ \bar{L}(1,2,3,4) &= L^0(1,2,3,4) + \int d(5678)\, L^0(1,2,5,6)\bar{K}(5,6,7,8)\bar{L}(7,8,3,4) \end{aligned} \tag{3.23}$$

where the kernels K and $\bar{K}$ are

$$\begin{aligned} K(5,6,7,8) &= \delta(5,6)\delta(7,8)v(5,7) + i\Xi(5,6,7,8) \\ \bar{K}(5,6,7,8) &= \delta(5,6)\delta(7,8)\bar{v}(5,7) + i\Xi(5,6,7,8) \end{aligned} \tag{3.24}$$

and Ξ is defined as

$$\Xi(1,2,3,4) = \frac{\delta\Sigma(1,3)}{\delta G(2,4)}.$$

The connection with the irreducible polarizability passes through the 4-point extension of (1.34) (having defined the 4-point extension of the Coulomb potential $v(1,2,3,4) = \delta(1,2)\delta(3,4)v(1,3)$)

$$\begin{aligned} \bar{L}(1,2,3,4) &= \tilde{L}(1,2,3,4) + \int d(5678)\, \tilde{L}(1,2,3,4)\bar{v}(5,6,7,8)\bar{L}(7,8,3,4) \\ L(1,2,3,4) &= \tilde{L}(1,2,3,4) + \int d(5678)\, \tilde{L}(1,2,3,4)v(5,6,7,8)L(7,8,3,4), \end{aligned} \tag{3.25}$$

which, combined with

$$\tilde{L}(1,2,3,4) = L^0(1,2,3,4) + i\int d(5678)\, L^0(1,2,5,6)\Xi(5,6,7,8)\tilde{L}(7,8,3,4) \tag{3.26}$$

give (3.23).[15]

In order to calculate the absorption spectrum, we need a two-point contraction of the resulting polarizability, and the limit of vanishing momentum transfer to obtain the macroscopic dielectric function

$$\varepsilon_M(\omega) = 1 - \lim_{\mathbf{q}\to 0} v(\mathbf{q}) \int d\mathbf{r} d\mathbf{r}' \, e^{i\mathbf{q}\cdot(\mathbf{r}-\mathbf{r}')} \bar{L}(\mathbf{r}, \mathbf{r}, \mathbf{r}', \mathbf{r}', \omega) \tag{3.27}$$

whose imaginary part gives the absorption spectrum. The electron energy loss spectrum for vanishing momentum transfer is instead given, if in the latter, $\bar{L}$ is substituted by L.

As stated in (3.24), the kernel K is composed of two terms: the 4-point Coulomb interaction, also called *electron-hole exchange*,[16] and the variation of the self-energy upon the variation of the Green function. Let's now specify a shape for the self-energy, taking e.g. the GWA self-energy $\Sigma = iG(1,2)W(2,1)$. This directly leads to

$$K(1,2,3,4) = \delta(1,2)\delta(3,4)\bar{v}(1,3) - \delta(1,3)\delta(2,4)W(1,2) \tag{3.28}$$

where in the derivation of the self-energy we have omitted the term $iG(1,2)\frac{\delta W(1,2)}{\delta G(3,4)}$, i.e. the variation of the screening due to the excitation.[17]

Intrinsic two-particle character of the BSE

If W were zero in (3.28), only the Coulomb term would appear in (3.24) and then in (3.23), i.e. it would be possible to find a two-point representation of the the formula contracting the indices. But, because of the presence of Ξ, the BSE can be never written in a 2-point framework (in (3.28), the arguments of the delta functions multiplying $W(1,2)$ prevents any contraction of indices), even if the GWA is used for the self-energy. This demonstrates the intrinsic two-particle character of the BSE.

3.3.1 Effective two-particle equations

The four time variables, implicitly contained in a 4-point polarizability, can be reduced to just one, considering the propagation and the interaction of the two particles, the electron and the hole, as simultaneous and instantaneous,[18] and considering the translational

[15] The relation between (3.26) and the 2-point polarizability occurring in Hedin's equations can be obtained multiplying (3.12) by a pair of Green functions $-GG$, and using (3.14). This operation gives a 4-point polarizability ${}^4\tilde{P}$, related to $\tilde{L}$ via $\tilde{L} = -{}^4\tilde{P}$.

[16] In spite of the name, whose meaning will be clarified in Par. 6.1, this term is related to the Hartree potential, and not to Fock exchange.

[17] This term is supposed to be small [191–193].

[18] This corresponds to $(t_2 = t_1^+ \, ; t_4 = t_3^+)$ and $W(1,2) = W(\mathbf{r}_1, \mathbf{r}_2)\delta(t_1 - t_2)$.

invariance in time. Thus, thanks to a Fourier transform, we have

$$\begin{aligned} L(1,2,3,4) &\longrightarrow L(1,2,3,4|\omega) \\ \bar{L}(1,2,3,4) &\longrightarrow \bar{L}(1,2,3,4|\omega) \end{aligned}$$

where i only indicates (from now on) the spatial and spin variables, but not the time anymore. This is also the function $\bar{L}$ occurring in Eq. (3.27) For simplicity, the frequency-dependence will not be specified, if not necessary. Given the Eq. (3.23) for the $\bar{L}$ (or L in case of EELS), one needs to invert a 4-point function, at each frequency, which is a very demanding task.

It is possible to exploit the two-particle nature of the BSE, mapping the problem onto an effective two-particle equation, where the basis set is represented by pairs of single-particle ϕ's, i.e. by transitions, trusting that only a small number of transitions will contribute to the description of each part of the spectrum. In this paragraph we have essentially followed the scheme described in Ref. [194, 195].

The first step is to change basis and define the polarizability in the transition space, via

$$L_{(n_1n_2)(n_3n_4)} = \int d\mathbf{r}_1 d\mathbf{r}_2 d\mathbf{r}_3 d\mathbf{r}_4 L(1,2,3,4)\phi_{n_1}(\mathbf{r}_1)\phi^*_{n_2}(\mathbf{r}_2)\phi^*_{n_3}(\mathbf{r}_3)\phi_{n_4}(\mathbf{r}_4) \tag{3.29}$$

where the index n now includes the band and wave vector index. Eq. (3.23) becomes

$$\bar{L}_{(n_1n_2)(n_3n_4)} = L^0_{(n_1n_2)(n_3n_4)} + L^0_{(n_1n_2)(n_5n_6)} K_{(n_5n_6)(n_7n_8)} \bar{L}_{(n_7n_8)(n_3n_4)} \tag{3.30}$$

with a diagonal expression for L^0, if the ϕ's are the KS wavefunctions[19] used to construct L^0,

$$L^0_{(n_1n_2)(n_3n_4)} = \frac{(f_{n_2} - f_{n_1})\,\delta_{n_1,n_3}\delta_{n_2,n_4}}{E_{n_2} - E_{n_1} - \omega - i\eta}.$$

Eq. (3.30) can be formally solved giving

$$L_{(n_1n_2)(n_3n_4)} = \left[\frac{1}{1 - L^0 K}\right] L^0 = \Pi L^0 \tag{3.31}$$

with

$$\begin{aligned} \Pi_{(n_1n_2)(n_3n_4)} = [&(E_{m_2} - E_{m_1} - \omega)\,\delta_{m_1,m_3}\delta_{m_2,m_4} \times \\ &\times (f_{m_1} - f_{m_2})\,K_{(m_1m_2)(m_3m_4)}]^{-1}_{(n_1n_2)(n_3n_4)}\,(E_{m_2} - E_{m_1} - \omega)\,, \end{aligned}$$

[19] In reality, the $\{\phi\}$ can be any complete set of eigenfunctions and we chose it such that the function $L^0_{(n_1n_2)(n_3n_4)}$ is diagonal.

having used

$$\left[\delta_{ij} - \frac{1}{b_i} a_{ij}\right]^{-1}_{\alpha\beta} = \left[\frac{1}{b_i}\left(b_i\delta_{ij} - a_{ij}\right)\right]^{-1}_{\alpha\beta} = \left(b_i\delta_{ij} - a_{ij}\right)^{-1}_{\alpha\beta} b_\beta.$$

We can define the two-particle Hamiltonian or *excitonic* Hamiltonian

$$H^{2p}_{(n_1n_2)(n_3n_4)} = \left(E_{n_2} - E_{n_1}\right)\delta_{n_1,n_3}\delta_{n_2,n_4} + \left(f_{n_1} - f_{n_2}\right) K_{(n_1n_2)(n_3n_4)} \tag{3.32}$$

which permits one to rewrite Eq. (3.31) as

$$\bar{L}_{(n_1n_2)(n_3n_4)} = \left[H^{2p} - I\ \omega\right]^{-1}_{(n_1n_2)(n_3n_4)} \left(f_{n_3} - f_{n_4}\right). \tag{3.33}$$

The structure of the excitonic Hamiltonian is quite complicated; it is schematically represented by a triangular block matrix

$$H^{2p}_{(n_1n_2)(n_3n_4)} = \begin{pmatrix} A & B \\ 0 & D \end{pmatrix}$$

or, specifying A,B and D,

$$H^{2p}_{(n_1n_2)(n_3n_4)} = \left(\begin{array}{c|cccc} {\scriptstyle (n_3n_4)\rightarrow \atop (n_1n_2)\downarrow} & \{v'c'\} & \{c'v'\} & \{v'\tilde{v}'\} & \{c'\tilde{c}'\} \\ \hline \{vc\} & H^{2p,reso}_{(vc)(v'c')} & K_{(vc)(c'v')} & K_{(vc)(v'\tilde{v}')} & K_{(vc)(c'\tilde{c}')} \\ \{cv\} & -[K_{(vc)(v'c')}]^* & -[H^{2p,reso}_{(cv)(c'v')}]^* & -K_{(cv)(v'\tilde{v}')} & -K_{(cv)(c'\tilde{c}')} \\ \{v\tilde{v}\} & 0 & 0 & (E_{\tilde{v}} - E_v)\delta_{vv'}\delta_{\tilde{v}\tilde{v}'} & 0 \\ \{c\tilde{c}\} & 0 & 0 & 0 & (E_{\tilde{c}} - E_c)\delta_{cc'}\delta_{\tilde{c}\tilde{c}'} \end{array}\right).$$

Here, we have omitted the index $\mathbf{k}$, associated to each vertical transition $v\mathbf{k} \rightarrow c\mathbf{k}$. The occupied KS states are indicated by the indices $v, v', \tilde{v}, \tilde{v}'$, while the empty states by $c, c', \tilde{c}, \tilde{c}'$. The presence of the factor $(f_{n_4} - f_{n_3})$ in (3.33) means that only the $\{n_3, n_4\} = \{v', c'\}$ or $\{n_3, n_4\} = \{c', v'\}$ components of the inverse matrix M^{-1}

$$\mathsf{M}^{-1}_{(n_1n_2)(n_3n_4)} = \left[H^{2p} - I\omega\right]^{-1}_{(n_1n_2)(n_3n_4)}$$

will contribute, i.e. only the first column of M.[20] Thus, since we are interested only in $[A - I\omega]$, we reduce the two-particle Hamiltonian only to the interesting part, defining the $H^{2p,exc}$

$$H^{2p,exc} = \begin{pmatrix} H^{2p,reso}_{(vc)(v'c')} & K^{coupling}_{(vc)(c'v')} \\ -\left[K^{coupling}_{(vc)(c'v')}\right]^* & -\left[H^{2p,reso}_{(vc)(v'c')}\right]^* \end{pmatrix} \tag{3.34}$$

[20] Because $\mathsf{M} = [H^{2p} - I\omega]$ is a upper triangular block matrix.

where the matrix $H^{2p,reso}$ only involve positive frequency transitions, and it is called *resonant term*

$$H^{2p,reso}_{(vc)(v'c')} = (E_c - E_v)\,\delta_{v,v'}\delta_{c,c'} + K_{(vc)(v'c')}. \tag{3.35}$$

One can see that if all the lifetime effects are neglected, the $H^{2p,reso}$ is a Hermitian matrix. The fourth term, involving negative frequency transitions is called *anti-resonant term*, while the out of diagonal blocks mix positive and negative frequency transitions, so they are called *coupling terms*.

We have not yet solved the problem of inverting a matrix at each frequency. For this purpose, let us define the important spectral representation of the inverse excitonic Hamiltonian

$$\left[H^{2p,exc} - I\omega\right]^{-1}_{(n_1n_2)(n_3n_4)} = \sum_{\lambda,\lambda'} \frac{A^{(n_1n_2)}_{\lambda}\, \mathsf{S}^{-1}_{\lambda\lambda'}\, A^{*(n_3n_4)}_{\lambda'}}{E^{exc}_{\lambda} - \omega} \tag{3.36}$$

that is valid for a general non-Hermitian matrix defined by

$$H^{2p,exc}_{(n_1n_2)(n_3n_4)} A^{(n_3n_4)}_{\lambda} = E^{exc}_{\lambda} A^{(n_1n_2)}_{\lambda} \tag{3.37}$$

and solved by diagonalization. The overlap matrix S is given by

$$\mathsf{S}_{\lambda\lambda'} = \sum_{n_1n_2} A^{*(n_1n_2)}_{\lambda}\, A^{(n_1n_2)}_{\lambda'}$$

and differs from the identity because of the non-orthogonality of eigenstates of a non-Hermitian matrix, like $H^{2p,exc}$.

If, due to the approximation chosen for the self-energy, the $H^{2p,reso}$ is an Hermitian matrix (that also means that $K^{coupling}$ is symmetric), the excitonic eigenvalues E^{exc}_{λ} are real, and the corresponding excitation has an infinite lifetime.

The advantage of the spectral representation of the excitonic Hamiltonian is clear. The problem of inverting a matrix at each frequency has been mapped onto the problem of diagonalizing that matrix, *once for all*. The results of the diagonalization, $\{A_\lambda\}$ and $\{E_\lambda\}$, are used to build the polarizability function in the transition framework

$$\bar{L}_{(n_1n_2)(n_3n_4)} = \sum_{\lambda,\lambda'} \frac{A^{(n_1n_2)}_{\lambda}\, \mathsf{S}^{-1}_{\lambda\lambda'}\, A^{*(n_3n_4)}_{\lambda'}}{E^{exc}_{\lambda} - \omega} \tag{3.38}$$

which, once transformed in real space, can be put into Eq. (3.27) and give

$$\begin{aligned}\varepsilon_M(\omega) = 1 - \lim_{\mathbf{q}\to 0} v_0(\mathbf{q}) \sum_{\lambda\lambda'} \Bigg[\sum_{(n_1n_2)} \left\langle n_1 | e^{-i\mathbf{q}\cdot\mathbf{r}} | n_2 \right\rangle \frac{A^{(n_1n_2)}_{\lambda}}{E^{exc}_{\lambda} - \omega - i\eta} \times \\ \times \mathsf{S}^{-1}_{\lambda\lambda'} \sum_{(n_3n_4)} \left\langle n_4 | e^{i\mathbf{q}\cdot\mathbf{r}'} | n_3 \right\rangle A^{*(n_3n_4)}_{\lambda} \left(f_{n_4} - f_{n_3}\right) \Bigg].\end{aligned} \tag{3.39}$$

If we now consider only the resonant part of the excitonic Hamiltonian, i.e., the part which mixes only positive frequency transitions, the eigenstates A_λ are mutually orthogonal if $H^{2p,reso}$ is Hermitian and, in this case a simple formula holds

$$\varepsilon_M(\omega) = 1 - \lim_{\mathbf{q}\to 0} v_0(\mathbf{q}) \sum_\lambda \frac{\left|\sum_{(n_1 n_2)} \langle n_1 | e^{-i\mathbf{q}\cdot\mathbf{r}} | n_2 \rangle \, A_\lambda^{(n_1 n_2)}\right|^2}{E_\lambda^{exc} - \omega - i\eta}. \tag{3.40}$$

The use of (3.40) turned out to be a very good approximation, especially for the absorption spectra of semiconductors. Neglecting the coupling means neglecting the mixing between positive frequency and negative frequency transitions [196, 197]. This is in general no problem for the absorption spectrum, which involves the imaginary part of the dielectric function. Instead, for all quantities involving the real part of the dielectric matrix, like EELS, transitions at positive and negative frequency are naturally mixed, by the Kramers Kronig transformation, and the coupling term has turned out to be sometimes very important. An example of EELS for silicon is reported in Ref. [198].

3.3.2 Ingredients and approximations

In this paragraph we want to report the ingredients of the BSE method. The resonant part of the excitonic Hamiltonian (3.35)

$$H^{reso}_{(vc\mathbf{k})(v'c'\mathbf{k}')} = (E_{c\mathbf{k}} - E_{v\mathbf{k}})\,\delta_{vv'}\delta_{cc'}\delta_{\mathbf{k}\mathbf{k}'} + 2v^{v'c'\mathbf{k}'}_{vc\mathbf{k}} - W^{v'c'\mathbf{k}'}_{vc\mathbf{k}} \tag{3.41}$$

is composed of three parts: a diagonal part concerning the quasi-particle energies (calculated in the GW approximation)

$$H^{diag}_{(vc\mathbf{k})(v'c'\mathbf{k}')} = (E_{c\mathbf{k}} - E_{v\mathbf{k}})\,\delta_{vv'}\delta_{cc'}\delta_{\mathbf{k}\mathbf{k}'} \tag{3.42}$$

where all the indices have been specified (even the $\mathbf{k}$ point); the second and the third part are the electron-hole exchange and the screened electron-hole interaction part, given respectively by

$$H^{exch}_{(vc\mathbf{k})(v'c'\mathbf{k}')} = 2v^{v'c'\mathbf{k}'}_{vc\mathbf{k})} = \int d\mathbf{r} \int d\mathbf{r}' \phi^*_{c\mathbf{k}}(\mathbf{r})\phi_{v\mathbf{k}}(\mathbf{r}) \frac{2}{|\mathbf{r}-\mathbf{r}'|} \phi_{c'\mathbf{k}'}(\mathbf{r}')\phi^*_{v'\mathbf{k}'}(\mathbf{r}') \tag{3.43}$$

and

$$\begin{aligned} H^{scr}_{(vc\mathbf{k})(v'c'\mathbf{k}')} =& -\int d\mathbf{r} \int d\mathbf{r}' \int d\mathbf{r}_1 \phi^*_{c\mathbf{k}}(\mathbf{r})\phi_{c'\mathbf{k}'}(\mathbf{r})\varepsilon^{-1}(\mathbf{r},\mathbf{r}_1)\frac{1}{|\mathbf{r}_1-\mathbf{r}'|}\phi_{v\mathbf{k}}(\mathbf{r}')\phi^*_{v'\mathbf{k}'}(\mathbf{r}') = \\ = W^{v'c'\mathbf{k}'}_{vc\mathbf{k}} =& -\int d\mathbf{r} \int d\mathbf{r}' \phi^*_{c\mathbf{k}}(\mathbf{r})\phi_{c'\mathbf{k}'}(\mathbf{r}) W(\mathbf{r},\mathbf{r}')\phi_{v\mathbf{k}}(\mathbf{r}')\phi^*_{v'\mathbf{k}'}(\mathbf{r}') \end{aligned} \tag{3.44}$$

where we have summed up the spin[21] and only a static screening has been used $\varepsilon^{-1}(\mathbf{q}, \omega = 0)$. This further approximation has been implemented in the light of results [200, 201], showing that dynamical effects in the screening are partially compensated by those of the Green function, at least in simple semiconductors, so suggesting to neglect them both. In practice we evaluate (3.43) and (3.44) in momentum space, as

$$H^{exch}_{(vc\mathbf{k})(v'c'\mathbf{k}')} = 2\frac{4\pi}{\Omega}\sum_{\mathbf{G}\neq 0}\frac{1}{|\mathbf{G}|^2}\left\langle c\mathbf{k}\left|e^{i\mathbf{G}\cdot\mathbf{r}}\right|v\mathbf{k}\right\rangle\left\langle v'\mathbf{k}'\left|e^{-i\mathbf{G}\cdot\mathbf{r}}\right|c'\mathbf{k}'\right\rangle \tag{3.45}$$

$$H^{scr}_{(vc\mathbf{k})(v'c'\mathbf{k}')} = -\frac{4\pi}{\Omega}\sum_{\mathbf{G}\mathbf{G}'}\frac{\varepsilon^{-1}_{\mathbf{G}\mathbf{G}'}(\mathbf{q})}{|\mathbf{q}+\mathbf{G}|^2}\left\langle c\mathbf{k}\left|e^{i(\mathbf{q}+\mathbf{G})\cdot\mathbf{r}}\right|c'\mathbf{k}'\right\rangle\left\langle v'\mathbf{k}'\left|e^{-i(\mathbf{q}+\mathbf{G}')\cdot\mathbf{r}'}\right|v\mathbf{k}\right\rangle\delta_{\mathbf{k}-\mathbf{k}',\mathbf{q}}. \tag{3.46}$$

Before concluding this chapter, it is worth summarizing the steps of the method and the approximations that we use in the determination of optical spectra in BSE. We will follow Fig. 3.VI:

- First, one has to perform a ground state calculation, in order to find the KS eigenvalues $\{\epsilon_i\}$ and wavefunctions $\{\phi_i\}$.
  Approximations: use of pseudo-potentials and LDA for the exchange-correlation potential.

- Second, the calculation of the dielectric function is performed, once we have obtained the independent-particle polarizability χ^0.
  Approximations: dielectric matrix calculated within the RPA.

- Third, the standard GWA is applied to find the quasi-particle energies E_i.
  Approximations: use of the GW approximation where $\Sigma = iG^0W^0$. Plasmon-pole model applied to the frequency dependence of ε^{-1}.

- Fourth, the screening W and the independent-quasi-particle polarizability[22] P^0 are calculated.
  Approximations: The static limit is taken for W. The LDA wavefunctions are used to build P^0.

- Finally, the BSE calculation is performed, using P^0 and $K = \bar{v} - W^0$.
  Approximations: only the resonant part of the excitonic Hamiltonian is considered.

[21] The spin structure of the BSE would deserve a wide paragraph on its own [199]. Here we only consider that (1) the spin-orbit interaction in the system is negligible (so that the single particle states can be labelled by spin-up or spin-down states), (2) only the spin-singlet class of solution is taken into account.

[22] If one uses Eq. (3.35) the calculation of P^0 is not strictly necessary, because the quasi-particle energies are contained in the diagonal part of that equation. However, P^0 gives, for $\omega > 0$, the GW-RPA spectrum, which is very useful, in comparing with the BSE result, to infer about the excitonic effects. Also, $W(\omega = 0)$ might have already been calculated in the previous step.

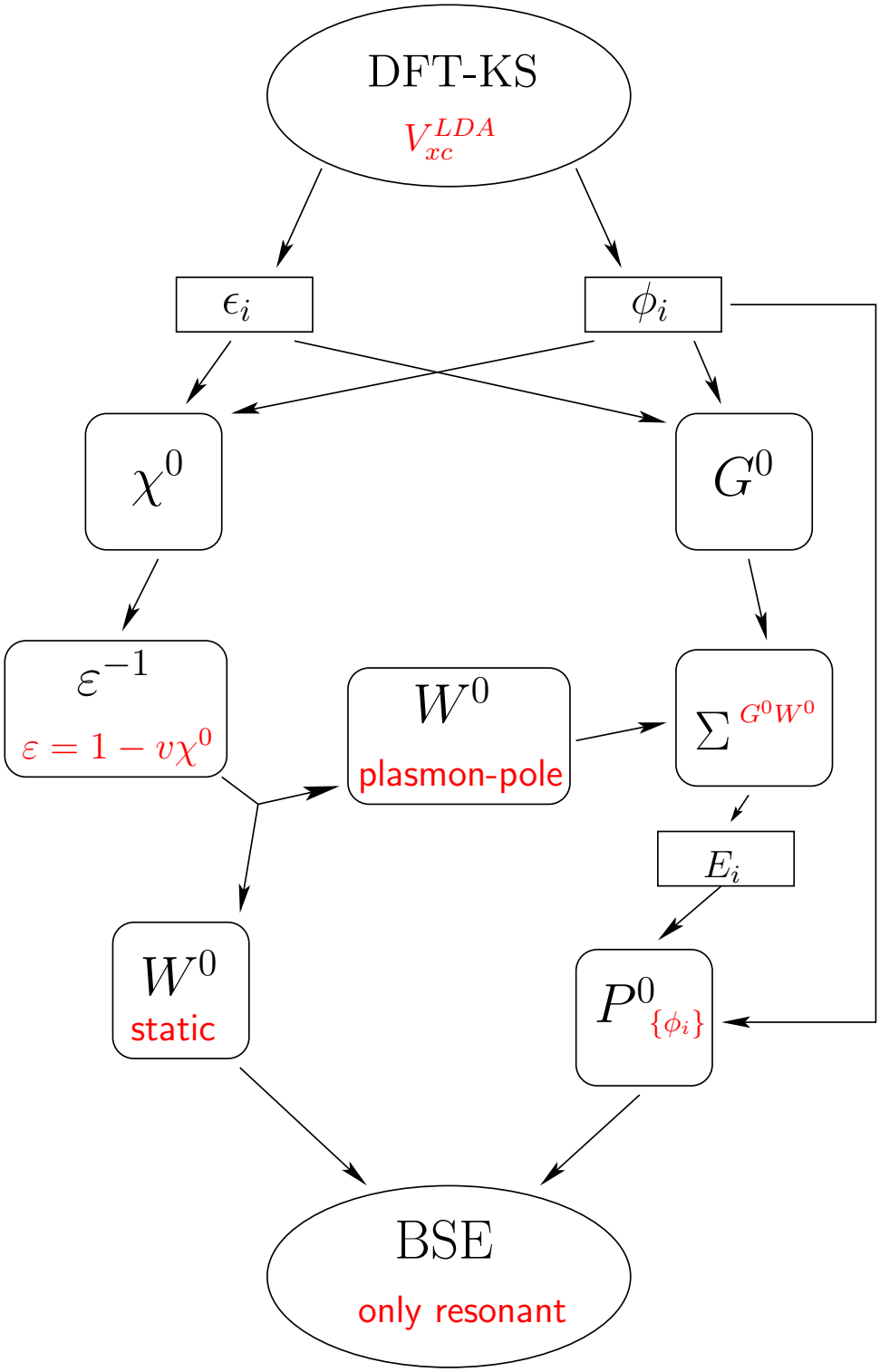

Figure 3.VI: Scheme for the determination of Optical Spectra in BSE.

Despite the number (and the level) of approximations occurring ("we are far from a full self-consistence resolution of the Hedin's equation"), the BSE method has achieved very good results.

Hanke and Sham [191] have managed to explain the absorption spectrum of silicon using the BSE together with a semi-empirical band structure. See also Ref.s [172, 202–205], to cite some of the first applications of modern *ab initio* BSE approach.

In Fig. 3.VII we show the results of the absorption spectrum of bulk silicon calculated with RPA, GW-RPA, BSE, compared with the experiment. The BSE result is in good

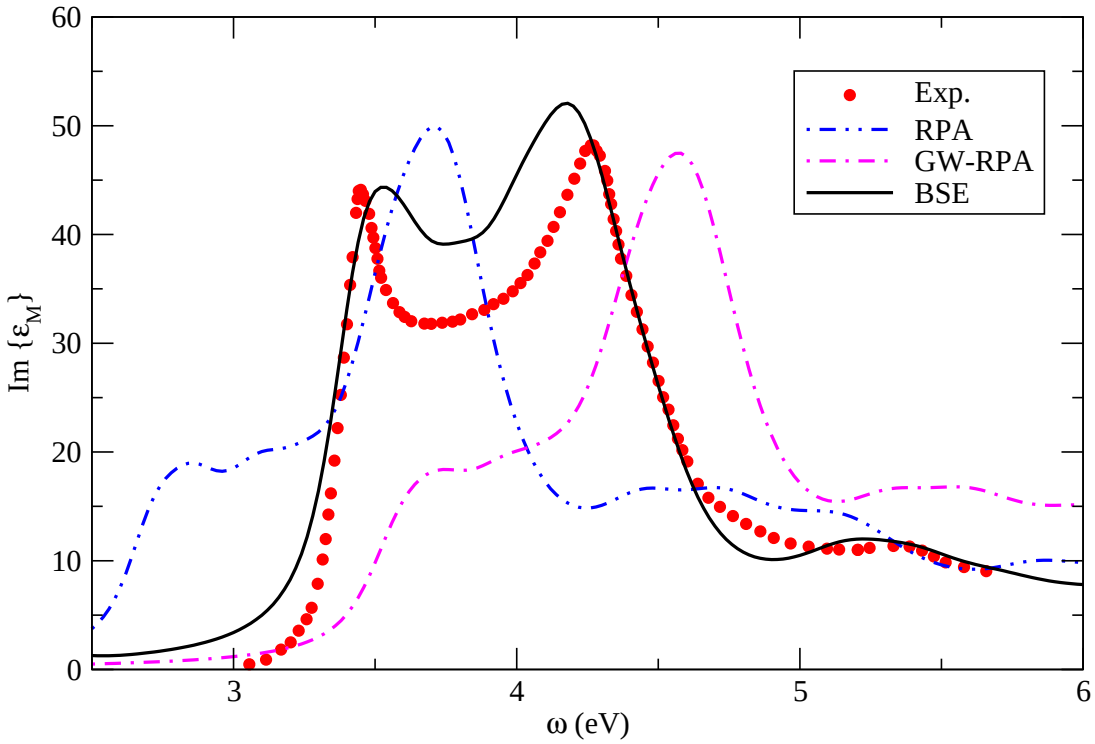

Figure 3.VII: Absorption Spectrum for bulk silicon. RPA, GW-RPA and BSE results compared to the experiment [189].

agreement with the experiment; in particular, the relative strength of the two peaks, now is correct. If we look at the results of Fig. 3.VII, we understand why the BSE is considered the final point of a three-steps procedure: first, the RPA spectrum can be obtained, using DFT-LDA eigenvalues and eigenfunctions (dashed curve); second, the GW corrections are calculated and the GW-RPA spectrum is built using LDA wavefunctions, but quasi-particle energies[23] (double-dot dashed curve); finally the BSE is applied, using again LDA wavefunctions and quasi-particle energies. The effect of the second step has been

[23]LDA energies + GW corrections

to shift (almost rigidly) the RPA spectrum towards higher energy, though without any improvement in the line-shape. The red-shift of the RPA has become the blue-shift of the GW-RPA, with respect to experiment. The very crucial step, the third one, moves (red-shift) the GW-RPA peaks in the right position and improves the line-shape of the spectrum (full line). Let us summarize the mathematical expression of the polarizability at the three stages (schematically):

$$\begin{aligned} \text{DFT-LDA} &\Rightarrow \chi_0^{RPA} = G^0(\epsilon_i)G^0(\epsilon_i) \\ \text{GW-RPA} &\Rightarrow P_0 = G^0(E_i)G^0(E_i) \\ \text{BSE} &\Rightarrow \tilde{P} = P_0 + P_0 W \tilde{P} = (1 - P_0 W)^{-1} P_0 \end{aligned}$$

We recognize that in both DFT-LDA and GW-RPA cases, the polarizability is given by the propagation of the electron and the hole *separately* (product of two one-particle Green functions), whereas in BSE the propagation of the two particles is correlated by the term $(1 - P_0 W)^{-1}$, which is nothing but the vertex term Γ, as follows from (3.12) and (3.14). This vertex term is responsible for excitonic effects, i.e. for the electron-hole interaction, giving rise to the two-particle character of the BSE.

Despite its three-step algorithm, the physics of the BSE picture is quite clear, and it is also easy to recognize the level of approximations occurring at each stage. Moreover the results one can achieve, within BSE, are remarkable, in a large variety of systems, like bulk semiconductors [202–207] or insulators [204, 208, 209], surfaces [210, 211], atoms [212], molecules [172], clusters [213], or even polymers [214–216]; and not only for the optical spectrum, but also, e.g. for the EELS [198, 217]. However, because of its 4-point character, the BSE calculations are necessarily cumbersome. The bottleneck of the calculation can be identify either in the construction of the $(N_v \times N_c \times N_{\mathbf{k}})^2$ matrix element of the $H^{2p}_{(vc\mathbf{k})(v'c'\mathbf{k}')}$, or in the diagonalization of the matrix itself, which involves a scaling of $(N_v \times N_c \times N_{\mathbf{k}})^3$, where $N_v, N_c, N_{\mathbf{k}}$ are the numbers of valence bands, of conduction bands, and of k-points used to sample the Brillouin zone, respectively.

It is also important to point out that the algorithm shown here to describe the solution of the Bethe-Salpeter equation, is neither the only possible one, nor the the most efficient. Several approaches, in fact, have been recently proposed, to have a numerically more efficient resolution, by a group [218–220] in the United States or by a group [211, 221] in Jena. Still, the calculations remain cumbersome, and far from applicable to systems of interest in material science, like defects, multi-wall nanotubes or quantum dots.

The heaviness of calculations is, of course, an important point, sufficient to justify the search for alternative approaches. The most promising is the Time Dependent Density Functional Theory, object of next chapter.

Chapter 4

Time Dependent DFT

Ποταμῷ οὐκ ἔστιν ἐμβῆναι δὶς τῷ αὐτῷ

῾Ηράκλειτος ὁ ᾽Εφέσιος

4.1 The problem

The Hohenberg-Kohn-Sham theory we saw in Chap. 2 is a time-independent theory. It is therefore not generally applicable to problems involving time-dependent fields, thus excluding the calculation of optical properties, electronic spectra, photo-chemistry, etc. The first extension of DFT, in order to deal with time-dependent external fields, was pursued by Peuckert [222] and Zangwill and Soven [223]. In particular, Zangwill and Soven, firstly applied the adiabatic Local Density Approximation for the calculation of "static polarizabilities, total photo-absorption cross sections, and selected partial photo-absorption cross sections of the rare gases which yield results in good agreement with experiment" [223]. A rigorous formal justification of the approach suggested by this work came only later, when a generalization of the basic formalism of DFT to the time-dependent case has been given by Runge, Gross and Kohn [224, 225]. In the work of Runge and Gross a theory similar to the Hohenberg-Kohn-Sham theory has been developed for time-dependent potentials. Several reviews of the foundation of TDDFT can be found in Ref.s [226–229]. For a comparison with the MBPT approach, see also Ref. [94].

TDDFT: 1st theorem ...

Suppose to have an N-electrons system, described by the Schrödinger equation:

$$H(t)\varphi(t) = i\frac{\partial}{\partial t}\varphi(t)$$

with $H(t) = T + V + W(t) = -\frac{1}{2}\sum_{i=1} \nabla_i^2 + \sum_{i<j} \frac{1}{|\mathbf{r}_i - \mathbf{r}_j|} + \sum_{i=1} V_{ext}(\mathbf{r}_i, t)$ sum of the kinetic energy, Coulomb potential and external (time-dependent) potential. The latter has to be expandable in a Taylor series around t_0, so that $V_{ext}(\mathbf{r}, t_0) = V_{ext}(\mathbf{r})$. Runge and Gross showed that *the densities $n(\mathbf{r}, t)$ and $n'(\mathbf{r}, t)$ evolving from the common initial state $\varphi(t_0) = \varphi_0$, under the influence of two external potential $V_{ext}(\mathbf{r}, t)$ and $V'_{ext}(\mathbf{r}, t)$, both Taylor expandable around t_0, are always different provided that the external potentials differ by more than a purely time-dependent function $c(t)$*. This is the time-dependent analogue of the first H&K theorem. As a consequence, the time-dependent density uniquely determines the external potential (up to a purely time-dependent function $c(t)$). On the other hand the potential determines the time-dependent wave function, unique functional of the density up to a purely time-dependent phase:

$$\varphi(t) = e^{-i\alpha(t)}\varphi[n, \varphi_0](t).$$

So for an operator $\widehat{O}(t)$, which is a function of time but not of any derivative or integral operators on t, this phase factor cancels out when taking the expectation value, which is hence a unique functional of the density:

$$\langle\varphi(t)|\, \widehat{O}(t)\, |\varphi(t)\rangle = O[n](t).$$

... and 2nd one

The analogue of the second H&K theorem, where the Rayleigh-Ritz minimum principle is used for the total energy, is given in the time-dependent theory by the stationary principle of the Hamiltonian action integral, as no minimum energy principle is available. We know, in fact, that in quantum mechanics the time-dependent Schrödinger equation, with the initial condition $\varphi(t_0) = \varphi_0$ corresponds to a stationary (not necessarily minimum) point of the quantum mechanical action integral[1]

$$A = \int_{t_0}^{t_1} dt\, \langle\varphi(t)|\, i\frac{\partial}{\partial t} - H(t)\, |\varphi(t)\rangle\,.$$

A is a functional of the density and has a stationary point at the correct time-dependent density. This density can hence be obtained solving the Euler equations $\frac{\delta A[n]}{\delta n(\mathbf{r}, t)} = 0$ with the appropriate initial conditions. Now exactly as we did for the time-independent case, we can write the functional A as:

$$A[n] = B[n] - \int_{t_0}^{t_1} dt \int d\mathbf{r} n(\mathbf{r}, t) V_{ext}(\mathbf{r}, t) \tag{4.1}$$

[1]This should not leave one surprised. Even in classical mechanics the equations of motion (the trajectory) of a material are given by solving the *stationary* principle for the Hamiltonian or Lagrangian (thus giving the Hamilton equations or Lagrange equations respectively); whereas the static equilibrium position is given by *minimizing* the potential energy.

with the universal[2] functional $B[n]$ given by

$$B[n] = \int_{t_0}^{t_1} dt \, \langle \varphi(t)| \, i\frac{\partial}{\partial t} - T - V \, |\varphi(t)\rangle \, .$$

As for the time-independent DFT one can define a Kohn-Sham scheme by introducing a non-interacting system with exactly the same density $n(\mathbf{r}, t)$. Once the v-representability of the time-dependent densities is proven [230], we can apply the stationary condition to Eq. (4.1) under the condition $n(\mathbf{r}, t) = \sum_i |\phi_i(\mathbf{r}, t)|^2$, in order to obtain the time-dependent Kohn-Sham equations:

$$\left[-\frac{1}{2}\nabla^2 + V_{tot}(\mathbf{r}, t)\right] \phi_i(\mathbf{r}, t) = i\frac{\partial}{\partial t}\phi_i(\mathbf{r}, t) \tag{4.2}$$

where

$$V_{tot}(\mathbf{r}, t) = V_{ext}(\mathbf{r}, t) + \int v(\mathbf{r}, \mathbf{r}')n(\mathbf{r}', t)d\mathbf{r}' + V_{xc}(\mathbf{r}, t) \tag{4.3}$$

analogous to Eq. (2.9) and Eq. (2.10) respectively.

Up to here we have presented the very basic formalism, only taking into account the quantum nature of electrons. As for the time-independent case, generalizations are required, in order to treat coupling of nuclear and electronic motion or to deal with magnetic fields and time-dependent electromagnetic fields.[3]

4.2 TD Density Response Functional Theory

The solutions of Eq. (4.2) are the Kohn-Sham orbitals which yield the true charge density. This means that any property which depends only on the density, can be exactly obtained (in principle) by the Kohn-Sham formalism. Here we are interested in excitations energies and polarizabilities within linear response (although TDDFT can, of course, also describe non-linear response) which leads to some simplifications.

The linear response theory (see Appendix A) can be applied here to study the effect of a small perturbation $V_{ext}(\mathbf{r}, t)$ on the system. In the linear approximation the induced charge density is related to the external potential

$$n_{ind}(\mathbf{r}, t) = \int d\mathbf{r}'dt'\chi(\mathbf{r}, \mathbf{r}', t - t')V_{ext}(\mathbf{r}', t') \tag{4.4}$$

via the *response function* $\chi(\mathbf{r}, \mathbf{r}', t - t')$ which is called full polarizability. The analogy with the function P defined by (3.19) is evident, the difference being represented by the fact that P is a time-ordered function, whereas χ is a retarded function (see Par. 3.2).

[2]It is however φ_0-dependent.

[3]It is crucial, for example, to deal with superconductors [231].

The function χ is non-zero only for $t > t'$ because of the causality condition. In the (TD)KS-scheme it is also possible to describe the response of the system (i.e. in terms of induced charge density) to an *effective* total[4] potential V_{tot}, given by Eq. (4.3), via the

$$n_{ind}(\mathbf{r}, t) = \int d\mathbf{r}' dt \chi^0(\mathbf{r}, \mathbf{r}', t - t') V_{tot}(\mathbf{r}', t') \tag{4.5}$$

where the independent-particle polarizability χ^0 is the linear response of the fictitious Kohn-Sham system (non-interacting one), and has the well known form (see Eq. 2.25 and Appendix A)

$$\chi^0(\mathbf{r}, \mathbf{r}', \omega) = \sum_{vc} \frac{(f_v - f_c)\, \phi_v^*(\mathbf{r})\phi_c(\mathbf{r})\phi_c^*(\mathbf{r}')\phi_v(\mathbf{r}')}{\omega - (\epsilon_c - \epsilon_v) + i\eta}, \tag{4.6}$$

directly translated in frequency domain.[5] Here f_v and f_c are Fermi occupation numbers, ϵ_c and ϵ_v are KS eigenvalues, and the sums run over all KS orbitals (continuum states included). The two response functions χ and χ^0 are related by Eq. (4.3), giving

$$\begin{aligned}\chi = \frac{\delta n}{\delta V_{ext}} = \frac{\delta n}{\delta V_{tot}} \frac{\delta V_{tot}}{\delta V_{ext}} = \chi^0 \left[\frac{\delta V_{ext}}{\delta V_{ext}} + \frac{\delta V_H}{\delta V_{ext}} + \frac{\delta V_{xc}}{\delta V_{ext}} \right] = \\ = \chi^0 \left[1 + \frac{\delta V_H}{\delta n} \frac{\delta n}{\delta V_{ext}} + \frac{\delta V_{ext}}{\delta n} \frac{\delta n}{\delta V_{ext}} \right] = \chi^0 + \chi^0 (v + f_{xc})\, \chi\end{aligned}$$

or, more explicitly,

$$\begin{aligned}\chi(\mathbf{r}, \mathbf{r}', \omega) = \chi^0(\mathbf{r}, \mathbf{r}', \omega) + \\ + \iint d\mathbf{r}'' d\mathbf{r}''' \left[\chi^0(\mathbf{r}, \mathbf{r}'', \omega) \Big(v(\mathbf{r}'', \mathbf{r}''') + f_{xc}(\mathbf{r}'', \mathbf{r}''', \omega) \Big) \chi(\mathbf{r}''', \mathbf{r}', \omega) \right].\end{aligned} \tag{4.7}$$

The fact that the variation of the Hartree and exchange-correlation potentials appear in determining the response function, derives from the fact that the total perturbation acting on the system is calculated self-consistently.

Here the quantity

$$f_{xc}(\mathbf{r}, \mathbf{r}', t, t') = \frac{\delta V_{xc}([n]\mathbf{r}, t)}{\delta n(\mathbf{r}', t')}$$

has been introduced. It is called exchange-correlation kernel and takes into account all dynamical exchange and correlation effects to linear order in the perturbing potential. A

[4] It is important to notice that the total potential V_{tot} defined here also contains the exchange-correlation contribution, whereas the (classical) total potential U defined by (3.19) does not.

[5] The pure imaginary part $i\eta$ has been inserted to make the Fourier transform feasible. This damping factor is also used for a Lorentzian broadening of χ^0. Its sign distinguishes between time-ordered and retarded response.

formally exact representation of the exchange-correlation kernel is the inversion of (4.7), supposing that the inverse of χ^0 and χ exist,

$$f_{xc}(\mathbf{r},\omega) = \chi_0^{-1}(\mathbf{r},\mathbf{r}',\omega) - \chi^{-1}(\mathbf{r},\mathbf{r}',\omega) - \frac{1}{|\mathbf{r}-\mathbf{r}'|}. \tag{4.8}$$

4.3 Adiabatic Local Density Approximation

Of course, the exact time dependent exchange-correlation potential and kernel are unknown and realistic calculations rely on some approximations. A widely used approximations is the adiabatic local density approximation (ALDA), in which f_{xc} is taken as the (ω-independent, i.e. adiabatic) functional derivative of the static LDA exchange-correlation potential (described in Par. 2.4)

$$f_{xc}^{ALDA}(\mathbf{r},\mathbf{r}') = \delta(\mathbf{r}-\mathbf{r}')\frac{\partial V_{xc}^{LDA}(n(\mathbf{r}),\mathbf{r})}{\partial n(\mathbf{r})}. \tag{4.9}$$

This approximation is chosen on top of the approximation chosen for the static potential V_{xc} to determine the ground state, and hence to determine χ^0. In principle the exchange-correlation kernel should always be the functional derivative of an exchange-correlation potential, if one wants the sum rules to be fulfilled (see also Par. 4.5).

The local adiabatic approximation (ALDA) has proven to be quite successful in applications to finite systems, such as molecules and clusters up to several hundred atoms in size. However, the ALDA results obtained for spectra appear to be less systematically satisfactory than those generally obtained using the LDA for ground state calculations. For example, the ALDA description of the photo-absorption spectrum of small cluster can be satisfactory or even very good (Na_4 [232], benzene [233]) or rather bad (SiH_4 [232]). The Rydberg series is not reproduced by the local adiabatic approximation (see Par. 4.4), and the ALDA systematically fails in the description of absorption spectra of solids (see Par. 4.5 and Ref.s [94, 234]). An example is shown in Fig. 4.I, where the ALDA calculation of solid silicon is compared to the RPA, GW-RPA and BSE calculations. The experiment is also reported [98].

4.4 Excited States in TDDFT

We have seen that, in static DFT, the interpretation of one-particle eigenvalues as quasi-particle energies, is not formally justified and it leads to the well known band-gap problem. Much better results can be obtained using the ΔSCF-DFT scheme, even if it is restricted to finite systems.

In the Green function approach, the standard GW approximation led to a great improvement of the description of quasi-particle energies, both for occupied and empty levels

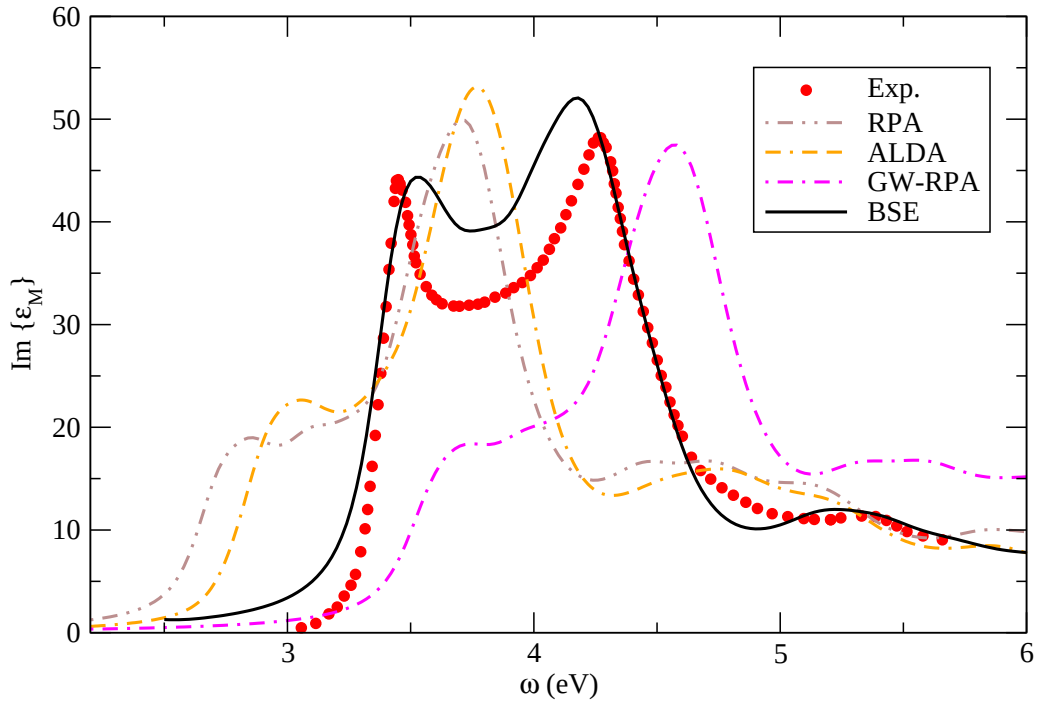

Figure 4.I: Absorption spectrum of solid silicon. ALDA, RPA, GW-RPA and BSE calculations are compared with the experiment.

(see Fig. 3.IV), and the BSE yields a good description of neutral excitations spectra, like absorption and electron energy loss spectra.

Also the time-dependent density functional theory permits one to calculate the excited states energies of a many-body system [235, 236]. In fact, in Eq. (4.7), rewritten as

$$\left[1 - \chi^0(v + f_{xc})\right] \chi = A\chi = \chi^0 \tag{4.10}$$

one can observe that the χ has poles at the true excitation energies $\Omega_j = (E_j^N - E_0^N)$, where E_0^N is the ground state energy and E_j^N an (j^{th}) excited state energy of a N-particle system, as we have discussed in Appendix A. The χ^0 (right part of Eq. (4.10)), instead, has poles at the one-particle excitation energies $(\epsilon_i - \epsilon_j)$ (KS eigenvalue differences) which are different of the true excitation energies. The relation (4.10), then, holds only if the operator $A(\omega)$ is not invertible in those frequencies where $\omega = \Omega_j$. This is because zeroes of $A(\omega)$ must cancel the singularities of χ. Therefore, the problem of finding the excitation energies of a N-particle system, reduces to find those frequencies for which $A(\omega)$ is not invertible, which are exactly $\omega = \Omega_j$. The application of TDDFT (in describing excitations of finite systems) are quite promising [232, 233, 235, 237–243], but they often require to go beyond the ALDA.

In Par. 4.3 we have mentioned the fact that the ALDA description of excited energies

completely misses the description of Rydberg states. This is due to the incorrect asymptotic behavior of the adiabatic local density exchange-correlation potential, which decays exponentially instead of the correct $1/r$. Other problems, related to the use of the local density (or even gradient corrected) approximations, already show up in the one-particle properties, for example (i) the fact that negative atomic ions are not bound, or (ii) that the ionization potentials are too small.

Several attempts have been proposed to overcome these problems, like to correct the tail of the LDA exchange-correlation potential [244], or, within the optimized effective potential (OEP) scheme [235, 245–248] handling the exchange part of the potential exactly (which again yields the correct asymptotic behavior), and the correlation part in LDA or GGA. Concerning solids, only more recently the community has tried to go beyond ALDA, within TDDFT.

Before comparing TDDFT to the BSE approach, it is useful to realize what a TDDFT calculations means in practice, for the case of a solid and for a finite system.

4.5 Electronic Spectra in TDDFT - Application to solids

In Fourier space[6], the independent-particle polarizability (4.6) is written as

$$\chi^0(\mathbf{q},\mathbf{G},\mathbf{G}',\omega) = \frac{2}{\Omega}\sum_{v,c,\mathbf{k}}(f_{c,\mathbf{k+q}} - f_{v,\mathbf{k}})\frac{\left\langle v,\mathbf{k}|e^{-i(\mathbf{q}+\mathbf{G})\cdot\mathbf{r}}|c,\mathbf{k}+\mathbf{q}\right\rangle\left\langle c,\mathbf{k}+\mathbf{q}|e^{i(\mathbf{q}+\mathbf{G}')\cdot\mathbf{r}'}|v,\mathbf{k}\right\rangle}{\omega-(\epsilon_{c,\mathbf{k+q}}-\epsilon_{v,\mathbf{k}})+i\eta}$$

$$\chi^0(\mathbf{q},\mathbf{G},\mathbf{G}',\omega) = \frac{2}{N_\mathbf{k}}\sum_{v,c,\mathbf{k}}\frac{(f_{c,\mathbf{k+q}} - f_{v,\mathbf{k}})\tilde{\rho}_{vc\mathbf{k}}(\mathbf{q},\mathbf{G})\,\tilde{\rho}^*_{vc\mathbf{k}}(\mathbf{q},\mathbf{G}')}{\omega-(\epsilon_{c,\mathbf{k+q}}-\epsilon_{v,\mathbf{k}})+i\eta} \tag{4.11}$$

where the one-particle states are Bloch wave functions, labeled by wave vector $\mathbf{k}$ and band index $v(c)$.[7] The sum over spins is responsible for the factor 2. The response function is normalized with the volume Ω of the system which reads $\Omega = \Omega_{cell}\cdot N_\mathbf{k}$, i.e. number of k-points times the volume of the unit cell. The polarisation matrices $\tilde{\rho}_{vc\mathbf{k}}(\mathbf{q},\mathbf{G}) = \left\langle v,\mathbf{k}|e^{-i(\mathbf{q}+\mathbf{G})\cdot\mathbf{r}}|c,\mathbf{k}+\mathbf{q}\right\rangle$ have also been introduced to simplify the successive comparison with the Green functions theory.

As we have described in Chap. 1, in order to connect the macroscopic (measurable) optical quantities and the microscopic electronic structure, we need to define a dielectric function ε. In the linear approximation, the effective potential V_{tot} is related to the external potential V_{ext} via

$$V_{tot}(\mathbf{r},\omega) = \int d\mathbf{r}'\varepsilon^{-1}(\mathbf{r},\mathbf{r}',\omega)V_{ext}(\mathbf{r}',\omega) \tag{4.12}$$

[6]The most natural to deal with bulk systems, having a translational periodicity.

[7]v (or c) stands for valence (or conduction) band index if the system is a semiconductor or an insulator.

where the inverse dielectric function ε^{-1} acts as a screening for the external potential. From the latter and the Eq.s (4.3) and (4.4) one can easily find the connection between the dielectric function and the polarizability. However, the portion of screening that has to be included in the ε^{-1}, depends on the probe (different probes will be "screened" by different parts of the response function). We have to read that in two steps[8]:

1 The external perturbation V_{ext} produces an induced charge density in the system $n_{ind} = \chi\, V_{ext}$ with χ as response function. When V_{ext} can be considered to be classical, $\chi\, V_{ext}$ depends only on the nature of the system (in our case, a gas of interacting electrons, so $\chi = (1 - \chi^0 v - \chi^0 f_{xc})^{-1}\chi^0$).

2 The induced charge creates a screening, described by ε^{-1} which depends on the nature of the perturbation to be screened. If the probe is a test-particle, it has no exchange-correlations effects with the responding electron gas. On the contrary an electron (test-electron) "feels" not only an induced classical potential vn_{ind}, but also an induced exchange-correlation potential $V_{xc} = f_{xc}n_{ind}$. Therefore

$$\varepsilon^{-1}_{TP} = 1 + v\,\chi \tag{4.13}$$

$$\varepsilon^{-1}_{TE} = 1 + v\,\chi + f_{xc}\chi \tag{4.14}$$

for the test-particle and test-electron cases, respectively.

In this thesis, we need the test-particle dielectric matrix, hence in reciprocal space,

$$\varepsilon^{-1}_{\mathbf{G},\mathbf{G}'}(\mathbf{q},\omega) = \delta_{\mathbf{G},\mathbf{G}'} + v_{\mathbf{G}}(\mathbf{q})\,\chi_{\mathbf{G},\mathbf{G}'}(\mathbf{q},\omega). \tag{4.15}$$

Following Par. 1.5, the macroscopic dielectric function can then be calculated as

$$\varepsilon_M(\omega) \equiv \lim_{\mathbf{q}\to 0} \frac{1}{\left[\varepsilon^{-1}(\mathbf{q},\omega)\right]_{\mathbf{G}=\mathbf{G}'=0}}.$$

and Absorption and Electron Energy Loss Spectra from

$$\text{Abs} = \Im\left\{\varepsilon_M\right\} \qquad ; \qquad \text{EELS} = -\Im\left\{\frac{1}{\varepsilon_M}\right\}.$$

We can now summarize the steps leading[9] to the determination of an optical spectrum in TDDFT.

[8] For further discussions see [145, 249–251].

[9] This clearly is just the approach adopted in this thesis. For a real space and real time approach, see [233, 237, 239, 252–254] and references therein.

Summary: optical spectra in 4 steps

1) **A ground state calculation** is usually done in the DFT framework, where a reasonable exchange-correlation potential V_{xc} has been chosen, e.g. the V_{xc}^{LDA}. This first step permits one to obtain the ground state electronic structure in terms of the (ground state) wavefunctions ϕ_i and eigenvalues ϵ_i.

   Approximations involved: $V_{xc}([n], \mathbf{r}) \approx V_{xc}^{LDA}(n(\mathbf{r}))$ and pseudo-potentials.

2) **The Independent-Particle polarizability** $\chi^{\mathbf{0}}$ can be built using wavefunctions and eigenvalues obtained in the previous step, via the $\chi^0 \sim \sum_{vc} \frac{\phi_v \, \phi_c \, \phi_c \, \phi_v}{\omega - (\epsilon_c - \epsilon_v)}$.

   Approximations involved: None, except the linear response framework.

3) **The full polarizability** χ can be obtained then, if an expression for the exchange-correlation kernel f_{xc} exists. $\chi = (1 - \chi^0 v - \chi^0 f_{xc})^{-1} \chi^0$.

   Approximations involved: in f_{xc}. The simplest choice, namely the Random Phase Approximation (RPA), is to put the kernel to zero $f_{xc}^{\mathrm{RPA}} = 0$. The ALDA $f_{xc}^{ALDA} = \delta(\mathbf{r} - \mathbf{r}') \frac{\partial V_{xc}^{LDA}(n(\mathbf{r}), \mathbf{r})}{\partial n(\mathbf{r})}$ is another possibility. In this thesis, more successful kernel have been developed.

4) **The dielectric function**, calculated as $\varepsilon^{-1} = 1 + v\chi$, permits one to obtain both absorption and EELS via the macroscopic function $\varepsilon_M = 1/\varepsilon_{00}^{-1}$.

   Approximations involved: None.

Before concluding this paragraph, two remarks are necessary.

1st observation: the crucial step of the previous summary is clearly the third one. In Eq. (4.7) two terms have to be included. The first, and known, term is the Coulomb potential and its importance will be described in the next chapter. The second term, the *unknown* f_{xc}, is the key of TDDFT, and its goal is to reproduce all the quasi-particle and excitonic effects, which are not contained in the RPA (which is the starting point, since $f_{xc}^{RPA} = 0$). The exchange-correlation kernel will be extensively analyzed in the following chapters.

2nd observation: the TDDFT scheme we have used here, the most convenient to deal with solids,[10] is based on the linear response framework (which is not a limit of TDDFT), it works in the Fourier space and in frequency domain. Another difference with respect to real-space real-time TDDFT, where one lets the density $n(\mathbf{r})$ evolve according to $V_{ext}(\mathbf{r}, t)$, maintaining the self-consistency between $n(\mathbf{r})$ and $V_{ext}(\mathbf{r}, t)$, is that here it is quite natural to decouple the ground state calculation from that one of the response. Mathematically, that means that not necessarily $f_{xc} = \frac{\partial V_{xc}}{\partial n}$. On one hand, this constitutes an advantage because one can calculate the ground state using a reasonable V_{xc}, e.g. the LDA one[11]

[10] It has also successfully used for finite systems, using the super-cells method.

[11] LDA wavefunctions can be safely used in solids [255].

(steps 1 and 2 of the summary), then make the great effort modeling the f_{xc}. This is the way followed in this thesis.[12] On the other hand caution must be taken, when $f_{xc} \neq \frac{\partial V_{xc}}{\partial n}$, because possible violation of sum-rules can occur. See for that [122, 123, 256].

4.6 Electronic Spectra in TDDFT - Finite systems

Finite systems are described through the usual (linear-) response function χ that relates the induced density to the external applied field (either photon or electron), as Eq. (4.4). We follow here the basic idea, firstly suggested by Zangwill and Soven, to find the dynamic photo-response of a finite system.

If the variation of the external field, e.g. the photon wavelength in case of an electromagnetic perturbation, is much larger than the size of the system,[13] we can consider the response of the system as described by changes in the dipole moment $\mathbf{p}(t)$.
Taking the electric field as external perturbation, we can develop the dipole moment [257]

$$\mathbf{p}(t) = \alpha(\omega)\mathsf{E}cos(\omega t) + \frac{1}{2!}\beta(0)\mathsf{E}\mathsf{E} + \frac{1}{2!}\beta(2\omega)\mathsf{E}\mathsf{E}cos(2\omega t) + \\ + \frac{1}{3!}\gamma(\omega)\mathsf{E}\mathsf{E}\mathsf{E}cos(\omega t) + \frac{1}{3!}\gamma(3\omega)\mathsf{E}\mathsf{E}\mathsf{E}cos(3\omega t) + ... \quad (4.16)$$

where only the time coupling between external perturbation and response function has been taken into account.[14] The linear dynamical polarizability $\alpha(\omega)$ is a tensor of rank one, while the non-linear hyper-polarizabilities $\beta, \gamma, ...$ are higher order tensors.

If one neglects non-linear terms in Eq. (4.16) [257], the induced dipole moment becomes

$$\mathbf{p}(\omega) = \alpha(\omega)\mathsf{E}cos(\omega t) \quad (4.17)$$

while the external potential applied to the system can be chosen as

$$V_{ext} = \frac{1}{2}zeE^0$$

where E^0 is the magnitude of the electric field along the direction $\hat{\mathbf{z}}$. From Eq. (4.17) and knowing that $\mathsf{E} = -\nabla V_{ext}$, we have

$$\alpha(\omega) = -\frac{\mathbf{p}(\omega)}{\frac{1}{2}eE^0}.$$

[12] In principle, one can of course also decouple V_{xc} and f_{xc} in a real space real time code by letting only a part of the potential evolve in time.

[13] See Appendix D for a brief discussion of size effects in finite systems.

[14] This is justified for finite systems, like an atom or a molecule, but not for a solid where also a spatial coupling occurs: $\int d\mathbf{r}'\alpha(\mathbf{r}, \mathbf{r}', \omega)\mathsf{E}(\mathbf{r}', \omega)$.

Since the definition of the dipole moment is $\mathbf{p}(\omega) = \int d\mathbf{r}\, z\, n(\mathbf{r}, \omega)$, the dynamical dipole-polarizability α is

$$\begin{aligned} \alpha(\omega) &= -\frac{2}{eE^0} \int d\mathbf{r} z n_{ind}(\mathbf{r}, \omega) \\ &= -\frac{2}{eE^0} \int d\mathbf{r} z \left[\int d\mathbf{r}' \chi(\mathbf{r}, \mathbf{r}', \omega) \frac{1}{2} eE^0 z' \right] \\ &= -\int d\mathbf{r} d\mathbf{r}' z \chi(\mathbf{r}, \mathbf{r}', \omega) z' \end{aligned} \tag{4.18}$$

and whose imaginary part represents the (measurable) photo-absorption cross section $\sigma(\omega)$

$$\sigma(\omega) = \frac{4\pi\omega}{c} \Im\{\alpha(\omega)\} \tag{4.19}$$

which is the function to compare with spectroscopy experiments.

Eq. (4.18) is nothing but a special (dipole) case of the more general dynamical polarizability

$$\alpha(\omega) = -\int d\mathbf{r} d\mathbf{r}' V_{ext}(\mathbf{r}, \omega) \chi(\mathbf{r}, \mathbf{r}', \omega) V_{ext}(\mathbf{r}', \omega). \tag{4.20}$$

The first atomic applications of TDDFT are reviewed in [226, 231, 258].

Chapter 5

BSE & TDDFT:

Così tra questa
~~immensità~~ infinità s'annega il pensier mio:
E 'l naufragar m'è dolce in questo mare.

from L'INFINITO, Giacomo Leopardi

BSE calculations generally yield good agreement between the calculated and experimental absorption spectra for both finite and infinite systems, but the intrinsic two-particle nature of the BSE makes the calculation very cumbersome. The alternative approach is represented by TDDFT, whose two-point (density-propagation) character can lead, in principle, to simpler calculations. The leading equations of the two methods are

$$\begin{aligned} \text{BSE} \quad &\leftrightarrow \quad {}^4\bar{L} = {}^4P^0 + {}^4P^0\left({}^4\bar{v} - {}^4W\right){}^4\bar{L} \\ \text{TDDFT} \quad &\leftrightarrow \quad \bar{\chi} = \chi^0 + \chi^0\left(\bar{v} - f_{xc}\right)\bar{\chi} \end{aligned} \tag{5.1}$$

for what concerns absorption. The same can be done for EELS, provided that $\bar{v}$ has been substituted by v. Here we have put the top-left exponent ${}^4\square$ to explicitly indicate a 4-point function.

In spite of its two-point character, the description of optical spectra of solids in TDDFT (often using ALDA) has been quite unsatisfying up to not long time ago. The reason relies on the difficulty to find efficient approximations for the exchange-correlation potential v_{xc} and kernel f_{xc}.

The main advantage of the BSE is the immediate physical meaning of each ingredient of the theory. Be able to discern if an ingredient is essential or not, recognize where errors possibly cancel, immediately leads to very efficient approximations within the BSE.

This is not so easy in TDDFT, where one has to deal only with f_{xc} (or v_{xc}). In fact, if we look at Eq. (5.1), in order for the two approaches to give the same result, the TDDFT

kernel f_{xc} must: (1) correct the DFT Kohn-Sham energies (towards the quasi-particle energies, contained in ${}^4P^0$; (2) simulate the excitonic effects, i.e. the W term in the BSE; even though the two contribution partially cancel each other. This is, of course, a very big task, and it will be the aim of next chapters.

Here, we want to show that, since the two equations (5.1) have the same structure, it is possible to make a direct comparison between the two methods. To do so, we have to extend the TDDFT to the 4-point formalism (it is not possible to find a two-point expression for the BSE):

$$ {}^4\bar{\chi} = {}^4\chi^0 + {}^4\chi^0 \left({}^4\bar{v} + {}^4f_{xc} \right) {}^4\bar{\chi} $$

where

$$ {}^4\bar{v} = \delta(12)\delta(34)\bar{v}(13) \quad ; \quad {}^4f_{xc} = \delta(12)\delta(34)f_{xc}(13) \tag{5.2} $$

while in the BSE

$$ {}^4W = \delta(13)\delta(24)W(12). \tag{5.3} $$

We can observe that, if the quasi-particle corrections are directly inserted[1] into the χ^0, via a χ^0_{GW}, obtained simply by replacing ϵ_i with the E_i in χ^0, the equations in BSE and TDDFT can be unified, leading to[2]

$$ S = P^0 + P^0 K S $$

with P^0 representing an independent-(quasi)particle polarizability and the kernel of the Dyson equation composed of two terms $K = v + \Xi$. Two are then, besides P^0, the ingredients to consider for the calculation of a spectrum:

- the Coulomb term v (for energy loss) or $\bar{v}$ (for Absorption), which is common in BSE and TDDFT
- the exchange-correlation (electron-hole) interaction Ξ, which instead distinguishes BSE and TDDFT results

In next chapter we will discuss in detail the importance and the role of the first (common to TDDFT and BSE) term; whereas Chap. 7 and the following will be centered on Ξ, with several approximations proposed. In particular, in Chap. 8, a new fully *ab initio*, parameter-free kernel will be described and implemented. It is based on the comparison of BSE and TDDFT, and on its formulation in transitions space, where Eq.s (5.1) become (following (3.33))

$$ \begin{aligned} \bar{L}_{(n_1n_2)(n_3n_4)} &= \left[H^{2p,reso}_{\mathrm{BSE}} - I\omega \right]^{-1}_{(n_1n_2)(n_3n_4)} (f_{n_3} - f_{n_4}) \\ \bar{\chi}_{(n_1n_2)(n_3n_4)} &= \left[H^{2p,reso}_{\mathrm{TDDFT}} - I\omega \right]^{-1}_{(n_1n_2)(n_3n_4)} (f_{n_3} - f_{n_4}) \,. \end{aligned} \tag{5.4} $$

[1] This is a choice that has turned out to be successful.

[2] Again, in principle we have to distinguish between time-ordered and retarded response functions. In practice we suppose to be at $\omega > 0$.

The 2-particle Hamiltonians (following Eq. (3.35)) are

$$H^{\mathrm{BSE}}_{(vc\mathbf{k})(v'c'\mathbf{k}')} = (E_{c\mathbf{k}} - E_{v\mathbf{k}})\,\delta_{vv'}\delta_{cc'}\delta_{\mathbf{k}\mathbf{k}'} + 2v^{v'c'\mathbf{k}'}_{vc\mathbf{k}} - W^{v'c'\mathbf{k}'}_{vc\mathbf{k}} \tag{5.5}$$

for the BSE, with v given by (3.43) and W given by (3.44), and

$$H^{\mathrm{TDDFT}}_{(vc\mathbf{k})(v'c'\mathbf{k}')} = (\epsilon_{c\mathbf{k}} - \epsilon_{v\mathbf{k}})\,\delta_{vv'}\delta_{cc'}\delta_{\mathbf{k}\mathbf{k}'} + 2v^{v'c'\mathbf{k}'}_{vc\mathbf{k}} + F^{\mathrm{TDDFT}}_{(vc\mathbf{k})(v'c'\mathbf{k}')} \tag{5.6}$$

with F given by

$$F^{\mathrm{TDDFT}}_{(vc\mathbf{k})(v'c'\mathbf{k}')} = 2\int d\mathbf{r}\int d\mathbf{r}'\phi^*_{c\mathbf{k}}(\mathbf{r})\phi_{v\mathbf{k}}(\mathbf{r})f_{xc}(\mathbf{r},\mathbf{r}',\omega)\phi_{c'\mathbf{k}'}(\mathbf{r}')\phi^*_{v'\mathbf{k}'}(\mathbf{r}'). \tag{5.7}$$

As one can see, the term containing the Coulomb interaction is common to BSE and TDDFT, whereas the exchange-correlation kernel (in TDDFT) and the screened interaction (in BSE) have different nature.

Part II

Developments and Applications

Chapter 6

Role of the Coulomb interaction v

> There was things which he streched, but mainly he told the truth.
>
> from The Adventures of Huckleberry Finn, Mark Twain

In this chapter we address some fundamental questions related to the role of the Hartree potential (or rather, its functional derivative, the Coulomb interaction v) in the dielectric response of finite and infinite systems. We briefly review the most important equations for both absorption and energy-loss using the formulation described in Par.1.5.1, which puts into evidence the different components of the Hartree term and therefore facilitates the comparison between the two neutral excitations spectra, for both finite and infinite systems. In order to compare finite and infinite systems, we decided to follow one possible path, namely to go from a periodic solid to isolated objects (atoms, molecules or clusters) by increasing the "lattice parameter". This path is easier to follow than the alternative one, namely to increase the size of an isolated object up to the bulk limit. Moreover, in this way, we can also address the performance of a solid-state approach (reciprocal space with periodic boundary conditions, i.e. a super-cell technique) to describe an isolated system.

Even though the formalism of TDDFT is used in this chapter, all discussions, results and conclusions are also valid within BSE.

This chapter will be resumed in F. Sottile, V. Olevano, A. Rubio and L. Reining, *Importance of the coulombian term in absorption and electron energy-loss spectra: finite versus infinite systems*, in preparation.

6.1 The local fields: $\bar{v}$

Eq. (3.15) reads, in reciprocal space, and in its retarded version,

$$\varepsilon_{\mathbf{G},\mathbf{G}'}(\mathbf{q},\omega) = \delta_{\mathbf{G},\mathbf{G}'} - v_{\mathbf{G}}(\mathbf{q})\tilde{\chi}_{\mathbf{G},\mathbf{G}'}(\mathbf{q},\omega). \tag{6.1}$$

Now, if ε were diagonal in $\mathbf{G}, \mathbf{G}'$, then $\varepsilon_M = \lim_{\mathbf{q}\to 0} \frac{1}{\varepsilon^{-1}_{00}} = \lim_{\mathbf{q}\to 0} \varepsilon_{00}(\mathbf{q},\omega)$ which is the case of the homogeneous electron gas. But normally, the dielectric matrix is not diagonal in $\mathbf{G}$ space, i.e. the microscopic dielectric function is position dependent and not only distance dependent. The local field effects (LFE) translate exactly this behavior: all elements in the matrix contribute to one element of the inverse matrix; LFE account for *inhomogeneities* at the microscopic level and can be very important for both photon and electron spectroscopies. As an approximation, one can of course define the macroscopic dielectric function without local fields (NLF) as

$$\varepsilon_M^{NLF} = \lim_{\mathbf{q}\to 0} \varepsilon_{00}(\mathbf{q},\omega) = \lim_{\mathbf{q}\to 0} [1 - v_0(\mathbf{q})\tilde{\chi}_{00}(\mathbf{q},\omega)] \tag{6.2}$$

which is just the macroscopic average of the microscopic dielectric function. $\varepsilon_M^{NLF} \neq \varepsilon_M$, except for the homogeneous electron gas.

We have given, in Par. s 1.5 and 2.7, a definition for the absorption (and EELS) in the framework of one-particle Fermi's golden-rule and static DFT, respectively. From a direct comparison between the Eq.s (6.2) and (1.31), one can see that the level of approximation of (1.31) (or even (2.23)) is the Random Phase Approximation (putting i.e. $\tilde{\chi} = \chi^0$), *but neglecting the local field effects*.

It is interesting and useful to remind that the term $\bar{v}$, as defined via (1.35), can be considered the responsible for the crystal local field effects.[1] This is quite easy to see within the RPA, i.e. putting $f_{xc}^{\mathrm{RPA}} = 0$ in the evaluation of the full polarizability (or equivalently $\tilde{\chi} = \chi^0$ in the (6.1))

$$\chi^{RPA} = (1 - \chi^0 v)^{-1}\chi^0.$$

In this matrix expression, now, we want to neglect $\bar{v}$, i.e. use only the $\mathbf{G} = 0$ contribution v_0 instead of the total v. Since the matrix $\chi^0 v_0$ has only the first column different from zero, so that the matrix $\mathsf{B} = 1 - \chi^0 v_0$ has the following peculiar structure (first column and main diagonal different from zero):

$$\mathsf{B} = \left(\begin{array}{c|c} 1 - v_0\chi^0_{00} & 0 \\ \hline -v_0\chi^0_{00} & \mathsf{I} \end{array}\right).$$

[1] In the following we just talk about "local fields" when referring to the crystal local fields, i.e. we do not include f_{xc} in the local fields, although this is sometimes done in literature.

The inverse dielectric matrix is

$$\varepsilon^{-1} = 1 + v\left(1 - \chi^0 v_0\right)^{-1}\chi^0$$

but, since we are only interested in the head of this matrix, we can directly write

$$\varepsilon^{-1}_{00} = 1 + v_0 \sum_{\mathbf{G}} (\mathsf{B})^{-1}_{0\mathbf{G}}\, \chi^0_{\mathbf{G}0}.$$

Because of the form of B, any element of the first line of B^{-1} vanishes, except the head

$$\mathsf{B}^{-1}_{00} = \frac{1}{\mathsf{B}_{00}} = \frac{1}{1 - v_0\chi^0_{00}}.$$

The head of the dielectric matrix becomes hence

$$\varepsilon^{-1}_{00} = 1 + v_0\frac{\chi^0_{00}}{1 - v_0\chi^0_{00}} = \frac{1}{1 - v_0\chi^0_{00}}$$

and therefore

$$\varepsilon_M = \frac{1}{\varepsilon^{-1}_{00}} = 1 - v_0\chi^0_{00} = \varepsilon^{NLF}_M.$$

This demonstrates that $\bar{v}$ is indeed responsible for the local field effects.[2]

This result has general validity and can be applied even if f_{xc} is taken into account. It is, in fact, sufficient to consider $\chi = (1 - \hat{\chi}v)^{-1}\hat{\chi}$, with $\hat{\chi} = (1 - \chi^0 f_{xc})^{-1}\chi^0$.

We have said that the local fields take into account the microscopic *inhomogeneities* of the system, but also the microscopic polarizability of the system itself is an important factor. The system, in fact, can be highly inhomogeneous, but if *locally* the polarizability is small, even the contribution of the local fields will be negligible. An example is shown in Fig. 6.I. The RPA response (with and without local fields) of an atom of beryllium (calculated in an fcc supercell) is reported in the upper panel of Fig. 6.I, showing an important contribution of the local fields. As a comparison, in the inset of the same

[2]We can also observe that, starting from an independent-particle polarizability χ^0, as defined in Eq. (2.21), that is just a sum of independent transitions, if the matrix inversion of ε is properly carried out, i.e. if LFE are included, the formerly independent transitions mix. In fact, the microscopic components of the Coulomb interaction $\bar{v}$ are part of the kernel of the Bethe-Salpeter equation (second of (3.23)). Even if the screened Coulomb interaction W is set to zero, the presence of $\bar{v}$ in the BSE prevents the eigenvectors of the excitonic Hamiltonian (3.37) to be δ-functions. This implies, hence, that there is a contribution due to the mixing of transitions in the calculation of the absorption spectrum (3.40). It is clear that this term is a Hartree, and not an exchange contribution. However, if we look at the diagonal part of (3.43) and (3.44), we have schematically, $H^{scr} \sim \int |\phi_c|^2 W |\phi_v|^2$ for the screened Coulomb interaction part of the Hamiltonian and $H^{exch} \sim \int \phi_c \phi_v^* \bar{v} \phi_v \phi_c^*$ for the electron-hole exchange part. The name "electron-hole exchange" then, follows from the shape of the latter, which is similar to the exchange term of the Hartree-Fock theory.

figure, the response of the correspondent bulk system (clearly more homogeneous than an isolated atoms in empty space), shows to which extent in this case the contribution of local fields is negligible.[3] However, in an atom of argon, whose RPA response is reported in the lower panel of Fig. 6.I, the difference between the response with local fields and the response without local fields is not enormous, even though the system (again an atom in empty space) is as inhomogeneous as before. This is because the atom of argon is not as polarizable as the beryllium one, and hence not capable of creating a strong microscopic local field. Moreover in the argon solid, which is less homogeneous than the beryllium solid, the local fields still have a not negligible contribution.

6.2 Absorption and EELS - Towards finite systems

We have seen in Par. 1.5 that ε_M determines the measured absorption (*Abs*) and Electron Energy Loss Spectra (EELS) as:

$$\text{Abs} = \Im\{\varepsilon_M\} \qquad ; \qquad \text{EELS} = -\Im\left\{\frac{1}{\varepsilon_M}\right\}.$$

It is evident that EELS and absorption are very closely related quantities (they both carry information about the electronic response of the system). At this point it is worth reminding that EELS is traditionally associated to collective plasmon excitations whereas particle-hole excitations (roughly proportional to the joint density-of-states) are thought to build up the absorption spectra. This argument stems directly form the fact that in an independent particle picture, the imaginary part of the microscopic dielectric function is given by Eq. (2.21), showing that single particle excitations dominate absorption. Instead the structure in EELS is mainly given by regions where both real and imaginary parts are close to zero, that is the classical condition for a collective (plasmon) mode (Chap. 2). Fig. 6.II schematically illustrates this behavior.

Following the formulation giving in Par. 1.5.1 for the absorption spectrum

$$\text{Abs} = -\Im\left\{\lim_{\mathbf{q}\to 0} v_0(\mathbf{q})\bar{\chi}_{00}(\mathbf{q},\omega)\right\} \quad ; \quad \bar{\chi} = \tilde{\chi} + \tilde{\chi}\bar{v}\bar{\chi}$$

and EELS

$$\text{EELS} = -\Im\left\{\lim_{\mathbf{q}\to 0} v_0(\mathbf{q})\chi_{00}(\mathbf{q},\omega)\right\} \quad ; \quad \chi = \tilde{\chi} + \tilde{\chi}v\chi = \tilde{\chi} + \tilde{\chi}(v_0 + \bar{v})\chi,$$

we can now elucidate the role of the Coulomb potential in the response function framework: the term $\bar{\boldsymbol{v}}$ **is responsible for the local field effects**, and the long range component $\boldsymbol{v_0}$ **is responsible for the difference between absorption and electron**

[3] To be precise, the bulk beryllium shown here is the fcc phase, and not the equilibrium bcc one. However, this does not influence the conclusions.

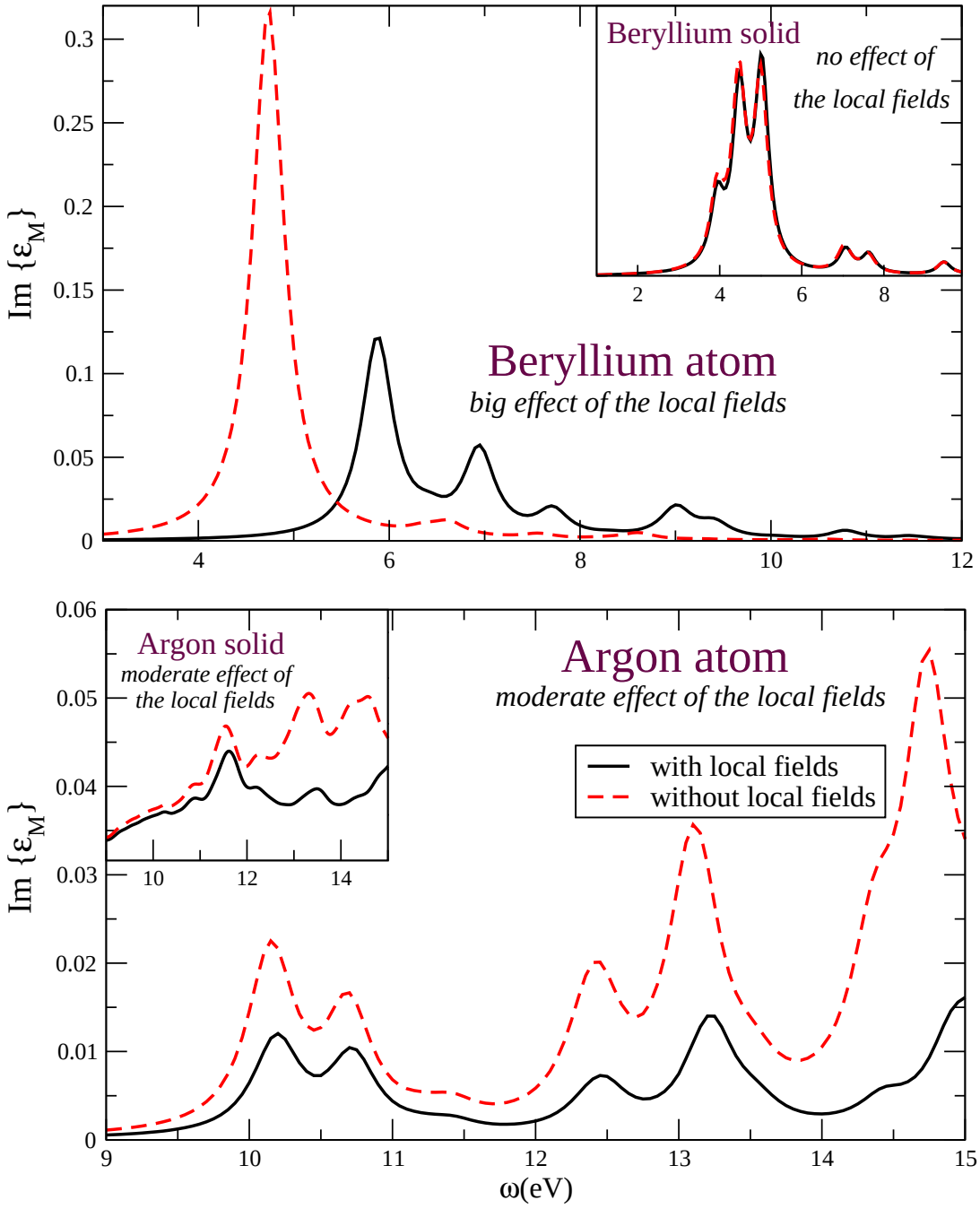

Figure 6.I: Imaginary part of the macroscopic dielectric function, with and without local field effects. Upper panel: atom of beryllium (unit cell parameter 48 a.u.). In the inset: the solid of beryllium. Lower panel: atom of argon (unit cell parameter 45 a.u.). In the inset: the solid of argon. The legend is the same for both panels.

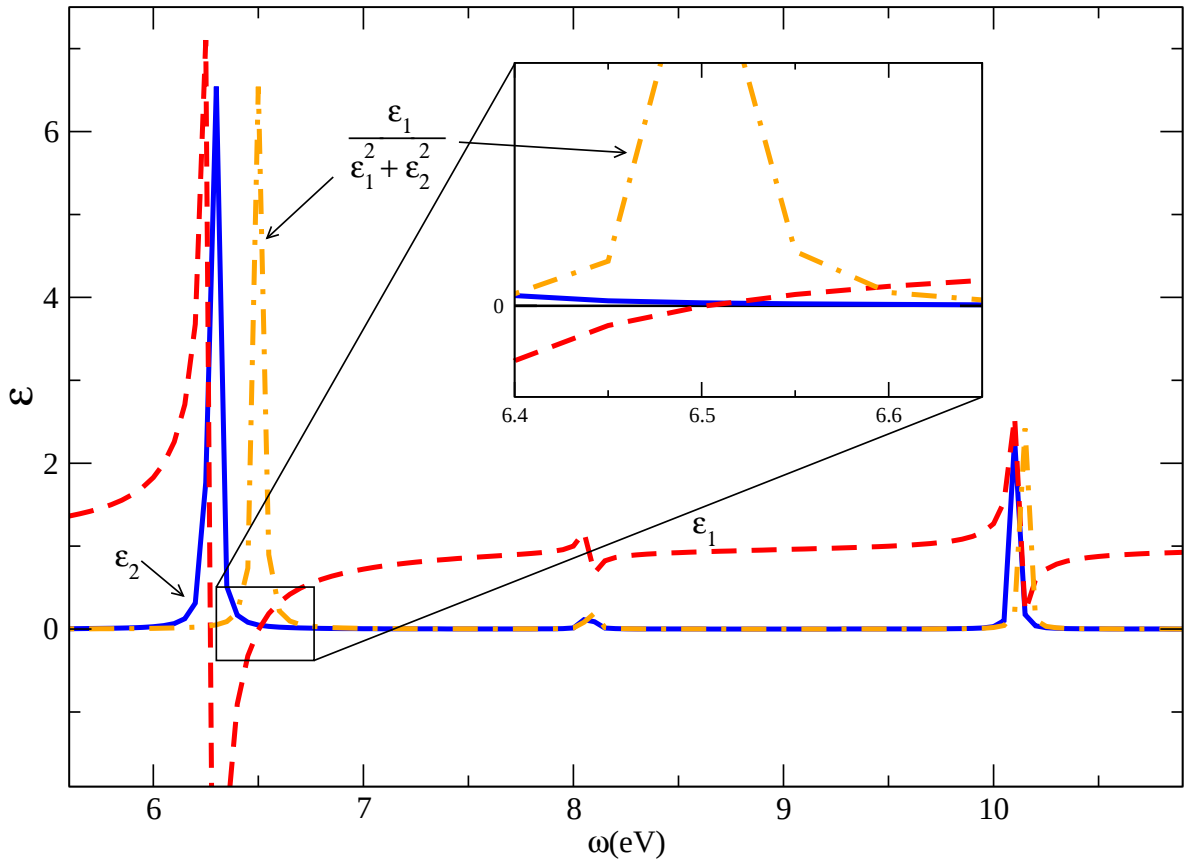

Figure 6.II: The absorption spectrum is given by the imaginary part of the (macroscopic) dielectric function (continuous curve). To a peak of the absorption spectrum corresponds an anomalous dispersion of the real part (dashed curve), i.e. the negative first derivative. The crossing of the real part ε_1 with the axis of frequency, leads to a peak in the loss function $-\Im\{\frac{1}{\varepsilon_M}\} = \frac{\varepsilon_2}{\varepsilon_1^2+\varepsilon_2^2}$ (dot-dashed curve). This collective excitation, called *plasmon*, can be excited using electron energy loss spectroscopy.

energy-loss. The latter, apparently subtle, difference is crucial for extended systems, as we can see in Fig. 6.II and, for a more realistic case, Fig. 6.V, showing EELS (plasmon peak at 16.8 eV) and absorption (at the range 3-5 eV) of bulk silicon. Since coming from the solid, one knows that the optical and electron energy-loss spectra are very different, one might expect that the same is true for finite systems. This is however not the case, as can be immediately understood: we have shown that the difference comes entirely from v_0. Whenever this contribution is negligible, absorption and electron energy loss spectra are equivalent.[4]

It is instructive to illustrate the previous discussion for the simplest case when LFE

[4]Since a finite system cannot explore infinite distances, one can expect that the long range term v_0 does not have a big effect in a finite system.

are neglected, i.e., $\bar{v} = 0$. In this case $\bar{\chi} = \tilde{\chi}$ and $\chi = \tilde{\chi} + \tilde{\chi} v_0 \chi$, and the description of absorption and EELS is then

$$\begin{cases} \text{Abs} = -v_0 \Im\{\bar{\chi}_{00}\} = -v_0 \Im\{\tilde{\chi}_{00}\} \\ \text{EELS} = -v_0 \Im\{\chi_{00}\} = -v_0 \Im\left\{\dfrac{\tilde{\chi}_{00}}{1 - v_0 \tilde{\chi}_{00}}\right\} \end{cases} . \tag{6.3}$$

Here it appears obvious that χ and $\bar{\chi}$ are fundamentally different (in χ, $\tilde{\chi}_{00}$ is screened, but not in $\bar{\chi}$), and that this fact is entirely due to the apparently tiny difference of the kernel in Eq. (1.34).

In order to make a comparison between absorption and EELS for both finite and infinite systems, we apply those equations for the case of a solid where the lattice parameter is increased, in order to go towards the limit of an isolated system. In doing this limit, we exploit the fact that $v_0 \tilde{\chi}_{00} \propto \frac{1}{\Omega}$ where Ω is the volume of the unit cell of the lattice. Thus the ratio between EELS and Abs given by Eq. (6.3) is

$$\frac{\text{Abs}}{\text{EELS}} = \left[1 + \frac{\alpha}{\Omega} + \frac{\beta}{\Omega^2}\right] \tag{6.4}$$

which clearly shows how absorption and EELS tend to give the same spectrum in an isolated system, when $\Omega \to \infty$. Here α and β are functions of the frequency and depend of course on the polarisation function $\tilde{\chi}$.

Eq. (6.3) can be straightforwardly generalized to the case when all LFE are included (see Appendix C for the derivation). This general case is obtained directly by replacing $\tilde{\chi}$ by $\bar{\chi}$ in Eq. (6.3), that is:

$$\begin{cases} \text{Abs} = & -v_0 \Im\{\bar{\chi}_{00}\} \\ \text{EELS} = -v_0 \Im\left\{\dfrac{\bar{\chi}_{00}}{1 - v_0 \bar{\chi}_{00}}\right\} \end{cases} . \tag{6.5}$$

It is clear that the same limiting behavior (6.4) still holds.

6.2.1 A simple model: "one-pole model"

Here we derive the frequency dependence of the α and β functions, appearing in Eq. (6.4) for the simplest case where only a single transition with frequency ω_0 dominates the response function. In this "one-pole model" the imaginary part of the dielectric function is given by a delta function in energy, that is:

$$\Im\{\varepsilon\} = \Im\{1 - v_0 \tilde{\chi}_{00}\} = \frac{v_0 A}{\Omega} \left[\delta(\omega - \omega_0) + \delta(\omega + \omega_0)\right], \tag{6.6}$$

and the corresponding real part is, by Kramers-Kronig

$$\Re\{\varepsilon(\omega)\} = 1 - \frac{2 v_0 A}{\pi \Omega} \frac{\omega_0}{\omega^2 - \omega_0^2}. \tag{6.7}$$

From this we can evaluate the ration between EELS and absorption to be

$$\frac{\text{Abs}}{\text{EELS}} = 1 - \frac{1}{\Omega}\left(\frac{4v_0 A\omega_0}{\pi(\omega^2-\omega_0^2)}\right) + \frac{1}{\Omega^2}\left[v_0^2A^2\left(\frac{4}{\pi^2}\frac{\omega_0^2}{(\omega^2-\omega_0^2)^2} + [\delta(\omega-\omega_0)+\delta(\omega+\omega_0)]^2\right)\right]. \quad (6.8)$$

Comparing with Eq. (6.4) we can infer the frequency dependence of $\alpha(\omega)$ and $\beta(\omega)$ for this model. We note that from (6.7), $\Re\{\varepsilon\}$ crosses the frequency axis when:

$$\omega = \pm\sqrt{\omega_0^2 + \frac{2v_0 A\omega_0}{\pi\Omega}}$$

this result shows how the plasmon peak corresponding to $\Re\{\varepsilon\} = 0$ moves towards the absorption peak at ω_0 as the cell volume Ω increases.

6.2.2 Importance of the limit $\mathbf{q} \to 0$

The electron energy loss, as defined up to now, has been limited to vanishing momentum transfer. It is worth reminding that a momentum transfer, when an electron (a massive particle) is involved, can be much greater than zero,[5] so that the case in study here ($\mathbf{q} \to 0$) is only one of a wide range of possibilities. However, we have limited ourselves to this case for the EELS results shown here, in order to compare with absorption, for which one assumes a vanishing momentum transfer $\mathbf{q}$.[6] Moreover, EELS is concerned with the response of the system to an external moving electron charge and probes the longitudinal response of the system for a finite transfer of momentum q. This is in contrast with absorption where the transverse photon-field response is addressed. It is worth here reminding that we are working with dipolar excitations. In fact, in the limit $\mathbf{q} \to 0$, the optical absorption can be described in the longitudinal gauge as the response of the system to a constant external E field, due to a potential linear in space. In this description, some similarity with the EELS, which probes the response of the system to the dipolar potential create by the moving charge is to be expected (there still is a subtle difference between photon and electron spectroscopy, due to the polarisation of the photon).

Experimentally the limit $q \to 0$ in EELS is very difficult to achieve, however if the size of the system is much smaller than $2\pi/q$, the response of the system can indeed be described in the limit $q \to 0$. When the dimension of the system is of the same order of magnitude as $2\pi/q$, then *size effects* appear, the limit $q \to 0$ is not fulfilled and the previous results are not applicable in this case.[7] We refer to the Appendix D for further discussions.

In the following hence, when referring to "absorption" and "EELS", we simply mean the imaginary part of ε_M and $-1/\varepsilon_M$, respectively.

[5] This is also true for X-rays, due to their high frequency, and it is used, for example, in Inelastic X-rays scattering, e.g. [259].

[6] Correct in the optical range, and for the systems and precision considered here.

[7] One above all: absorption and energy-loss spectra start to deviate from each other, and the long-range part of the electron-electron interaction is not negligible anymore.

6.3 Absorption versus EELS: Numerical analysis

We will now show the numerical results that illustrate the analytical conclusions in the previous section, and, on the other hand, remark some important results from a practical point of view. We have performed numerical simulations of a fcc-periodic array of Be atoms with an increasing lattice parameter in order to have atoms further apart from each other, i.e. a periodic representation of an isolated system. We have used the standard super-cell plane-wave representation of the electronic wavefunction for the ground state electronic structure and the Random Phase Approximation (RPA) for the response function,[8] i.e. $\tilde{\chi} = \chi^0$. Moreover, since we want to analyze the behavior of the system going towards a finite system, we sample the Brillouin zone only with the Γ point.

In the two panels of Fig. 6.III we show those results for the fictitious solids formed by Be atoms at various inter-atomic distances. We clearly see how the absorption and EELS spectra become similar as the cell size increases, considering or not local field effects. In particular for a cell with a lattice parameter of 55 a.u., both spectra are indistinguishable (the intensity of all the spectra of Fig. 6.III has been scaled by the factor $\frac{1}{\Omega}$, with $\Omega =$ volume of the unit cell).

Another fact that emerges from the calculations shown in Fig. 6.III is that the absorption spectrum converges much faster, with cell size, than the EELS one. This could be expected from the fact that the energy-loss spectrum is, by construction, more sensitive to long-range effects, therefore larger sizes are needed in order to numerically being able to eliminate interactions with neighbor cells. For a given cell-size the absolute error is going to be smaller in a super-cell calculation of absorption than in EELS. This provides us with a practical rule for computational purposes of spectra of finite-size structures.

This behavior is in perfect agreement with the analytical conclusions of Par. 6.2. We can make the comparison between EELS and absorption more quantitative by plotting the difference between the position of the first peak of both spectra as a function of cell size. This analysis is presented in Fig. 6.IV together with the extrapolation to large cell-volume of the analytical expression of equation (6.8). This extrapolation is done via a simple fitting function

$$f(\Omega) = a + \frac{b}{\Omega}$$

where f is the difference between the position of the peak of absorption and that of EELS; Ω is the volume of the unit cell. The parameters of the extrapolation appear in the legend and the fact that the asymptotic value $a = -0.004$ is very close to zero means a perfect superposition of the peaks of absorption and EELS in the limit of infinitely distance atoms, i.e, in the isolated atom limit. The good agreement of the fit gives further support to the analysis presented in previous Par. 6.2.

[8] Inclusion of better exchange-correlation functionals will not modify the conclusions of the present analysis.

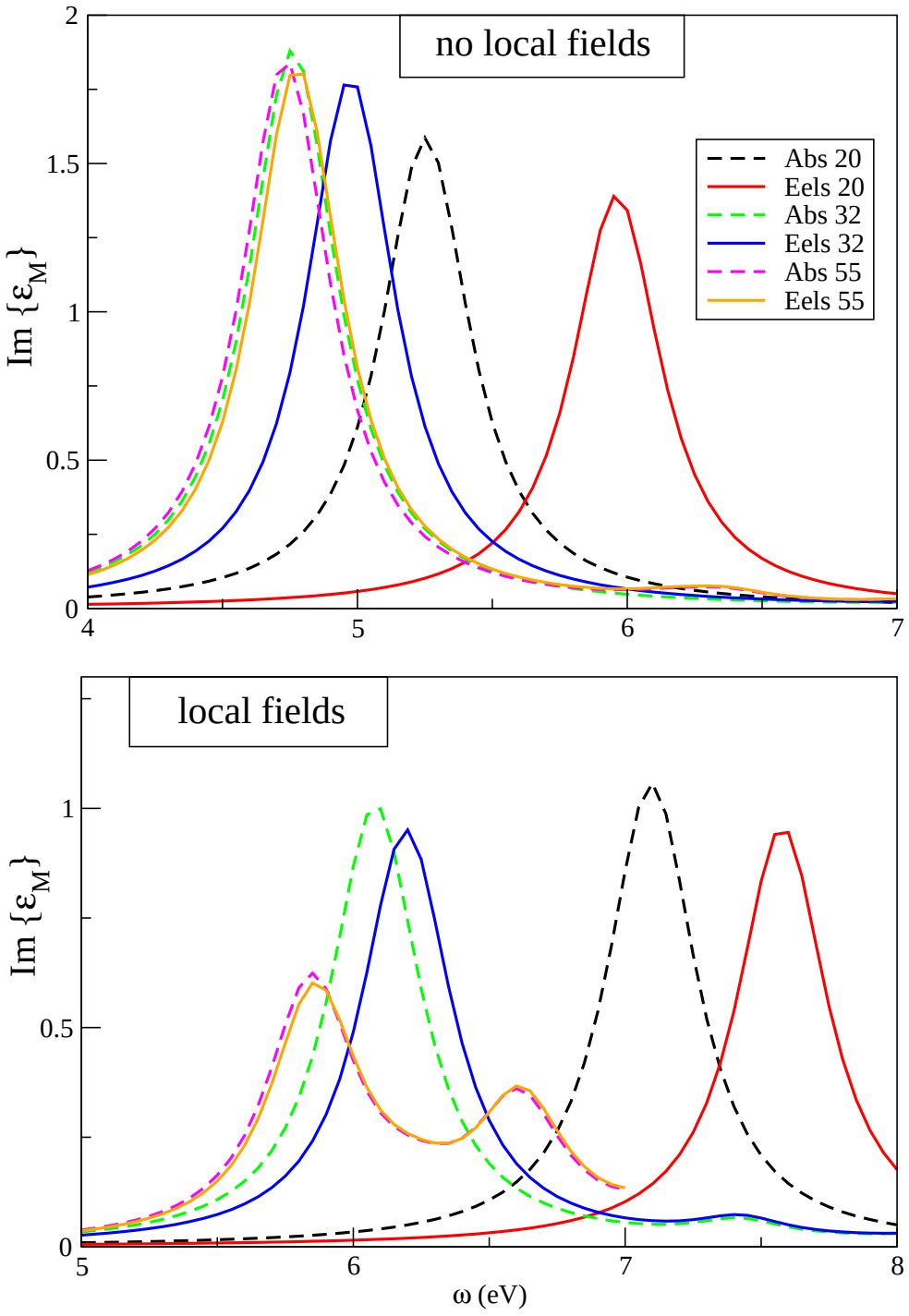

Figure 6.III: Absorption and EELS for several cell sizes: 20, 32, and 55 a.u. Upper panel: calculations made neglecting local fields. Bottom panel: local field effects included. The legend is the same for both panels.

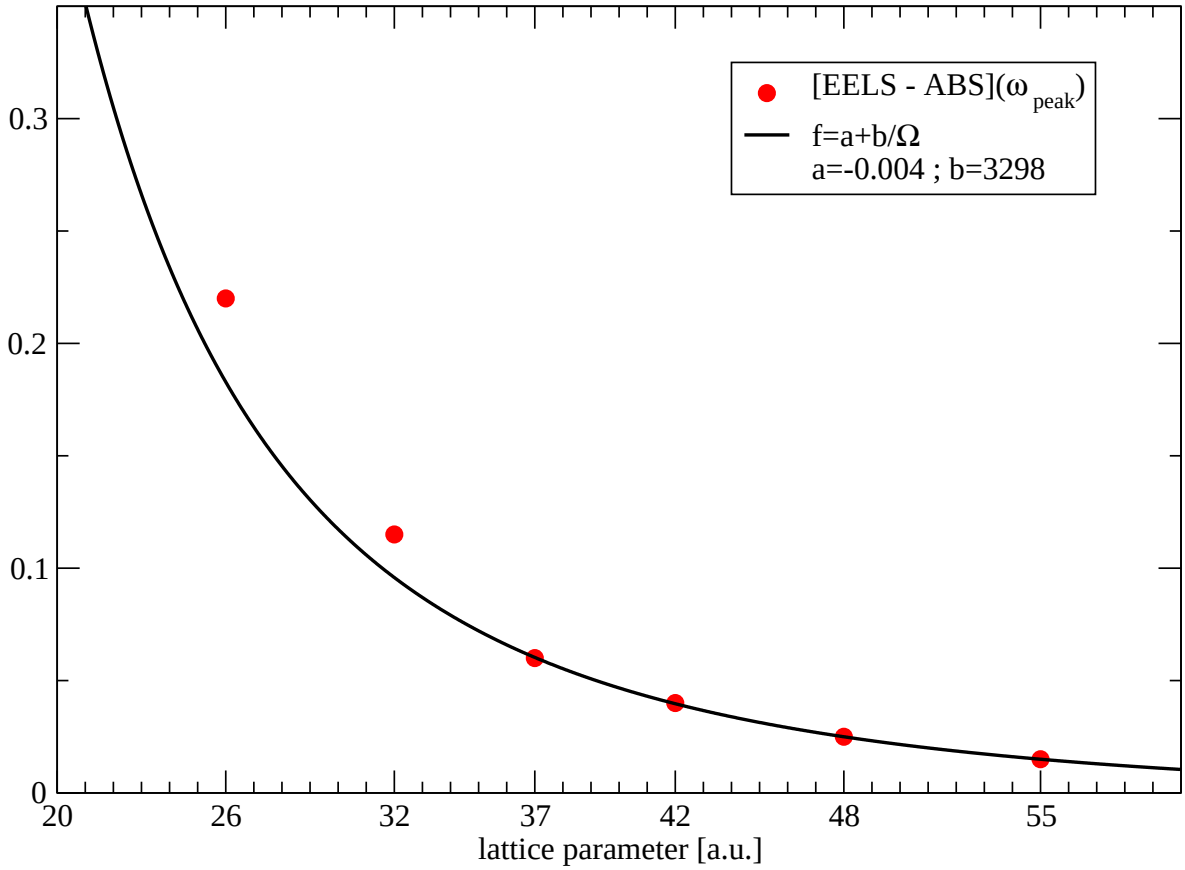

Figure 6.IV: Difference of the position of peaks of absorption and EELS as a function of the cell parameter. The extrapolation is represented by the full line.

6.3.1 Case of silicon: an "adiabatic connection"

Now let's have a look at a solid system. It is very useful to see the absorption and energy-loss spectra (within RPA and with local fields) for a real system, like silicon, in the same figure (Fig. 6.V). Following Eq. (1.33), the generalized spectrum $Z(\omega)$ defines EELS or absorption depending if the long-range component v_0 has been included or not:

$$\left.\begin{array}{r}\text{Abs}\\ \text{EELS}\end{array}\right\} = Z(\omega) = -\Im\{v_0(\mathbf{q}\to 0)S_{00}(\mathbf{q}\to 0,\omega)\}$$

with

$$S(\omega) = \left(1-\chi^0\alpha v_0 - \chi^0\bar{v}\right)^{-1}\chi^0.$$

If $\alpha = 1$, $Z(\omega) =$ EELS, and if $\alpha = 0$, $Z(\omega) =$ Abs. But we can also see in Fig. 6.V, how the EELS turns into Abs when v_0 is continuously (*adiabatically*) switched off. The case

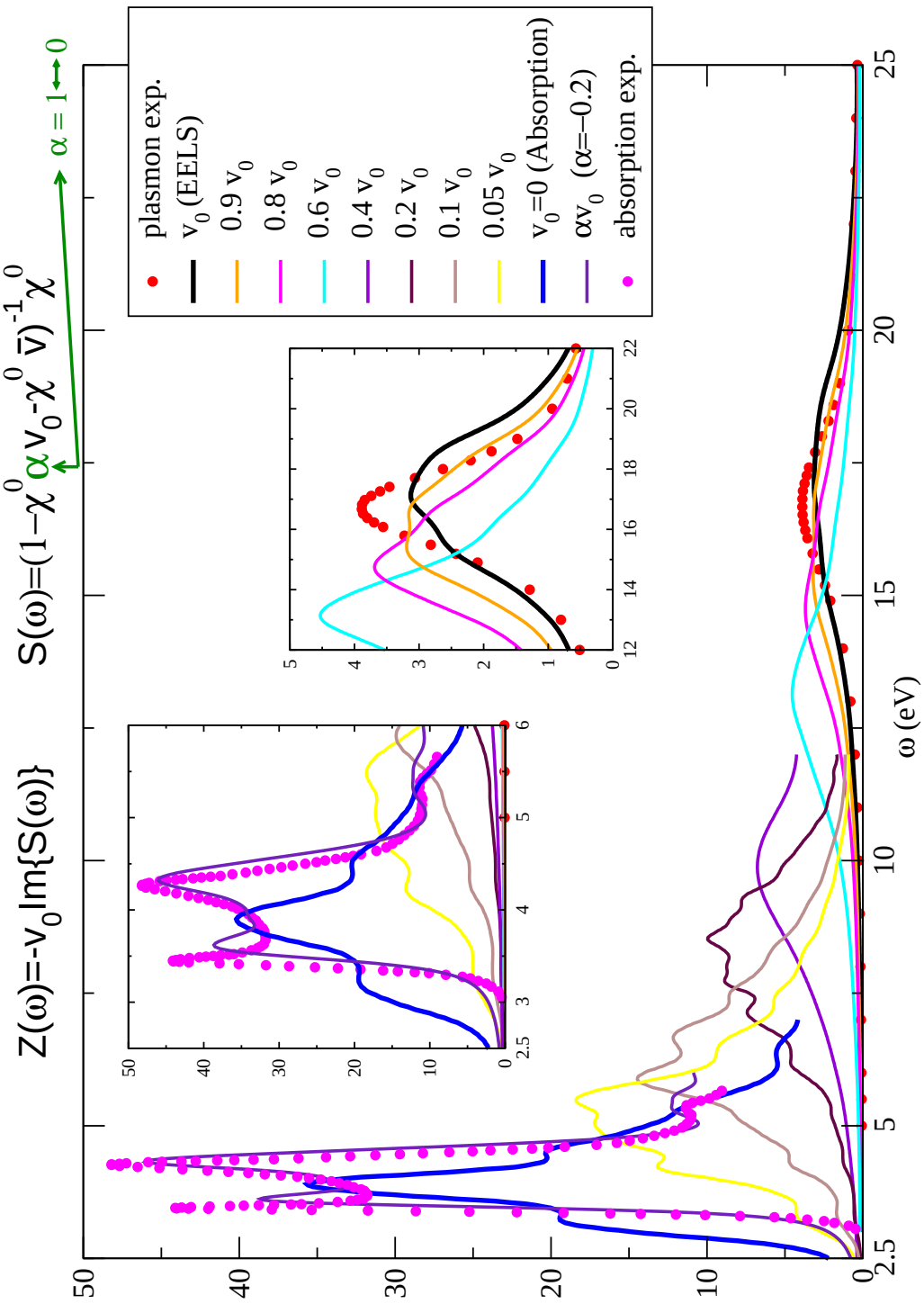

Figure 6.V: Continuous connection between EELS and Abs, via v_0. Experiments from references [98] (absorption) and [260] (EELS).

of the little *negative* portion of v_0, leading to a good agreement with the experiment,[9] corresponds to put an exchange-correlation kernel $f_{xc} = \alpha v_0 = -\frac{0.2}{4\pi q^2}$, that simulates excitonic effects, and will be discussed in Chap. 7. This illustrative example shows very well the action of the long-range component, and how its inclusion or exclusion can make the big difference between absorption and electron energy loss spectra.

6.4 Concluding remarks

In this chapter we have analyzed some fundamental questions related to the calculations of absorption and EELS spectra in finite and infinite systems. We have seen that the effects of the macroscopic contribution to the self-consistent variation of the Hartree potential turn out to be the key factor in determining the differences between absorption and EELS for extended systems. Instead, when the wavelength of the perturbation is much larger than the system size, the absorption and the electron energy loss spectra coincide. We have also discussed the role of this long-range contribution in order to address related questions of technical interest, demonstrating, in particular, that in a super-cell technique for finite systems, it is more suitable to calculate absorption than EELS, in order to obtain the same final result.

[9] In this case, a scissor operator (0.8 eV) has also been applied in order to reproduce the self-energy contribution, and let the kernel take care only of the e-h contribution. See Chap. 7.

Chapter 7

role of Ξ

> The sciences do not try to explain, they hardly even try to interpret, they mainly make models. By a model is meant a mathematical construct which, with the addition of certain verbal interpretations, describes observed phenomena. The justification of such a mathematical construct is solely and precisely that it is expected to work.
>
> John von Neumann

In this chapter we want to discuss about the second ingredient which plays an important role in the description of optical spectra of solids, namely the exchange-correlation kernel of TDDFT or, in the BSE, screened electron-hole interaction. We approximate this interaction in various ways, and discuss in particular the results obtained for a local contact potential. This, in fact, allows us to straightforwardly make the link to the TDDFT approach, and to discuss the exchange-correlation kernel f_{xc} that corresponds to the contact exciton [261, 262]. Our main results, illustrated at the examples of bulk silicon and argon, are that (i) the simple contact exciton model, used on top of an *ab initio* calculated band-structure, yields reasonable absorption spectra; (ii) qualitatively extremely different f_{xc} can be derived approximatively from the same Bethe-Salpeter equation. These kernels can however yield very similar spectra; (iii) a *static* f_{xc}, both with or without a long-range component, can create transitions in the quasi-particle gap. This is the first time that TDDFT has been shown to be able to reproduce bound excitons.

This chapter is resumed in

• F. Sottile, K. Karlsson, L. Reining and F, Aryasetiawan *Macroscopic and microscopic components of exchange-correlation interactions*, accepted by Phys. Rev. B.

• S. Botti, F. Sottile, N. Vast, V. Olevano, H.-Ch. Weissker and L. Reining, G. Onida, A. Rubio, R. W. Godby and R. Del Sole", *Long-range contribution to the exchange-correlation kernel of time-dependent density functional theory*, submitted to Phys. Rev. B.

7.1 Introduction

The electronic structure of semiconductors and insulators is well described by reliable *ab inito* methods [41, 42, 159, 263]. However, calculated optical properties adopting a scheme using free quasi-particle transitions exhibit severe shortcomings compared to experiment [33]. We have seen one example in Fig. 3.V, where both the Kohn-Sham and the GW-corrected band structures were used to calculate the transitions giving rise to the absorption spectrum of bulk silicon, neither of them leading to satisfactory agreement with the experiment. The neglect of the electron-hole interaction leads to an overall disagreement in the absorption strength as well as the complete failure to reproduce bound excitons. In fact, the calculated optical spectra typically underestimate the absorption strength at low energies and overestimate it at high energies. Early attempts to overcome these failures by including two-particle effects were made successfully using the effective-mass approximation [264] for bound excitons, and the solution of the Bethe-Salpeter equation (BSE) in a tight-binding approximation [191, 265] for the continuum spectra. Later the BSE has been solved on the basis of more realistic band-structures [94, 172, 202–204, 206, 207, 266]. In these works, essentially the BSE is written as an effective two-particle Schrödinger equation that contains the electron-hole interaction (3.35). This is also the approach adopted in this thesis. The agreement with experiment is greatly improved with respect to calculations in the Random Phase Approximation (RPA), where the electron-hole Coulomb interaction is neglected. Again, bulk silicon (shown in Fig. 3.VII) is a good illustration. Of course, the associated computational cost is relatively large.

One might try to overcome this difficulty either by searching for good approximations to the BSE that could make the calculations more efficient, or by adopting an alternative scheme for the description of electron-hole excitations, that could avoid the two-particle picture. In the next sections, we explore and relate both points of view. In particular, we go back to the old contact exciton idea [261, 262, 267]. Ultra-short ranged interactions like contact excitons seem at first sight not suitable for wide applications. However, the contact exciton model has been successfully used for the description of continuum exciton effects in a wide range of applications [261, 262, 268], and model calculations have also shown that it is able to produce one bound state [268, 269].

7.2 The contact exciton

As mentioned above, we will now consider the contact exciton approximation. It is clear that restricting the range of $W(\mathbf{r},\mathbf{r}')$ in Eq. (3.44) does not simplify the following calculations significantly, since the size of the matrix $W_{vc\mathbf{k}}^{v'c'\mathbf{k}'}$ is not decreased, contrary to what happens when a localized basis is used (as e.g. in the work of Hanke and Sham, Ref.s [191, 265]). In that case, the introduction of a contact interaction would of course be very useful and straightforward. However, for the purpose of discussion we have simulated the effect of a cutoff r_c in W in a Bloch-transition-space code [172, 202, 203]. To do so, we have replaced $W(\mathbf{r},\mathbf{r}')$ by $(W_0/4\pi)v(\mathbf{r}-\mathbf{r}')\Theta(r_c-|\mathbf{r}-\mathbf{r}'|)$. This expression is particularly easy to handle in a plane wave code, since its Fourier transform is simply $\delta_{\mathbf{G},\mathbf{G}'}(W_0/\Omega)v(\mathbf{G})(1-cos(r_c|\mathbf{G}|))$, where Ω is the crystal volume. With the parameters W_0 and r_c we can tune the interaction strength and -radius, keeping in mind that we expect an increase in W_0 to partially cancel a decrease in r_c. We have moreover introduced an additional parameter β multiplying the bare electron-hole exchange interaction $2\bar{v}_{vc\mathbf{k}}^{v'c'\mathbf{k}}$ from (3.43). Although, as pointed out in the previous chapters, this term is (despite its name "electron-hole exchange") not due to exchange-correlation but to Hartree effects, we found it useful to tune it by introducing β, for two main reasons: first, often the contact exciton model is discussed by neglecting this term (i.e. β=0 instead of the full expression with β=1); second, when we will make below the link to TDDFT all exchange-correlation terms will take a form similar to this contribution, which makes it important to investigate its effects from the beginning.

7.2.1 Technical details of the calculation of the spectra

The spectra have been obtained sampling the Brillouin zone with 256 shifted k-points (silicon) and 256 special Monkhorst-Pack points (argon; this case corresponds to 10 k-points in the irreducible Brillouin zone), and using 6 (3 valence and 3 conduction) bands. The number of $\mathbf{G}$ vectors $N_{\mathbf{G}}$ required by the BSE, GW-RPA and RPA calculations for both silicon and argon is $N_{\mathbf{G}} = 59$. The $N_{\mathbf{G}}$ requested for the contact exciton model calculation is $N_{\mathbf{G}} = 169$ and $N_{\mathbf{G}} = 411$ for silicon and argon, respectively. On the contrary, the long-range model in TDDFT turned out to require only 59 $\mathbf{G}$-vectors, as an RPA calculation. The self-energy shift for silicon (GW-RPA calculation) has been obtained using the GW-corrections, calculated in the plasmon pole model approximation; whereas for solid argon, a "scissor operator" (of 6.0 eV) has been applied, to simulate the GW-corrections, and hence to reproduce the experimental quasi-particle gap.

7.2.2 Bethe-Salpeter equation for variable interaction strength and radius: results

We first look at the effect of a variable interaction radius on a continuum exciton. Fig. 7.I shows results obtained for bulk silicon, in the two extreme limits: the continuous curve is the result of our Bethe-Salpeter calculation (same as Fig. 3.VII), known to be in good agreement with experiment [172, 202–204, 206], and significantly different from the GW-RPA one (dot-double-dashed curve, same as Fig. 3.V), i.e. the result that is obtained when $W_{vc\mathbf{k}}^{v'c'\mathbf{k}'}$ is neglected in (3.41). Crystal local field effects are correctly included through β=1, and, although screened, the electron-hole Coulomb interaction is naturally long-ranged, asymptotically proportional to $1/r$. The dashed curve has instead been obtained in the limit $r_c \to 0$, i.e. the Fourier transform of W is simply taken to be $(A/\Omega)\delta_{\mathbf{G},\mathbf{G}'}$, where $A = 2\pi W_0 r_c^2$ has a finite value (A=30 in atomic units) since an increasingly strong W_0 is supposed to compensate the vanishing r_c. This result is surprisingly close to the full BSE one, because the effect of all the long-range part of W has been incorporated in the strong value of W_0 and hence A. Consequently, also intermediate values of W_0 and r_c can be used to produce similar results: the dot-dashed curve is an example for $r_c = 3.8$ a.u. (which corresponds to half the next-neighbor distance in silicon), with $W_0 = 3.8$, whereas the dotted curve has been obtained with $r_c = 7.3$ and $W_0 = 2.5$ Up to here, the parameter β was always set to 1, i.e. to its default value for the correct description of local field effects. Playing with β it turns out that the effect of an increasing β can to a certain extent be canceled by an increase in W_0 (in fact, the contributions have opposite sign): the double-dot-dashed curve shows the result for $r_c = 3.8, W_0 = 4.4$ and $\beta = 2$.

Next, let us look at a strongly bound exciton, taking solid argon as an example.[1] The dots in Fig. 7.II represent the experimental absorption spectrum [270, 271], with the clear spin-orbit splitted $n = 1$ bound exciton peak at 12.1 eV, and a weaker $n = 2$ peak at about 13.8 eV. The continuous curve in Fig. 7.II is the GW-RPA result, where as above the electron-hole interaction is neglected but quasi-particle energies are used, instead of Kohn-Sham eigenvalues: of course, there are no structures in the quasi-particle gap. Instead, it is well known that the BSE using the full long-range W can reproduce bound excitons (see e.g. [94, 204, 206, 209, 272]) both concerning peak positions and intensities. It is now interesting to see whether reasonable results concerning the position of the $n = 1$ peak, its oscillator strength, as well as the presence of the higher-order peaks, can be obtained with a contact interaction W in the *ab initio* framework. The dashed, dotted, dot-dashed and double-dot-dashed curves are the results of the contact exciton obtained with $A = 20, 50, 52$, and 60, respectively. In fact a strong enough A succeeds to split a peak out of the continuum. This peak moves to lower energies with increasing A,

[1] We will again look at solid argon in Chap. 10, including careful convergence tests, precise BSE calculations and more precise analyses. For the qualitative discussions in the present chapter, these details are not essential.

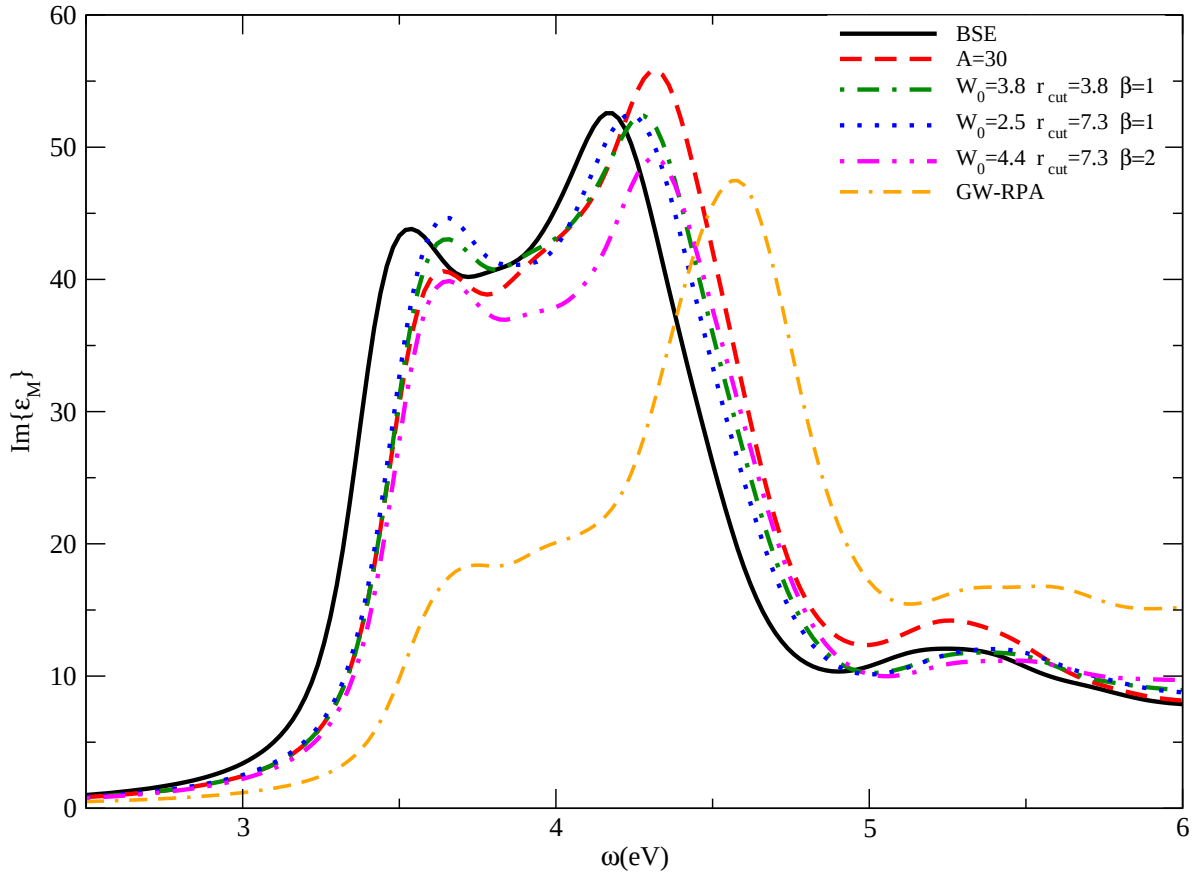

Figure 7.I: Imaginary part of the macroscopic dielectric function for silicon. Continuous curve: solution of the full BSE, Eq. (3.41), with (3.44). Dashed curve: contact exciton, strength of the contact interaction A=30. Dot-dashed, dotted, and double-dot-dashed curves: Solution of the BSE with a model Coulomb interaction of range r_c and strength W_0, and with an electron-hole exchange weighted by a factor β (see text); r_c = 3.8, 7.3 and 7.3; W_0 = 3.8, 2.5 and 4.4; β = 1, 1, and 2, respectively. Dot-double-dashed curve: GW-RPA, i.e. solution of Eq. (3.27) with $W = 0$.

and can in this way, with $A = 52$, be put on top of the experimental position. However, the relative intensity of the continuum close to the onset (at 14.1 eV) is underestimated, whereas a strong artificial peak appears at about 15.5 eV (not shown here). Moreover, no additional peaks in the quasi-particle gap are found. The intensity can be changed by changing β. For decreasing β (which corresponds to subtracting local field effects), oscillator strength is transferred to lower energies within the continuum, but the $n = 1$ bound exciton peak looses intensity, and almost disappears for $\beta = -1$ and A=42.

The results of this subsection can be summarized as follows: *a short-ranged but strong electron-hole Coulomb interaction can simulate the effect of the true, screened long-ranged one, to a certain extent: continuum exciton effects can be well reproduced, and one exciton*

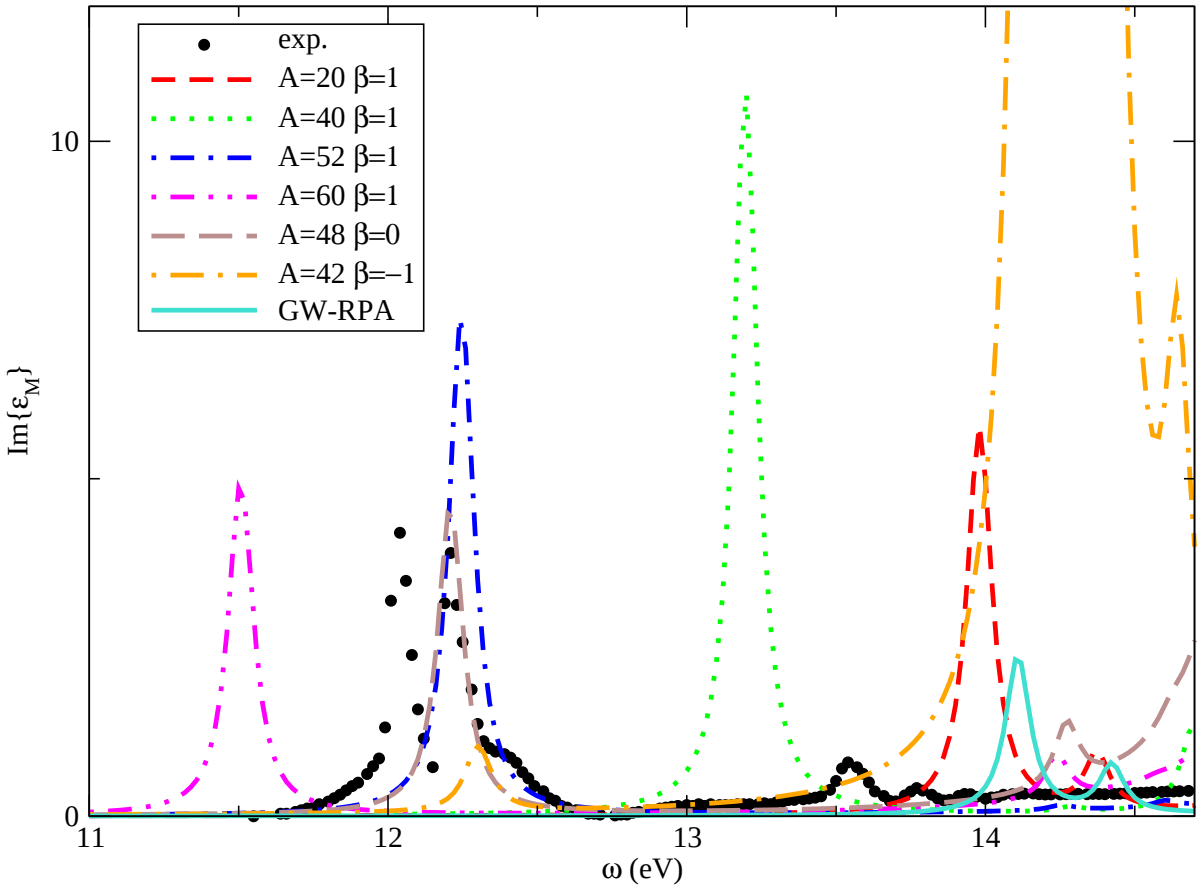

Figure 7.II: Imaginary part of the macroscopic dielectric function for solid argon. Dots: experiment [270, 271]. Continuous curve: GW-RPA, i.e. solution of Eq. (3.27) with $W = 0$. Dashed, dotted dot-dashed and double-dot-dashed curves: contact exciton, whose interaction strength varies from A=20 to 60 (see legend).

can be created. However, the continuum is not well described, and no higher-order peaks of the series are obtained, at least within the range of parameters explored here. Tuning the electron-hole exchange contribution allows to tune intensities, but still, the description of a whole series seems out of reach. Nevertheless, it is important to see that such a simple model can in principle yield a bound exciton.

In the following, we will see how these findings can be used in the context of TDDFT.

7.3 Links between the Bethe-Salpeter equation and TDDFT

7.3.1 The contact exciton and the TDDFT kernel

Although derived in a different framework, the BSE and the TDDFT equations can be written in a very similar way, as we have seen in Chap. 5 (Eq.s (5.4)), which suggests that it is straightforward to exchange information between the two approaches. This is of course not completely true in view of the fundamental difference between the matrices W and f_{xc} (Eq.s (3.44) and (5.7), respectively). It is hence not surprising to encounter a number of seeming contradictions or at least ambiguities. The most obvious one is the question whether f_{xc} should be short- or long-ranged. The usefulness of a long-range contribution in f_{xc} has been suggested and/or confirmed by various authors [188, 273–278], including calculations done in the framework of this thesis [188]. On the other side, having strongly bound electron-hole pairs might suggest that one is dealing with short-range effects. Let us take as the most striking example the contact exciton model. Two approaches to the problem of finding the corresponding f_{xc} are then possible. First, in TDDFT one can obtain the macroscopic dielectric function from the same modified response function $\bar{\chi}$ as in the BSE framework, through

$$\Im\{\varepsilon_M\} = -v_0(\mathbf{q})\Im\{\bar{\chi}_{00}(\mathbf{q},\omega)\};$$

however, now $\bar{\chi}(\mathbf{G},\mathbf{G}';\mathbf{q},\omega)$ can be directly found from a two-point matrix screening equation, analogous to that one for χ in Eq. (4.7):

$$\bar{\chi} = \chi^0 + \chi^0(\bar{v} + f_{xc})\bar{\chi}. \tag{7.1}$$

If f_{xc} is supposed to have only a $\mathbf{G} = \mathbf{G}' = 0$, i.e. the long-range, contribution, this equation can be re-written as [275]

$$(\varepsilon_M(\omega) - 1) = (\varepsilon_M^{RPA}(\omega) - 1) + (\varepsilon_M^{RPA}(\omega) - 1)\frac{f_{xc}}{v_{\mathbf{G}=0}}(\varepsilon_M(\omega) - 1), \tag{7.2}$$

where $\varepsilon_M^{RPA}(\omega)$ is defined to be the RPA macroscopic dielectric function, i.e. $\varepsilon_M^{RPA} = 1 - v\bar{\chi}$ using (7.1) when f_{xc} is neglected. This, as already pointed out in Ref. [275], is equal to the contact exciton Eq. (7) of Ref. [261, 262]

$$(\varepsilon_M^{RPA} - 1) = \frac{(\varepsilon_M^{RPA} - 1)}{1 + g(\varepsilon_M^{RPA} - 1)}$$

when the scalar factor g in that work is identified to be $g = -f_{xc}/v(\mathbf{G} = 0)$. In other words, the short-range contact exciton approximation to the BSE seems to be equivalent to the long-range-kernel approximation in TDDFT, since one obtains $f_{xc} = -g4\pi/q^2$.

This latter approach is in fact known to yield a good description of continuum exciton effects [273].

On the other hand, however, one could simply write down (in the here, as usual, adopted static approximation for the electron-hole interaction) the exchange-correlation contribution to the Bethe-Salpeter kernel in real space:

$$^4W(\mathbf{r}_1, \mathbf{r}_2, \mathbf{r}_3, \mathbf{r}_4) = -\delta(\mathbf{r}_1 - \mathbf{r}_3)\delta(\mathbf{r}_2 - \mathbf{r}_4)W(\mathbf{r}_1, \mathbf{r}_2) \tag{7.3}$$

and compare to the corresponding four-point expression for f_{xc}:

$$^4f_{xc}(\mathbf{r}_1, \mathbf{r}_2, \mathbf{r}_3, \mathbf{r}_4) = 2\delta(\mathbf{r}_1 - \mathbf{r}_2)\delta(\mathbf{r}_3 - \mathbf{r}_4)f_{xc}(\mathbf{r}_1, \mathbf{r}_3). \tag{7.4}$$

If one replaces in (7.3) $W(\mathbf{r}_1, \mathbf{r}_2)$ by the contact approximation $W(\mathbf{r}_1, \mathbf{r}_2) = A\delta(\mathbf{r}_1 - \mathbf{r}_2)$, it is easily possible to choose the kernels $^4W(\mathbf{r}_1, \mathbf{r}_2, \mathbf{r}_3, \mathbf{r}_4)$ and $^4f_{xc}(\mathbf{r}_1, \mathbf{r}_2, \mathbf{r}_3, \mathbf{r}_4)$ (and hence the resulting spectra) to be equal, namely by postulating

$$f_{xc}^{contact}(\mathbf{r}_1, \mathbf{r}_3) = -\frac{1}{2}\delta(\mathbf{r}_1 - \mathbf{r}_3)A : \tag{7.5}$$

an ultra-short range kernel is found, in apparent contradiction to the above considerations and to the finding of Ref. [275].

In order to reconcile the two contradictory - i.e. the short-range and the long-range - f_{xc}'s one has to realize that we are talking about *effective* kernels. I.e., we are performing a certain number of mappings that allow one to obtain a desired final result (namely a given spectrum), and that are not necessarily unique if the number of equations that have to be fulfilled is inferior to the number of free parameters. The contact exciton problem is a very good illustration for this point. First, of course, within the BSE framework the true screened long-range Coulomb interaction is mapped upon a short-range function of modified strength; this is just the starting point which is the same for both the derivation of a long-range and of a short-range f_{xc}. Once this starting point is fixed, the short-range f_{xc} (Eq. (7.5)) is in fact an *exact* solution of the problem, for any number of transitions or part of the spectrum that is considered. Instead, when one (as it is often done in the framework of the contact exciton) neglects microscopic components (the local field effects), a new mapping has to be done. Now, the sole $\mathbf{G} = \mathbf{G}' = 0$ element of f_{xc} has to reproduce the effect of the full Fourier transform of f_{xc}, i.e. of $A\delta_{\mathbf{G}\mathbf{G}'}$, which is significant, in particular since it is not decaying with increasing $|\mathbf{G}|$. In order to have a non-negligible effect with the sole head element of f_{xc}, the latter must of course diverge as $1/q^2$ since in (7.1) f_{xc} is multiplied with χ^0, that goes to zero as q^2. $f_{xc} = -\alpha/q^2$ should hence yield an approximate, even though possibly very good (with respect to the contact-BSE calculation), spectrum. In principle, it could even yield the correct spectrum (i.e. a spectrum identical to that resulting from the corresponding contact-BSE calculation) if α was chosen to be frequency-dependent: if only an absorption spectrum (i.e. $1/\varepsilon^{-1}(0, 0, \omega)$, and not the whole matrix $\varepsilon^{-1}(\mathbf{G}, \mathbf{G}', \omega)$) is asked for, one additional degree of freedom is

in fact sufficient to allow for an exact solution of Eq. (7.2) with respect to f_{xc}. Note that an approximate quadratic dependence of α upon frequency is suggested by the formula given in Ref. [261, 262], stemming from the energy factor between the matrix elements of the velocity operator and those of the dipole operator.

In general, the "exact" kernel corresponding to a given W can of course not be derived so easily, and an approximate mapping has anyway to be performed. The question is then not so much to search for a kernel close to the "exact" one, but to work with a form of the kernel that allows a relatively straightforward mapping, preferably with few parameters, or parameters that can be determined from first principles. In this sense, a long-range version of f_{xc} has already proven to be successful [188, 273, 274], whereas a corresponding breakthrough for a hypothetical short-range version has not yet been achieved. This adds to the fact that of course a realistic W and the resulting f_{xc} *are* of long range.

7.3.2 Continuum excitons: numerical results for different TDDFT kernels

Let us first confirm these discussions with numerical results for the case of a continuum exciton, namely again in silicon. Fig. 7.III shows the standard result of a full BSE calculation (continuous curve), and the result of a fit using the long-range kernel $f_{xc} = -\alpha/q^2$ with $\alpha = 0.2$ (dotted curve), both known to be in good agreement with experiment (dots).[2] The dashed curve is now the result obtained for the ultra-short ranged f_{xc}, Eq. (7.5): it is, as it should be, identical to the contact exciton result (dashed curve of Fig. 7.I), since it has been calculated using the same strength of the interaction $A = 30$. Therefore, it is also in good agreement with the BSE and with experiment. *An ultra-short range kernel can hence yield very similar results to those of an ultra-long range one.*

7.3.3 The TDDFT kernel and bound excitons

Up to now, the question of bound excitons in solids has never been addressed in the framework of TDDFT, and could even seem to be out of reach. However, the situation is far from desperate. First, the above discussions and results for the contact exciton immediately tell us that already a simple, static, contact kernel must be able to produce at least one bound exciton peak, since it will yield the same results as a contact BSE calculation, which in turn yields a bound peak. Second, it is instructive to discuss how a scalar f_{xc} should look like in order to be able to produce bound excitons. To do so, we take the imaginary part of the scalar equation

$$\bar{\chi} = \chi^0 + \chi^0 f_{xc} \bar{\chi} \tag{7.6}$$

[2] This is the same result as the one shown in Fig. 6.V.

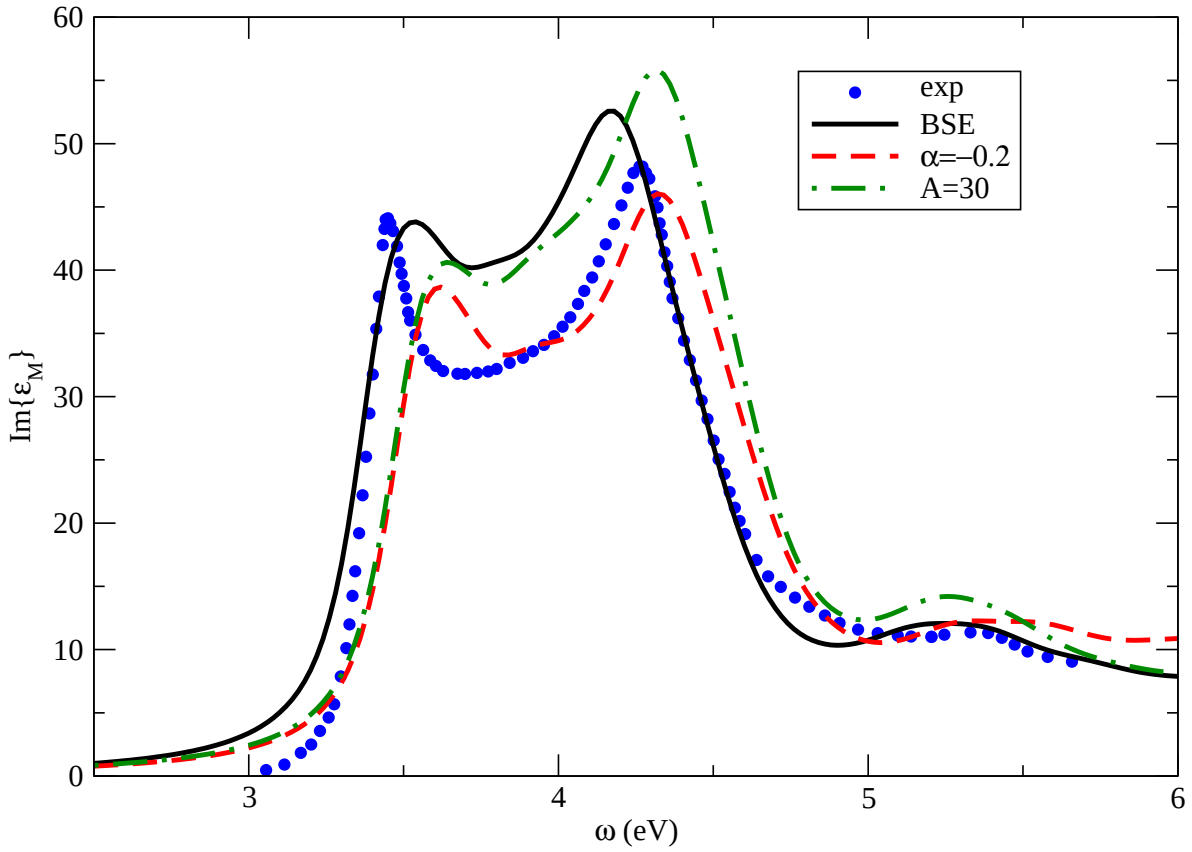

Figure 7.III: Imaginary part of the macroscopic dielectric function for bulk silicon. Continuous curve: BSE, i.e. solution of Eq. (3.41) with the full static RPA W. Dotted curve: TDDFT Result for $f_{xc} = -0.2/q^2$. Dashed curve: TDDFT contact kernel, strength of the contact kernel A/2=15. Dots: experiment [98].

("scalar" means that only the head ($\mathbf{G} = \mathbf{G}' = 0$) elements are treated for all matrices). As above χ^0 is supposed to be constructed using the quasi-particle band-structure and may or may not already include $\bar{v}$, i.e. crystal local field effects.[3] Below the quasi-particle gap, the imaginary part of χ^0 is hence vanishing, whereas, if bound excitons are present, at those frequencies the imaginary part of $\bar{\chi}$ does *not* vanish. Therefore, one obtains

$$\Im\{\bar{\chi}\} = \Im\left\{(1 - \chi^0 f_{xc})^{-1}\right\} \Re\{\chi^0\} \tag{7.7}$$

or

$$\Im\{\bar{\chi}\} = \frac{\Re\{\chi^0\}\Im\{f_{xc}\}}{(1 - \Re\{\chi^0\}\Re\{f_{xc}\})^2 + (\Re\{\chi^0\}\Im\{f_{xc}\})^2} \Re\{\chi^0\}. \tag{7.8}$$

[3]As a matter of fact, the Eq. (7.6) given above, does not contain the local fields, but a simple substitution of χ^0 with $\hat{\chi} = (1 - \chi^0 v)^{-1}\chi^0$ in (7.6) (and in the following), automatically permits one to correctly take into account the local field effects.

It is hence clear that sharp structures below the gap can show up when f_{xc} has a small or vanishing imaginary part, and when $\Re\{f_{xc}\} = 1/\Re\{\chi^0\}$. This can be rewritten as

$$\Re\{f_{xc}\} = -\frac{\alpha}{4\pi} v \tag{7.9}$$

with

$$\alpha = \frac{4\pi}{\Re\{\varepsilon_M^{RPA}(\omega_0)\} - 1}, \tag{7.10}$$

where we have introduced the parameter α by analogy to Ref. [273]. Note that $\varepsilon_M^{RPA}(\omega_0)$ has to be taken at the frequency ω_0 where the bound exciton occurs. For semiconductors with very weakly bound excitons, i.e. close to the onset of the continuum, $\Re\{\varepsilon_M^{RPA}\}$ is big (typically bigger than 10) and α becomes inversely proportional to the screening, as we have predicted in Ref. [188] for the continuum excitons. For insulators, the bound exciton peaks can occur far in the quasi-particle gap, where $\Re\{\varepsilon_M^{RPA}\}$ takes a value close to the static one, which can be almost 1.0 as in the case of argon. As a consequence, α has to be very large. Several features found above or below can immediately be understood from these formula: (i) when local field effects are included, $\Re\{\varepsilon_M^{RPA}\}$ becomes smaller, i.e. closer to 1, and therefore α, i.e. the strength of the contact interaction, must be increased in order to get the bound exciton; (ii) the size of an α able to create a strongly bound exciton must be such that, if it is taken to be static, its effect on the continuum must be dramatic. In other words, it is not very probable that such a scalar static f_{xc} can yield *at the same time* bound excitons and a good spectrum in the continuum. Due to (i), this must be even worse when local field effects are included; (iii) $\Re\{\chi^0\}$ being a smooth and monotonic function below the gap, a static f_{xc} will cross it only once along the frequency axis. It is hence impossible to obtain more than one bound exciton peak. In order to get a series of bound excitons a scalar f_{xc} has hence to be oscillating around $\Re\{\chi^0\}$. Bound exciton peaks will then occur at each crossing.

This suggests that one bound exciton can be created by a *static, scalar, long-range* kernel. We will in the following show numerical results for solid argon. Fig. 7.IV contains again the experimental result (dots) and also the best contact fit (dot-dashed curve, same as dot-dashed curve of Fig. 7.II, since, as we have shown, for the contact exciton case BSE and TDDFT results perfectly coincide[4]). The continuous curve is now obtained using f_{xc} from Eq. (7.9), choosing of course the position of the experimental peak for ω_0, which leads to $\alpha = 10$. As predicted, the static long-range kernel *is* able to produce one bound

[4]Note that this is only true at convergence. In fact, since the contact kernel is constant in reciprocal space, its head element alone, multiplied with $\chi^0(\mathbf{q} \to 0) \sim q^2$, does not have any effect. This is also the reason for the frequently heard opinion that a short-range kernel would have a negligible effect. A large number of **G**-vectors has to be included in the calculations, contrary to the case of $f_{xc} = -\alpha/q^2$ where $G = 0$ alone already yields results close to the converged ones. We have, in fact, carried out calculations [188] neglecting all $\mathbf{G} \neq 0$ terms, and obtained results (for silicon) that are indistinguishable from the ones that are obtained using also the $\mathbf{G} \neq 0$ components (of course, with the same α).

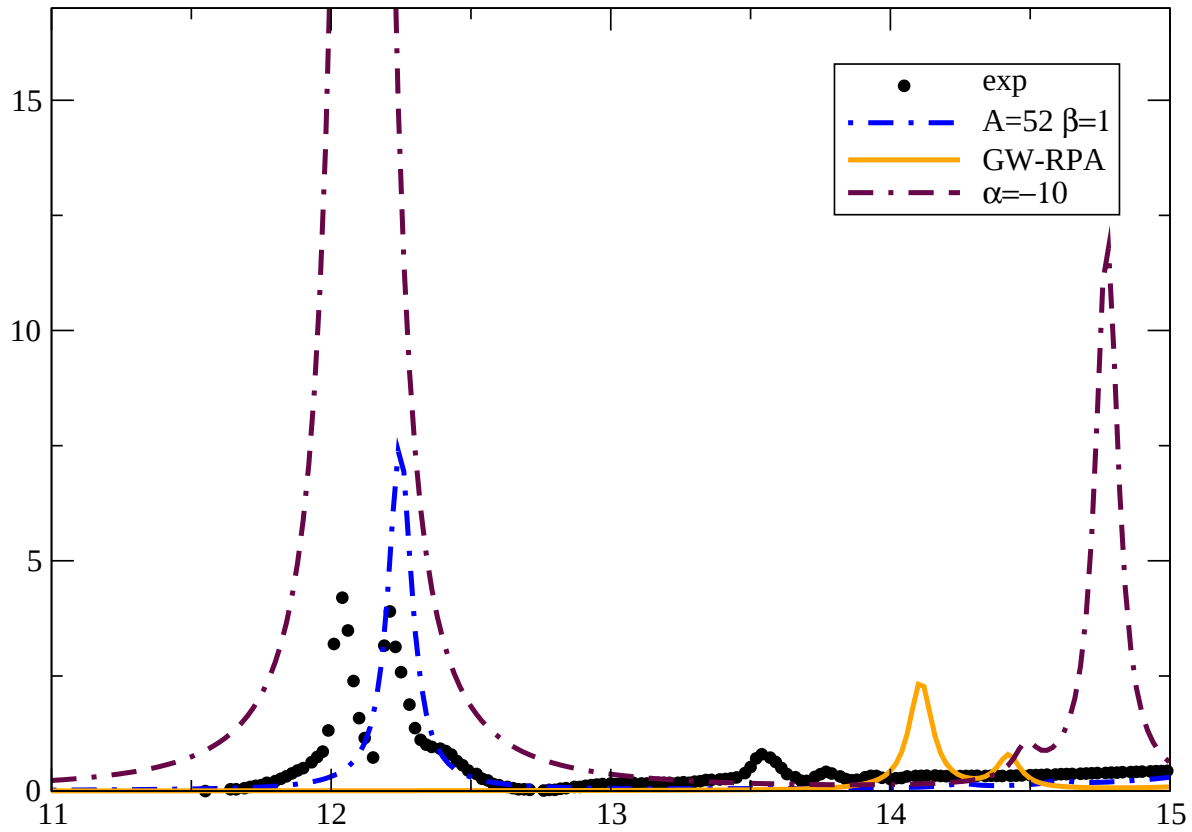

Figure 7.IV: Imaginary part of the macroscopic dielectric function for solid argon. Dots: experiment [270, 271]. Dot-dashed curve: contact exciton, strength of the contact interaction A=52. Continuous curve: TDDFT Result for $f_{xc} = -10/q^2$.

exciton peak. Its relative intensity, however, is now strongly overestimated, contrary to the contact case.

This suggests that a mixing of short- and long-range contributions in a still static model could be sufficient to obtain overall satisfying results.

It should be pointed out that building model f_{xc}'s based on short- and long-range Coulomb components is also suggested by several findings in the literature: first, $v_{xc}(\mathbf{r}) = -\int d\mathbf{r}'\rho(\mathbf{r}')v(\mathbf{r}-\mathbf{r}')$ and $f_{xc}(\mathbf{r},\mathbf{r}') = -v(\mathbf{r}-\mathbf{r}')$ yield exact results for the excitation energies of an isolated electron in an external potential [94, 279], and $f_{xc}(\mathbf{r},\mathbf{r}') = -v\Theta(r_{cut} - |\mathbf{r}-\mathbf{r}'|)$ has been suggested for a model system of non-overlapping valence electrons [94]. Further evidence is given for example by results obtained on bulk aluminum: an RPA calculation of the dynamical structure factor [280] shows that for large momentum transfer the results are considerably better when χ^0 instead of the full RPA response function $\chi = (1-\chi^0 v)^{-1}\chi^0$ is used, in other words, when the RPA kernel (i.e. the bare

Coulomb interaction v) is neglected: this is equivalent to choosing $f_{xc} = -v$.

7.4 Concluding remarks

The long-range Coulomb electron-hole interaction is the source of enormous complications concerning the efficient and reliable *ab initio* calculation of absorption spectra. In this chapter, we have therefore studied in detail the effects of its macroscopic and microscopic components, on the absorption spectra of various bulk semiconductors and insulators. We have used the insight gained in this way in order to propose models for a static exchange-correlation kernel f_{xc}, that yield promising results for continuum and bound excitons. More in particular, we have seen a series of results suggesting that a simple model for the exchange-correlation kernel as

$$f_{xc} = -\frac{\alpha}{4\pi|\mathbf{r} - \mathbf{r}'|} + \gamma\delta(\mathbf{r} - \mathbf{r}')$$

i.e., a contact plus a long-range interaction, might give results qualitatively, and sometimes quantitatively, in agreement with experiments.

In the next chapter, we provide an *ab initio* parameter-free kernel for the TDDFT, and we might therefore wonder whether models are still needed. However, even though, in principle, less cumbersome than the BSE, the use of a complicated *ab initio* kernel will always be more demanding than a RPA calculation, whereas model kernels proposed in the present chapter do not add computational complexity with respect to the RPA. Thus, the possibility to have a very simple model to verify a behavior, or also to rapidly obtain preliminary results, is still to be considered very useful. Besides this, the contact exciton model *is* used for applications [261, 262, 268], and so a "contact-TDDFT" could be. Moreover it is not *a priori* excluded that it will eventually be possible to determine the parameters without fitting to experiment.

The results are hence promising, in particular since we have shown for the first time that TDDFT, even in a static approximation, can yield bound excitons in a solid.

Chapter 8

TDDFT: parameter-free exchange-correlation kernel from the BSE

> The important thing in science is not so much to obtain new facts as to discover new ways of thinking about them.
>
> Sir William Bragg

We have seen, in the previous chapter, several attempts to go beyond the ALDA in practical calculations of solids, and how it is possible, to a certain extent, to improve the description of an optical spectrum of a crystal, in the framework of TDDFT, with respect to the RPA. Other examples can be found in literature. Ref.s [281, 282] contain a many-body diagrammatic expansion for the exchange-correlation kernel and discuss some fundamental questions, like the non-locality of f_{xc}. Ref. [283] is situated in the framework of current-density functional theory [284]. An effective long-range kernel is proposed that improves the RPA and ALDA results for the optical spectra of various bulk semiconductors, including silicon and diamond. In Ref. [285] an "exact exchange-only" (EXX) kernel is derived as the first order term of an expansion in the framework of the adiabatic-connection perturbation theory [286]. In Ref. [274] this kernel and the EXX potential are used to calculate the optical absorption spectrum of bulk silicon and again, the result is considerably improved with respect to the RPA. In Ref. [273] an analytical expression for f_{xc} is found from a comparison with MBPT, using the successful approximations of the latter, namely the GW form for the self-energy and a static electron-hole interaction in the BSE. Only the long-range limit (vanishing wave-vector q) of the resulting $f_{xc}(\mathbf{q})$ is then explicitly studied, which is sufficient to demonstrate that a $1/q^2$ divergence of f_{xc} can be able to reproduce excitonic effects in the optical spectra of bulk silicon. This approximation was also used in Chap. 7 of this thesis.

However, none of the above numerical calculations, included of course, the results presented in Chap. 7, are truly *ab initio*: empirical parameters, corrections or cutoffs are used in all cases to fit the results to experiment. In Ref. [283], material-dependent rigid shifts of the spectra and an empirical prefactor to adjust intensity ratios are used. In Ref. [274] finite, non negligible terms in the expression of the kernel are cut off to avoid the otherwise occurring "collapse" of the resulting spectra, and to fit the result to the experiment. Finally in Chap. 7 of this thesis, tuning the parameter(s) of the contact exciton model is crucial to fit the experiment, and the $1/q^2$ divergence in f_{xc}, as derived in Ref. [273], also has to be varied, via a parameter α, in order to get agreement with experiment, although for the case of simple semiconductors, the meaning of this parameter can be elucidated [188].

Only one parameter-free calculation of the frequency-dependence of the long-range contribution to f_{xc} has been published so far for a bulk material (namely for silicon and diamond) [275], but at the price of fully solving the BSE, which is of course not of immediate practical interest.

A suggestion of how to obtain excitonic effects without solving the BSE, and without using adjustable parameters, is given in Ref. [273]. However, it has never been shown how well this approach would work in practice. In fact, its success is *a priori* far from obvious, due to possible obstacles of principle (it relies on the invertibility of matrices) or practice (treatment of double poles). In this chapter, instead, we show that the approach originally proposed in Ref. [273], based on the comparison of TDDFT and BSE, exposed in Chap. 5, *is* in fact one possible *solution* for the long-standing problem of calculating *parameter-free* optical spectra, including excitonic effects, in the framework of TDDFT and *without solving the BSE*. We generalize the kernel given in that reference to a class of dynamical ones, and show that a static f_{xc}, when it exists, is just one of many possibilities which yield a good spectrum.

This chapter is resumed in F. Sottile, V. Olevano and L. Reining *Parameter-free calculation of response functions in time-dependent density-functional theory*, Phys. Rev. Lett. **91**, 56402 (2003).

8.1 The theory

The key of the comparison between BSE and TDDFT (see also Chap. 5) is of course the request to have *the same spectrum with the two approaches*. Since the optical spectrum is described by the macroscopic dielectric function, the necessary and sufficient condition,

in order to have the same spectrum, would be

$$\varepsilon^M_{\rm BSE}(\omega) = \varepsilon^M_{\rm TDDFT}(\omega) \tag{8.1}$$

i.e., the same macroscopic dielectric function, given by (3.27). However, since the equations of the polarizability can be written in the 4-point formalism (or transition space, here we recall Eq.s 5.4),

$$\begin{aligned} \bar{L}_{(n_1n_2)(n_3n_4)} &= \left[H^{2p,reso}_{\rm BSE} - I\omega\right]^{-1}_{(n_1n_2)(n_3n_4)} (f_{n_3} - f_{n_4}) \\ \bar{\chi}_{(n_1n_2)(n_3n_4)} &= \left[H^{2p,reso}_{\rm TDDFT} - I\omega\right]^{-1}_{(n_1n_2)(n_3n_4)} (f_{n_3} - f_{n_4})\,., \end{aligned} \tag{8.2}$$

it is much easier to give a stronger condition

$$\bar{L}(1,2,3,4) = \bar{\chi}(1,2,3,4) \tag{8.3}$$

i.e. the equality between the four-point response functions, or

$$\bar{L}_{(n_1n_2)(n_3n_4)} = \bar{\chi}_{(n_1n_2)(n_3n_4)} \tag{8.4}$$

the equality between the matrix elements in the transitions space.[1] The latter (or Eq. (8.3)) clearly is a sufficient condition (if it is true, Eq. (8.1) is true), but not a necessary one. It might even be impossible to fulfill this equation exactly. In the next paragraph we will come back to this point; for the moment we suppose that we can use Eq. (8.4). From the latter then, (3.35) and (3.42),(3.43) and (3.44), we have

$$\begin{aligned} &(\epsilon_{n_2} - \epsilon_{n_1})\,\delta_{n_1n_3}\delta_{n_2n_4} + \Bigg[2\int d\mathbf{r}d\mathbf{r}'\ \Phi(n_1n_2,\mathbf{r})\bar{v}(\mathbf{r}-\mathbf{r}')\Phi^*(n_3n_4,\mathbf{r}') \\ &\qquad\qquad +2\int d\mathbf{r}d\mathbf{r}'\Phi(n_1n_2,\mathbf{r})f_{xc}(\mathbf{r},\mathbf{r}',\omega)\Phi^*(n_3n_4,\mathbf{r}')\Bigg] = \\ &(E_{n_2} - E_{n_1})\,\delta_{n_1n_3}\delta_{n_2n_4} + \Bigg[2\int d\mathbf{r}d\mathbf{r}'\ \Phi(n_1n_2,\mathbf{r})\bar{v}(\mathbf{r}-\mathbf{r}')\Phi^*(n_3n_4,\mathbf{r}') \\ &\qquad\qquad -\int d\mathbf{r}d\mathbf{r}'\Phi(n_1n_3,\mathbf{r})W(\mathbf{r},\mathbf{r}',0)\Phi^*(n_2n_4,\mathbf{r}')\Bigg] \end{aligned} \tag{8.5}$$

[1] We have implicitly supposed that the single particle wavefunctions are the same in both BSE and TDDFT. In fact, even if Eq. (8.4) is fulfilled, in order to use the Eq. (3.27), we need the real space (or Fourier space) polarizabilities, which are obtained via $L(1234) = \sum_{n_1n_2n_3n_4} \phi^*_{n_1}(1)\phi_{n_2}(2)\phi^*_{n_3}(3)\phi_{n_4}(4)L_{(n_1n_2)(n_3n_4)}$. If the ϕ's (used in BSE and TDDFT) are not the same, then, the spectra could be different.

with $\Phi(n_1 n_2, \mathbf{r}) = \phi_{n_1}(\mathbf{r})\phi^*_{n_2}(\mathbf{r})$. Now, considering that the term involving the Coulomb potential is equal for both cases, we can express a relation between the BSE and TDDFT kernels in a more compact form

$$F^{\text{TDDFT}}_{(n_1n_2)(n_3n_4)} = (E_{n_2} - E_{n_1} - \epsilon_{n_2} + \epsilon_{n_1})\,\delta_{n_1n_3}\delta_{n_2n_4} + F^{\text{BSE}}_{(n_1n_2)(n_3n_4)}, \tag{8.6}$$

once we have defined the *transition space kernels* $F^{\text{TDDFT}}_{(n_1n_2)(n_3n_4)}$ and $F^{\text{BSE}}_{(n_1n_2)(n_3n_4)}$

$$\begin{aligned} F^{\text{TDDFT}}_{(n_1n_2)(n_3n_4)} &= 2\int d\mathbf{r}d\mathbf{r}'\Phi(n_1n_2,\mathbf{r})f_{xc}(\mathbf{r},\mathbf{r}',\omega)\Phi^*(n_3n_4,\mathbf{r}') \\ F^{\text{BSE}}_{(n_1n_2)(n_3n_4)} &= -\int d\mathbf{r}d\mathbf{r}'\Phi(n_1n_3,\mathbf{r})W(\mathbf{r},\mathbf{r}',0)\Phi^*(n_2n_4,\mathbf{r}'). \end{aligned} \tag{8.7}$$

The latter is equivalent to the $W^{v'c'\mathbf{k}'}_{vc\mathbf{k}}$ (defined by (3.44)) if $n_1n_2 = v\mathbf{k} \to c\mathbf{k}$ and $n_3n_4 = v'\mathbf{k}' \to c'\mathbf{k}'$. Let us stress, here, as discussed in Par. 7.3, that two different couples of Φ's are involved in the definition of the transition space kernels (8.7), depending if we are in the TDDFT framework, or in BSE framework. This prevents f_{xc} to be simply equal to $-W/2$. Eq. (8.6) illustrates that, in order for TDDFT and BSE to give the same spectra, the TDDFT kernel has to take into account the self-energy corrections and the electron-hole interaction, described by W in BSE.[2] We can observe that, if the quasi-particle corrections are directly inserted into the χ^0, via a χ^0_{GW}, obtained simply replacing ϵ_i by the E_i in χ^0, Eq. (8.6) becomes

$$F^{\text{TDDFT}}_{(n_1n_2)(n_3n_4)} = F^{\text{BSE}}_{(n_1n_3)(n_2n_4)}. \tag{8.8}$$

We would like, now, to exploit the relation (8.6). In Ref. [273] this was done by formally inverting the matrices Φ in Eq.s (8.7), leading to a static $f_{xc} = \Phi^{-1}F^{\text{BSE}}(\Phi^*)^{-1}$. Here, instead, we immadiately write a symmetric version of (4.7), with respect to χ^0

$$\begin{aligned} \bar{\chi} &= \left(1 - \chi^0\bar{v} - \chi^0 f_{xc}\right)^{-1}\chi^0 = \chi^0\left(\chi^0 - \chi^0\bar{v}\chi^0 - \chi^0 f_{xc}\chi^0\right)^{-1}\chi^0 \\ &= \chi^0\left(\chi^0 - \chi^0\bar{v}\chi^0 - T\right)^{-1}\chi^0. \end{aligned} \tag{8.9}$$

The term T can be explicitly written down (χ^0 given by (4.11)[3])

$$\begin{aligned} T(\mathbf{r},\mathbf{r}',\omega) &= \int d\mathbf{r}_1 d\mathbf{r}_2\,\chi^0(\mathbf{r},\mathbf{r}_1)f_{xc}(\mathbf{r}_1,\mathbf{r}_2,\omega)\chi^0(\mathbf{r}_2,\mathbf{r}') = \\ &= \int d\mathbf{r}_1 d\mathbf{r}_2 \sum_{\substack{n_1n_2\\n_3n_4}} \frac{\Phi^*(n_1n_2,\mathbf{r})\Phi(n_1n_2,\mathbf{r}_1)}{\omega - (\epsilon_{n_2} - \epsilon_{n_1}) + i\eta} f_{xc}(\mathbf{r}_1,\mathbf{r}_2,\omega)\frac{\Phi^*(n_3n_4,\mathbf{r}_2)\Phi(n_3n_4,\mathbf{r}')}{\omega - (\epsilon_{n_4} - \epsilon_{n_3}) + i\eta} = \\ &= \sum_{\substack{n_1n_2\\n_3n_4}} \frac{\Phi^*(n_1n_2,\mathbf{r})}{\omega - (\epsilon_{n_2} - \epsilon_{n_1}) + i\eta} F^{\text{TDDFT}}_{(n_1n_2)(n_3n_4)} \frac{\Phi(n_3n_4,\mathbf{r}')}{\omega - (\epsilon_{n_4} - \epsilon_{n_3}) + i\eta} \end{aligned} \tag{8.10}$$

[2] This also stresses the fact that having KS eigenvalues different from the QP energies is not a problem for neutral excitations spectra: this difference will be corrected by the kernel.

[3] Here we consider only the resonant part of χ^0, with $\tilde{\rho}(\mathbf{q} = 0) = \Phi$, in real space.

where the first of (8.7) has been used. If we use now (8.6), we obtain the searched relation

$$T(\mathbf{r},\mathbf{r}',\omega) = T_1 + T_2 = \sum_{n_1 n_2} \frac{\Phi^*(n_1 n_2,\mathbf{r})\Phi(n_1 n_2,\mathbf{r}')}{\left[\omega - (\epsilon_{n_2} - \epsilon_{n_1}) + i\eta\right]^2} \left[E_{c\mathbf{k}} - E_{v\mathbf{k}} - (\epsilon_{c\mathbf{k}} - \epsilon_{v\mathbf{k}})\right] + \sum_{\substack{n_1 n_2 \\ n_3 n_4}} \frac{\Phi^*(n_1 n_2,\mathbf{r})}{\omega - (\epsilon_{n_2} - \epsilon_{n_1}) + i\eta} F^{\mathrm{BSE}}_{(n_1 n_2)(n_3 n_4)} \frac{\Phi(n_3 n_4,\mathbf{r}')}{\omega - (\epsilon_{n_4} - \epsilon_{n_3}) + i\eta} \quad (8.11)$$

which is the key equation of this derivation of TDDFT from the BSE. Eq. (8.11) answers to the question: *What is the kernel to put into the TDDFT to obtain the same spectrum of the BSE ?*, if Eq. (8.4) can be fulfilled.

It is worth reminding that (1) only the resonant part of the response function, (2) a static electron-hole interaction and (3) KS-LDA wavefunctions occur in our BSE calculation, which turned out to be reasonable approximations (see Chap. 3).

We can write the explicit form of T_1 and T_2, in reciprocal space, and for a vanishing momentum transfer (vertical transitions from valence states $v\mathbf{k}$ to conduction states $c\mathbf{k}$)

$$T_1(\mathbf{G},\mathbf{G}',\omega) = \frac{2}{N_{\mathbf{k}}} \sum_{vc\mathbf{k}} \frac{\Phi^*(vc\mathbf{k},\mathbf{G})\Phi(vc\mathbf{k},\mathbf{G}')}{\left[\omega - (\epsilon_{c\mathbf{k}} - \epsilon_{v\mathbf{k}}) + i\eta\right]^2} \left[E_{c\mathbf{k}} - E_{v\mathbf{k}} - (\epsilon_{c\mathbf{k}} - \epsilon_{v\mathbf{k}})\right] \quad (8.12)$$

which is the trace of a diagonal matrix in the transition space framework, and

$$T_2(\mathbf{G},\mathbf{G}',\omega) = \frac{2}{N_{\mathbf{k}}^2} \sum_{\substack{v\,c\,\mathbf{k} \\ v'c'\mathbf{k}'}} \frac{\Phi^*(vc\mathbf{k},\mathbf{G})}{\omega - (\epsilon_{c\mathbf{k}} - \epsilon_{v\mathbf{k}}) + i\eta} F^{\mathrm{BSE}}_{(vc\mathbf{k})(v'c'\mathbf{k}')} \frac{\Phi(v'c'\mathbf{k}',\mathbf{G}')}{\omega - (\epsilon_{c'\mathbf{k}'} - \epsilon_{v'\mathbf{k}'}) + i\eta}. \quad (8.13)$$

Here the number of k-points N_k appears explicitly.[4]

This result, for the term T, is equal to Eq. (11) of Ref. [273], there are nevertheless important differences: first of all, our derivation is now *more general*, since it does not pass through an explicit inversion of the matrices $\Phi(vc\mathbf{k},\mathbf{G})$. In order to fulfill the invertibility condition, the matrix Φ has to have an equal number of transitions (N_t) and $\mathbf{G}$-vectors ($N_{\mathbf{G}}$). This is not easy to achieve, especially for system whose spectrum requires a lot of transitions to be described, because it would also require a huge number of $\mathbf{G}$-vectors for the characterization of the spectrum. Moreover the invertibility condition (if it holds) also implies f_{xc} to be static, whereas our general derivation does not require a static kernel.

It is then, clear why the present derivation is not only more general than the one of Ref. [273] (it does not require Φ to be invertible, it does not require a static kernel), but it is also of more practical interest, because of the considerable freedom in the choice of basis size ($N_{\mathbf{G}}$ can be chosen much smaller than N_t).

[4]The prefactor of χ^0 is the volume of the system, i.e. $\Omega = \Omega_{cell} \times N_{\mathbf{k}}$, but Ω_{cell} is included in the definition of the Φ's, see (4.11) and (2.26).

8.1.1 When the assumption is wrong...

The theory, as developed up to now, relies on the assumption (8.4), i.e. the equality between the 4-point polarizabilities (of BSE and TDDFT) has to be fulfilled. This (strong) condition is not necessary to have $\varepsilon_M^{\mathrm{BSE}} = \varepsilon_M^{\mathrm{TDDFT}}$. On the contrary, there are cases where it cannot be fulfilled. An example is reported in Ref. [273], taking plane waves as wavefunctions.

Here we want to show another example in which Eq. (8.4) cannot be satisfied. Let's write down the diagonal matrix elements F^{TDDFT} and F^{BSE} for the resonant case (having contracted the indices $n_1 \to v$,$n_2 \to c$)

$$F^{\mathrm{TDDFT,reso}}_{(vc)(vc)} = 2\int d(12)\phi_v(1)\phi_c(1)f_{xc}(1,2,\omega)\phi_v(2)\phi_c(2) \tag{8.14}$$

and

$$F^{\mathrm{BSE,reso}}_{(vc)(vc)} = -\int d(12)\phi_v(1)\phi_v(1)W(1,2)\phi_c(2)\phi_c(2), \tag{8.15}$$

and for the coupling case

$$F^{\mathrm{TDDFT,coupl}}_{(vc)(cv)} = 2\int d(12)\phi_v(1)\phi_c(1)f_{xc}(1,2,\omega)\phi_c(2)\phi_v(2) \tag{8.16}$$

and

$$F^{\mathrm{BSE,coupl}}_{(vc)(cv)} = -\int d(12)\phi_v(1)\phi_c(1)W(1,2)\phi_c(2)\phi_v(2). \tag{8.17}$$

Here we have considered the wavefunctions to be real for simplicity.

Let's consider then, as first approach, the resonant part and the coupling part *separately*. The two equalities (by which we can obtain an exchange-correlation kernel)

$$F^{\mathrm{TDDFT,reso}}_{(vc)(vc)} = F^{\mathrm{BSE,reso}}_{(vc)(vc)} \tag{8.18}$$

and

$$F^{\mathrm{TDDFT,coupl}}_{(vc)(cv)} = F^{\mathrm{BSE,coupl}}_{(vc)(cv)} \tag{8.19}$$

can be separately fulfilled and then a kernel could be found separately for the two cases. In particular in the case of coupling an exchange-correlation kernel can be immediately extrapolated from Eq. (8.19), i.e. $f_{xc}(\mathbf{r},\mathbf{r}') = -\frac{1}{2}W(\mathbf{r},\mathbf{r}')$.

Now, we want an exchange-correlation kernel which takes into account, the resonant, the anti-resonant, *and* also the coupling contribution. To have this, both Eq.s (8.18) and (8.19) have to be fulfilled, *simultaneously*. This leads to a contradiction. In fact, since in our example the wavefunctions are real, we have

$$F^{\mathrm{TDDFT,reso}}_{(vc)(vc)} = F^{\mathrm{TDDFT,coupl}}_{(vc)(cv)} \tag{8.20}$$

and

$$F^{\mathrm{BSE,reso}}_{(vc)(vc)} \neq F^{\mathrm{BSE,coupl}}_{(vc)(cv)}. \tag{8.21}$$

By virtue of (8.20) and (8.21), if the condition (8.18) is fulfilled, Eq. (8.19) cannot be satisfied, and vice versa. In conclusion, this is an (particular) example where the initial assumption

$$F^{\mathrm{TDDFT}}_{(vc)(v'c')} = F^{\mathrm{BSE}}_{(vc)(v'c')}$$

is wrong, leading to an internal contradiction. However, as we have mentioned before, a separate fulfillment of the Eq.s (8.18) and (8.19) is still possible, giving, then, a suggestion of how to overcome the problem. In other cases, it might not be possible to find a way to avoid the problem. In fact, if we had chosen to work with (8.3) instead of (8.4), the different indices in the δ-functions in (5.2) and (5.3), would have been a tough obstacle even for an approximate fulfillment of the equality. In principle (8.3) and (8.4) should of course be equivalent. In practice, however, (8.4) gives us some margin, due to the fact that only a finite number of transitions has to be considered for the spectrum in each energy range. Eq. (8.4) should hence be considered as an equation defining the *parameters* $F^{\mathrm{TDDFT}}_{(n_1n_2),(n_3n_4)}$, rather than matrix elements.

8.1.2 ...and when it is, instead, straightforward

There are instead cases where Eq. (8.8) is trivially satisfied. Let us consider, as first example, the contact exciton model for the (resonant) electron-hole contribution to the Bethe-Salpeter equation (see Chap. 7)

$$\begin{aligned} F^{\mathrm{BSE}}_{(vc)(v'c')} &= -\int d\mathbf{r}d\mathbf{r}'\phi_v(\mathbf{r})\phi^*_{v'}(\mathbf{r})A\delta(\mathbf{r}-\mathbf{r}')\phi^*_c(\mathbf{r}')\phi_{c'}(\mathbf{r}') \\ &= -A\int d\mathbf{r}\phi_v(\mathbf{r})\phi^*_{v'}(\mathbf{r})\phi^*_c(\mathbf{r})\phi_{c'}(\mathbf{r}) \\ &= -A\int d\mathbf{r}\phi_v(\mathbf{r})\phi^*_c(\mathbf{r})\phi^*_{v'}(\mathbf{r})\phi_{c'}(\mathbf{r}). \end{aligned}$$

Since the transition space exchange-correlation kernel $F^{\mathrm{TDDFT}}_{(vc)(v'c')}$ is given by the first of Eq.s (8.7), Eq. (8.8) reads

$$2\int d\mathbf{r}d\mathbf{r}'\phi_v(\mathbf{r})\phi^*_c(\mathbf{r})f_{xc}(\mathbf{r},\mathbf{r}',\omega)\phi^*_{v'}(\mathbf{r}')\phi_{c'}(\mathbf{r}') = -A\int d\mathbf{r}\phi_v(\mathbf{r})\phi^*_c(\mathbf{r})\phi^*_{v'}(\mathbf{r})\phi_{c'}(\mathbf{r})$$

which gives the equation (7.5)

$$f^{contact}_{xc}(\mathbf{r},\mathbf{r}') = -\frac{1}{2}\delta(\mathbf{r}-\mathbf{r}')A.$$

The contact exciton model hence constitutes a case in which the initial assumption is fully satisfied, leading to a simple shape for the exchange-correlation kernel.

Also a two-level model (where one has only one transition), or a model of N independent transitions are cases where Eq. (8.8) can be perfectly fulfilled.

8.2 Technical analysis

In order to elucidate the validity of the above derivation, and also to make the link to the derivation in Ref. [273], it is, besides calculating a few examples, crucial to analyze the behavior of the different terms. We will do this, looking at the macroscopic dielectric function $1/\varepsilon^{-1}_{\mathbf{G}=\mathbf{G}'=0}(\mathbf{q} \to 0, \omega)$ of bulk silicon, that has been studied in previous publications [273, 274, 283].

It is easier to understand some important relations using first a very coarse sampling of the BZ. We therefore use only 2 special k-points in the irreducible BZ, and 6 (3 valence and 3 conduction) bands for all calculations in the following illustrations, meant to show the effects of Eq.s (8.12) and (8.13).

8.2.1 The term T_1

The Fig. 8.I shows the result of a standard RPA calculation (i.e. $T = 0$ in Eq. (8.9); dotted curve), a GW-RPA result (where the $\chi^0_{\mathrm{GW}}(\{E_i\})$ is used instead of $\chi^0(\{\epsilon_i\})$, but still T is neglected: dashed curve), and the result of a BSE calculation (continuous curve). The matrix dimension $N_{\mathbf{G}}$ required to converge such calculations is $N_{\mathbf{G}} = 59$.

We have then obtained the absorption spectrum using χ^0 plus the contribution T_1. The resulting curve (dots) yields results that are indistinguishable from the GW-RPA ones. As a consequence, *the contribution T_1 correctly acts as an effective self-energy shift*. Such a shift of poles is far from trivial and could not be obtained by simpler approximations, like the one discussed in Ref.s [188, 273]; see, for that, also Ref. [278]. It is, in fact, important to see that this self-energy shift is obtained in a very different way using the two approaches (GW-RPA or using T_1): in the case of GW-RPA, the quasi-particle corrections are added to the DFT-LDA energies, with the consequent shifts of the poles of χ^0. This is *not* a big task, if the quasi-particle corrections are known.[5] On the contrary, the action of the term T_1 is not that simple, because the shifts appear in a more complicated way in Eq. (8.12). Here the shift is obtained wiping out the oscillator strengths of certain frequencies and strengthening those of other frequencies, thus constituting a demanding effort. In particular a big spatial complexity is required to have the oscillator strength in the right position. This behavior is illustrated in Fig. 8.II: when the number of **G**-vectors increases, the line-shape of the spectrum improves, up to achieve the convergence (coincidence with the GW-RPA spectrum), but only when $N_{\mathbf{G}} = 307$. We remind that well converged spectra within RPA, GW-RPA and BSE

[5] Often this step is substituted by the simple application of a "scissor operator" [287], if the quasi-particle corrections are quite constant in the considered transitions.

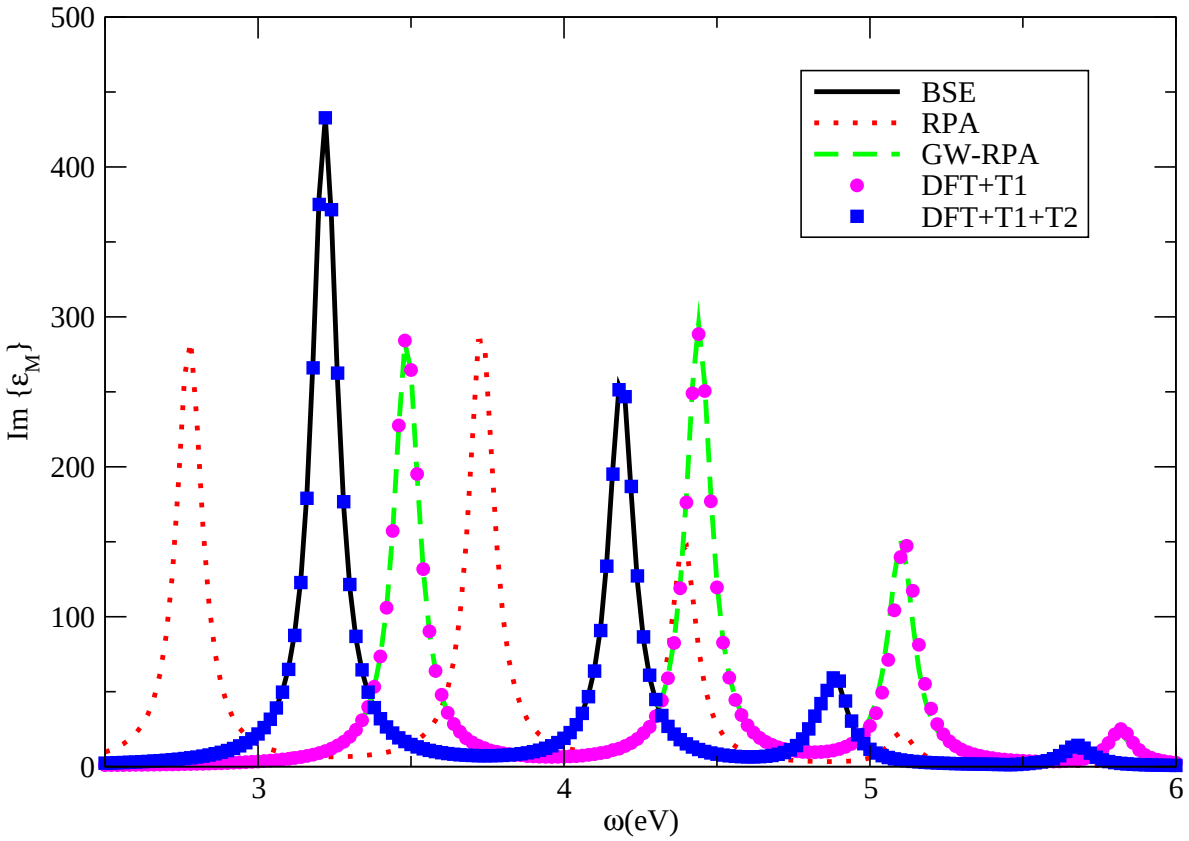

Figure 8.I: RPA, GW-RPA and BSE results, represented by dotted, dashed and continuous curves, respectively. Dots represent the insertion of T_1 and boxes the whole kernel $T_1 + T_2$.

were obtained with only $N_{\mathbf{G}} = 59$, considerably less than 307, thus showing the intrinsic difficulty to obtain the self-energy shift using the kernel T_1.

This difficulty to obtain the self-energy shift using the term T_1 is strongly related to the initial assumption, namely to have the same matrix elements in TDDFT and BSE, i.e. (so restricting Eq. (8.6) to the self-energy shift only):

$$F_{tt'}^{\mathrm{TDDFT}} = (\Delta E_t - \Delta\epsilon_t)\delta_{tt'} \tag{8.22}$$

having called t the transition $n_1 n_2$. In order to fulfill Eq. (8.22), F^{TDDFT} has to satisfy the double condition

$$\begin{aligned} F_{tt}^{\mathrm{TDDFT}} &= \int d\mathbf{r}d\mathbf{r}'\Phi(t,\mathbf{r})f_{xc}(\mathbf{r},\mathbf{r}',\omega)\Phi(t,\mathbf{r}') = (\Delta E_t - \Delta\epsilon_t) \\ F_{tt'}^{\mathrm{TDDFT}} &= \int d\mathbf{r}d\mathbf{r}'\Phi(t,\mathbf{r})f_{xc}(\mathbf{r},\mathbf{r}',\omega)\Phi(t',\mathbf{r}') = 0, \quad t' \neq t. \end{aligned} \tag{8.23}$$

The request for the matrix elements to satisfy both Eq.s (8.23) is troublesome; in particular, the more similar transitions there are, the more the relations (8.23) will be difficult

to fulfill. If we increment the number of k-points N_k, for instance, the two relations schematically read

$$\begin{aligned} F^{\mathrm{TDDFT}}_{k,k} &= (\Delta E_k - \Delta\epsilon_k) \\ F^{\mathrm{TDDFT}}_{k,k+\Delta k} &= 0 \quad \forall \Delta k \neq 0. \end{aligned} \tag{8.24}$$

where k labels a transition in this case (we imagine that, in a realistic calculation, a lot of k-points and a few bands are used, to describe an optical spectrum). If N_k is big enough, Δk is small and the relation (8.24) becomes impossible to fulfill[6] and, as a consequence, the term T_1 is unable to reproduce the GW-RPA spectrum. This occurs already, for example, when 256 shifted k-points are used to sample the BZ of silicon, as reported in Fig. 8.III.

We expect hence, the inclusion of the term T_1 to be problematic, especially for realistic calculations. Above all, however, it does not present any practical interest (it does not avoid the calculation of the quasi-particle corrections). We have therefore decided, to avoid this term in all future calculations: this can be done by simply using χ^0_{GW}, instead of χ^0.

8.2.2 The term T_2

If one also includes, in Eq. (8.9), the term T_2, as given by (8.13), the spectrum *is now identical to the BSE result*, as shown by boxes in Fig.8.I, i.e. the term T_2 correctly *simulates the e-h interaction*, represented by W in the BSE. The numbers of **G**-vectors required for a well converged spectrum is $N_{\mathbf{G}} = 113$. As we can notice, the convergence of the spectrum is achieved well before that of the term T_1, so supporting the previous decision to avoid the latter and, more important, justifying the hope that T_2 will be useful in practice.

8.2.3 The (¿useless?) kernel f_{xc}

To further investigate T_2, we study $f^{\mathrm{e-h}}_{xc}(\omega) = \left(\chi^0_{\mathrm{GW}}(\omega)\right)^{-1} T_2(\omega) \left(\chi^0_{\mathrm{GW}}(\omega)\right)^{-1}$, i.e. the kernel one should use in the canonical equation

$$\bar{\chi} = \left(1 - \chi^0_{\mathrm{GW}}\bar{v} - \chi^0_{\mathrm{GW}} f_{xc}\right)^{-1} \chi^0_{\mathrm{GW}}.$$

This is, as it will turn out, a rather academic discussion, because the function to deal with, in our approach, is *not* f_{xc}, but $T_2 = \chi^0 f_{xc} \chi^0$.

The lower panel of Fig. 8.IV shows several results for $q^2 \Re\left\{f^{\mathrm{e-h}}_{xc}(\mathbf{q}, \mathbf{G} = \mathbf{G}' = 0, \omega)\right\}$ for vanishing momentum transfer $\mathbf{q}$. Other wing and body elements ($\mathbf{G} \neq 0$) behave similarly, and are therefore not shown here. The different curves have been obtained by

[6] The function Φ's are slowly varying functions, with respect to transitions.

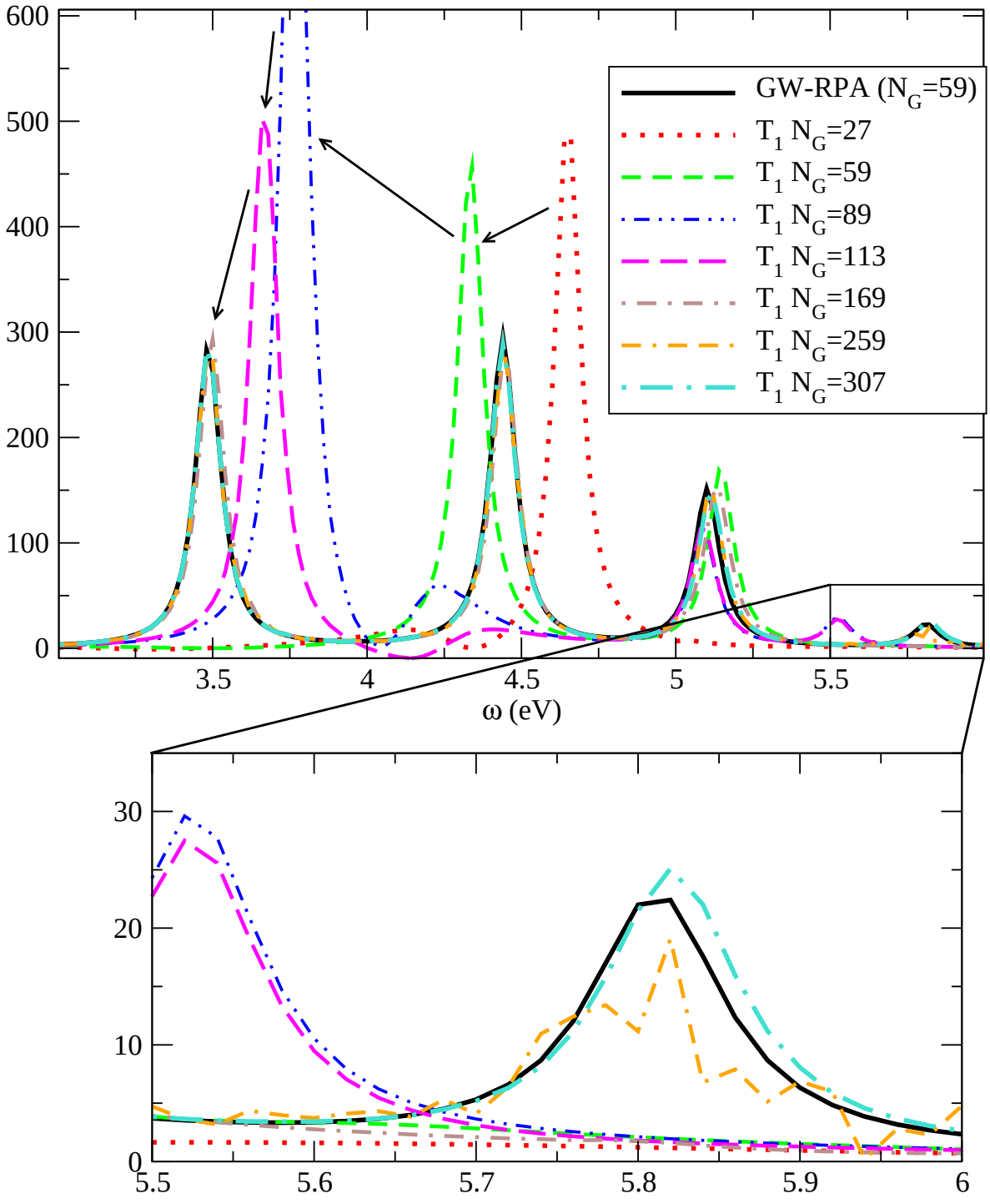

Figure 8.II: Behaviour of T_1 with an increasing $N_{\mathbf{G}}$, with respect to the GW-RPA calculation. In the lower panel, a particular range (from 5.5 to 6.0 eV) is shown.

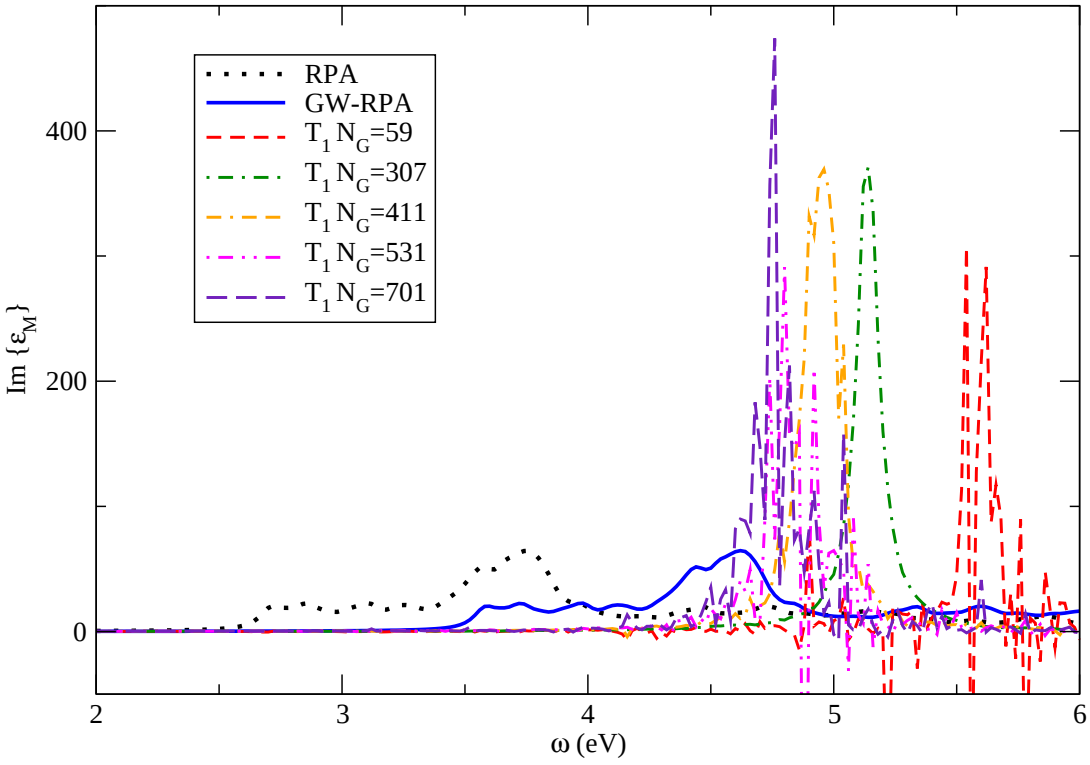

Figure 8.III: Behaviour of T_1 with an increasing $N_{\mathbf{G}}$. In this case, i.e. using 256 shifted k-points, a converged (shifted) spectrum is not achieved.

varying the dimension N_G of the matrices χ^0_{GW} and T_2. If we use N_G=1, the resulting kernel (dotted line) has a very sharp pole-like frequency dependence. With increasing N_G, this feature moves to higher energy, leaving behind an essentially flat $f_{xc}^{\mathrm{e-h}}$. At $N_G = 169$, $f_{xc}^{\mathrm{e-h}}$ is completely static in the optical range. In fact, only when N_G approaches the number of transitions N_t that are considered (288 in our example), the hypothesis of invertibility of the matrices Φ, made in the derivation of a static kernel in Ref. [273], can be valid. However, as explained above, using the present derivation this condition can be dropped. In fact, the upper panel of Fig. 8.IV shows the spectra that are obtained using N_G=1, 113, 169 and 307. Besides the clearly wrong result obtained in the first case, leading even to negative absorption, all other results are equally virtually perfect. This set of results includes the one shown already in Fig. 8.I, which had been obtained with N_G=113, the result for N_G=169 corresponding to a static kernel (note that the static limit $f_{xc}^{\mathrm{e-h}}(\omega = 0)$ has been used to produce the absorption curve for this value), and it is even true for N_G=307. Now, $N_G > N_t$, and χ^0_{GW} has several eigenvalues close to zero. This is because χ^0 is a sum of products $\chi^0(\mathbf{G}, \mathbf{G}', \omega) = \sum_t \Phi_t^*(\mathbf{G})\Phi_t(\mathbf{G}')f_t(\omega)$, where $t = v\mathbf{k} \rightarrow c\mathbf{k}$ is again the transition index. A sum of products of vectors cannot be inverted if the dimension of the vectors is greater than the number of products. Therefore

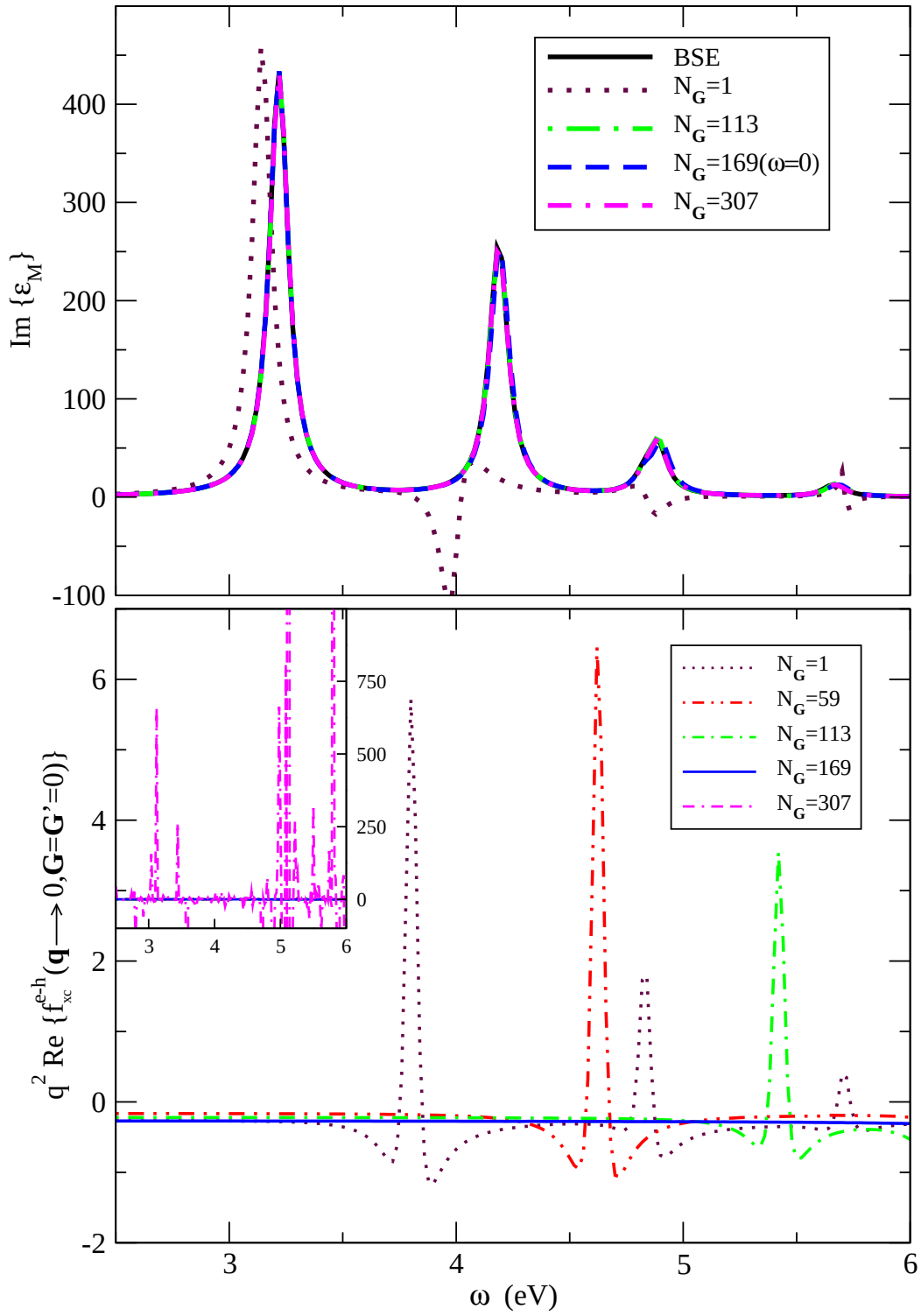

Figure 8.IV: Analysis of the kernel $f_{xc}^{\mathrm{e-h}}(\omega)$.

$f_{xc}^{\mathrm{e-h}}$ is scattered and out of the vertical range (see the out of scale inset of Fig. 8.IV, lower panel), but since this meaningless kernel is finally used in a multiplication with χ^0_{GW}, the result remains so surprisingly excellent.[7] It is worth, therefore, also looking at the inversion of χ^0, from a numerical point of view. To do this, we plot the real part of one element (the head) of the $(\chi^0)^{-1}$ as a function of energy, in the optical range. We expect then, that when N_G is of the same order[8] of N_t, invertibility problems occur and the $(\chi^0)^{-1}$ should be scattered out and meaningless. This is what happens, indeed, and it is shown in Fig. 8.V. In the central panel of the figure, the case treated up to now (32 total k-points, 6 bands, then $N_t = 3 \times 3 \times 32 = 288$ transitions) is shown, and the result confirms our prediction, i.e. when N_G approaches (229) the number of transitions (288), the χ^0 is not invertible anymore. In the upper panel a smaller case, where only two bands are taken into account, is shown. Here the number of transitions is reduced to 32, and, in fact, the χ^0 shows invertibility problem already when $N_G = 27$. Finally in the lower panel of Fig. 8.V, we show the case with the number of bands N_b is increased up to 8, which leads to $N_t = 480$ transitions. Also in this case, the first invertibility problems occur when $N_G(387)$ approaches the number of transitions.[9]

Overall, the findings concerning T_2 are very ensuring: everything happens consistently with the derivation of the equations, and the results are perfect. Moreover, they are of potential practical interest since, if one does not require explicitly the Φ's to be invertible and the kernel to be static, the basis size N_G can be chosen to be much smaller than N_t (basis size of the BSE). Finally the fact that not f_{xc}, but f_{xc} multiplied with χ^0 is the key quantity, clearly is the reason for stable results and an important hint for future research.

Nevertheless, before coming to real applications, a last important issue related to the exchange-correlation kernel is:

Is the f_{xc} kernel static, or dynamic ?

If the initial assumption (8.8) is perfectly fulfilled (the quasi-particle corrections are taken into account in the independent-particle polarizability), since the BSE kernel $W(\mathbf{r}, \mathbf{r}')$ is static, so the f_{xc} kernel should also be static. There are nevertheless several important remarks. The way we have followed to obtain the kernel can be summarized in three steps: first, we have imposed the (8.8); second, we have obtained the term T_2 from F^{BSE} via (8.13) (now T_2 is dynamic); third, we have derived the exchange-correlation kernel via $f_{xc} = (\chi^0)^{-1} T_2 (\chi^0)^{-1}$ (and we have seen that it can be static or dynamic) by considering

[7] This is of course only true when numerical errors due to the inversion of χ^0_{GW} are avoided.

[8] We say "same order" instead of same number because, in reality, the number to deal with is the number of *independent* transitions, which can be (much) less than the total number of transition N_t.

[9] These problems are of course only due to the fact that a limited number of bands, hence transitions, is taken into account.

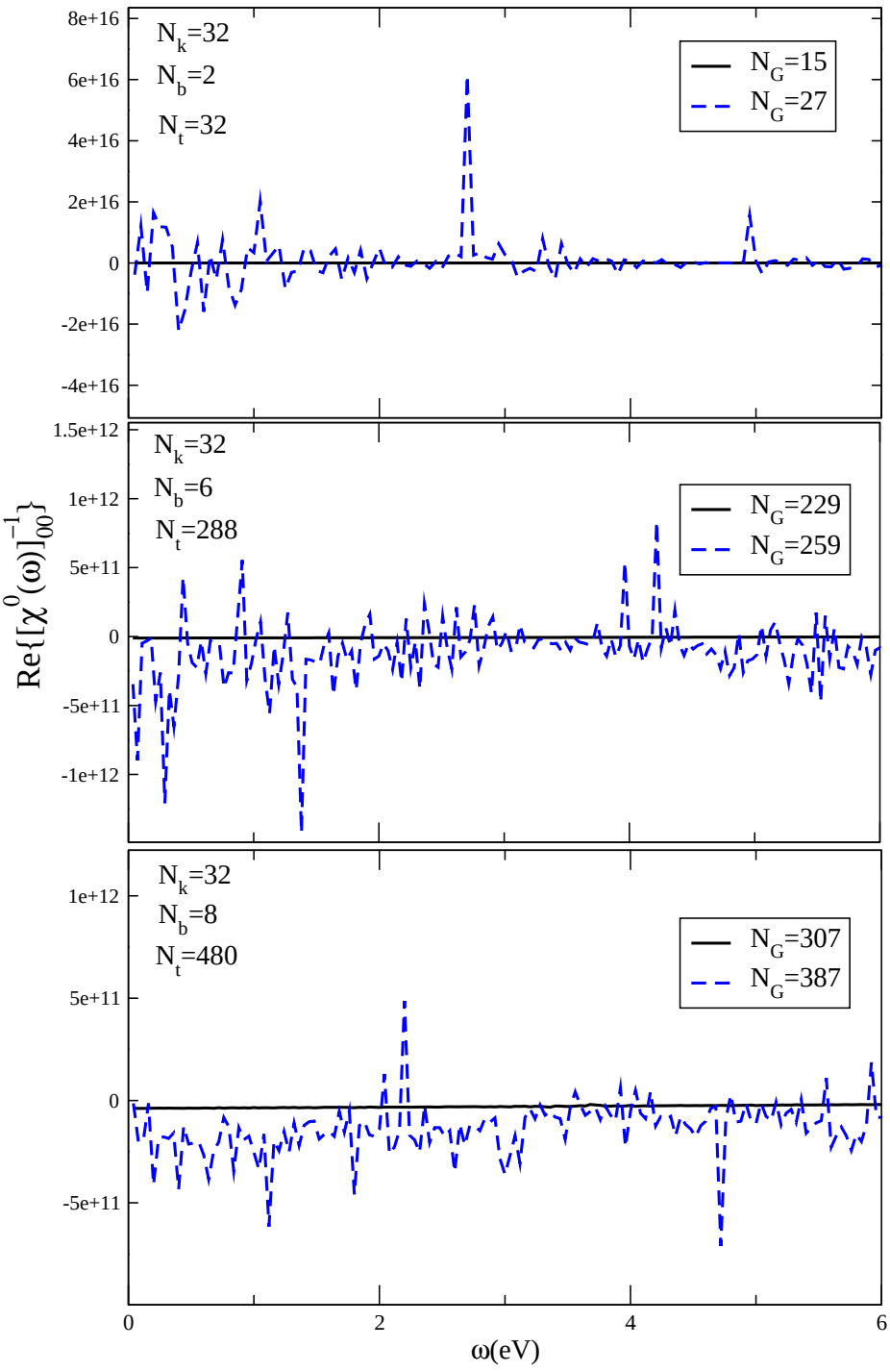

Figure 8.V: Real part of the head of the inverse independent particle polarizability. Upper panel: 2 bands equivalent to 32 transitions. Central panel: 6 bands equivalent to 288 transitions. Lower panel: 8 bands equivalent to 480 transitions.

the matrix χ^0 to be invertible. Only the second step is straightforward, whereas the first and the third steps require two conditions

C1) $F^{\mathrm{TDDFT}}_{(n_1n_2)(n_3n_4)} = F^{\mathrm{BSE}}_{(n_1n_2)(n_3n_4)}$

C2) χ^0 invertible

to be fulfilled in order to have a static kernel. It can occur that these two conditions cannot be both satisfied. Let's see the illustrative example of silicon, sampled with 2 k-points. We have seen that, if the cutoff is too low ($N_{\mathbf{G}} < 169$) the matrix χ^0 is invertible; however the condition C1) cannot be considered to be an equation for matrix elements of f_{xc}, because $f_{xc}(\mathbf{q} \to 0, \mathbf{G}, \mathbf{G}')$ has less degrees of freedom than N_t^2 equations to be fulfilled. As pointed out above, (8.6) should rather be interpreted as a choice of parameters. In fact, the resulting kernels are dynamic (see Fig. 8.IV, lower panel). If we increase the number of $\mathbf{G}$ vectors up to $N_{\mathbf{G}} = 169$, the condition C1) is now fulfilled and the matrix χ^0 is still invertible. As a consequence, the resulting exchange-correlation kernel is *static* (full curve in Fig. 8.IV, lower panel). Finally, if we now increase $N_{\mathbf{G}}$, whether the condition C1) is satisfied or not, the condition C2) is not satisfied anymore, because $N_{\mathbf{G}} > N_t$. Thus, in this model system, we have been able to find an intermediate cutoff where both C1) and C2) are fulfilled. In realistic systems, it can happen that we cannot achieve a perfect fulfillment of C1) before encountering invertibility problems in χ^0. In this case there are only two possibilities: either the parameters of the calculations have to be changed, e.g. increasing the number of bands (as we have seen before, this can permit one to increase a bit more the cutoff before having invertibility problems again; however it cannot remedy to cases as the examples (8.20) and (8.21), where the condition C1) is always wrong); or, more simply, one searches for a compromise, i.e. a reasonable cutoff, for whom a *converged spectrum is obtained, without taking care of* f_{xc}, because f_{xc} is never explicitly calculated nor used (but contained in the term T_2). It is clear that, in this case, the exchange-correlation kernel, if calculated via $f_{xc} = (\chi^0)^{-1} T_2 (\chi^0)^{-1}$, would be dynamic. The results, carried out on realistic systems (semiconductors and insulators), will largely justify this procedure, as we will soon verify, so showing that the *important function is not the kernel* f_{xc}, but the kernel combined with a response function.

8.3 The problems of χ^0, cautions and tricks.

Before applying this kernel to realistic systems, we want to warn the reader about possible problems that can occur when dealing with χ^0 and its inversion.

First, one could think that the results in Fig. 8.IV suffer of numerical problems, in particular when $N_{\mathbf{G}} = 307$. But it is *not* the case. In producing all those results, we have carefully verified that the (double) precision used for the inversion is sufficient to obtain a stable kernel and meaningful spectra. We have indeed verified that if single

precision is used, the inversion does lead to numerical problems.[10] In this case, the use of Singular Value Decomposition (SVD) [288], in order to deal with the numerical inversion of singular matrices, can be a solution.

The reason of non-invertibility of χ^0 rely in its vanishing eigenvalues. As Mearns and Kohn have shown [289], when the frequency range taken into account is above the first resonance, which is always the case for the absorption spectrum, non trivial vanishing eigenvalues occur (in the spectral decomposition of χ^0), so that in certain frequencies χ^0 is not invertible and caution is in order. Moreover, as we have explained before, for $N_{\mathbf{G}} > N_t$, χ^0 is not invertible for *all* frequencies. It is, therefore, clear that the f_{xc} (not the spectrum) displayed for the case $N_G = 307$ is *meaningless*: χ^0 is invertible in double precision because, probably due to the very small numerical errors in the calculation (in single precision) of χ^0 itself, eigenvalues are close, but not identical, to zero. The singularities (big numbers) in the inverse of χ^0 are then correctly counterbalanced by the zeros (small numbers) of the two χ^0 multiplying on the left and on the right the inverted matrix. This is the reason for the fact that the final correspondent spectrum is again perfect.

However, two remarks are here necessary, to certify the numerical stability of our results, despite the mentioned problems:

- Generalization of (8.9).
  Instead of multiplying Eq. (8.9) times χ^0, inside and outside the brackets, we can use another, *more general* function X, which leads to

  $$\bar{\chi} = X\left(X - \chi^0\bar{v}X - \chi^0 f_{xc}X\right)^{-1}\chi^0 = X\left(X - \chi^0\bar{v}X - T'\right)^{-1}\chi^0.$$

  In order to extrapolate F^{TDDFT} from T' (to be able to use Eq. (8.6)), X has to be

  $$X(\mathbf{G},\mathbf{G}',\omega) = \sum_{vc\mathbf{k}} \Phi^*(vc\mathbf{k},\mathbf{G})\Phi(vc\mathbf{k},\mathbf{G}')f(vc\mathbf{k},\omega)$$

  i.e., built up by the Φ matrices and by an arbitrary function $f(vc\mathbf{k},\omega)$. It is easy to recognize χ^0 as a special case of X, with $f(vc\mathbf{k},\omega) \propto \frac{1}{\omega-(\epsilon_{c\mathbf{k}}-\epsilon_{v\mathbf{k}})+i\eta}$. We have obtained preliminary results for different choices of $f(vc\mathbf{k},\omega)$: they *are identical* to the ones with $X = \chi^0$, so supporting the correctness of the results shown here. This freedom in the choice of $f(vc\mathbf{k},\omega)$ might be exploited in the future to build up an X less singular than χ^0 in the frequency domain of interest.

- Linear solver technique
  The algorithm we have used to find the full polarizability $\bar{\chi}$ is perfectly stable, avoiding any explicit inversion. In fact, we calculate T, never f_{xc}, so that we do not have to invert χ^0. Moreover, since we are interested only in the head of $\bar{\chi}$, we also

[10] Which means, e.g., that $(\chi^0)^{-1}\chi^0 \neq 1$.

avoid the inversion of $(\chi^0 - \chi^0 \bar{v} \chi^0 - T)$, by using a linear system solver technique. This algorithm, explained in Appendix E, has the double advantage to be more stable than an inversion, and to be much more convenient, from a computational point of view.

Chapter 9

Absorption spectrum of semiconductors

> To electricity – so, for the present, continuing to call it – we *may* not be wrong in referring the various physical appearances of light, heat and magnetism; but far less shall be liable to err in attributing to this strictly spiritual principle the more important phenomena of vitality, consciousness and *Thought*.
>
> from EUREKA, Edgar Allan Poe.

In this chapter we apply the theory developed in Par. 8.1 to optical absorption spectra of semiconductors. Since only poor results can be obtained within ALDA/RPA in describing the optical spectra of the bulk silicon and silicon carbide (whereas the BSE leads to a good agreement with the experiment, for both systems), the choice of these two semiconductors is the perfect test to validate the kernel T_2, proposed, but applied only to a model system, in the previous chapter.

This chapter is resumed in F. Sottile, V. Olevano and L. Reining *Parameter-free calculation of response functions in time-dependent density-functional theory*, Phys. Rev. Lett. **91**, 56402 (2003).

9.1 Absorption spectra of Silicon ...

Once the ground-state has been obtained, the LDA-KS wavefunctions ϕ_i and eigenvalues ϵ_i can be used to build the independent-particle polarizability χ^0, according to (4.11). The use of the polarizability

$$\bar{\chi} = \left(1 - \chi^0 \bar{v}\right)^{-1} \chi^0 \tag{9.1}$$

in

$$\Im\{\varepsilon_M\} = -\lim_{\mathbf{q}\to 0} v_0(\mathbf{q}) \bar{\chi}_{00}(\mathbf{q}, \omega)$$

directly leads to the RPA spectrum. The local field effects are correctly included. The RPA spectrum (same as Fig. 2.III) is represented by the double-dot dashed curve in Fig. 9.I.

The inclusion of an exchange-correlation kernel (in the adiabatic local density approximation) f_{xc}^{ALDA}, following (4.7) and (4.9) leads to the ALDA spectrum, represented by the double-dash dotted curve in Fig. 9.I, same as Fig. 4.I.

As we have already seen, the results are very similar and both quite poor. The electron-hole interaction, contained only in the "true" f_{xc}, is missing in the RPA and largely underestimated in ALDA [234, 290], thus leading to the (typical) underestimation of absorption strength at low energy, and of its overestimation at high energies. Moreover, of course, the self-energy shift is missing.

Following the three steps algorithm, described in Par. 3.3.2 and illustrated in Fig. 3.VI, we can perform a BSE calculation, which includes the electron-hole interaction, passing through the determination of quasi-particle corrections. All the approximations described in Par. 3.3.2 are used here. The details of the calculations are the following: all the spectra (RPA, ALDA, GW-RPA and BSE) have been obtained sampling the BZ with 256 shifted k-points (see Appendix E.2), and using 6 (3 valence and 3 conduction) bands. The number of resulting transitions is $N_t = N_v N_c N_k = 3 \times 3 \times 256 = 2304$. The number of $\mathbf{G}$-vectors required in all cases is $N_{\mathbf{G}} = 59$. In Fig. 9.I we show the GW-RPA (dot-dashed curve) and the BSE spectrum (dashed curve). The former is only a (almost rigid) shift of the RPA spectrum towards higher energies, whereas the BSE calculation includes a description of the electron-hole interaction, which is, then, crucial, to obtain a good agreement with the experiments.

It remains to check how the kernel that we have developed in Chap. 5, works out in this realistic case. So, starting from Eq. (9.1), we add the term T_2, as described[1] in Par. 8.1 and Eq. (8.13). The result (solid line) is practically coincident with the BSE calculation!

To obtain this spectrum we have used $N_{\mathbf{G}} = 307$, which is bigger than the value used for the RPA calculation ($N_{\mathbf{G}} = 59$), but significantly lower than the number of transitions $N_t = 2304$, the dimension to deal with, in BSE calculations. With increasing N_t, our

[1]The self-energy corrections are automatically taken into account using a χ^0_{GW} instead of χ^0, hence avoiding the contribution T_1, as we have already mentioned.

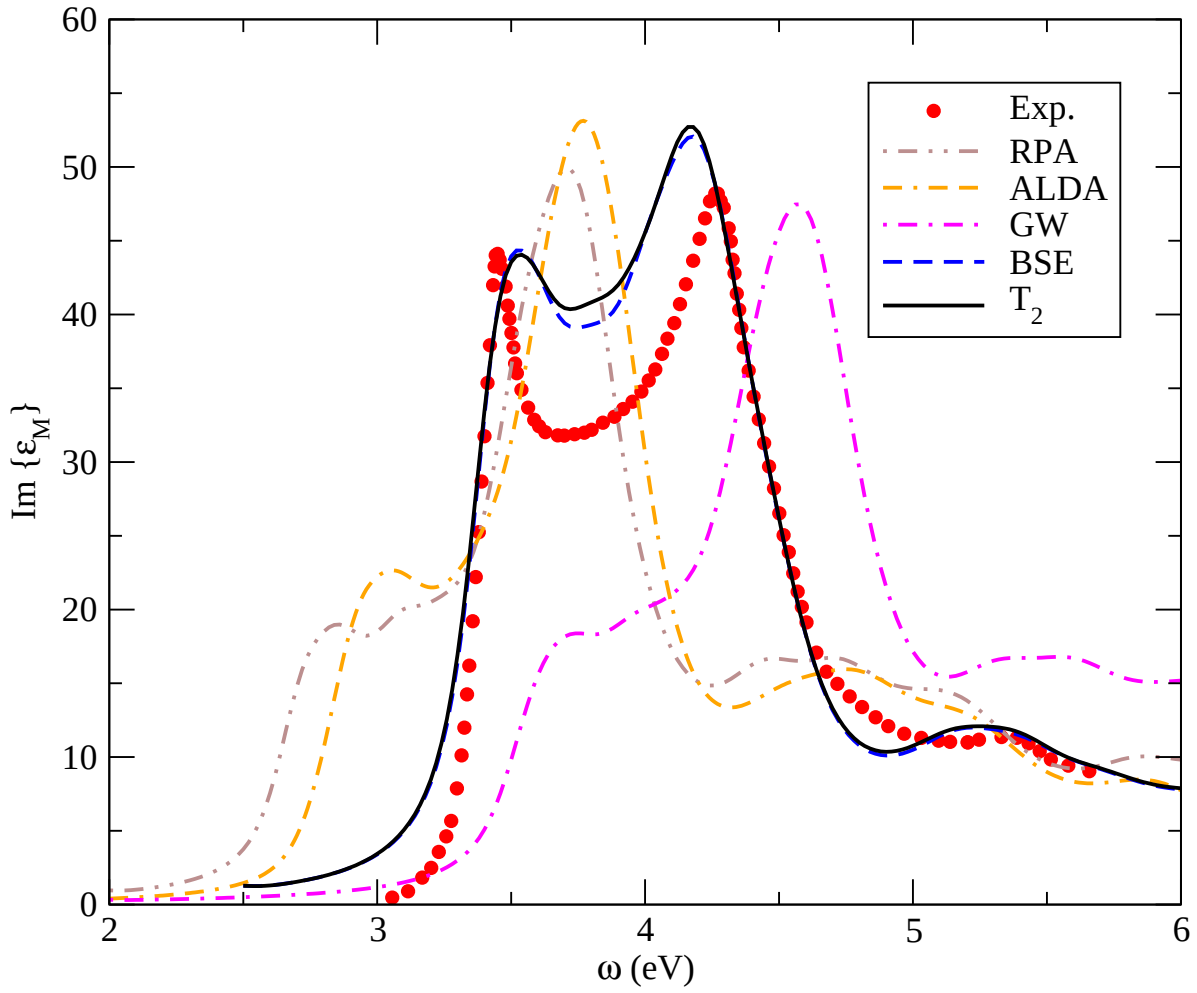

Figure 9.I: Imaginary part of the macroscopic dielectric function for solid silicon. Experiment from [98].

approach becomes more convenient, since the natural cutoff of the silicon wavefunctions prevents the basis from being equal, or even proportional, to N_t. However,with increasingly dense BZ sampling, one can find an increasing number of non-trivial eigenvalues of $\chi^0_{\rm GW}$ close to zero, even for $N_{\mathbf{G}} < N_t$. It happens, in fact, in the present calculation of silicon for $N_{\mathbf{G}} = 387$, which is considerably less than $N_t = 2304$ (see also the discussion in Par. 8.3). An immediate consequence for the calculations using the denser k-point sampling is the fact that, although we find an excellent spectrum, the kernel starts to be scattered at relatively low $N_{\mathbf{G}}$, so that the limit of a completely static kernel is never reached, as shown in Fig. 9.III.

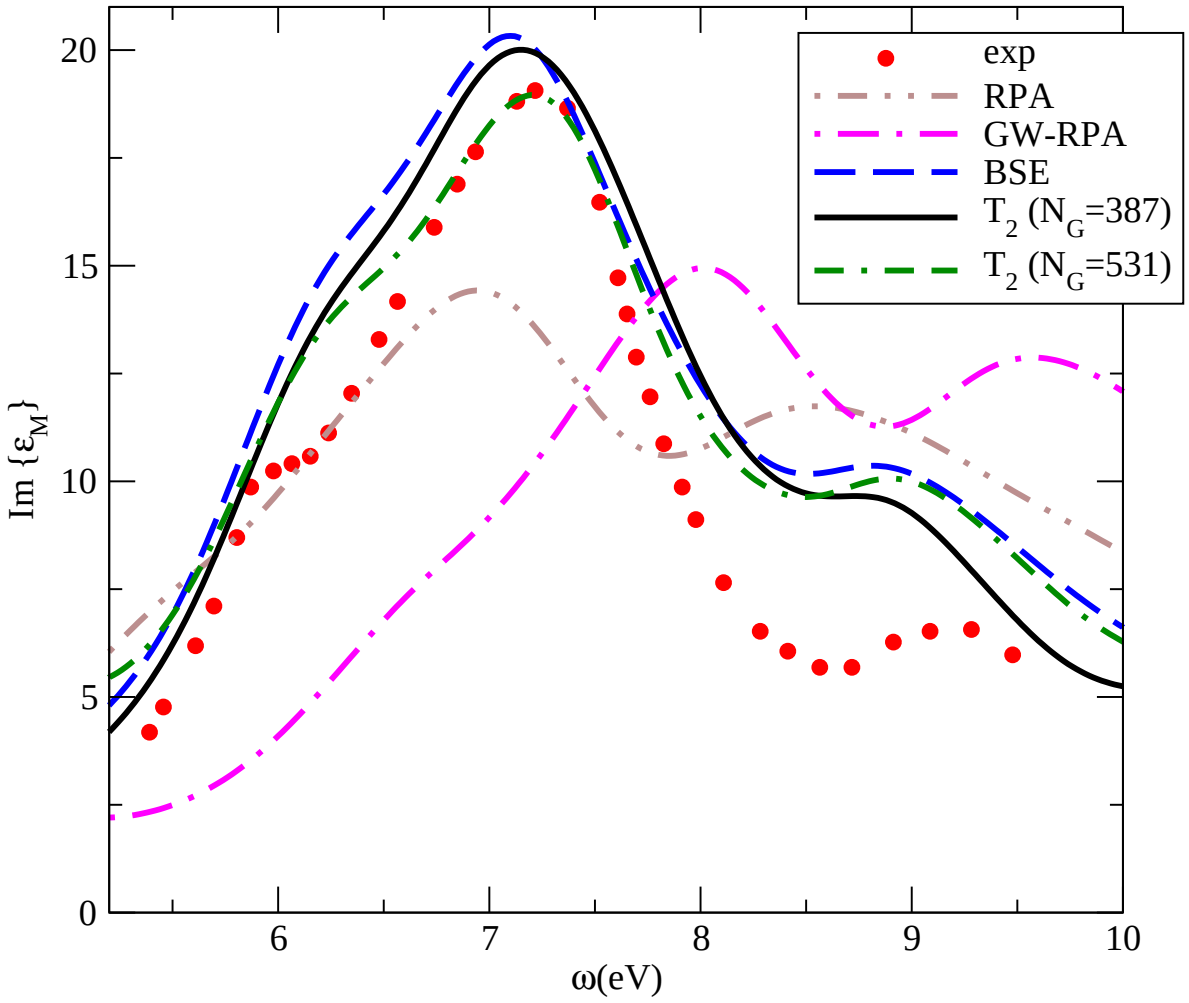

Figure 9.II: Imaginary part of the macroscopic dielectric function of SiC.

9.2 ... and of Silicon Carbide

The cubic SiC represents a severer test for the method. It is, in fact, a large-gap material with half the dielectric constant of silicon (hence twice the electron-hole interaction) which requires a considerably higher number of plane waves to describe the wavefunctions with respect to silicon. One might hence suspect that, contrary to the case of silicon, a well-converged spectrum cannot be obtained before $N_{\mathbf{G}}$ passes some critical value leading to absurd results.

In fact, we have found that also in the case of SiC, calculated with 3 valence and 3 conduction bands, and using 256 shifted k-points as in silicon, strong fluctuations in $\chi^{(0)-1}_{\mathrm{GW}}$ show up when N_G is chosen to be bigger than 387. However, in that range a

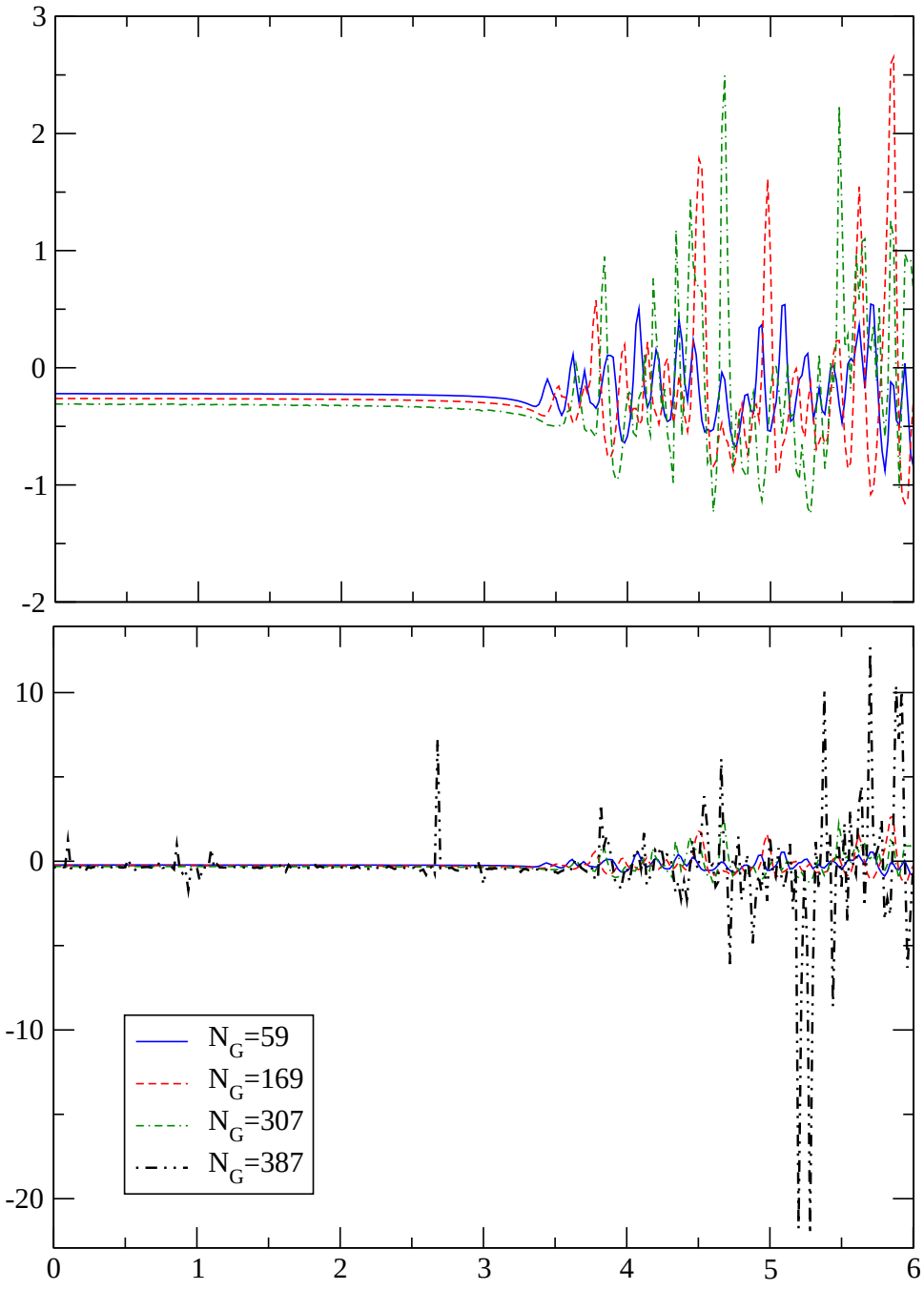

Figure 9.III: Kernel analysis of silicon. Upper panel: real part of $q^2 f_{xc}^{\mathrm{e-h}}(\omega)$ for three different values of $N_{\mathbf{G}}$. In the lower panel the same curves are reported, with the addiction of the case $N_{\mathbf{G}} = 387$ where the kernel starts to be scattered. The legend is the same for both panels.

reasonably converged spectrum is already in very good agreement with the result of BSE calculation, as one can see in Fig. 9.II. In this case the agreement between BSE (dashed line) and experiment (dots [291]) is not perfect, but the one between BSE and TDDFT (with our kernel T_2, continuous line) is still excellent, hence correcting most of the error of the GW-RPA result (dot-dashed line). The number of $\mathbf{G}$-vectors required to achieve the convergence is $N_{\mathbf{G}} = 387$, whereas for RPA (double dot-dashed line), GW-RPA and BSE spectra the convergence was achieved with $N_{\mathbf{G}} = 65$.

As we have already mentioned, the calculation of a spectrum is much less critical, and the results much more stable, than the calculation of f_{xc}. This is once again confirmed by the results of SiC. The TDDFT spectrum in Fig. 9.II (double-dash dotted line) is calculated using $N_{\mathbf{G}} = 531$. It is very good, even though the correspondent kernel $f_{xc} = (\chi^0_{\mathrm{GW}})^{-1} T_2 (\chi^0_{\mathrm{GW}})^{-1}$ is totally meaningless (see Fig. 9.IV).

9.3 Concluding remarks

In conclusion, the application of the kernel proposed in Chap. 8 to semiconductors, is to be considered extremely successful, leading to results which are almost indistinguishable from the BSE results. Moreover, since the two systems tested, silicon and silicon carbide, have a rather different band-gap energy (1.1 eV and 2.3 eV, for the experimental minimum gap, respectively), and consequently, a rather different electron-hole interaction contribution, it is reasonable to hope that the method will work out in a wide range of semiconductors.

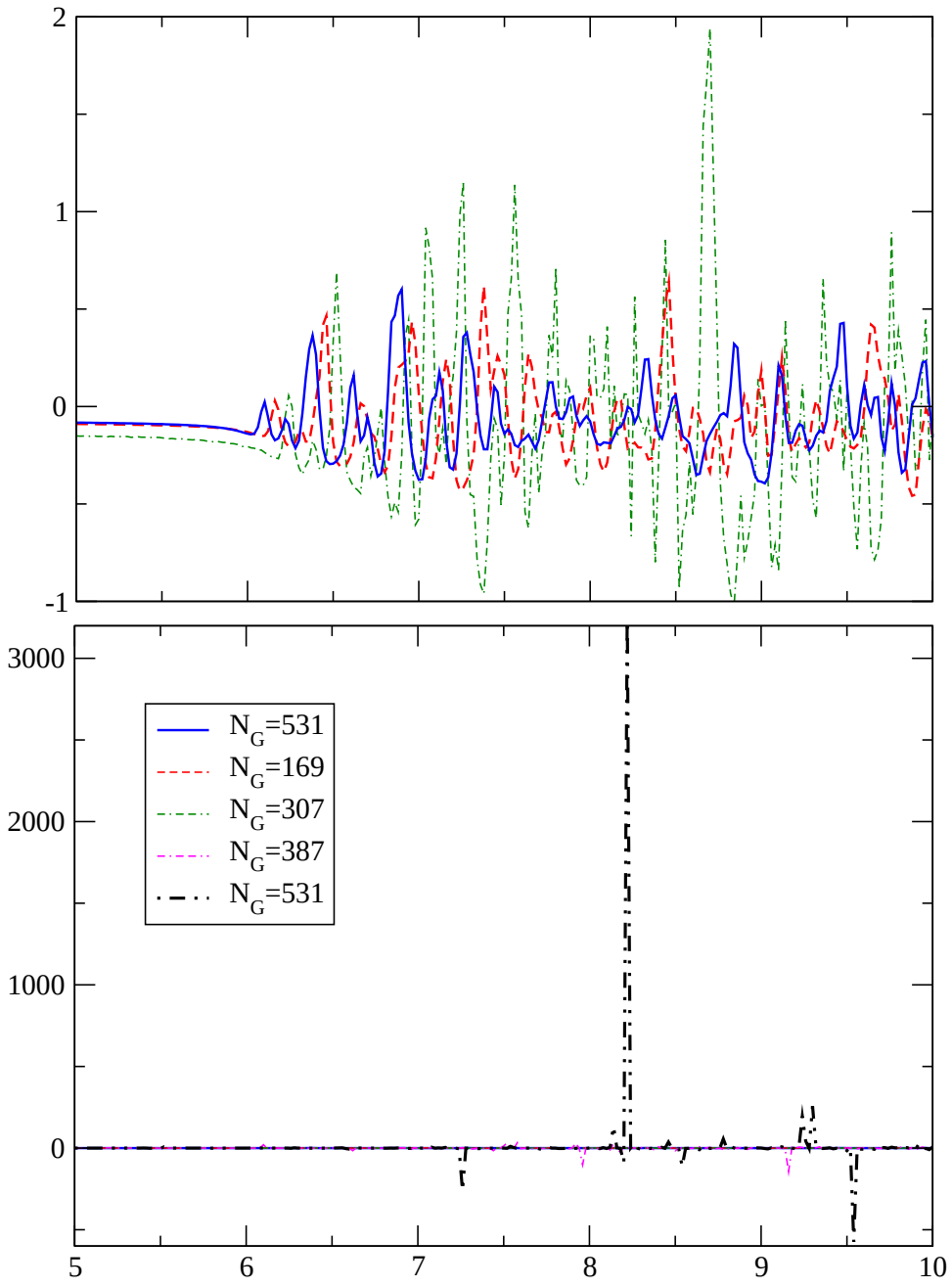

Figure 9.IV: Kernel analysis of SiC. Upper panel: real part of $q^2 f_{xc}^{\mathrm{e-h}}(\omega)$ for three different values of $N_{\mathbf{G}}$. In the lower panel the same curves are reported, with the addition of the cases $N_{\mathbf{G}} = 387$, the same value used for the calculation of the spectrum (but also the value where the kernel starts to be scattered), and $N_{\mathbf{G}} = 531$, when large fluctuations appear. The legend is the same for both panels.

Chapter 10

Bound excitons in TDDFT

> Veniet tempus quo posteri nostri tam aperta nos nescisse mirentur.
>
> from Naturales Quaestiones, Seneca

Up to now, in literature, bound excitons in solids have never been obtained by any attempt to calculate absorption spectra within TDDFT. Only in Chap. 7, we have shown, for the first time, that the TDDFT can lead to the description of bound excitons in solids, namely, in a static approximation and using the contact exciton model, for solid argon.

It seems obvious, now, in the light of the results of Chap. 9, to try to extend the application of the kernel T_2 to insulators, e.g. the solid argon tested in Chap. 7. However, before doing the same comparison (i.e. between BSE and TDDFT), made for the semiconductors in the previous chapter, we have to generate our reference result, i.e. the BSE result for solid argon.

This chapter will be resumed in F. Sottile, V. Olevano and L. Reining *Bound excitons in TDDFT*, in preparation.

10.1 BSE result for solid argon

The absorption spectrum of the molecular crystal of argon consists (see Fig. 10.I) of a strong excitonic peak at 12.1 eV, and a series of weaker peaks below the photoemission gap, whose value is 14.1 eV [270, 271, 292]. Starting from the DFT-LDA ground state, we have simulated the GW corrections to the DFT-LDA eigenvalues simply by applying a scissor operator of 6.0 eV. The result is the dot-dashed curve (GW-RPA) shown in

Fig. 10.I. We have then applied the BSE, obtaining the same results (BSE, continuous curve) as V. Olevano [209], and compared them with the experiment (dots).[1] The dotted curve, instead, represents the ALDA result.

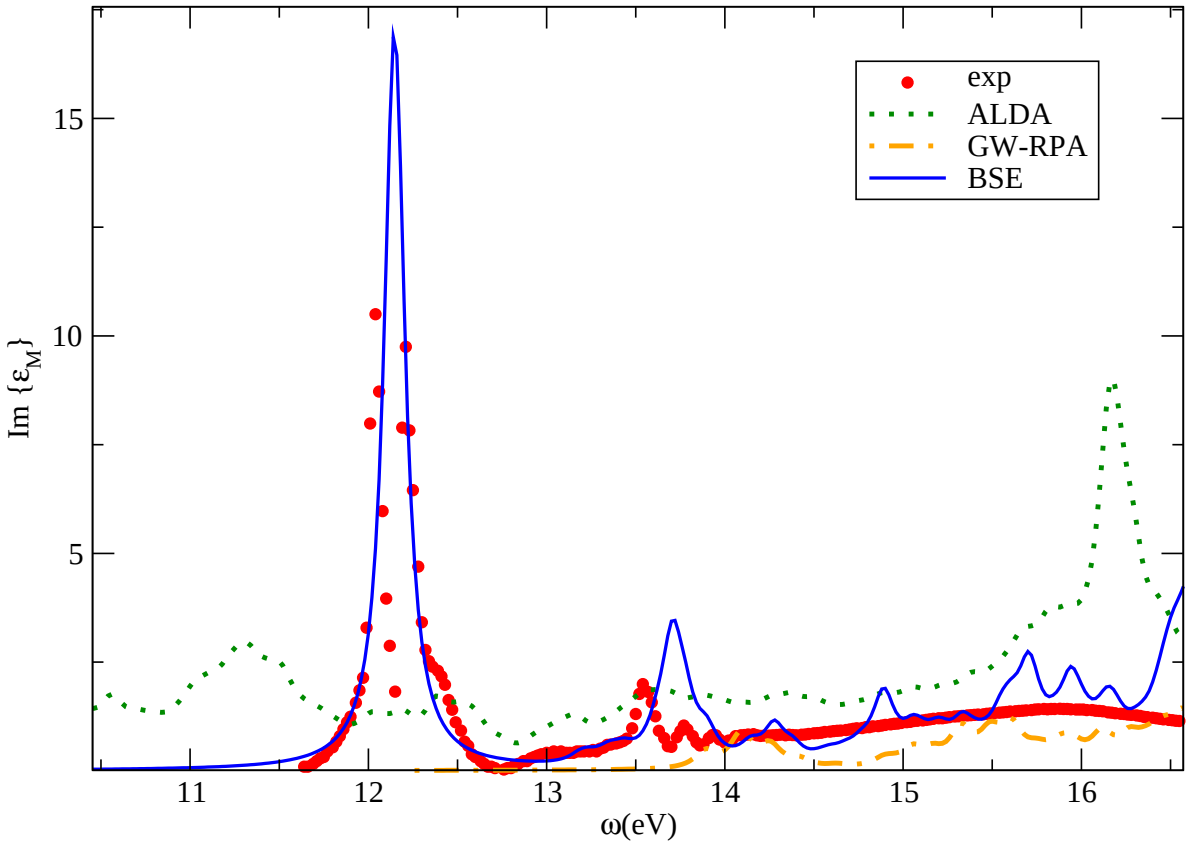

Figure 10.I: Solid argon. Comparison between ALDA, GW-RPA, BSE results with experiment. The calculations have all been performed using 256 shifted k-points and 6 (3 valence and 3 conduction) bands. The experiment is in arbitrary units.

As one can see from Fig. 10.I, the effect of the electron-hole interaction is huge, leading to a first strongly bound (2 eV) exciton. It is perfectly described by the BSE calculations. Less accurate is the description of the series of peaks weakly bound at $13.5 \div 14$ eV, at least with the k-points sampling used here (256 shifted k-points). This point, however, deserves a more detailed investigation.

[1] Note that the experimental result shows a spin-orbital split that is not contained in our calculation.

10.1.1 k-points sampling

In the case of calculation of the absorption spectra of silicon and other semiconductors, the use of shifted k-points (see Appendix E.2) has led to a big improvement with respect to the use of the special Monkhorst-Pack k-points. As one can see from Fig. 10.II, in the upper panel, the calculation (reasonably converged) of the absorption spectrum of silicon (same curve as reported in Fig. 9.I) using 256 shifted k-points is much more in agreement with the experiment, than the same calculation performed sampling the BZ with 256 Monkhorst-Pack k-points, corresponding to only 10 (crystallographically different) k-points in the irreducible BZ (dot-dashed curve). However it is important to distinguish between the effect of the sampling on the band structure, and the effect of the sampling on the characterization of the electron-hole interaction. The former can be investigated looking at the GW-RPA results shown in Fig. 10.IV, for both silicon and argon. The difference between the two samplings (10 k-points and 256 k-points) in silicon is big, even using a quite large broadening,[2] whereas the same difference for the argon is less important: the broadening used for argon is only 0.07 eV (absolute Lorentzian). A larger broadening, e.g. the same as the one used for silicon, has led to a very small difference between the two samplings (inset of the lower panel of Fig. 10.IV). If now we come back to Fig. 10.II we realize that the different sampling has also an effect on the description of the electron-hole interaction: in particular, in silicon, the difference between the spectra is still enforced, while in argon it is further reduced and, in the region of the first excitonic peak, almost vanishing. This is reasonable: the series of bound peaks in argon is in fact similar to the hydrogen-like series predicted by the Wannier-Mott exciton model [293, 294] (although the first peak is rather Frenkel-like [295, 296]). Therefore the $n = 1$ peak mixes a rather large portion of k-space, which allows a rough sampling, whereas the higher order peaks only mix transitions close and closer to the Γ point. This behavior is illustrated in Fig. 10.III. This implies that, in order to describe the first excitonic peak of argon, not only few k-points are sufficient, but also the nature of the sampling (if special or shifted k-points) is not so important.

Instead, 256 k-points are not enough to converge the spectrum of solid argon, for a good description of the excitonic series starting from 13.5 eV. For this reason, we have performed a calculation for the optical spectrum of argon, using 2048 shifted k-points and only 4 (3 valence and 1 conduction) bands.[3] The choice of a restricted number of bands, dictated by computer-time reasons, turned out not to worsen the convergence of

[2]The broadening used for GW-RPA and BSE calculations of silicon is the following: absolute Lorentzian broadening = 0.05 eV. In addition a relative Lorentzian and Gaussian broadening (1.5%) have been applied (which corresponds to add about 0.15 eV).

[3]Passing from 256 to 2048 k-points had, as a consequence, the reduction of the DFT-LDA band-gap, because we are sampling closer to the Γ point. In order to simulate the experimental photoemission gap, we had hence to increase the "scissor" operator up to 6.4 eV (it was 6.0 eV for the case of 256 k-points). It is important, however, to point out that the electron-hole binding energy is has not been influenced by this shift.

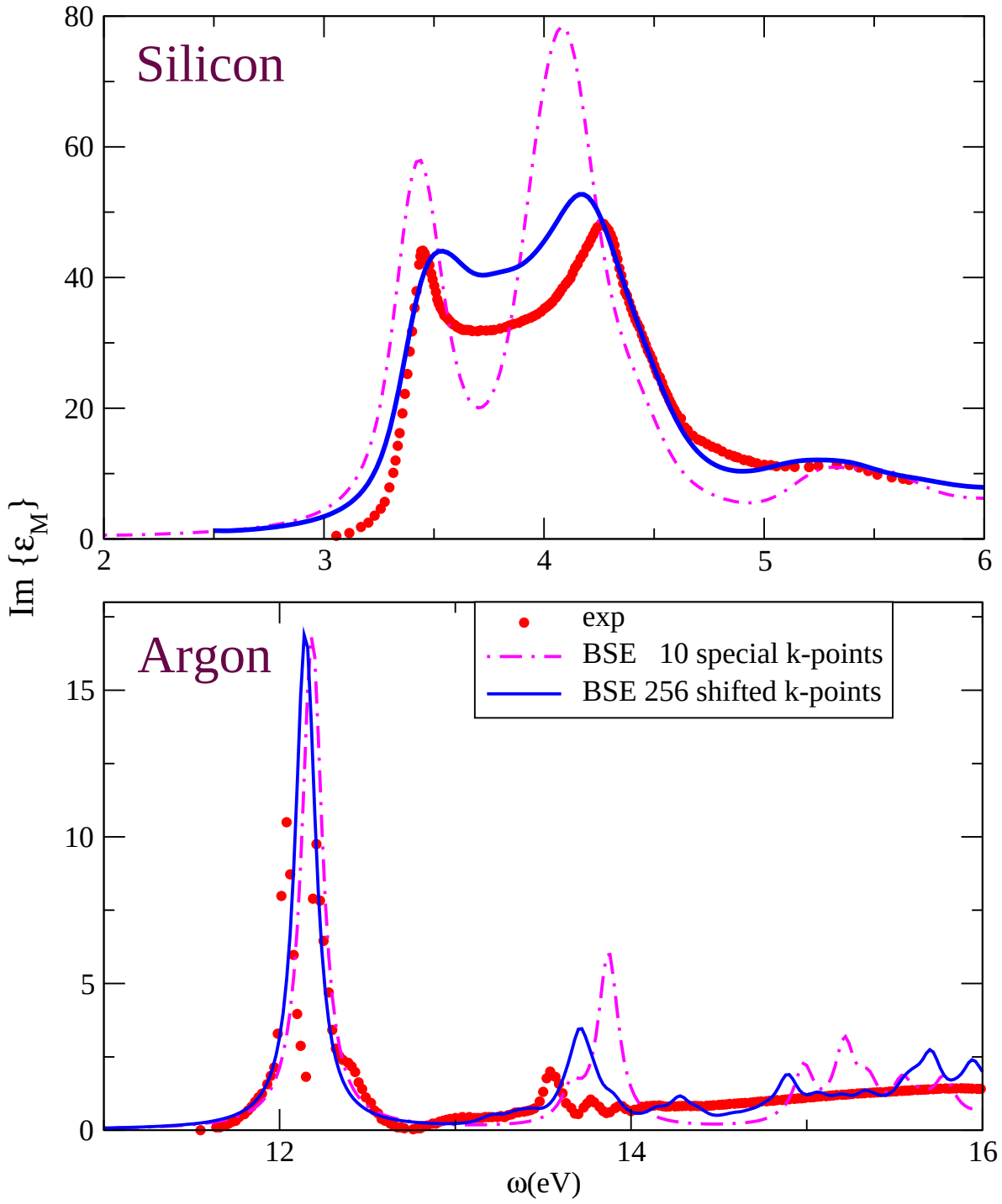

Figure 10.II: Imaginary part of macroscopic dielectric function of silicon (upper panel) and argon (lower panel). Comparison between BSE calculations (two different samplings of the BZ) and experiment. The legend is the same for both panels.

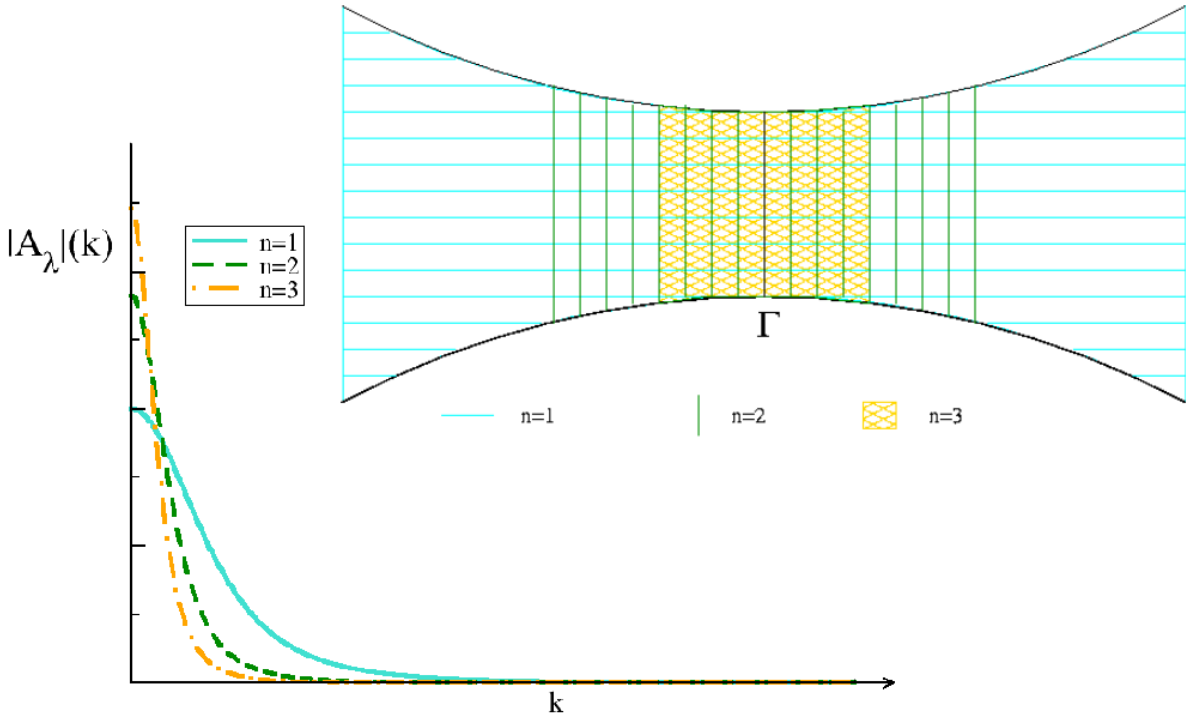

Figure 10.III: In the Wannier-Mott exciton model, the eigenvectors A^k_λ of the excitonic Hamiltonian (3.37) have the shape described [297, 298] by the continuous, dashed and dot-dashed curves, for $n = 1, 2, 3$, respectively. The number of k-points required for a given accuracy of the k-sampling (supposed homogeneous) is clearly bigger for an higher n.

the spectrum below the onset. Of course, this choice prevents any inference about the continuum, for which much more bands would be necessary.

The result is shown in Fig. 10.V, where both calculations (256 and 2048 shifted k-points) are compared with the experiment. The position of the first peak is still well described, but now, with the finer sampling, it has been possible to describe the n=2 and n=3 peaks which are in good agreement with the experiment, both for position and their relative intensity. Using the BSE, the description of the strong excitonic effects occurring in the optical spectrum of solid argon is hence possible, and very successful.

10.2 TDDFT description of Argon

The issue of bound excitons in solids has been addressed in the framework of TDDFT in Chap. 7, for the first time. Now we want to apply the kernel developed in Par. 8.1, and more precisely the term T_2 (the term T_1 is contained in χ^0_{GW}), in order to verify if the description of bound excitons in solid is possible even by a fully *ab initio* parameter-free

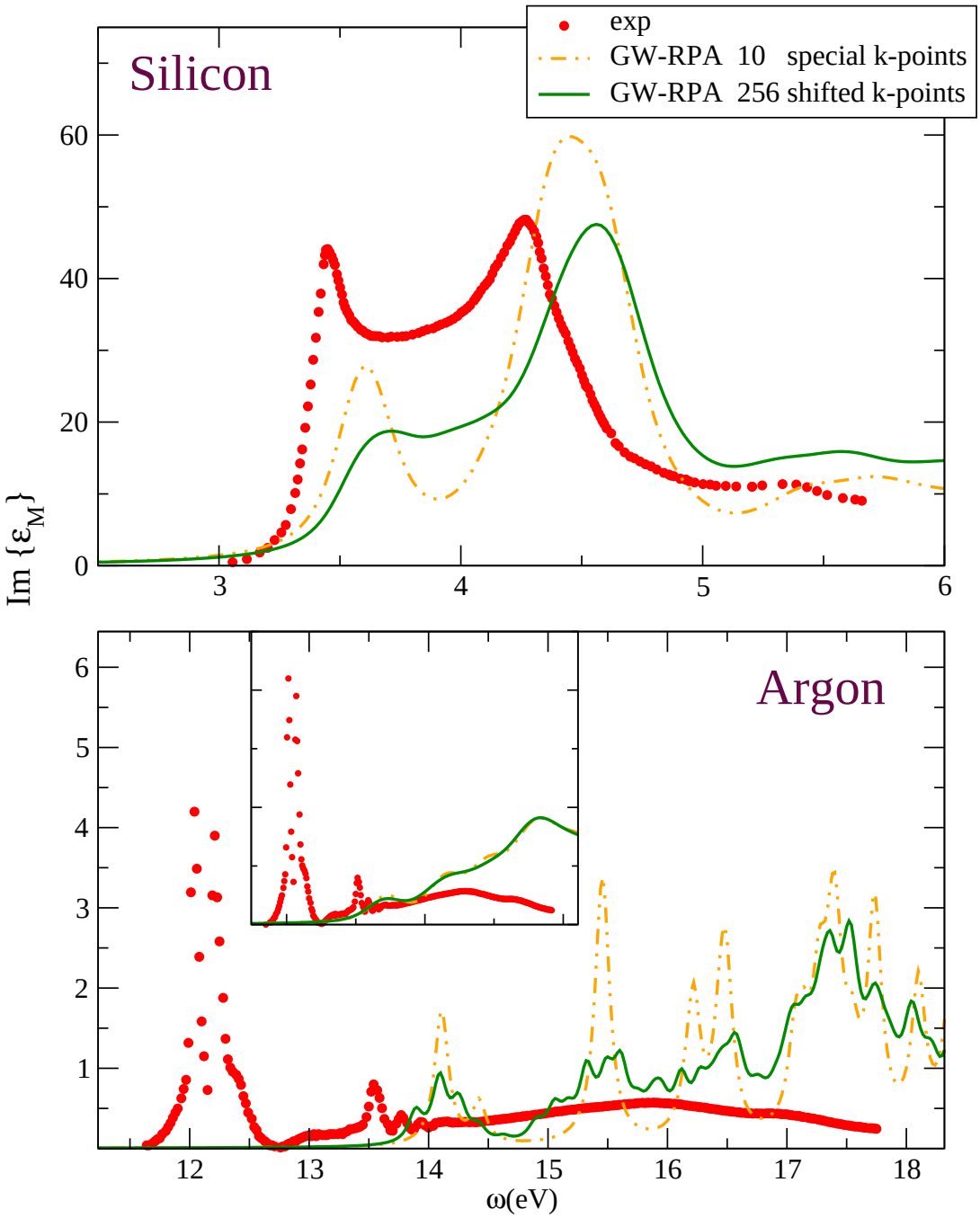

Figure 10.IV: Imaginary part of macroscopic dielectric function of both silicon (upper panel) and argon (lower panel). Comparison between calculations (using two different samplings of the BZ) and experiment. Inset of the lower panel: GW-RPA calculation of solid argon, using the same broadening as in the silicon case. The legend is the same for both panels.

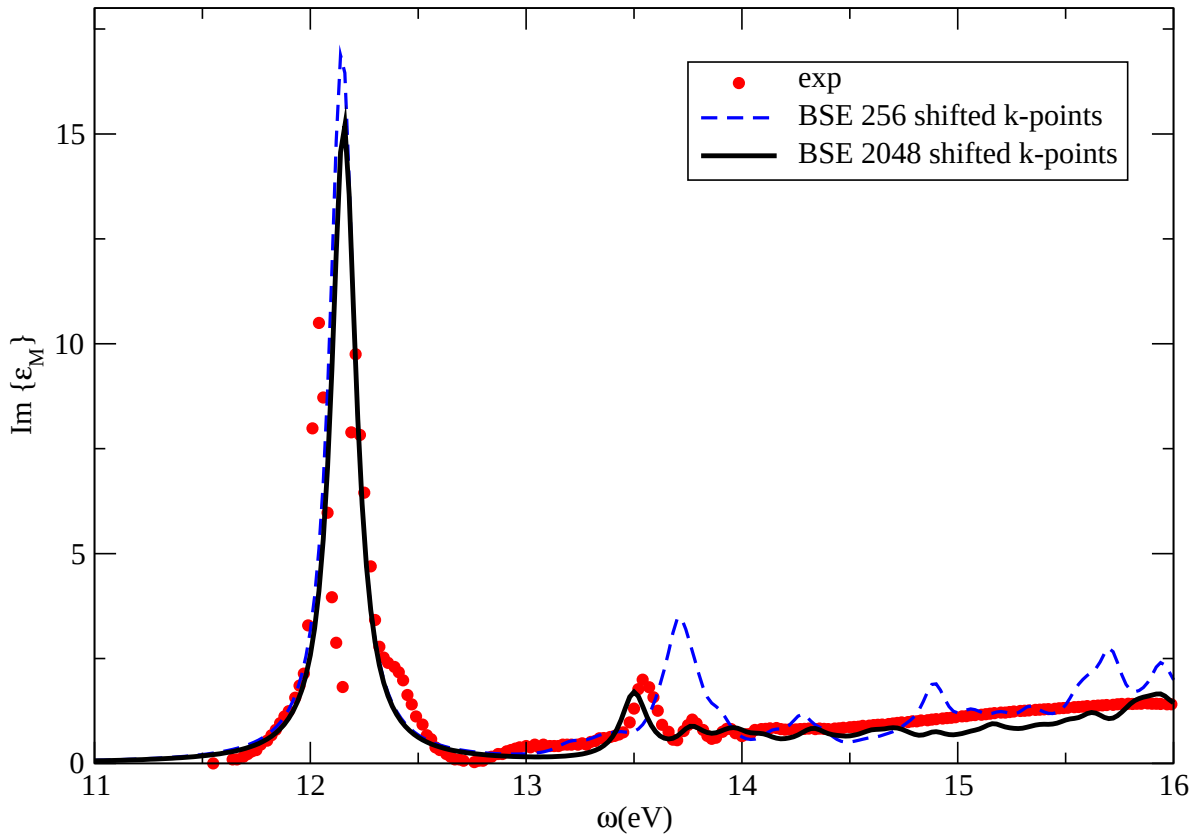

Figure 10.V: Imaginary part of macroscopic dielectric function for solid argon. Two different samplings of the BZ (256 and 2048 k-points) are compared with the experiment.

TDDFT approach, like the one proposed here.

We have then calculated the imaginary part of the macroscopic dielectric function in TDDFT, via Eq. (8.9), for different values of $N_{\mathbf{G}}$, and compared the results with our reference, i.e. the BSE calculations. We have first used 256 shifted k-points and 6 (3 valence and 3 conduction) bands, obtaining the results shown in Fig. 10.VI. Contrary to the ALDA result in Fig. 10.I, our TDDFT approach creates a strong transition in the gap. The description of the first peak is not bad, even though a small (about 0.3 eV) blue-shift occurs, but the second peak, inside the gap, is not reproduced. Moreover, because of the small broadening,[4] large fluctuations (leading also to negative absorption) can be seen in the spectrum. Nevertheless, the results shown are remarkable: the kernel T_2 (8.13) *is* able to describe bound excitons in solids, in a parameter-free approach within TDDFT.

However, we are not fully satisfied. The agreement between TDDFT and BSE was, for semiconductors, much more impressive; a deeper analysis is, then, crucial to better

[4]We have used the same broadening as in the BSE calculation, i.e. 0.07 eV (Lorentzian).

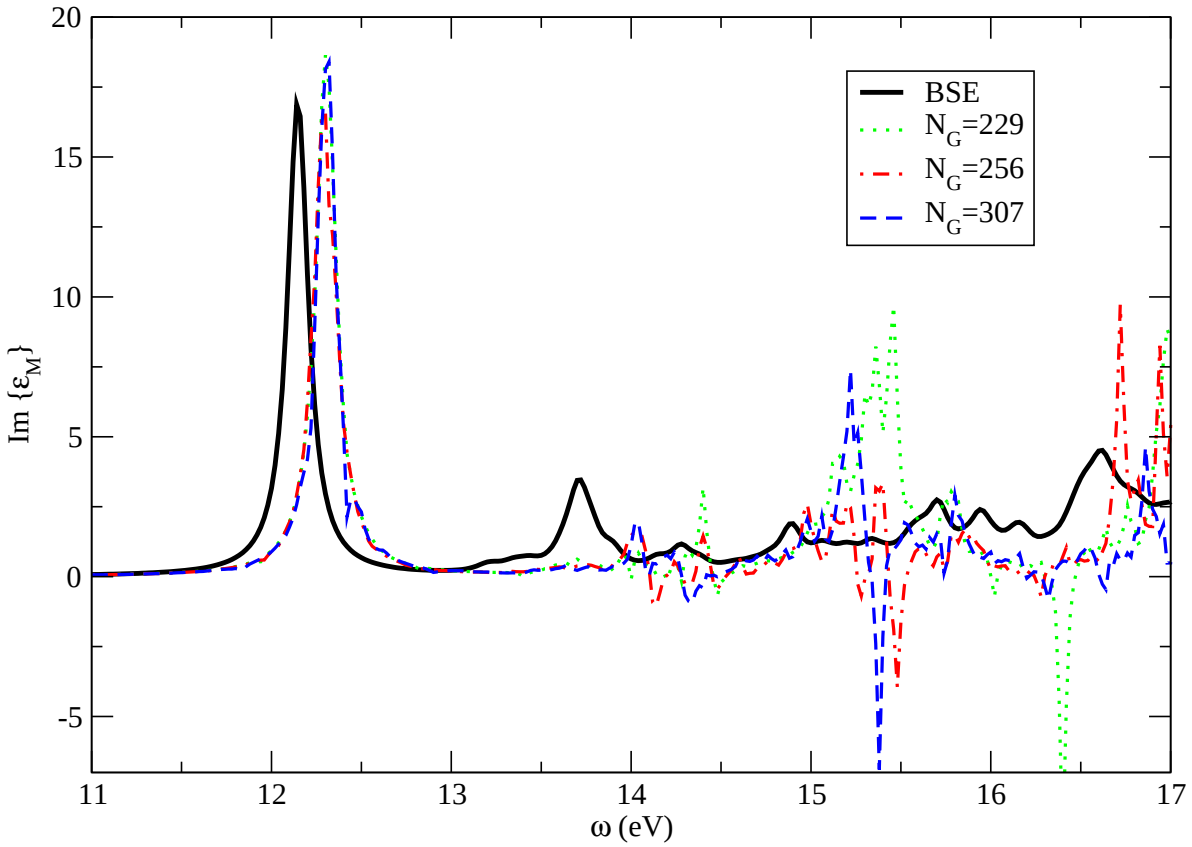

Figure 10.VI: Imaginary part of the macroscopic dielectric function of argon. The TDDFT results (different cutoff $N_{\mathbf{G}}$) are compared with the BSE result. 256 shifted k-points.

understand the behavior of TDDFT calculation of optical spectra of insulators.

10.2.1 Diagonal contribution of T_2: a problem.

In order to build the term T_2, a small contribution comes from the particular case $(vc\mathbf{k}) = (v'c'\mathbf{k}')$, i.e. from the contribution that is diagonal in transitions. This contribution, that we call T_2^d, is given by

$$T_2^d(\mathbf{G},\mathbf{G}',\omega) = \frac{2}{N_k^2}\sum_{vc\mathbf{k}} \frac{\Phi^*(vc\mathbf{k},\mathbf{G})F^{\mathrm{BSE}}_{(vc\mathbf{k})(vc\mathbf{k})}\Phi(vc\mathbf{k},\mathbf{G}')}{\left[\omega-(E_{c\mathbf{k}}-E_{v\mathbf{k}})+i\eta\right]^2}. \tag{10.1}$$

The term T_2^d has exactly (except for the prefactor) the same shape as the term T_1. We have already seen that the latter is problematic and, that it should not to be taken into account in realistic calculations. The same conclusion should hold for T_2^d. Let's investigate, then, the value of $F^{\mathrm{BSE}}_{(vc\mathbf{k})(vc\mathbf{k})}$, for each transition $vc\mathbf{k}$. The results, shown in

Fig. 10.VII, clearly demonstrate that the term $F^{\mathrm{BSE}}_{(vc\mathbf{k})(vc\mathbf{k})}$ is, indeed, almost constant in the transition space, with a value -0.76 ± 0.01 eV.

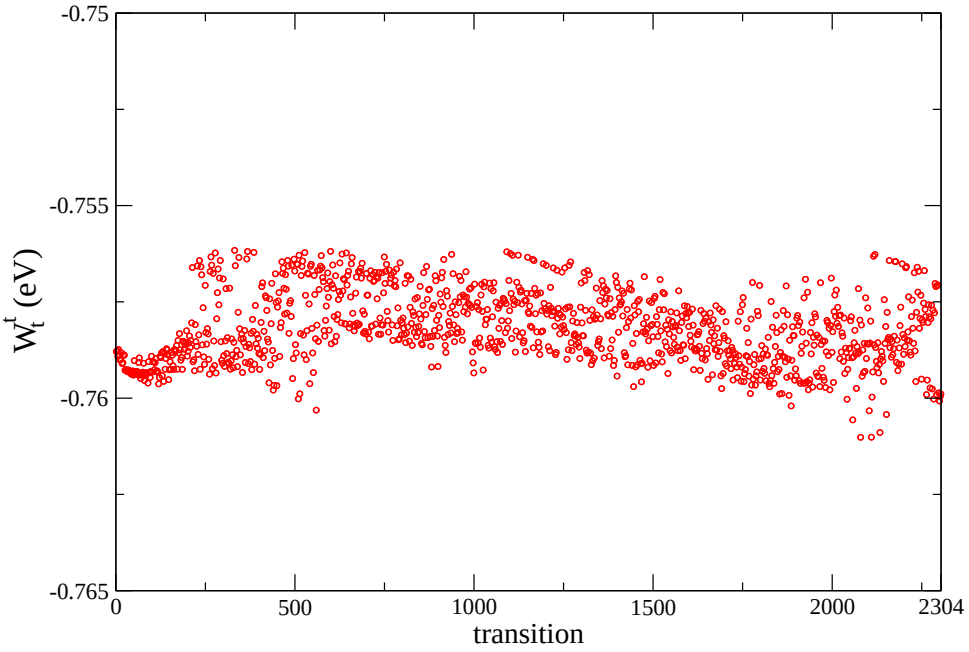

Figure 10.VII: Value of $F^{\mathrm{BSE}}_{(vc\mathbf{k})(vc\mathbf{k})} = W_t^t$ per transition ($N_t = 2304$). 256 shifted k-points.

Its effects should only be to shift the spectrum (towards lower energies, by 0.76 eV). Since its shape is that of T_1, it could be responsible for the convergence difficulties shown in Fig. 10.VI. To be sure of that, we have, firstly, calculated the optical spectrum of argon subtracting from T_2, the diagonal contribution T_2^d, thus leading to the dot-dashed curve in Fig. 10.IX; second, we have simulated the missing diagonal contribution by a rigid shift (given, of course, by the value of $F^{\mathrm{BSE}}_{(vc\mathbf{k})(vc\mathbf{k})} = -0.76$ eV (dashed curve in Fig. 10.IX)). The agreement between BSE and TDDFT is now very good, both for the first and second excitonic peak. This confirms again, that the diagonal contribution T_2^d worsens (or even prevents) the convergence, exactly like the term T_1 does. Another more rigorous possibility, instead of putting a rigid shift, could be to insert the diagonal contribution T_2^d directly in the χ^0 matrix [299], as we have already done for the term T_1. χ^0 would then become a $\chi^0_{\mathrm{GW},T_2^d}$ matrix.

It is important to notice that the diagonal contribution T_2^d, at the contrary of T_1, vanishes for $N_k \to \infty$, because of the prefactor $\frac{2}{N_k^2}$. A calculation with an increased number of k-points then, is crucial, not only to obtain better results to compare with the experiment (we have seen that 256 k-points are not sufficient for a good description of the spectrum), but also to verify the decreasing importance of T_2^d. This will be done in the following.

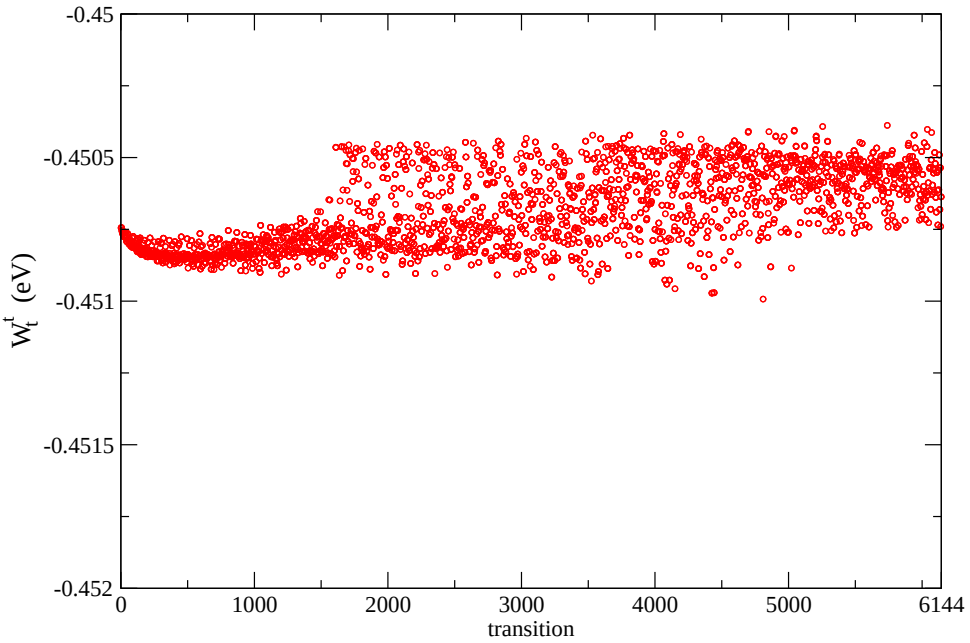

Figure 10.VIII: Value of $F^{\mathrm{BSE}}_{(vc\mathbf{k})(vc\mathbf{k})} = W^t_t$ per transition ($N_t = 6144$). 2048 shifted k-points.

10.2.2 Comparison with experiment

We use now 2048 shifted k-points and 4 (3 valence and 1 conduction) bands to calculate the absorption spectrum, in TDDFT, first using the full term T_2 (Fig. 10.X), for different $N_{\mathbf{G}}$. Then, we have followed the procedure of the previous paragraph, replacing the diagonal contribution T_2^d with a rigid shift (of an amount of 0.45 eV, extrapolated from Fig. 10.VIII), whose result is shown in Fig. 10.XI. Even for 2048 shifted k-points, when the whole T_2 is used, its diagonal prevents the achievement of convergence with the number of **G**-vectors $N_{\mathbf{G}}$. In this case, however, T_2^d is smaller and the spectrum is qualitatively better than the one using 256 shifted k-points: in particular the second bound peak is present, even though in a wrong position (the shift describing the missing T_2^d, is now decreased, as expected, although the behavior of $F^{\mathrm{BSE}}_{(vc\mathbf{k})(v'c'\mathbf{k}')}$ when the number of k-points N_k increases is not as $1/N_k$, but slower [5]). The agreement between BSE and TDDFT becomes impressive, when the diagonal contribution T_2^d is separately treated (i.e. subtracted from T_2 and simulated by a simple rigid shift), with a difference of only 0.04 eV between BSE and TDDFT on the first peak.

[5] This is due to the fact that roughly $W^{k'}_k$ goes as $1/|k-k'|^2$, and, for $k = k'$, the divergence is integrated over a small volume around zero.

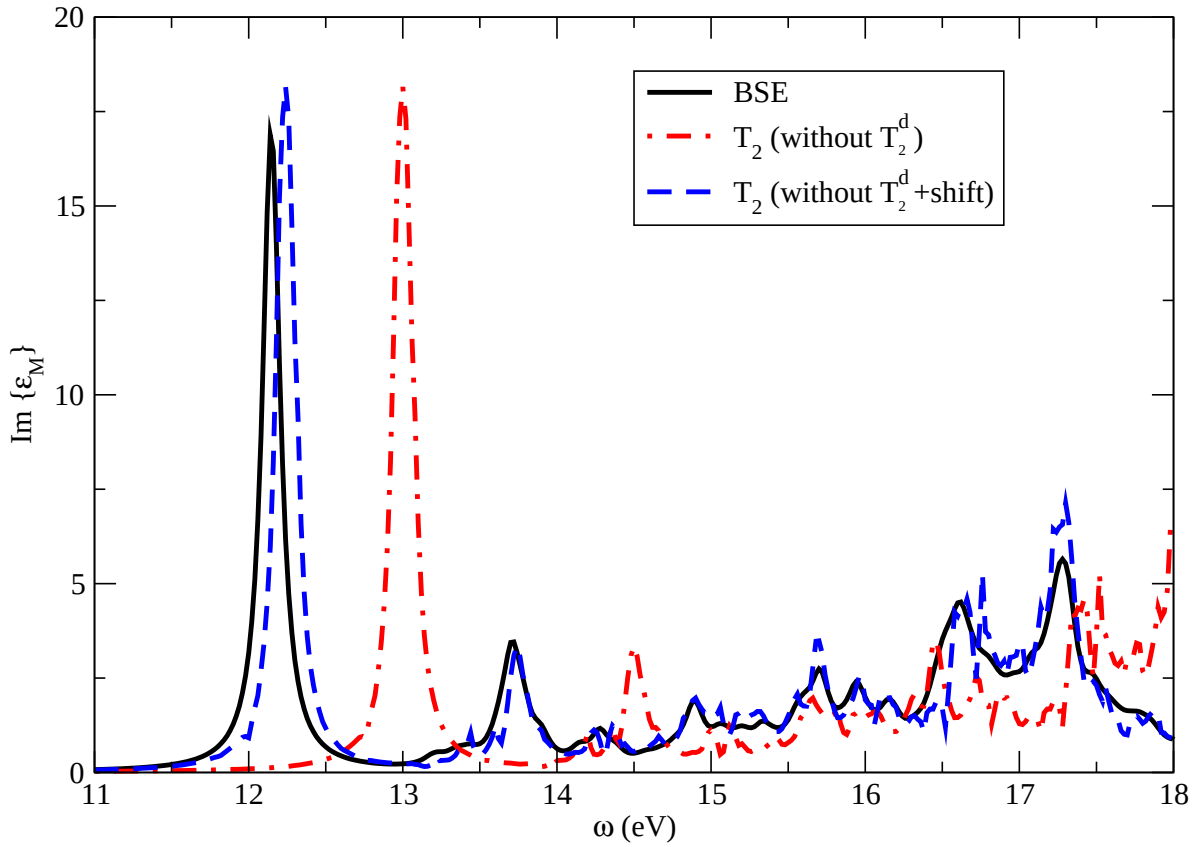

Figure 10.IX: Imaginary part of the macroscopic dielectric function of argon. The dot-dashed curve represents the TDDFT results obtained subtracting the term T_2^d to the full T_2, whereas in the dashed curve this diagonal contribution has been simulated by a rigid shift of the spectrum (by a value of -0.76 eV). 256 shifted k-points.

10.3 Results of other groups

The same formula for the electron-hole contribution to the exchange-correlation kernel in TDDFT (8.13) has been derived independently by a group in Rome [300, 301], following a different approach. Although still based on a comparison between BSE and TDDFT, in that work the kernel is developed in a perturbative series in terms of the screened interaction W. The first order of this perturbative series coincides with our formula (8.13). This is not a contradiction: we have already seen in Par. 8.1.1 that our initial assumption (8.6) cannot always be fulfilled, and we have given counter examples. Instead, for the examples given in Par. 8.1.2, where Eq. (8.6) can be exactly fulfilled, all the higher (than the first) order, in the perturbation series of the approach followed in Rome, vanish. In principle, the second order perturbation term [299] could be taken into account to overcome the problems that arise when (8.6) cannot be fulfilled. However, it seems that

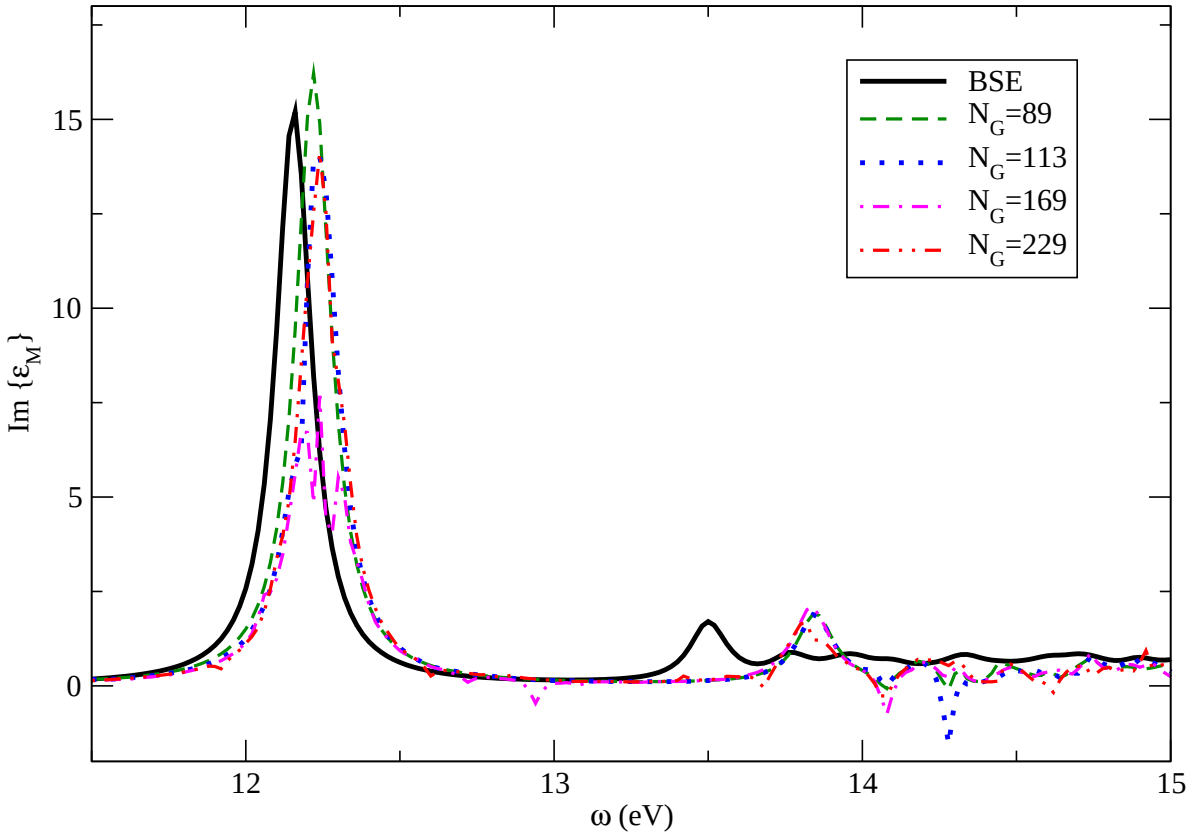

Figure 10.X: Imaginary part of the macroscopic dielectric function of argon. The TDDFT results (various cutoffs $N_{\mathbf{G}}$) are compared with the BSE result. The diagonal contribution T_2^d is included in T_2. 2048 shifted k-points.

this is only partially true. For example, the description of a shift, i.e. what we have called T_2^d (10.1), or a T_1 (8.12), does not improve. The convergence of the perturbation series is not simply due to the magnitude of some parameter,[6] in fact, the case of the contact exciton model (Par. 7.2) is an example where our initial assumption is perfectly fulfilled (which means that all the perturbative orders higher than the first have to vanish) even when the screened interaction W is *not* "small".

More comparisons will have to be done to elucidate the links between the two approaches in detail. In any case, we have been informed by our colleagues that the application of T_2 (8.13) yields excellent results also for other systems, like LiF and SiO_2, which is an additional demonstration of the accuracy and the potentiality of the kernel here proposed.

[6] It could be supposed, in fact, that such a perturbative series only converges rapidly if W is "small".

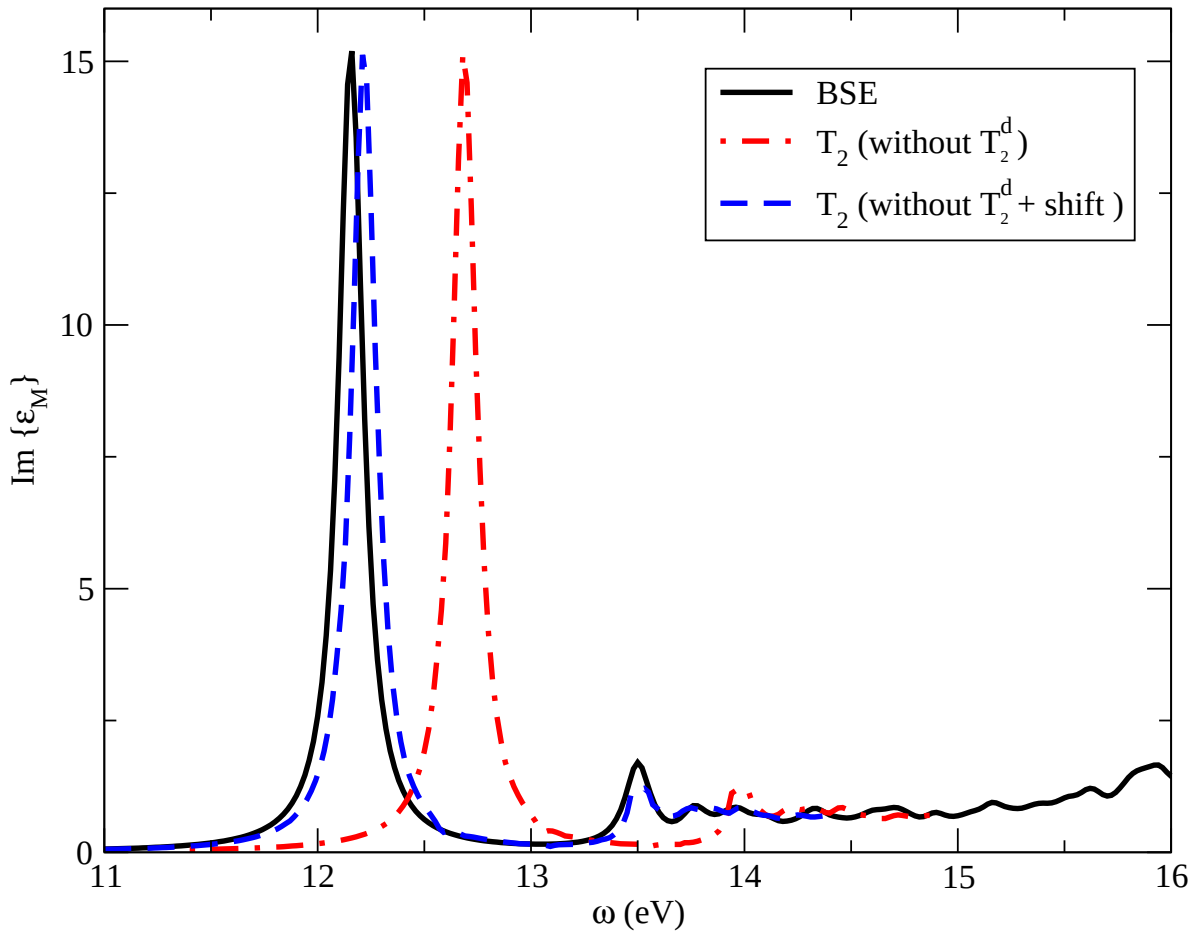

Figure 10.XI: Imaginary part of the macroscopic dielectric function of argon. The dot-dashed curve represents the TDDFT results obtained subtracting the term T_2^d from the full T_2, whereas in the dashed curve this diagonal contribution has been simulated by a rigid shift of the spectrum (by a value of -0.45 eV). 2048 shifted k-points.

10.4 Concluding remarks

Analogously to what we have seen for semiconductors, even in the case of insulators the application of the kernel T_2 is extremely successful, leading to results which are almost indistinguishable from the BSE ones, in their turn in good agreement with experimental results. We are therefore confident that this method can be proposed as a general solution for the calculation of excitonic effects in materials.

Conclusions

Non senza fatiga si giunge al fine.

Toccata Nona of Girolamo Frescobaldi

In this thesis, we have dealt with the description of optical properties of materials, with a particular interest in bulk materials.

The state-of-the-art of first principle calculations of optical absorption of solids has been represented, up to recently, by the Bethe-Salpeter equation (BSE) approach. The results one can achieve within BSE are in good agreement with experiments and, moreover, the range of applicability of BSE goes well beyond the solids. Absorption spectra of atoms, molecules, clusters or surfaces are usually well described by the Bethe-Salpeter approach. The heaviness of the calculations involved, however, prevents a large-scale application to more complex systems, that are the systems of great interest in material science like, e.g., quantum dots, multi-wall nanotubes, biological molecules or defects in solids.

The most prominent alternative to the Bethe-Salpeter approach is the Time Dependent Density Functional Theory, which is density-based and, therefore, could in principle lead to simpler calculations. A widely used approximation to the TDDFT is the adiabatic local density approximation (ALDA). Despite its (partial) success in finite systems the ALDA has led to poor results in the description of optical absorption of solids. The search for an efficient description of optical spectra of solids in TDDFT has become, hence, one of the major problems related to the optical response of a material.

In this thesis new inroads have been made in the comprehension of the optical response of a material. Starting from a joint analysis of the BSE approach and the TDDFT framework, it has been possible to calculate the optical spectra of solids, semiconductors and insulators, with the inclusion of the excitonic effects, *without solving the BSE but obtaining results of the same precision.*

To do so, we have derived, or re-derived in a more general way, the most relevant formulas, and implemented them in existing computer codes.[7] In order to increase the efficiency and the stability of the calculations, the codes have also been optimized, and, in

[7]Details about local computer codes are in Ref. [105].

particular, a linear solver technique has been implemented to avoid all matrix inversions. A large number of calculations for a detailed analysis of the models used and for all hypotheses made, had then to be performed. Finally we have illustrated our findings for bulk silicon, silicon carbide, and solid argon.
More in detail, after the theoretical framework, presented in chapters 1-4,

- In chapter 5 we have recalled the fact that TDDFT and BSE have the same mathematical structure, and that the response function in both approaches can be written as

  $$S = S^0 + S^0 K S$$

  whose solution gives the searched absorption or energy loss spectrum. The link between the response of an independent particle (or quasi-particle) system S^0 and the full response S is given by the kernel K in this Dyson-like screening equation. The kernel K contains the Coulomb interaction v, which is common to both TDDFT and BSE, and the exchange-correlation (in TDDFT) or electron-hole (BSE) contribution, which is instead different in the two approaches.

- The role of the Coulomb potential v has been elucidated in chapter 6. We have discussed its long-range component v_0, which is responsible for the difference between the absorption and the electron energy loss spectra in solids. To further illustrate this result, we have shown, analytically and numerically that, in the limit of an isolated system, where the long-range component of the Coulomb interaction is negligible, the absorption and the electron energy-loss (at vanishing momentum transfer) spectra are the same. The microscopic components of the Coulomb interaction, instead, are responsible for the local field effects.

- We have then addressed the second term of the kernel K, namely the exchange-correlation kernel f_{xc} (in TDDFT). The study made in chapter 7 has allowed us to show that simple static approximations for the exchange-correlation kernel f_{xc} can yield spectra of semiconductors and insulators in qualitative agreement with the experiments.

- In chapter 8 we have generalized a previously proposed, but never tested, expression for an exchange-correlation kernel f_{xc}, within the time dependent density functional theory framework, which is fully *ab initio* and parameter-free. We have also investigated the different contributions to the kernel and found out how and when the generalized kernel $\chi^0 f_{xc} \chi^0$ works in principle.

- In chapter 9 the kernel here developed is applied and tested for two semiconductors, namely bulk silicon and silicon carbide, while

- in chapter 10 the kernel is tested for an insulator, taking solid argon as an example. In both semiconductors and insulators the results of the TDDFT (using the kernel developed in chapter 8) and those of BSE are almost indistinguishable.

We have hence contributed to the solution of the long-standing problem of how to calculate the absorption spectra of solids, in the framework of TDDFT, without solving the BSE.

To have dealt with this problem, has allowed us to address, answer or simply illustrate several questions:

→ classical Coulomb (Hartree) contributions play an important role in electronic spectra, and it is worthwhile to discuss their effects before addressing the problems of exchange and correlation. Their short-range and long-range parts are crucial for understanding the link between absorption and energy loss, and the transition between finite and infinite systems.

→ satisfactory optical spectra of semiconductors and insulators can be obtained by using very simple models for the electron-hole interaction (in BSE) or for the exchange-correlation kernel (in TDDFT); these models, of course, depend on parameters that one has to adjust to fit the experiment. However the computational complexity of these calculations is that of the RPA, and one might try to find ways to determine these parameters from first principles;

→ to obtain an exchange-correlation kernel from the BSE is not straightforward. However, apart from some counter examples, discussed in chapter 8, in most cases an approximate mapping from one theory (the BSE) to the other (the TDDFT) is possible. A first consequence of the existing difficulties is that the resulting f_{xc} kernel can suffer of convergence problem (requiring a lot of $\mathbf{G}$-vectors or presenting strong fluctuations in frequency). There can also be several possible approximate mappings: an example is reported in chapter 7 where two exchange-correlations kernels, a long-range and an ultra short-range one, give similar (good) results. These two kernels are derived starting from the same model (the contact exciton model) within the BSE;

→ an important finding, following the discussions of chapter 8, is that the key quantity of the theory is not the kernel f_{xc}, but f_{xc} multiplied by a response function;

→ finally, we are now able to obtain very good results for the optical spectra of solids, well describing both the continuum and bound excitons, within a parameter-free TDDFT framework.

Future Developments

The thesis focused on the description of optical spectra of solids, in the appealing framework of TDDFT. However the concepts and approaches here developed have to be ex-

tended in order to improve their applicability and "workability". Concerning the latter, we will have to search for the most convenient algorithm to numerically evaluate the proposed expressions. We also plan to take advantage of the fact that, in our formulation, k-points are simply summed over, instead of being the indices of matrices that have to be inverted or diagonalized.

Concerning the applications, a short term perspective is to apply the method to the description of the electron energy loss spectra, for which the resonant and anti-resonant part of the response function have to be taken into account. We also plan to study finite systems. Moreover the introduction of the spin degree of freedom could allow to enlarge the target of our study, towards polarised systems, both finite and infinite, also subject to magnetic fields.

Appendices

Appendix A

Linear Response Theory

A linear response function χ to an applied external field F is defined through the relation:

$$\delta \langle p \rangle = \langle p \rangle - p_0 = \chi F \tag{A.1}$$

where p_0 is the value of the operator p when $F = 0$.[1] So $\delta \langle p \rangle$ is the response of the system to an applied field F, and χ is the *response function*, which is in the $F \to 0$ limit, independent of the applied field. More in detail, for any measurable property $p(\mathbf{r}, t)$:

$$\delta \langle p(\mathbf{r}, t) \rangle = \int d\mathbf{r}' \int dt' \chi \left(\mathbf{r}, \mathbf{r}'; t - t'\right) F(\mathbf{r}', t')$$

where the *causality* condition is used in the time integral.
The Fourier transform of χ is a complex function $\chi(\omega) = \chi_1 + i\chi_2$:

$$\chi(\omega) = \int dt \chi(t) e^{-i\omega t}$$

for a response function to a purely time-dependent applied field $F(t) = F_0\, e^{-i\omega t}$. The causality condition implies that $\chi(\omega)$ is analytic in the upper half plane of the complex plane[2], with precise relations between real and imaginary part of χ, namely the Kramers-Kronig [302–304] relations:

$$\chi_1(\omega) = \frac{2}{\pi} \mathrm{P} \int_0^\infty d\omega' \frac{\omega' \chi_2(\omega')}{\omega'^2 - \omega^2} \quad ; \quad \chi_2(\omega) = -\frac{2\omega}{\pi} \mathrm{P} \int_0^\infty d\omega' \frac{\chi_1(\omega')}{\omega'^2 - \omega^2}.$$

If $F(\mathbf{r}, t)$ is the external perturbation, the corresponding term that has to be added to the system's Hamiltonian is

$$H_1(t) = \int g(\mathbf{r}) F(\mathbf{r}, t) d\mathbf{r}$$

[1] p can be, for example, the macroscopic magnetisation of a sample subject to a magnetic field (F). χ, the response function, plays then the role of the magnetic susceptibility.

[2] Or the lower half plane if, by convention, we let the field to oscillate as $e^{i\omega t}$ instead of $e^{-i\omega t}$.

where $g(\mathbf{r})$ is the coupling variable between the perturbation and the system, and H_1, the perturbing contribution to the Hamiltonian, is expressed in the interaction picture. Within this scheme it is possible to derive the linear response function in terms of ground state quantities. First order time-dependent perturbation theory yields the Kubo formula (see, e.g. Ref. [119]) for the response function:

$$\chi\left(\mathbf{r},\mathbf{r}',t-t'\right)=-i\left\langle N\right|\left[g(\mathbf{r},t),g(\mathbf{r}',t')\right]\left|N\right\rangle\Theta(t-t')$$

with $|N\rangle$ many-body ground state ($|N\rangle=\varphi^0$).

A.1 The *full* polarizability

An important example is given by an electronic system subject to an external potential V_{ext}, which causes an induced charge density n_{ind} as

$$n_{ind}\left(\mathbf{r},t\right)=\int dtd\mathbf{r}'\chi\left(\mathbf{r},\mathbf{r}',t-t'\right)V_{ext}\left(\mathbf{r}',t'\right) \tag{A.2}$$

where χ is called polarizability of the electronic system. Here the perturbative Hamiltonian is

$$H_1(t)=\int n(\mathbf{r},t)V_{ext}(\mathbf{r},t)d\mathbf{r}$$

where the electron density $n(\mathbf{r})$ represents the coupling variable. So the polarizability is

$$\chi\left(\mathbf{r},\mathbf{r}',t-t'\right)=-i\left\langle N\right|\left[n(\mathbf{r},t),n(\mathbf{r}',t')\right]\left|N\right\rangle\Theta(t-t'). \tag{A.3}$$

The analytical structure of the linear response function is very important. Let's define $|j_N\rangle$ as the j^{th} N-particle state. The Eq. (A.3) becomes (putting $\tau=t-t'$)

$$\chi\left(\mathbf{r},\mathbf{r}',\tau\right)=-i\Theta(\tau)\sum_j\left\langle N\right|n(\mathbf{r},\tau)\left|j_N\right\rangle\left\langle j_N\right|n(\mathbf{r},0)\left|N\right\rangle+c.c.$$

Now, according to the Dirac picture, we can use the time-evolution density operator $n(\mathbf{r},t)=e^{iH_0t}n(\mathbf{r},0)e^{-iH_0t}$ in the linear response function in order to obtain:

$$\chi\left(\mathbf{r},\mathbf{r}',\tau\right)=-i\Theta(\tau)\sum_j\left[f_j(\mathbf{r})f_j^*(\mathbf{r}')e^{i(E_0^N-E_j^N)\tau}-c.c.\right]$$

where $f_j(\mathbf{r})=\left\langle N\right|n(\mathbf{r},0)\left|j_N\right\rangle$ and E_j^N is the energy of the j^{th} N-particle excited state. The Fourier transform of χ is to

$$\chi\left(\mathbf{r},\mathbf{r}',\omega\right)=\sum_j\left[\frac{f_j(\mathbf{r})f_j^*(\mathbf{r}')}{\omega-\Omega_j+i\eta}+\frac{f_j(\mathbf{r}')f_j^*(\mathbf{r})}{\omega+\Omega_j+i\eta}\right] \tag{A.4}$$

where we can see that the polarizability of an electronic system has poles at $\Omega_j=\pm(E_0^N-E_j^N)$, i.e. the excitation energies of the N-particle system. The first and the second term of (A.4) are called resonant and anti-resonant term, respectively.

A.2 The independent-particle polarizability

A frequently studied case, in condensed matter theory, is represented by an independent-particle electronic system, subject to an external perturbation. This time the N-particle state can be represented by the independent-particle state vector

$$|N\rangle = |f_{\mathbf{k}_1}, f_{\mathbf{k}_2}, ..., f_{\mathbf{k}_i}, ...\rangle \tag{A.5}$$

in the occupation numbers $f_{\mathbf{k}_i}$ formalism. Here all the quantum numbers are contained in the label $\mathbf{k}$ and the independent-particle states are $|\mathbf{k}\rangle$. The normalization rule for the vector (A.5) is

$$\langle f_{\mathbf{k}_1}, f_{\mathbf{k}_2}, ..., f_{\mathbf{k}_i}, ...| \, a^\dagger_{\mathbf{k}_i} a_{\mathbf{k}_j} \, |f_{\mathbf{k}_1}, f_{\mathbf{k}_2}, ..., f_{\mathbf{k}_j}, ...\rangle = \delta_{\mathbf{k}_i \mathbf{k}_j} f_{\mathbf{k}_j} \tag{A.6}$$

where $f_{\mathbf{k}}$ is the occupation number of the state $\mathbf{k}$ and $a^\dagger_{\mathbf{k}}, a_{\mathbf{k}}$ are the creation and annihilation operators, respectively.

In order to write the independent-particle polarizability, we observe that

$$n(\mathbf{r}) = \psi^\dagger(\mathbf{r})\psi(\mathbf{r}) \tag{A.7}$$

with the field operator $\psi(\mathbf{r})$ (annihilation field operator) related to $a_{\mathbf{k}}$ by

$$\psi(\mathbf{r}) = \sum_k^{occ} \phi_{\mathbf{k}}(\mathbf{r}) a_{\mathbf{k}}$$

where $\phi_{\mathbf{k}}$ are single-particle wave functions.
We can now calculate the analogous of Eq. (A.4), by specifying for the independent-particle case the oscillator strengths $f_j(\mathbf{r}) = \langle N| \, n(\mathbf{r}, 0) \, |j_N\rangle$

$$f_j(\mathbf{r}) = \left\langle N \left| \psi^\dagger(\mathbf{r})\psi(\mathbf{r}) \right| j_N \right\rangle = \left\langle N \left| \sum_{\mathbf{k}_1 \mathbf{k}_2} \phi^*_{\mathbf{k}_1}(\mathbf{r}) \phi_{\mathbf{k}_2}(\mathbf{r}) a^\dagger_{\mathbf{k}_1} a_{\mathbf{k}_2} \right| N_{(-\mathbf{k}+\mathbf{k}')} \right\rangle$$

where $a_{\mathbf{k}_2}$ has to destroy the electron in $\mathbf{k}'$ and $a^\dagger_{\mathbf{k}_1}$ has to create an electron in $\mathbf{k}$. The same reasonment holds for $f_j(\mathbf{r}')$. The independent-particle polarizability then becomes

$$\chi^0(\mathbf{r}, \mathbf{r}', \omega) = \sum_{\mathbf{k}\mathbf{k}'} \frac{f_{\mathbf{k}} \left(1 - f_{\mathbf{k}'}\right) \phi^*_{\mathbf{k}}(\mathbf{r}) \phi_{\mathbf{k}'}(\mathbf{r}) \phi^*_{\mathbf{k}'}(\mathbf{r}') \phi_{\mathbf{k}}(\mathbf{r}')}{\omega - \omega_{\mathbf{k}\mathbf{k}'} + i\eta} + a.r.^3 \tag{A.8}$$

where $\omega_{\mathbf{k}\mathbf{k}'} = \epsilon_{\mathbf{k}} - \epsilon_{\mathbf{k}'}$ is the energy difference of two single-particle levels and $f_{\mathbf{k}}$ is the occupation number of the k^{th} single-particle orbital. As we can see, the independent particle polarizability has poles at the independent-particle excitation energies. If the anti-resonant term is explicitly taken into account, we have the well known result

$$\chi^0(\mathbf{r}, \mathbf{r}', \omega) = \sum_{\mathbf{k}\mathbf{k}'} \frac{\left(f_{\mathbf{k}} - f_{\mathbf{k}'}\right) \phi^*_{\mathbf{k}}(\mathbf{r}) \phi_{\mathbf{k}'}(\mathbf{r}) \phi^*_{\mathbf{k}'}(\mathbf{r}') \phi_{\mathbf{k}}(\mathbf{r}')}{\omega - \omega_{\mathbf{k}\mathbf{k}'} + i\eta}. \tag{A.9}$$

[3] anti-resonant term, as in Eq. (A.4).

Appendix B

Dyson-like screening equation for the macroscopic dielectric function ε_{M}

Here we remind, following the lines of Ref.s [194, 305, 306], how one can put the local field effects into evidence by performing analytically the inversion of the microscopic dielectric matrix defined in Eq. (1.30). Thus, a general $(N_{\mathbf{G}}) \times (N_{\mathbf{G}})$ matrix of the form

$$M = \begin{pmatrix} m_{00} & \mathbf{m}_a^T \\ \mathbf{m}_b & \mathsf{m} \end{pmatrix}, \tag{B.1}$$

with m_{00} being a complex number and m a $(N_{\mathbf{G}} - 1) \times (N_{\mathbf{G}} - 1)$ matrix, has the inverse formally given by

$$M^{-1} = \frac{1}{(m_{00} - \mathbf{m}_a^T \mathsf{m}^{-1} \mathbf{m}_b)} \begin{pmatrix} 1 & -\mathbf{m}_a^T \mathsf{m}^{-1} \\ -\mathsf{m}^{-1}\mathbf{m}_b & m_{00}\mathsf{m}^{-1} \end{pmatrix}. \tag{B.2}$$

If M is now the dielectric function $\varepsilon = 1 - v\tilde{\chi}$ taken in its reciprocal space matrix representation (**G**,**G**'), then

$$\varepsilon_M = \frac{1}{\varepsilon_{00}^{-1}} = \left[\varepsilon_{00} - \varepsilon_a^T \epsilon^{-1} \varepsilon_b\right]. \tag{B.3}$$

In this equation, the quantities ε_{00}, ε_a^T, ε_b and ϵ are formally given by

$$\begin{aligned} \varepsilon_{00} &= 1 - v_0 \tilde{\chi}_{00}, && && \text{(B.4)} \\ \left[\varepsilon_a^T\right]_{\mathbf{G}} &= v_0 \tilde{\chi}_{0\mathbf{G}}, && \mathbf{G} \neq 0, && \text{(B.5)} \\ \left[\varepsilon_b\right]_{\mathbf{G}'} &= v_{\mathbf{G}'} \tilde{\chi}_{\mathbf{G}'0}, && \mathbf{G}' \neq 0, && \text{(B.6)} \\ \left[\epsilon\right]_{\mathbf{G}\mathbf{G}'} &= v_{\mathbf{G}} \tilde{\chi}_{\mathbf{G}\mathbf{G}'}, && \mathbf{G}, \mathbf{G}' \neq 0 && \text{(B.7)} \end{aligned}$$

where $v_0 = v_{\mathbf{G}=0}$.

This yields the following general expression for the macroscopic dielectric function

$$\varepsilon_M = 1 - v_0\tilde{\chi}_{00} - \sum_{\mathbf{G},\mathbf{G}'\neq 0} v_0\tilde{\chi}_{0\mathbf{G}}\epsilon^{-1}_{\mathbf{G}\mathbf{G}'}v_{\mathbf{G}'}\tilde{\chi}_{\mathbf{G}'0}. \tag{B.8}$$

As our goal is to write this in a compact matrix form, now one defines a new function $\bar{\varepsilon}_{\mathbf{G}\mathbf{G}'}$ such that

$$\bar{\varepsilon}_{\mathbf{G}\mathbf{G}'} \equiv \delta_{\mathbf{G},\mathbf{G}'} - \bar{v}_{\mathbf{G}}\tilde{\chi}_{\mathbf{G}\mathbf{G}'}, \tag{B.9}$$

with a modified Coulomb interaction (1.35)

$$\bar{v}_{\mathbf{G}} \equiv \begin{cases} 0, & \mathbf{G} = 0 \\ v_{\mathbf{G}}, & \mathbf{G} \neq 0 \end{cases}, \tag{B.10}$$

i.e. $\bar{v}$ indicates that the $\mathbf{G} = 0$ contribution of the bare Coulomb interaction is not considered. In matrix notation this yields

$$\bar{\varepsilon}_{\mathbf{G}\mathbf{G}'} = \begin{pmatrix} 1 & 0^T \\ \varepsilon_b & \epsilon \end{pmatrix}. \tag{B.11}$$

Then the inverse of $\bar{\varepsilon}$ is given by, using Eq. (B.2),

$$\bar{\varepsilon}^{-1}_{\mathbf{G}\mathbf{G}'} = \begin{pmatrix} 1 & 0^T \\ -\epsilon^{-1}\varepsilon_b & \epsilon^{-1} \end{pmatrix}. \tag{B.12}$$

Thus Eq. (B.8) can be written as $\varepsilon_M(\omega) = 1 - \lim_{\mathbf{q}\to 0}\left[v_0(\mathbf{q})\bar{\chi}_{\mathbf{G}=\mathbf{G}'=0}(\mathbf{q},\omega)\right]$ if in the latter, $\bar{\chi}$ is defined as

$$\bar{\chi}_{\mathbf{G}\mathbf{G}'} \equiv \chi_{\mathbf{G}\mathbf{G}'} + \sum_{K,K'} \chi_{\mathbf{G}K}\bar{\varepsilon}^{-1}_{KK'}\bar{v}_{K'}(q)\chi_{K'\mathbf{G}'}. \tag{B.13}$$

This gives the wanted matrix expression

$$\bar{\chi} = \chi + \chi\bar{\varepsilon}^{-1}\bar{v}\chi, \tag{B.14}$$

and, together with $\bar{\varepsilon}^{-1} = (1 - \bar{v}\chi)^{-1}$, the Dyson-like equation $\bar{\chi} = \chi + \chi\bar{v}\bar{\chi}$ of Eq.s (1.34). It is now relevant to compare this equation with the one that satisfies the response function χ giving the inverse microscopic dielectric function $\varepsilon^{-1} = 1 + v\chi$, namely $\chi = \tilde{\chi} + \tilde{\chi}v\chi$. The difference between the two Eq.s (1.34) leads to the difference between EELS (related to ε^{-1}) and absorption (related to ε_M). Formally the two equations are very much alike, but there is a long-range term v_0 appearing in the kernel of the Dyson-like screening equation for χ, that is absent in the case of $\tilde{\chi}$. See Chap. 6 for a discussion of the consequences of this difference in finite and infinite systems.

Appendix C

EELS versus Abs: LFE included

Here we show that Eq. (6.3) can also be derived when the local field effects are included. Starting from the second of (1.34) we have

$$\tilde{\chi} = \chi\Big(1 + v\chi\Big)^{-1} \tag{C.1}$$

that substituted into the first of (1.34):

$$\begin{aligned} \bar{\chi} &= \chi(1+v\chi)^{-1} + \chi(1+v\chi)^{-1}\bar{v}\bar{\chi} \\ &= \Big[(1+v\chi)\chi^{-1}\Big]^{-1}(1+\bar{v}\bar{\chi}) \\ &= \Big[\chi^{-1}+v\Big]^{-1}(1+\bar{v}\bar{\chi}) \end{aligned} \tag{C.2}$$

so

$$\Big[\chi^{-1}+v\Big]\bar{\chi} = (1+\bar{v}\bar{\chi}) \quad \rightarrow \quad \chi^{-1}+v = \bar{\chi}^{-1}+\bar{v} \tag{C.3}$$

and

$$\chi^{-1} = \bar{\chi}^{-1} + \bar{v} - v = \bar{\chi}^{-1} - \Delta v \tag{C.4}$$

$$\chi = \Big[\bar{\chi}^{-1} - \Delta v\Big]^{-1} = \bar{\chi}\Big[1 - \Delta v\bar{\chi}\Big]^{-1} \tag{C.5}$$

If we want to consider only the head, χ_{00} :

$$\chi_{00} = \sum_{\mathbf{G}_1} = \bar{\chi}_{0\mathbf{G}_1}\Big[(\delta_{\mathbf{G}\mathbf{G}'} - \Delta v_{\mathbf{G}}\bar{\chi}_{\mathbf{G}\mathbf{G}'})^{-1}\Big]_{\mathbf{G}_1 0} \tag{C.6}$$

where

$$\Delta v_{\mathbf{G}} = \begin{cases} v_0 & \mathbf{G}=0 \\ 0 & \text{else} \end{cases} . \tag{C.7}$$

Inverting the matrix $(\delta_{\mathbf{G}\mathbf{G}'} - \Delta v_{\mathbf{G}}\bar{\chi}_{\mathbf{G}\mathbf{G}'})$ we can write:

$$\chi_{00} = \frac{\bar{\chi}_{00}}{1 - v_0\bar{\chi}_{00}}. \tag{C.8}$$

Appendix D

Size effects in finite systems

The optical response of finite systems normally depends on the size of the system. Here we would like to briefly monitorize the development of collective effects in the simplest structural model of a spherical metallic cluster, namely the jellium model, in which the ionic background is smeared out to form a homogeneous distribution of positive charge $n_+(n_+ = n\,\Theta(R-r)$, where the radius R is related to the homogeneous bulk electron density $\frac{4}{3}\pi R^3 = n$). Clusters of alkali elements turn out to be well described by this model [307, 308].

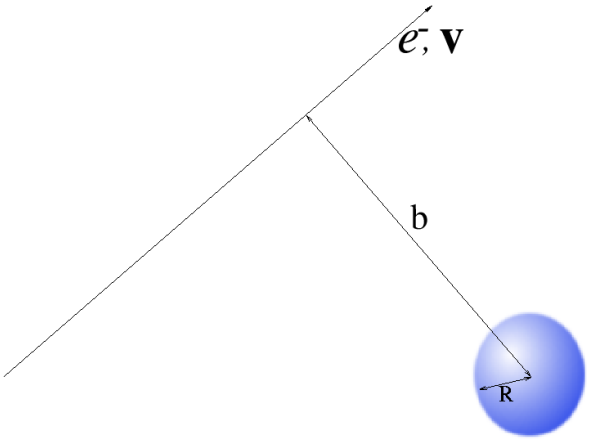

To discuss the relation to EELS experiments, it is useful to write down the energy loss probability $P(\omega)$ corresponding to an electron with velocity $|\mathbf{v}| = v$ interacting with an isolated sphere of dielectric function $\epsilon(\omega)$ at a distance b (impact parameter). Integrating over the electron trajectory and neglecting retardation effects in the induced potential, the final result [309] is:

$$P(\omega) = \frac{4R}{\pi v^2} \sum_{l=1} \sum_{m=0}^{l} \frac{2-\delta_{m0}}{(l+m)!(l-m)!} \times \times \left[\frac{\omega R}{v}\right]^{2l} K_m^2[\omega b/v]\; \Im\{\gamma_l(\omega)\}, \quad \text{(D.1)}$$

where $K_m(x)$ is a the modified Bessel function and $\gamma_l(\omega)$ is the sphere surface response given by:

$$\gamma_l(\omega) = \frac{l(1-\varepsilon(\omega))}{l\varepsilon(\omega)+l+1}. \quad \text{(D.2)}$$

Eq. (D.1) takes into account the contribution of all the multipolar terms of the induced potential created by the moving charge. Quantum mechanical effects are embodied in $\epsilon(\omega)$. The excitation frequencies are determined by the zeros of the denominator of γ_l. For a simple metal (described by a Drude-like dielectric response $\varepsilon(\omega) = 1 - \omega_p^2/\omega^2$) they are given by the classical Mie multipolar plasmon frequencies ω_l [310]

$$\omega_l = \omega_p \sqrt{\frac{l}{2l+1}} \tag{D.3}$$

where l is the angular momentum quantum number and ω_p is the plasma frequency related to the "homogeneous" electron density n of the system by $\omega_p = 4\pi n e^2/m_e$.

The dipolar term, i.e. $l = 1$ which takes to the well known limit $\omega = \frac{\omega_p}{\sqrt{3}}$, is dominant[1] only when *the sphere radius is much smaller than the range of variation of the field* $R << v/\omega \sim 2\pi/q$ or *when the probe electron travels far away from the target* $b >> R$ [309]. However, when the radius is of the order of v/ω (or bigger) many l-terms contribute: the induced density piles up in a small region close to the probe; thus many multipolar terms are needed in the expansion of the potential created by such a localized charge. In this case, $l = \infty$ turns out to be the dominant term in the absorption spectra and the main excitation frequency occurs at:

$$\omega = \omega_p \sqrt{\frac{l}{2l+1}} = \frac{\omega_p}{\sqrt{2}},$$

which is the result for a flat surface. In the usual case of large impact parameter, the dipolar term becomes the dominant one in Eq. (D.1) and in this case the EELS and the dipolar optical absorption (4.18) are proportional, as both are related to the imaginary part of χ (Chap. 6).

Surface and volume plasmons as pure transverse and longitudinal excitations are not well defined for small cluster sizes, and they can be excited by both electron and photons. However as the size increases this distinction is relevant and the proper longitudinal (EELS) and transverse (photon) external fields have to be included in the calculation of the response.

This appendix illustrates and corroborates the general discussions made in Chap. 6.

[1] This is also the case of optical spectra of small metallic cluster [307] where the spectra is dominated by a single excitation.

Appendix E

Technical details

E.1 Linear system solver

A straightforward, but inconvenient way to obtain $\bar{\chi}_{00}$, i.e.

$$\bar{\chi}_{00} = \left[\chi^0 \left(\chi^0 - \chi^0 \bar{v} \chi^0 - T\right)^{-1} \chi^0\right]_{00} \tag{E.1}$$

would be to perform the inversion of $A = (\chi^0 - \chi^0 \bar{v} \chi^0 - T)$, followed by the double matrix multiplication $\chi^0 A^{-1} \chi^0$. In this case, all the elements of $\bar{\chi}$ would be found, whereas we are interested in the head only.

If only one element is required, namely the head, only the first line of the left χ^0 and first column of $X = A^{-1}\chi^0$ are necessary. By virtue of the latter, we can solve the linear system

$$AX = \chi^0 \quad \Rightarrow \quad \sum_{\mathbf{G}'} A_{\mathbf{G}\mathbf{G}'} X_{\mathbf{G}'0} = \chi^0_{\mathbf{G}0} \tag{E.2}$$

where X and χ^0 are now column vectors. This permits us to find $X_{\mathbf{G}0}$. The final vector product $\sum_{\mathbf{G}} \chi^0_{0\mathbf{G}} X_{\mathbf{G}0}$ gives the searched $\bar{\chi}_{00}$.

The advantage of the algorithm is clear, because no useless term has been calculated.

We have followed this idea also for the RPA case, where

$$\bar{\chi} = \left(1 - \chi^0 \bar{v}\right)^{-1} \chi^0 \tag{E.3}$$

is immediately transformed in the linear system problem

$$\left(1 - \chi^0 \bar{v}\right) \bar{\chi} = \chi^0 \tag{E.4}$$

which leads directly to $\bar{\chi}_{0\mathbf{G}}$, and hence to the head $\bar{\chi}_{00}$.

The resolution of the linear system turned out to be, not only much more efficient (no useless information is calculated), but also more stable than an inversion, which is crucial when the matrix to be inverted is χ^0 or $(\chi^0 - \chi^0 \bar{v} \chi^0 - T)$ (see text, Par. 8.3).

E.2 The k sampling of the Brillouin zone

In the calculation of electronic spectra of semiconductor or insulator crystals, several occupied and unoccupied bands N_v and N_c are usually taken into account, as well as several hundred k-points (N_k) for the first BZ's sampling. The number of transitions $N_t = N_v N_c N_k$ is involved in the determination of optical spectra, both in BSE and in TDDFT (when electron spectroscopy is described, the number of unoccupied states usually has to be increased, with a much bigger N_t, since often plasmons are measured at higher energies that the interband transitions), and constitutes a strong bottleneck for the calculation. It is, then, crucial to reduce as much as possible the number of k-points used in the calculations. To do that, for almost all spectra of this thesis, we have used *shifted k-points* [199, 205, 206]. The effect of shifting an uniform k-points set (usually created starting from high symmetry BZ points), is to break any symmetry, in order to achieve a maximum number of non-equivalent k-points and hence a better sampling. In fact, let us take an fcc lattice as example, whose first BZ is sampled by 256 k-points [311]. The number of crystallographically unequivalent points is only 10! Instead a little (even random) shift (not along the high symmetry directions of the crystal) immediately leads to 256 crystallographically unequivalent k-points, with a consequent better spectral resolution.

Caution:

The effect of shifting the k-points can introduce a spurious anisotropy in systems which experimentally present an isotropic response. In this thesis, only the limit $\mathbf{q} \to 0$ has been considered for the electronic spectra, so, whenever shifted k-points are used, three different directions of $\mathbf{q}$ contribute to the spectrum, namely the cartesian directions $\hat{\mathbf{x}}, \hat{\mathbf{y}}, \hat{\mathbf{z}}$. This average is not necessary when the high symmetry k-points are used in a cubic crystal; in this case, in fact, any (and only one) direction for $\mathbf{q}$ can be safely chosen.[1] Of course, if $N_k \to \infty$, even when shifted k-points are used the effective drift goes to zero and no spurious anisotropy occurs.

[1] This arbitrariness of course only holds if the system is isotropic.

List of publications related with the thesis

- F. Sottile, V. Olevano and L. Reining, *Parameter-free calculation of response functions in time-dependent density-functional theory*, Phys. Rev. Lett. **91**, 56402 (2003).
- S. Botti, F. Sottile, N. Vast, V. Olevano, H.-Ch. Weissker and L. Reining, G. Onida, R. W. Godby, A. Rubio and R. Del Sole, *Long-range contribution to the exchange-correlation kernel of time-dependent density functional theory*, submitted to Phys. Rev. B.
- F. Sottile, K. Karlsson, L. Reining and F. Aryasetiawan, *Macroscopic and microscopic components of exchange-correlation interactions*, accepted by Phys. Rev. B.
- F. Sottile, V. Olevano, A. Rubio, and L. Reining, *Importance of the coulombian term in absorption and electron energy-loss spectra: finite versus infinite systems*, in preparation.
- F. Sottile, V. Olevano and L. Reining, *Bound excitons in time-dependent density-functional theory*, in preparation.
- F. Sottile, V. Olevano and L. Reining, *Time dependent density functional theory: an exchange-correlation kernel from the Bethe-Salpeter equation*, in preparation.

References and Literature

[1] G. Gugliotta, The Washington Post p. A14 (May 10, 2002).

[2] S. J. Langford, F. M. Raymo, and J. F. Stoddart, in *Molecular Electronics* (Blackwell, London, 1998), p. 325.

[3] V. Balzani, M. Gómez-López, and J. F. Stoddart, Acc. Chem. Res. **31**, 405 (1998).

[4] V. Balzani, A. Credi, F. M. Raymo, and J. F. Stoddart, Angew. Chem. Int. Ed. **39**, 3348 (2000).

[5] A. Credi, Ph.D. thesis, Università degli studi di Bologna (1998).

[6] S. F. Boys, Proc. R. Soc. **A200**, 542 (1950).

[7] A. Szabo and N. S. Ostlund, *Modern Quantum Chemistry* (MacMillan, New York, 1983).

[8] C. E. Dykstra, *Ab initio Calculations of the Structure and Properties of Molecules* (Elsevier, Amsterdam, 1988).

[9] J. Cizek, Adv. Chem. Phys. **14**, 35 (1969).

[10] W. Kutzelnigg, in *Modern Theoretical Chemistry*, edited by H. F. Shaefer (Plenum, New York, 1977), vol. 3.

[11] R. Ahlrichs, Comput. Phys. Commun. **17**, 31 (1979).

[12] H. Kümmel, K. H. Lührmann, and J. G. Zabolitzky, Phys. Lett. **36C**, 1 (1978).

[13] F. Coester and H. Kümmel, Nucl. Phys. **17**, 477 (1960).

[14] D. M. Ceperley, in *Recent Progress in Many-Body Theories* (Springer-Verlag, Berlin, 1981), p. 262.

[15] P. J. Reynolds, D. M. Ceperley, B. J. Alder, and W. A. Lester, J. Chem. Phys. **77**, 5593 (1982).

[16] D. M. Ceperley and B. J. Alder, J. Chem. Phys. **81**, 5833 (1984).

[17] M. H. Kalos, in *Monte Carlo Method in Quantum Physics* (Reidel, Dordrecht, 1984), p. 19, NATO ASI series.

[18] G. Senatore and N. H. March, Rev. Mod. Phys. **66**, 445 (1994).

[19] W. M. C. Foulkes, L. Mitas, R. J. Needs, and G. Rajagopal, Rev. Mod. Phys. **73**, 33 (2001).

[20] K. Becker and P. Fulde, J. Chem. Phys. **91**, 4223 (1989).

[21] P. Fulde, *Electron Correlation in Molecules and Solids* (Springer, Heidelberg, 1995).

[22] L. Hedin and S. Lundqvist, Solid State Physics **23**, 1 (1969).

[23] G. Grosso and G. Pastori Parravicini, *Solid State Physics* (Academic Press, 2000).

[24] J. C. Maxwell, Philos. Trans. Roy. Soc. London **155**, 459 (1865).

[25] F. Stern, Solid State Physics **15**, 299 (1965).

[26] J. D. Jackson, *Classical Electrodynamics* (John Wiley & Sons; 3rd edition, 1999).

[27] K. Riedling, *Ellipsometry for Industrial Applications* (Springer-Verlag Wein, New York, 1988).

[28] H. G. Tompkins, *A User's Guide to Ellipsometry* (Academic Press, New York, 1993).

[29] H. G. Tompkins and W. A. McGahan, *Spectroscopic Ellipsometry and Reflectometry: A User's Guide* (John Wiley & Sons, New York, 1999).

[30] Goldstein, *Classical Mechanics* (Addison-Wesley, 1981), second edition.

[31] S. L. Adler, Phys. Rev. **126**, 413 (1962).

[32] N. Wiser, Phys. Rev. **129**, 62 (1963).

[33] R. D. Sole and R. Girlanda, Phys. Rev. B **48**, 11789 (1993).

[34] M. Born and J. M. Oppenheimer, Ann. Physik **84**, 457 (1927).

[35] J. M. Ziman, *Principles of the Theory of Solids* (Cambridge University Press, 1972).

[36] H. Hellmann, *Einfuhrung in die Quantumchemie* (Franz Deutsche, Leipzig, 1937).

[37] R. P. Feynman, Phys. Rev. **56**, 530 (1939).

[38] R. P. Feynman and A. R. Hibbs, *Quantum Mechanics and Path Integrals* (McGraw-Hill, 1965).

[39] D. R. Hartree, Proc. Cambridge Philos. Soc. **24**, 89 (1928).

[40] V. Fock, Z. Phys. **61**, 126 (1930).

[41] P. Hohenberg and W. Kohn, Phys. Rev. **136**, B864 (1964).

[42] W. Kohn and L. J. Sham, Phys. Rev. **140**, A1133 (1965).

[43] S. Lundqvist and N. H. March, eds., *Theory of the Inhomogeneous Electron Gas* (Plenum, New York, 1983).

[44] R. M. Dreizler and E. K. U. Gross, *Density Functional Theory* (Springer Verlag, 1990).

[45] J. M. Seminario, ed., *Recent Developments and Applications of Modern Density Functional Theory* (Elsevier, Amsterdam, 1996).

[46] H. B. Callen, *Thermodynamics and an introduction to thermostatics* (John Wiley & sons, 1985), second edition.

[47] E. H. Lieb, Int. J. Quantum Chem. **24**, 243 (1983).

[48] R. Fukuda, T. Kotani, Y. Suzuki, and S. Yokojima, Prog. Theor. Phys. **92**, 833 (1994).

[49] N. Argaman and G. Makov, physics/9806013 (1999).

[50] M. C. Payne, M. P. Teter, D. C. Allan, T. A. Arias, and J. D. Joannopoulos, Rev. Mod. Phys. **64**, 1045 (1992).

[51] R. Evans, Adv. in Phys. **28**, 143 (1979).

[52] N. D. Mermin, Phys. Rev. **137**, A1441 (1965).

[53] M. Levy, Phys. Rev. A **26**, 1200 (1982).

[54] R. Erdhal and V. H. Smith, *Density Matrices and Density Functionals* (Reidel, Dordrecht, 1987).

[55] W. Kohn, in *Highlights of Condensed Matter Theory* (North-Holland, Amsterdam, 1985).

[56] E. S. Kryachko, Int. J. Quant. Chem. **18**, 1029 (1980).

[57] G. Vignale and M. Rasolt, Phys. Rev. Lett. **59**, 2360 (1987).

[58] G. Vignale and M. Rasolt, Phys. Rev. B **37**, 10685 (1988).

[59] L. N. Olivera, E. K. U. Gross, and W. Kohn, Phys. Rev. Lett. **60**, 2430 (1988).

[60] W. Kohn, E. K. U. Gross, and L. N. Olivera, J. de Physique (Paris) **50**, 2601 (1989).

[61] A. K. Rajagopal and J. Callaway, Phys. Rev. B **7**, 1912 (1973).

[62] A. K. Rajagopal, J. Phys. C **11**, L943 (1978).

[63] A. H. MacDonald and S. H. Vosko, J. Phys. C **12**, 2977 (1979).

[64] H. Englisch and R. Englisch, Phys. Stat. Sol. **B123**, 711 (1984).

[65] H. Englisch and R. Englisch, Phys. Stat. Sol. **B124**, 373 (1984).

[66] D. M. Ceperley and B. J. Alder, Phys. Rev. Lett. **45**, 566 (1980).

[67] S. Moroni, D. M. Ceperley, and G. Senatore, Phys. Rev. Lett. **75**, 689 (1995).

[68] G. Ortiz, M. Harris, and P. Ballone, Phys. Rev. Lett. **82**, 5317 (1999).

[69] O. Gunnarsson, M. Jonson, and B. I. Lundqvist, Phys. Rev. B **20**, 3136 (1979).

[70] S. H. Vosko and M. N. L. Wilk, Can. J. Phys. **58**, 1200 (1980).

[71] D. C. Langreth and J. P. Perdew, Phys. Rev. B **21**, 5469 (1980).

[72] J. P. Perdew and Y. Wang, Phys. Rev. B **33**, 8800 (1986).

[73] J. P. Perdew, J. A. Chevary, S. H. Vosko, K. A. Jackson, M. R. Pederson, D. J. Singh, and C. Fiolhais, Phys. Rev. B **46**, 6671 (1992).

[74] R. J. Barlett, in *Chemistry for the 21st Century* (Wiley-VCH, Weinheim, 2000), p. 271.

[75] M. E. Casida, in *Accurate Description of Low-Lying Molecular States and Potential Energy Surfaces, ACS Symposium Series 828* (ACS Press: Washington, D.C., 2001), pp. 199–220.

[76] J. P. Perdew and A. Zunger, Phys. Rev. B **23**, 5048 (1981).

[77] R. G. Parr and W. Yang, *Density-Functional Theory of Atoms and Molecules* (Oxford University Press, 1989).

[78] J. P. Perdew, S. Kurth, A. Zupan, and P. Blaha, Phys. Rev. Lett. **82**, 2544 (1999).

[79] J. P. Perdew, S. Kurth, A. Zupan, and P. Blaha, Phys. Rev. Lett. **82**, (E) 5179 (1999).

[80] S. Kurth, J. P. Perdew, and P. Blaha, Int. J. Quantum Chem. **75**, 889 (1999).

[81] R. H. Hertwig, , and W. Koch, Chem. Phys. Lett. **268**, 345 (1997).

[82] T. A. Koopmans, Physica **1**, 104 (1933).

[83] J. P. Perdew and M. R. Norman, Phys. Rev. B **26**, 5445 (1982).

[84] C. O. Almbladh and U. von Barth, Phys. Rev. B **31**, 3231 (1985).

[85] E. G. Maksimov, I. I. Mazin, S. Y. Savrasov, and Y. A. Uspenski, J. Phys.:Cond. Matter **1**, 2493 (1989).

[86] A. Svane, Phys. Rev. B **35**, 5496 (1987).

[87] P. Horsch, Solid State Commun. **54**, 741 (1985).

[88] A. E. Carlsson, Phys. Rev. B **31**, 5178 (1985).

[89] F. Perrot, Physics Status Solidi **52**, 163 (1972).

[90] S. T. Pantelides, D. S. Mickish, and A. B. Kunz, Phys. Rev. B **10**, 5203 (1974).

[91] R. O. Jones and O. Gunnarsson, Rev. Mod. Phys. **61**, 689 (1989).

[92] C. Massobrio, A. Pasquarello, and R. Car, Phys. Rev. Lett. **75**, 2104 (1995).

[93] C. Massobrio, A. Pasquarello, and R. Car, Phys. Rev. B **54**, 8913 (1996).

[94] G. Onida, L. Reining, and A. Rubio, Rev. Mod. Phys. **74**, 601 (2002).

[95] R. W. Godby and I. D. White, Phys. Rev. Lett. **80**, 3161 (1998).

[96] A. Marinopoulos, L. Reining, V. Olevano, A. Rubio, T. Pichler, X. Liu, M. Knupfer, and J. Fink, Phys. Rev. Lett. **89**, 76402 (2002).

[97] V. Olevano and L. Reining, Phys. Rev. Lett. **86**, 5962 (2001).

[98] P. Lautenschlager, M. Garriga, L. Viña, and M. Cardona, Phys. Rev. B **36**, 4821 (1987).

[99] N. W. Ashcroft and N. D. Mermin, *Solid State Physics* (Saunders College Publishing, 1976).

[100] W. Jones and N. H. March, *Theoretical Solid State Physics* (John Wiley & Sons, 1973), volume I.

[101] W. Jones and N. H. March, *Theoretical Solid State Physics* (John Wiley & Sons, 1973), volume II.

[102] E. Fermi, Il Nuovo Cimento **11**, 157 (1934).

[103] J. C. Phillips and L. Kleinman, Phys. Rev. **116**, 287 (1959).

[104] W. E. Pickett, Computer Physics Report **9**, 115 (1989).

[105] http://theory.polytechnique.fr/codes/codes.html.

[106] http://www.abinit.org/ABINIT/Psps/LDA_TM/lda.html.

[107] M. Troullier and J. L. Martins, Phys. Rev. B **43**, 1993 (1991).

[108] http://www.abinit.org.

[109] D. R. Hamann, Phys. Rev. B **40**, 2980 (1989).

[110] H. J. Monkhorst and J. D. Pack, Phys. Rev. B **13**, 5188 (1976).

[111] L. D. Landau, Sov. Phys. JETP **3**, 920 (1957).

[112] L. D. Landau, Sov. Phys. JETP **5**, 101 (1957).

[113] L. D. Landau, Sov. Phys. JETP **8**, 70 (1959).

[114] D. Pines, *Elementary Excitations in Solids* (Addison-Wesley, New York, 1963).

[115] D. Pines and P. Nozières, *The Theory of Quantum Liquids* (Addison-Wesley, New York, 1989).

[116] A. L. Fetter and J. D. Walecka, *Quantum Theory of Many-Particle Systems* (McGraw-Hill, New York, 1971).

[117] J. W. Negele and H. Orland, *Quantum Many-Particle Systems* (Addison-Wesley, Redwood City, 1988).

[118] G. D. Mahan, *Many Particle Physics* (Plenum, New York, 1990).

[119] A. A. Abrikosov, L. P. Gorkov, and I. E. Dzyaloshinski, *Methods of Quantum Field Theory in Statistical Physics* (Prentice-Hall, Englewood Cliffs, NJ, 1963).

[120] L. D. Landau and E. M. Lifschitz, *Statistical Physics Part II* (Pergamon, Oxford, 1980).

[121] B. Farid, Phil. Mag. B **76**, 145 (1997).

[122] B. Farid, Philos. Mag. Lett. **79**, 581 (1999).

[123] B. Farid, in *Electron Correlation in the Solid State*, edited by N. H. March (1999), pp. 103–262.

[124] J. Schwinger, Phys. Rev. **82**, 914 (1951).

[125] J. Schwinger, Proc. Natl. Acad. Sci. **37**, 452 (1951).

[126] J. Schwinger, Proc. Natl. Acad. Sci. **37**, 455 (1951).

[127] J. A. Anderson, Phys. Rev. **94**, 703 (1954).

[128] T. Matsubara, Progr. Theor. Phys. **14**, 351 (1955).

[129] P. C. Martin and J. Schwinger, Phys. Rev. **115**, 1342 (1959).

[130] T. Kato, T. Kobayashi, and M. Namiki, Progr. Theor. Phys. Suppl. **15**, 3 (1960).

[131] L. Hedin, Phys. Scr. **21**, 477 (1980).

[132] G. Strinati, Nuovo Cimento **11**, 1 (1988).

[133] V. M. Galitskii and A. B. Migdal, Sov. Phys. JETP **7**, 96 (1958).

[134] B. Farid, R. W. Godby, and R. J. Needs, in *The Physics of Semiconductors* (World Scientific, Singapore, 1990), vol. 3, p. 1759.

[135] F. J. Dyson, Phys. Rev. **75**, 486 (1949).

[136] F. J. Dyson, Phys. Rev. **75**, 1736 (1949).

[137] G. F. Roach, *Green's Functions. Introductory Theory with Applications* (Van Nostrand Reinhold Co., London, 1970).

[138] A. E. Taylor and D. C. Lay, *Introduction to Functional Analysis* (Krieger Publ. Co. Malabar, Florida, 1986), cap. V.

[139] E. N. Economou, *Green's Functions in Quantum Mechanics* (Springer-Verlag, Berlin, 1979).

[140] S. Boffi, *Da Heisenberg a Landau. Introduzione alla teoria dei sistemi a molte particelle.*, lecture notes.

[141] C.-O. Almbladh and L. Hedin, in *Handbook on Synchrotron Radiation* (North-Holland, Amsterdam, 1983), vol. 1, p. 607.

[142] L. Hedin, Phys. Rev. **139**, 796 (1965).

[143] J. Lindhard, K. Dan. Vidensk. Selsk. Mat. Fys. Medd. **28**, 57 (1954).

[144] M. S. Hybertsen and S. G. Louie, Phys. Rev. Lett. **55**, 1418 (1985).

[145] M. S. Hybertsen and S. G. Louie, Phys. Rev. B **34**, 5390 (1986).

[146] M. Rohlfing, P. Krüger, and J. Pollmann, Phys. Rev. B **48**, 17791 (1993).

[147] K.-H. Hellwege and O. Madelung, eds., *Numerical Data and Functional Relationships in Science and Technology*, vol. 17a and 22a (Springer-Verlag New York, 1982).

[148] R. W. Godby, M. Schlüter, and L. J. Sham, Phys. Rev. B **37**, 10159 (1988).

[149] G. Baldini and B. Bosacchi, Physics Status Solidi **38**, 325 (1970).

[150] X. Zhu and S. G. Louie, Phys. Rev. B **43**, 14142 (1991).

[151] A. Rubio, J. L. Corkill, M. L. Cohen, E. L. Shirley, and S. G. Louie, Phys. Rev. B **48**, 11810 (1993).

[152] O. Zakharov, A. Rubio, X. Blase, M. L. Cohen, and S. G. Louie, Phys. Rev. B **50**, 10780 (1994).

[153] U. Schönberger and F. Aryasetiawan, Phys. Rev. B **52**, 8788 (1995).

[154] R. C. Whited, C. J. Flaten, and W. C. Walker, Solid State Commun. **13**, 1903 (1973).

[155] F. Bechstedt, in *Festköperprobleme/Advances in Solid State Physiscs* (Braunschweig/Wiesbaden, 1992), vol. 32, p. 161.

[156] R. W. Godby, in *Topics in Applied Physics* (Springer, New York, 1992), vol. 69.

[157] R. W. Godby, M. Schlüter, and L. J. Sham, Phys. Rev. Lett. **56**, 2415 (1986).

[158] R. W. Godby, M. Schlüter, and L. J. Sham, Phys. Rev. B **36**, 6497 (1987).

[159] F. Aryasetiawan and O. Gunnarsson, Rep. Prog. Phys. **61**, 237 (1998).

[160] I. Campillo, J. M. Pitarke, A. Rubio, E. Zarate, and P. M. Echenique, Phys. Rev. Lett. **83**, 2230 (1999).

[161] I. Campillo, J. M. Pitarke, A. Rubio, and P. M. Echenique, Phys. Rev. B **62**, 1500 (2000).

[162] I. Campillo, J. M. Pitarke, A. Goldman, A. Rubio, and P. M. Echenique, Phys. Rev. Lett. **85**, 3241 (2000).

[163] I. Campillo, J. M. Pitarke, A. Rubio, V. M. Silkin, E. V. Chulkov, and P. M. Echenique, Phys. Rev. B **61**, 13484 (2000).

[164] P. M. Echenique, J. M. Pitarke, E. Chulkov, and A. Rubio, J. Chem. Phys. **251**, 1 (2000).

[165] R. Keyling, W.-D. Schne, and W. Ekardt, Phys. Rev. B **61**, 1670 (2000).

[166] V. M. Silkin, T. Balasubramanian, E. V. Chulkov, A. Rubio, and P. M. Echenique, Phys. Rev. B **64**, 85334 (2001).

[167] C. D. Spataru, M. A. Cazalilla, A. Rubio, L. X. Benedict, P. M. Echenique, and S. G. Louie, Phys. Rev. Lett. **87**, 246405 (2001).

[168] A. Fleszar and W. Hanke, Phys. Rev. B **62**, 2466 (2000).

[169] W. von der Linden and P. Horsch, Phys. Rev. B **37**, 8351 (1988).

[170] N. Hamada, M. Hwang, and A. J. Freeman, Phys. Rev. B **41**, 3620 (1990).

[171] G. E. Engel and B. Farid, Phys. Rev. B **47**, 15931 (1993).

[172] G. Onida, L. Reining, R. W. Godby, R. D. Sole, and W. Andreoni, Phys. Rev. Lett. **75**, 818 (1995).

[173] E. L. Shirley, Phys. Rev. B **54**, 7758 (1996).

[174] W.-D. Schöne and A. G. Eguiluz, Phys. Rev. Lett. **81**, 1662 (1998).

[175] B. Holm and U. von Barth, Phys. Rev. B **57**, 2108 (1998).

[176] B. Holm and F. Aryasetiawan, Phys. Rev. B **62**, 4858 (2000).

[177] P. García-González and R. W. Godby, Phys. Rev. B **63**, 75112 (2001).

[178] P. Sánchez-Friera and R. W. Godby, Phys. Rev. Lett. **85**, 5611 (2000).

[179] P. García-González and R. W. Godby, Phys. Rev. Lett. **88**, 56406 (2002).

[180] F. Aryasetiawan, T. Miyake, and K. Terakura, Phys. Rev. Lett. **88**, 166401 (2002).

[181] G. Baym and L. P. Kadanoff, Phys. Rev. **124**, 287 (1961).

[182] G. Baym, Phys. Rev. **127**, 1391 (1962).

[183] L. P. Kadanoff and G. Baym, *Quantum Statistical Mechanics* (Benjamin, New York, 1962).

[184] R. T. M. Ummels, P. A. Bobbert, and W. van Haeringen, Phys. Rev. B **57**, 11962 (1998).

[185] Y. Takada, Phys. Rev. Lett. **87**, 226402 (2001).

[186] W. Ku and A. G. Eguiluz, Phys. Rev. Lett. **82**, 2350 (1999).

[187] M. L. Tiago, S. Ismail-Beigi, and S. G. Louie, cond-mat/0307181 (2003).

[188] S. Botti, F. Sottile, N. Vast, V. Olevano, H.-C. Weissker, L. Reining, G. Onida, A. Rubio, R. W. Godby, and R. D. Sole (2003), submitted.

[189] P. Lautenschlager, M. Garriga, L. Vina, and M. Cardona, Phys. Rev. B **36**, 4821 (1987).

[190] E. E. Salpeter and H. A. Bethe, Phys. Rev. **84**, 1232 (1951).

[191] W. Hanke and L. J. Sham, Phys. Rev. B **21**, 4656 (1980).

[192] G. Strinati, Phys. Rev. Lett. **49**, 1519 (1982).

[193] G. Strinati, Phys. Rev. B **29**, 5718 (1984).

[194] S. Albrecht, Ph.D. thesis, Ecole Polytechnique, France (1999).

[195] W. Hanke, Adv. Phys. **27**, 287 (1978).

[196] R. Zimmerman, Phys. Status Solidi **41**, 23 (1970).

[197] R. D. Sole and A. Selloni, Phys. Rev. B **30**, 883 (1984).

[198] V. Olevano and L. Reining, Phys. Rev. Lett. **86**, 5962 (2001).

[199] M. Rohlfing and S. Louie, Phys. Rev. B **62**, 4927 (2000), and references therein.

[200] F. Bechstedt, K. Tenelsen, B. Adolph, and R. D. Sole, Phys. Rev. Lett. **78**, 1528 (1997).

[201] A. Marini, unpublished.

[202] S. Albrecht, G. Onida, and L. Reining, Phys. Rev. B **55**, 10278 (1997).

[203] S. Albrecht, L. Reining, R. D. Sole, and G. Onida, Phys. Rev. Lett. **80**, 4510 (1998).

[204] L. X. Benedict, E. L. Shirley, and R. B. Bohn, Phys. Rev. Lett. **80**, 4514 (1998).

[205] M. Rohlfing and S. G. Louie, Phys. Rev. Lett. **81**, 2312 (1998).

[206] L. X. Benedict, E. L. Shirley, and R. B. Bohn, Phys. Rev. B **57**, R9385 (1998).

[207] B. Arnaud and M. Alouani, Phys. Rev. B **63**, 85208 (2001).

[208] L. X. Benedict and E. L. Shirley, Phys. Rev. B **59**, 5441 (1999).

[209] V. Olevano, bound excitons in solid Argon, unpublished.

[210] M. Rohlfing, M. Palummo, G. Onida, and R. D. Sole, Phys. Rev. Lett. **85**, 5440 (2000).

[211] P. H. Hahn, W. G. Schmidt, and F. Bechstedt, Phys. Rev. Lett. **88**, 16402 (2002).

[212] M. Rohlfing and S. G. Louie, Phys. Rev. B **62**, 4927 (2000).

[213] M. Rohlfing and S. G. Louie, Phys. Rev. Lett. **80**, 3320 (1998).

[214] M. Rohlfing and S. G. Louie, Phys. Rev. Lett. **82**, 1959 (1999).

[215] J.-W. van der Horst, P. A. Bobbert, M. A. J. Michels, G. Brocks, and P. J. Kelly, Phys. Rev. Lett. **83**, 4413 (1999).

[216] A. Ruini, M. J. Caldas, G. Bussi, and E. Molinari, Phys. Rev. Lett. **88**, 206403 (2002).

[217] J. A. Soninen and E. L. Shirley, Phys. Rev. B **61**, 16423 (2000).

[218] L. X. Bendict, E. L. Shirley, and R. B. Bohn, Phys. Rev. B **57**, R9385 (1998).

[219] R. Haydock, Solid State Physics **35**, 215 (1980).

[220] R. Haydock, Comput. Phys. Commun. **20**, 11 (1980).

[221] W. G. Schmidt, S. Glutsch, P. H. Hahn, and F. Bechstedt, Phys. Rev. B **67**, 85307 (2003).

[222] V. Peuckert, J. Phys. C **11**, 4945 (1978).

[223] A. Zangwill and P. Soven, Phys. Rev. A **21**, 1561 (1980).

[224] E. Runge and E. K. U. Gross, Phys. Rev. Lett. **52**, 997 (1984).

[225] E. K. U. Gross and W. Kohn, Phys. Rev. Lett. **55**, 2850 (1985).

[226] E. K. U. Gross and W. Kohn, Adv. Quant. Chem. **21**, 255 (1990).

[227] E. K. U. Gross, F. J. Dobson, and M. Petersilka, *Density Functional Theory* (Springer, New York, 1996).

[228] J. Dobson, G. Vignale, and M. P. Das, eds., *Electronic Density Functional Theory: An approach to the Quantum Many-Body Problem* (Plenum, New York, 1997).

[229] R. van Leeuwen, Int. J. Mod. Phys. B **15**, 1969 (2001).

[230] R. van Leeuwen, Phys. Rev. Lett. **82**, 3863 (1999).

[231] E. K. U. Gross, F. J. Dobson, and M. Petersilka, *Density Functional Theory* (Springer, 1996).

[232] M. Marques, A. Castro, and A. Rubio, J. Chem. Phys. **115**, 3006 (2001).

[233] K. Yabana and G. F. Bertsch, Int. J. Quantum Chem. **75**, 55 (1999).

[234] V. I. Gavrilenko and F. Bechstedt, Phys. Rev. B **55**, 4343 (1997).

[235] M. Petersilka, U. J. Gossmann, and E. K. U. Gross, Phys. Rev. Lett. **76**, 1212 (1996).

[236] H. Appel, E. K. U. Gross, and K. Burke, Phys. Rev. Lett. **90**, 43005 (2003).

[237] A. Rubio, J. A. Alonso, X. Blase, L. C. Balbás, and S. G. Louie, Phys. Rev. Lett. **77**, 247 (1996).

[238] N. H. March, A. Rubio, and J. A. Alonso, J. Phys. B **32**, 2173 (1999).

[239] K. Yabana and G. F. Bertsch, Phys. Rev. B **54**, 4484 (1996).

[240] K. Yabana and G. F. Bertsch, Phys. Rev. A **60**, 1271 (1999).

[241] I. Vasiliev, S. Oğüt, and J. R. Chelikowsky, Phys. Rev. Lett. **82**, 1919 (1999).

[242] I. Vasiliev, S. Oğüt, and J. R. Chelikowsky, Phys. Rev. B **65**, 115416 (2002).

[243] M. E. Casida, F. Gutierrez, J. Guan, F. X. Gadea, D. Salahub, and J. P. Daudey, J. Chem. Phys. **113**, 7062 (2000).

[244] M. E. Casida and D. Salahub, J. Chem. Phys. **113**, 8918 (2000).

[245] A. Görling, Phys. Rev. Lett. **83**, 5459 (1999).

[246] M. Petersilka, E. K. U. Gross, and K. Burke, Int. J. quantum Chem. **80**, 532 (2000).

[247] T. Grabo, M. Petersilka, and E. K. U. Gross, J. Mol. Struct.: THEOCHEM **501**, 353 (2000).

[248] M. Stener and A. Görling, J. Chem. Phys. **114**, 7816 (2001).

[249] S. P. Singhal and J. Callaway, Phys. Rev. B **14**, 2347 (1976).

[250] L. Kleinman, Phys. Rev. **160**, 585 (1967).

[251] L. Kleinman, Phys. Rev. **172**, 383 (1968).

[252] A. Rubio, J. A. Alonso, X. Blase, L. C. Balbás, and S. G. Louie, Phys. Rev. Lett. **77**, E5442 (1996).

[253] A. Rubio, J. A. Alonso, X. Blase, L. C. Balbás, and S. G. Louie, Int. J. Mod. Phys. B **11**, 2727 (1997).

[254] G. F. Bertsch, J. I. Iwata, A. Rubio, and K. Yabana, Phys. Rev. B **62**, 7998 (2000).

[255] M. Hybertsen and S. Louie, Phys. Rev. B **35**, 5585 (1987).

[256] A. Liebsch, Phys. Rev. B **32**, 6255 (1985).

[257] P. W. Langhoff, S. T. Epstein, and M. Karplus, Rev. Mod. Phys. **44**, 602 (1972).

[258] G. D. Mahan and K. R. Subbaswamy, *Local Density Theory of Polarizability* (Plenum, New York, 1990).

[259] S. Galambosi, J. A. Soininen, K. Hämäläinen, E. L. Shirley, and C.-C. Kao, Phys. Rev. B **64**, 24102 (2001).

[260] J. Stiebling, Z. Phys. B **31**, 355 (1978).

[261] J. Rowe and D. Aspnes, Phys. Rev. Lett. **25**, 162 (1970).

[262] J. Rowe and D. Aspnes, Phys. Rev. Lett. **25**, (E) 979 (1970).

[263] L. Hedin, Phys. Rev. **139**, A796 (1965).

[264] L. J. Sham and T. M. Rice, Phys. Rev. **144**, 708 (1966).

[265] W. Hanke and L. J. Sham, Phys. Rev. Lett. **43**, 387 (1979).

[266] M. Rohlfing and S. G. Louie, Phys. Rev. Lett. **81**, 2312 (1998).

[267] R. M. Martin, J. E. R. J. A. van Vechten, and D. E. Aspnes, Phys. Rev. B **6**, 2500 (1972).

[268] N. F. Schwabe and R. J. Elliott, Phys. Rev. B **53**, 5318 (1996).

[269] I. Egri, Physics Report **119**, 363 (1985), and references therein.

[270] V. Saile, M. Skibowski, W. Steinmann, P. Gürtler, E. E. Koch, and A. Kozevnikov, Phys. Rev. Lett. **37**, 305 (1976).

[271] V. Saile, Ph.D. thesis, Universität München (1976).

[272] E. K. Chang, M. Rohlfing, and S. G. Louie, Phys. Rev. Lett. **85**, 2613 (2000).

[273] L. Reining, V. Olevano, A. Rubio, and G. Onida, Phys. Rev. Lett. **88**, 066404 (2002).

[274] Y. Kim and A. Görling, Phys. Rev. Lett. **89**, 96402 (2002).

[275] R. D. Sole, G. Adragna, V. Olevano, and L. Reining, Phys. Rev. B **67**, 45207 (2003).

[276] W. Aulbur, L. Jönsson, and J. Wilkins, Phys. Rev. B **54**, 8540 (1996).

[277] X. Gonze, P. Ghosez, , and R. Godby, Phys. Rev. Lett. **74**, 4035 (1995).

[278] P. Ghosez, X. Gonze, and R. W. Godby, Phys. Rev. B **56**, 12811 (1997).

[279] M. Taut, J. Phys C **4**, 9595 (1992).

[280] A. Fleszar, A. A. Quong, and A. G. Eguiluz, Phys. Rev. Lett. **74**, 590 (1995).

[281] I. V. Tokatly and O. Pankratov, Phys. Rev. Lett. **86**, 2078 (2001).

[282] I. V. Tokatly, R. Stubner, and O. Pankratov, Phys. Rev. B **65**, 113107 (2002).

[283] P. L. de Boeij, F. Koostra, J. A. Berger, R. van Leeuwen, and J. G. Sniders, J. Chem. Phys. **115**, 1995 (2001).

[284] G. Vignale and W. Kohn, Phys. Rev. Lett. **77**, 2037 (1996).

[285] Y. Kim and A. Görling, Phys. Rev. B **66**, 35114 (2002).

[286] A. Görling and M. Levy, Phys. Rev. A **50**, 196 (1994).

[287] G. A. Baraff and M. Schlüter, Phys. Rev. B **30**, 3460 (1984).

[288] W. H. Press and al., *Numerical Recipies* (Cambridge University Press, 1992), chapter 2.

[289] D. Mearns and W. Kohn, Phys. Rev. A **35**, 4796 (1987).

[290] F. Kootstra, P. L. de Boeji, and J. G. Snijders, Phys. Rev. B **62**, 7071 (2000).

[291] S. Logothetidis and J. Petalas, J. Appl. Phys **80**, 1768 (1996).

[292] V. Saile, M. Skibowski, W. Steinmann, P. Gürtler, E. E. Koch, and A. Kozevnikov, Applied Optics **15**, 2559 (1976).

[293] G. H. Wannier, Phys. Rev. **52**, 191 (1937).

[294] N. F. Mott, Trans. Faraday Soc. **34**, 500 (1938).

[295] J. Frenkel, Phys. Rev. B **37**, 17 (1931).

[296] R. Peierls, Ann. Phys. **13**, 905 (1932).

[297] F. Bassani and G. Pastori Parravicini, *Electronic States and Optical Transitions in Solids* (Pergamon Press, 1975).

[298] P. W. Anderson, *Concepts in Solids* (World Scientific, 1997).

[299] A. Marini, private communication.

[300] G. Adragna, R. Del Sole, and A. Marini, accepted by Phys. Rev. B.

[301] G. Adragna, Ph.D. thesis, Università degli Studi di Roma "Tor Vergata" (2003).

[302] H. A. Kramers, Nature **117**, 775 (1926).

[303] H. A. Kramers, Atti Congr. Internat. Fisici **2**, 545 (1927), Como.

[304] R. de L. Kronig, J. Opt. Soc. Am. **15**, 547 (1926).

[305] R. M. Pick, M. H. Cohen, and M. Martin, Phys. Rev. B **1**, 910 (1970).

[306] S. K. Sinha, R. P. Gupta, and D. L. Price, Phys. Rev. B **9**, 2564 (1974).

[307] W. A. de Heer, Rev. Mod. Phys. **65**, 611 (1993).

[308] M. Brack, Rev. Mod. Phys. **65**, 677 (1993).

[309] T. L. Ferrel and P. M. Echenique, Phys. Rev. Lett. **55**, 1526 (1985).

[310] G. Mie, Ann. Phys. (Leipzip) [Folge 4] **25**, 377 (1908).

[311] D. J. Chadi and M. L. Cohen, Phys. Rev. B **8**, 5747 (1973).

Index